EPFL

Thèse n° 8854

Methods for functional connectivity and morphometry in neonatal neuroimaging to study neurodevelopment.

Présentée le 28 mai 2021

Faculté des sciences et techniques de l'ingénieur
Laboratoire de traitement d'images médicales
Programme doctoral en génie électrique

pour l'obtention du grade de Docteur ès Sciences

par

Serafeim LOUKAS

Acceptée sur proposition du jury

Prof. J.-Ph. Thiran, président du jury
Prof. D. N. A. Van De Ville, Prof. P. S. Hüppi, directeurs de thèse
Prof. F. Lazeyras, rapporteur
Dr Ph. Ciuciu , rapporteur
Prof. O. Blanke, rapporteur

■ École
polytechnique
fédérale
de Lausanne

2021

Η αρχή της σοφίας είναι η αναζήτηση.
— Σωκράτης

Στη μνήμη του πατέρα μου Λουκά, στη γυναίκα μου Σοφία,
στη μητέρα μου Σοφία και στον αδερφό μου Άγγελο...

Acknowledgements

First and foremost, I would like to sincerely thank my thesis supervisors, Professor Petra Hüppi and Professor Dimitri Van De Ville for giving me the opportunity to start my journey in the neuroscience field six years ago as a master's student, and next to pursuit a Ph.D. under their joint supervision. Being part of two laboratories (ChilDLab & MIPLab) has been an amazing experience combining perfectly my engineering background with my interest in neuroscience. Professor Petra Hüppi offered me the opportunity to discover the world of pediatrics and preterm birth and Professor Dimitri Van De Ville guided me through the methodological obstacles faced in the context of this doctoral work. Thank you for the opportunity to embark on this adventure, for your unique ideas, and for always providing solutions to any problem that I encountered along the way. Your guidance and expertise have guided and inspired me to discover the amazing field of computational neuroscience with application to prematurity. It has been a privilege being a Ph.D. student under your supervision.

I would like to thank Djalel-Eddine Meskaldji for his invaluable assistance and guidance throughout this journey. Your enthusiasm and love for statistics have made me see things from a different perspective. Thank you for patiently explaining to me complex statistical concepts and for providing such amazing ideas. I will miss our brainstorming discussions.

I thank my colleagues at ChilDLab for patiently introducing me to the clinical world of preterm birth. I also thank my colleagues at MIPLab for the fruitful methodological discussions about my projects but also the amazing personal moments that we spent together at the office (I will surely miss the coffee breaks and the mafia games at the red chairs). Thank you Maria Giulia Preti, Laura Vilaclara, Anjali Tarun, Lorena Freitas, Enrico Amico, Raphaël Liégeois, Alessandra Griffa, Elenor Morgenroth, and Nawal Kinany (I hope I did not forget anyone).

I would like also to sincerely thank my colleagues and friends Miljan Petrovic, Nicolas Gninenko, and Younes Farouj for the countless brainstorming coffee breaks at Campus Biotech but also for the amazing personal moments we shared.

My warmest thanks go to Lara Lordier, Joana Sa De Almeida, Vanessa Siffredi, and Maria-Chiara Liverani for spending countless hours at the MRI facility collecting data that were analyzed in the context of this dissertation. Thank you for making this thesis possible and for the amazing collaboration that we had on several projects.

Being part of the ChiDLab allowed me to work on a Horizon 2020 project, giving me the opportunity to meet and collaborate with amazing scientists spanning computational neuroscience and clinical neurology. I feel grateful and thrilled to have been part of the EuroPOND consortium. I specifically thank Neil Oxtoby and Daniel Alexander for the harmonic and fruitful

Acknowledgements

Abstract

Preterm birth is a major pediatric health problem that perturbs the genetically determined program of corticogenesis of the developing brain. As a consequence, prematurity has been strongly associated with adverse long-term neurodevelopmental outcome that may persist even into adulthood. Early characterization of the underlying neuronal mechanisms and early identification of infants at risk is of paramount importance since it allows better development of early therapeutic interventions aiming to prevent adverse outcomes through resilience. This dissertation aims to investigate the consequences of preterm birth on brain function and structure and their relation to adverse neurodevelopmental outcome, as well as to unveil the effect of an early music intervention on brain function. Research to date has mainly focused on the effect of early interventions on the long-term outcome but not on the effect of those interventions on brain function in preterm populations. Moreover, a clear consensus about the predictive utility of MRI volumetric data for long-term outcomes is still missing.

This dissertation consists of three main parts. First, we investigate the effects of an early musical intervention in preterm infants using a task-based and resting-state fMRI paradigm. We explore brain effective connectivity changes during task and functional connectivity (FC) modulations at rest. We show that music exposure during hospitalization promotes brain auditory processing maturation. We find increased FC between the auditory cortex and regions involved in familiarity and music processing, such as the thalamus and caudate nucleus. Moreover, we report increased rs-FC in regions involved in associative memory and multisensory processing, such as the calcarine and angular gyrus with a dosage-dependent effect on this modulation. Secondly, we examine brain volumetric development and whether brain volumes are associated with cognitive and behavioural long-term outcomes. We find that perinatal risk factors, such as asphyxia and sepsis have an impact on brain tissue volume. We also find that cognitive and behavioural outcomes are strongly associated with parental SES and that brain tissue volumes at TEA have moderate predictive power. Next, inspired by studies that have characterized the progression of neurodegenerative diseases, we employ an advanced technique to unveil the sequence of biological events along the course of prematurity. Our novel findings might be of clinical use as they allow more targeted early interventions aiming to improve long-term outcomes. Finally, we propose a framework that enables the spectral graph theory analysis of the functional connectome at the voxel level. Our results indicate the presence of both functional gradients and community structure revealing fine-grained connectivity patterns. The proposed framework opens a new avenue for spectral

Abstract

graph theory research at the voxel level.

Keywords: Preterm birth, functional MRI, neurodevelopmental outcome, connectomics, brain networks, multivariate modeling.

iv

Résumé

La prématurité est un problème de santé publique majeur qui perturbe le programme génétique qui contrôle le processus de corticogenèse du cerveau pendant le développement. En conséquence, la prématurité peut entraîner des séquelles neurodéveloppementales sur le long terme, qui peuvent persister même à l'age adulte. La caractérisation des mécanismes neuronaux sous-jacents et l'identification précoce des nourrissons à risque sont d'une importance capitale car elles permettent de déployer de meilleures interventions thérapeutiques anticipées visant à prévenir les effets indésirables grâce à la résilience. Cette thèse vise à étudier les conséquences de l'accouchement prématuré sur la fonction et la structure du cerveau et leur relation avec les complications neurodéveloppementales, ainsi que de dévoiler l'effet d'une intervention musicale précoce sur la fonction cérébrale. La recherche à ce jour s'est principalement concentrée sur l'effet des interventions précoces aux résultats à long terme, mais pas sur l'effet de ces interventions sur la fonction cérébrale dans les populations prématurées. En outre, il n'existe toujours pas un consensus clair sur l'utilité prédictive des données volumétriques IRM pour les résultats à long terme.

Cette thèse se compose de trois parties principales. D'abord, nous étudions les effets d'une intervention musicale précoce chez les nourrissons prématurés en utilisant un paradigme d'IRMf fondé sur les tâches et l'état de repos. Nous explorons les changements de connectivité effective du cerveau pendant les modulations de tâche et de connectivité fonctionnelle (FC) au repos. Nous montrons que l'exposition à la musique pendant l'hospitalisation favorise la maturation du traitement auditif cérébral. Nous trouvons une FC accrue entre le cortex auditif et les régions impliquées dans la familiarité et le traitement de la musique, comme le thalamus et le noyau caudé. De plus, nous rapportons une augmentation de la FC au repos dans les régions impliquées dans la mémoire associative et le traitement multisensoriel, comme la scissure calcarine et le gyrus angulaire avec un effet dépendant de la dose sur cette modulation. Deuxièmement, nous examinons le développement volumétrique du cerveau et si les volumes cérébraux sont associés à des résultats cognitifs et comportementaux à long terme. Nous constatons que les facteurs de risque périnatals tels que l'asphyxie et la septicémie ont un impact sur le volume du tissu cérébral. Nous constatons également que les résultats cognitifs et comportementaux sont fortement associés au SSE parental et que les volumes de tissu cérébral à TEA peuvent apporter des prédictions modérées. Ensuite, inspirés des études qui ont caractérisé la progression des maladies neurodégénératives, nous utilisons une technique avancée pour dévoiler la séquence des événements biologiques au cours de la prématurité. Nos nouvelles découvertes pourraient être d'une utilité clinique car

Résumé

elles permettent des interventions précoces plus ciblées visant à améliorer les résultats à long terme. Enfin, nous proposons un cadre qui permet l'analyse de la théorie spectrale des graphes du connectome fonctionnel au niveau du voxel. Nos résultats indiquent la présence à la fois de gradients fonctionnels et d'une structure communautaire révélant des modèles de connectivité à grain fin. Le cadre proposé ouvre une nouvelle voie pour la recherche en théorie spéctrale des graphes au niveau du voxel.

Mots-clés: naissance prématurée, IRM fonctionnelle, séquelles neurodéveloppementales, étude connectomique, réseaux cérébraux, modélisation multivariée.

Contents

Contents

1 Introduction

1.1 Motivation

Preterm birth, defined as the birth that occurs prior to 37 weeks of gestation, is considered a major pediatric health problem. Every year approximately 15 million babies are born preterm worldwide and the main causes underpinning preterm birth have yet to be fully understood (Blencowe et al., 2013). The economic impact of preterm birth is tremendous as it has been estimated that the hospitalization cost of preterm infants ranges from 25-fold to 68-fold those of full-term born infants, depending on the severity of each case (Tommiska et al., 2003; Beam et al., 2020). Moreover, prematurity has been reported to be the direct cause of 35% of all neonatal deaths (Blencowe et al., 2013) and preterm-born infants (PT) have an increased risk of suffering from chronic health issues, infections, as well as feeding problems. Although recent advances in neonatal care have increased the survival rates for these neonates, prematurity perturbs the genetically determined program of corticogenesis of the developing brain and it has been strongly associated with adverse neurodevelopmental outcome (Delobel-Ayoub et al., 2009; Marlow et al., 2005; Arpino et al., 2010; Doyle and Anderson, 2010). These adverse outcomes include cognitive, motor, and behavioural problems such as thinking and learning disabilities, walking problems, and poor social/interactive skills, respectively. Finally, preterms have three times the odds of meeting criteria for psychiatric diagnoses, compared to full-term born children (Treyvaud et al., 2013). Taken all these into account, the unveiling of the underlying neuronal mechanisms of preterm birth is crucial for the development of targeted and individualized early therapeutic interventions aiming to restore brain development and prevent adverse outcomes.

Magnetic resonance imaging (MRI) is a non-invasive, in vivo, neuroimaging technique that enables us to study the human brain. Due to its non-invasive nature, MRI is a perfect tool to study the sequelae of preterm birth and identify relevant neuroimaging biomarkers that are associated with adverse neurodevelopmental outcomes. Using this imaging technique, a plethora of neuroimaging studies have investigated the consequences of prematurity on brain microstructure, function, and tissue composition. Brain alterations due to preterm birth have

been associated to executive functions problems (Wehrle et al., 2018; Peterson et al., 2003; Gimenez et al., 2006), motor and cognitive disabilities (Pineda et al., 2014; Keunen et al., 2016; Nosarti et al., 2014; Peterson, 2000), psychiatric (Johnson and Marlow, 2011; Sinclair, 2012) and socio-emotional disorders (Treyvaud et al., 2013; Johns et al., 2019), hyperactivity and inattention (Montagna et al., 2020; Rommel et al., 2017) as well as to emotional processing deficits (Papini et al., 2016; Healy et al., 2013).

To prevent these adverse outcomes, early developmental interventions such as kangaroo mother care, maternal voice, and tactile stimulation have been provided in the clinical setting aiming to restore function and improve overall outcomes for these infants. Several studies have investigated the effectiveness of these interventions reporting a significant positive impact on cognitive development (Spittle et al., 2015), improved short-term growth and feeding outcomes, reduced respiratory support, decreased length of hospitalization, reduction of apnea or bradycardia, as well as improved neurodevelopmental outcomes at 2 years old age (Symington and Pinelli, 2006; Filippa et al., 2017; Anderson and Patel, 2018; Pineda et al., 2017; Haslbeck, 2012). Recently, new interventions have been introduced such as music therapy (Lejeune et al., 2019). However, there is little research about the effect of such interventions on brain function in preterm infants.

Thanks to its high spatial resolution and specificity, MRI can be an excellent tool to study the effectiveness of early interventions, to unveil the sequence of brain abnormality characterizing preterm birth, and to explore the potential associations between brain abnormalities and outcome.

1.2   Dissertation organization and main contributions

The present doctoral thesis aims to provide novel insights into the consequences of preterm birth on brain function and structure, as well as to investigate the effect of early interventions on the preterm brain, through the development of appropriate state-of-the-art methods and frameworks. Another objective of this dissertation is the characterization of the sequence of abnormality underlying preterm birth as well as the association of brain abnormalities to adverse neurodevelopmental outcomes. The thesis is organized as a compilation of two already published manuscripts, one manuscript submitted for publication, and three preprints in preparation for submission. Chapter 2 serves as the background for the studies presented in the following chapters, providing first an introduction to magnetic resonance imaging (MRI), a powerful, non-invasive method to study brain function and structure, followed by an overview of the state-of-the-art analytical tools for the different imaging techniques that are based on MRI. Next, the clinical aspects of preterm birth, as well as recent findings concerning the consequences of this major public health problem on the brain, are presented. Finally, a summary of the challenges and considerations in the neonatal neuroimaging field is provided. Chapters 3-5, include published manuscripts and articles in preparation that provide both novel insights but also complement existing knowledge. Finally, in Chapter 6, the conclusions

and future perspectives of the current research work are reported.

In the remainder of this section, a summary of the main research questions addressed in the context of the present dissertation and the contributions of each manuscript are provided. Throughout all the studies presented in this thesis, I have performed the data processing, statistical analysis, and visualization. Furthermore, I wrote or contributed equally to the manuscript preparation, and submission and revisions, where applicable. Finally, I would like to acknowledge that the research presented in this thesis is an outcome of interdisciplinary collaboration among several people.

Motivation

Preterm birth
- 15 million babies are born preterm every year
- Increased risk of suffering from neurodevelopment adverse outcome
- Deficits may persist even into adulthood
- Early developmental interventions can revert damage through brain resilience

Multivariate and predictive modeling
- MRI → non-invasive brain imaging technique → ideal to study the developing brain
- The effectiveness of early interventions on brain connectivity has not been studied
- Predictive utility of brain tissue volumes debate → more studies are needed
- Disease progression following preterm birth has yet to be investigated
- Parcellation of brain → sacrifice spatial resolution → data-driven methods are crucial
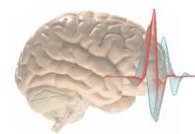
Contributions

Chapter 3: Unveiling the effects of intervention in preterm infants with task-based & resting-state fMRI

Lordier*, Loukas* et al., NeuroImage, 2018
- Psychophysiological interaction (PPI) analysis
- Brain effective connectivity of the auditory cortex (seed)
- Music exposure during hospitalization promotes brain auditory maturation
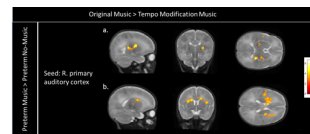
Loukas*, Lordier* et al., Human Brain Mapping, submitted
- Partial least squares multivariate (PLS) analysis
- Connectome-based statistical analysis
- Unveiled multivariate dosage-dependent modulation patterns in resting-state functional connectivity
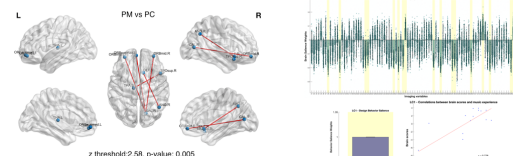
Chapter 4: Predictive utility of brain volumes for cognitive and behavioural long-term outcomes

Gui, Loukas et al., NeuroImage, 2019
- Longitudinal study of tissue growth in preterm infants
- Predictive modeling of brain volumetric data: linear discriminant analysis (LDA), model comparison
- Perinatal brain characteristics influence later functional development.
- Socioeconomic status is associated with adverse long-term outcome
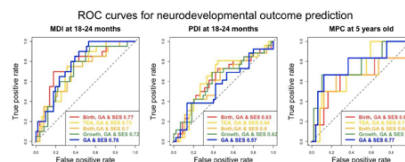
Loukas*, Liverani* et al., preprint, 2021
- Multivariate predictive modeling: support vector machines (SVM)
- Permutation importance assessments of best predictors
- Different sets of perinatal data predict different subcategories of behavioural outcome
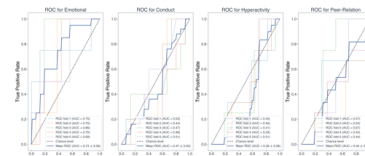
Chapter 5: Advanced models for neurodevelopment

Loukas et al., preprint, 2021
- Event-based modeling (EBM)
- Unveiled the disease progression underlying prematurity - progression sequence
- Brainstem is the first to become abnormal while subcortical GM the last
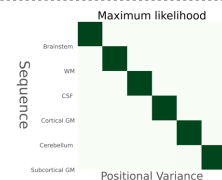
Loukas et al., preprint, 2021
- Data-driven, atlas-free, novel framework for the estimation of modularity & laplacian at the voxel level
- Recovered meaningful dominant patterns at the voxel-level
- Functional gradients and community structure is present at the voxel level
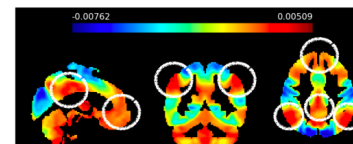
Figure 1.1 – **Thesis overview:** Main contributions on the underlying brain function in preterm birth.

Chapter 3: Unveiling the effects of intervention in preterm infants with task-based and resting-state fMRI

Soon after birth, preterm infants are admitted to the neonatal intensive care unit (NICU) where life support is provided and early developmental interventions aiming to restore development and prevent adverse outcomes are administrated (Delobel-Ayoub et al., 2009; Marlow et al., 2005; Arpino et al., 2010; Doyle and Anderson, 2010). Recently, musical interventions have been introduced in the clinical setting. To the best of our knowledge, at the time of this publication, no previous study has investigated the effect of such interventions on brain functional connectivity in preterm infants using fMRI. This chapter includes two fMRI studies. In the first study, we investigate the brain responses (task-based fMRI) of preterm infants that underwent musical intervention during hospitalization. On the other hand, in the second study, we explore the resting-state brain connectivity changes following the presentation of the same music used during the intervention, unveiling the beneficial effects of the early musical intervention.

Section 3.1: Music processing in preterm and full-term newborns: A psychophysiological interaction (PPI) approach in neonatal fMRI (Journal Article)

Lordier L*, Loukas S*, Grouiller F, Vollenweider A, Vasung L, Meskaldji DE, Lejeune F, Pittet MP, Borradori Tolsa C, Lazeyras F, Grandjean D, Van De Ville D, and Hüppi PS, Music processing in preterm and full-term newborns: A psychophysiological interaction (PPI) approach in neonatal fMRI, Neuroimage, 2019185:857-864, doi: 10.1016/j.neuroimage.2018.03.078.

- What are the neural processes underlying music processing in preterm infants?
- What is the effect of music therapy during NICU hospitalization on brain function?
- Is brain responding the same in preterm infants that were previously exposed to the music, compared to control preterm infants?

How the preterm brain processes music is an important question to ask before promoting the enrichment of the neonatal environment with music. In this study, we explore the brain networks implicated in music processing in newborns as well as the effect of music exposure during hospitalization on brain functional connectivity. Using task-based fMRI and by employing a psychophysiological interaction (PPI) analysis, we unveil, for the first time, the brain networks involved in music processing in preterm infants and we show that music exposure during hospitalization promotes brain auditory processing maturation. These novel findings highlight the beneficial aspects of early musical intervention on brain function in preterm infants.

Section 3.2: Musical memories in newborns: A resting-state functional connectivity study (Submitted Journal Article)

Loukas S*, Lordier L*, Meskaldji DE, Filippa M, Sa de Almeida J, Van De Ville D, and Hüppi PS, Musical memories in newborns: A resting-state functional connectivity study, Human Brain Mapping, 2021, Submitted.

- How does music listening modify the distributed resting-state brain networks in preterm and full-term newborns?
- Is there an intervention dosage effect on this modulation?
- Can we find brain traces of memory engrams?

While task-based fMRI paradigms allow us to understand how the brain works under specific cognitive demands or tasks, resting-state fMRI analyses provide valuable insight into intrinsic brain function (Fox, 2010; Lee et al., 2012). Using the same population as in the previous study, we investigate the effect of music listening on the resting-state functional connectivity (rs-FC) using connectomics-based statistical frameworks. Furthermore, to investigate the potential dosage effect of prior music listening on the rs-FC, we employ a multivariate partial least squares (PLS) correlation approach to associate the post music listening changes in rs-FC with the occurrence of the prior musical intervention - i.e., the dosage. We show that all infants experience changes in their rs-FC after music listening and that preterm infants who were previously repeatedly exposed to music increase their rs-FC between brain regions known to be involved in associative memory and multi-sensory processing. Finally, we report a dosage-dependent effect on this modulation.

Chapter 4: Predictive utility of brain volumes for cognitive and behavioural long-term outcomes

While functional MRI studies provide valuable insight into brain function, volumetric analyses are needed for the characterization of brain tissue abnormalities due to preterm birth (PTB). Even in the absence of major brain injury, PTB is often characterized by the presence of subtle alterations of cerebral structures, leading to potential disruption in the typical progression of a child's development and subsequent functional consequences. Some studies have reported associations of brain volumetric data with adverse neurodevelopmental outcome (Peterson et al., 2003; Beauchamp et al., 2008; Thompson et al., 2008) while others not (Shah et al., 2006; Lind et al., 2010; Lee et al., 2016). Moreover, recent reviews concluded that, so far, there is limited evidence regarding the value of neonatal brain volumetric information in predicting neurodevelopmental outcome in childhood (Keunen et al., 2012; Anderson et al., 2015). Thus, more studies aiming to investigate the predictive power of volumetric and clinical, as well as perinatal data are needed to shed more light on this open debate.

This chapter includes two volumetric MRI studies. The first study aims to investigate longitudinal brain development between birth and TEA in a cohort of relatively healthy PT infants, and to identify potential predictive biomarkers for the long-term *neurodevelopmental* outcome.

To the best of our knowledge, at the time of the publication, only a limited number of studies have tried to explore the association of longitudinal brain volumes with outcomes beyond 24 months of age. Finally, the second study tries to disentangle the association between brain volumes measured at TEA and long-term *behavioural* outcomes assessed through parental questionnaires in a preterm population.

Section 4.1: Longitudinal study of neonatal brain tissue volumes in preterm infants and their ability to predict neurodevelopmental outcome (Journal Article)

Gui L, Loukas S, Lazeyras F, Hüppi PS, Meskaldji DE, and Borradori-Tolsa C, Longitudinal study of neonatal brain tissue volumes in preterm infants and their ability to predict neurodevelopmental outcome, NeuroImage, 2019, 728-741, https://doi.org/10.1016/j.neuroimage.2018.06.034.

- How does the longitudinal brain development of preterm infants evolve between birth and TEA?
- Are there brain asymmetries already present at birth or at TEA?
- Can we predict long-term cognitive/motor outcomes using brain volumetric data?

Several studies have reported associations between neurodevelopmental outcomes and brain tissue volumes at term-equivalent-age (TEA) (Peterson et al., 2003; Beauchamp et al., 2008; Thompson et al., 2008; Keunen et al., 2016). Interestingly, others did not find evidence of such associations or found that these associations were weakened or not significant after adjustment for perinatal variables (Shah et al., 2006; Lee et al., 2016). In addition, a clear consensus about the predictive utility of MRI brain volumes for the prediction of long-term neurodevelopmental outcome has yet to be established (Keunen et al., 2012; Anderson et al., 2015). Therefore, more studies are needed in order to shed light on this ongoing controversy.

Early prediction of neurodevelopmental outcomes requires the identification of early perinatal biomarkers. In the context of this study, we first investigate the longitudinal brain development between birth and TEA in a cohort of relatively healthy PT infants. Furthermore, we investigate whether brain asymmetries are already present at birth or TEA, and finally, we explore the predictive utility of brain volumetric data in terms of cognitive/motor outcomes prediction at 18-24 months and 5 years of age using linear discriminant analysis (LDA). We demonstrate that cognitive outcomes at 18-24 months and 5 years of age are strongly associated with parental SES and that volumetric data at birth and at TEA contribute to the prediction of motor outcomes at 18-24 months, while brain volumes at TEA and tissue growth rates contribute to the prediction of the cognitive outcome at 5 years of age. These results suggest that perinatal brain characteristics in PT infants may influence later functional development.

Section 4.2: Behavioral outcome of very preterm children at five years of age: Prognostic utility of brain tissue volumes at TEA and perinatal factors (Journal Preprint)

Liverani MC*, Loukas S*, Gui L, Pittet MP, Pereira M, Bickle-Graz M, Truttmann AC, Hüppi PS, Meskaldji DE, and Borradori Tolsa C, Behavioral outcome of very preterm children at five years of age: Prognostic utility of brain tissue volumes at TEA and perinatal factors, Preprint.

- Is SDQ questionnaire able to distinguish behavioural problems among children at risk and those that are not?
- Is there a comorbidity between the behavioural symptoms as assessed by the SDQ questionnaire?
- Can we use brain volumetric data at TEA to predict behavioural outcome at 5 years of age in very preterm infants?

In a similar context to the previous study, we explore the association between brain volumes and *behavioural* long-term outcomes assessed via parental questionnaires in a cohort of preterm infants. We aim to enlighten the prognostic utility and usefulness of magnetic resonance imaging at birth, a point that is still controversial. Thus, the main objective of the study is to evaluate the predictive utility of brain volumetric data at TEA in terms of long-term behavioural outcome prediction using support vector machines. Additionally, we explore the contribution of perinatal factors and parental socioeconomic status to the prediction of the behavioural outcome at 5 years of age. We show that brain tissues at TEA could serve as biomarkers for the long-term prediction of emotional problems. Finally, we find that clinical variables predict long-term hyperactivity-related problems and that SES is associated with conduct and peer-relations problems.

Chapter 5: Advanced models for neurodevelopment

While functional, structural, and volumetric brain alterations due to prematurity have been previously investigated (Dewey et al., 2019; Karolis et al., 2017; Alexander et al., 2019; Gui et al., 2019; de Almeida et al., 2021; Inder, 2005), the exact *sequence* of brain abnormality following preterm birth has never been explored. Understanding the sequence of biological events of the encephalopathy of prematurity can provide valuable insights into the underlying pathology and can help intervention development. To this end, we employ an advanced model aiming to characterize the sequence of brain abnormalities. To the best of our knowledge, no previous study has tried to characterize the disease progression sequence of the encephalopathy of prematurity.

In the first section of this chapter, an advanced probabilistic model is used on brain tissue volumes on a large cohort of preterm infants aiming to estimate the sequence of the pathology in a probabilistic sense. In the second section of this chapter, we introduce a novel, data-driven framework for the estimation of the Laplacian and the modularity spectra at the voxel level. The proposed method can characterize, for the first time, the brain's fundamental organizational principles at the voxel level, without the use of a parcellation scheme. We validate and illustrate the importance of the proposed method using 40 subjects from the

Human Connectome Project (HCP).

Section 5.1: Fine-grained, image-based disease progression characterization of prematurity (Journal Preprint)

Loukas S, Oxtoby N, Meskaldji DE, Gui L, Van De Ville D, Hüppi PS, and Alexander D, Fine-grained, image-based disease progression characterization of prematurity, Preprint.

- Can we unveil the sequence of abnormality underlying the encephalopathy of prematurity?
- Which are the brain regions that become abnormal first?

Neurodevelopment is a dynamic process characterized by large macroscopic changes where brain abnormality compensation mechanisms are highly present (Young et al., 2020; de Silva et al., 2020). Conditions such a preterm birth may change the dynamic process of neurodevelopment and lead to adverse neurodevelopmental outcomes. Thus, understanding the sequence of biological events along the course of prematurity can provide valuable insights into the underlying pathophysiology and can help develop more targeted interventions.

In this study, we employ a data-driven approach to unveil the disease progression of prematurity, producing a fine-grained estimation of the sequence of brain abnormality in prematurely-born infants at TEA. The hypothesis is that preterm birth alters the dynamic process of neurodevelopment, similarly to disease progression, and thus, advanced disease progression models might be of potential clinical use. Our novel findings suggest that there is a robust ordering of brain tissue volume abnormality underpinning encephalopathy of prematurity at term age.

Section 5.2: A new framework for high-resolution spectral analysis of resting-state fMRI functional connectivity (Journal Preprint)

Loukas S, Meskaldji DE, Hüppi PS, and Van De Ville D, A new framework for high-resolution spectral analysis of resting-state fMRI functional connectivity, Preprint.

- How can we perform spectral graph theory analysis at the voxel level?
- Are there functional gradients and community structure at the voxel level?
- Can we recover meaningful modularity and laplacian-driven voxel-wise brain maps from resting-state fMRI data?

The investigation of functional connectomes has revealed interesting network-related characteristics such as small-world (Bassett and Bullmore, 2016), rich-hub (van den Heuvel and Sporns, 2011), and scale-free organization (Eguíluz et al., 2005). Furthermore, spectral graph theory has revealed the presence of a modular (Kabbara et al., 2019; Betzel et al., 2017; Zhigalov et al., 2017; Sporns and Betzel, 2016) and large-scale cortical gradient-based organization(Margulies et al., 2016; Huntenburg et al., 2018). While these studies provide valuable insights into brain function and organization, in most cases, the functional connectome is constructed based on a subjective, non-trivial choice of a predefined brain parcellation atlas.

This is done due to the high dimensionality of the fMRI data that prohibits the connectomics analysis at the voxel level. Importantly, it has been shown that the atlas resolution can affect the results and statistical outcomes of connectomics studies (Bellec et al., 2015; Wang et al., 2009; de Reus and van den Heuvel, 2013).

In this work, we introduce a framework that enables the spectral graph theory analysis at the voxel level overcoming the aforementioned limitations. To validate our framework, we estimate the group-level modularity and Laplacian spectrum of 40 subjects from the Human Connectome Project. Our results indicate the presence of both functional gradients and community structure at the voxel level revealing fine-grained, dominant, connectivity patterns. The proposed framework opens a new avenue for spectral graph theory research at the voxel level. Finally, the code developed to perform the analysis described in this work has been made available at https://github.com/seralouk/Voxel_wise_Laplace_Modularity.

2 Background

Magnetic resonance imaging (MRI) provides a non-invasive, in vivo technique to study brain function and structure. Over the past decades, MRI has provided valuable insights and has played a central role in studying the neonatal brain and identifying relevant neuroimaging biomarkers. The advantages, as well as disadvantages of this technique, can be better appreciated after understanding the principles underlying this neuroimaging technique. In this chapter, the principles of MRI and the different neuroimaging techniques are first introduced. Next, an overview of the state-of-the-art analytical tools for neuroimaging data is provided, followed by the introduction of the clinical aspects and implications of preterm birth. Finally, the main challenges and considerations in the neonatal neuroimaging field are summarized.

2.1   Magnetic resonance imaging (MRI) and brain research

Magnetic resonance imaging (MRI) allows us to study the anatomical structure, function, and tissue composition of the human brain, based on nuclear magnetic resonance (NMR). NMR refers to the interaction effects of specific atomic nuclei when they are exposed to radio-frequency (RF) waves, in the presence of an external static magnetic field. Paul Lauterbur was the first to create a 2D NMR image in 1973 (Lauterbur, 1973) and Raymond Damadian was the first to show that healthy tissue and tumors can be distinguished using MRI (Damadian et al., 1977), illustrating the tremendous clinical value of the technique for human imaging and pathology.

The main biologically relevant element that makes the use of MRI possible is the hydrogen (^{1}H) nucleus. It is estimated that the human body is made of approximately 63% of hydrogen atoms (Chou and Carrino, 2007). Each atomic nucleus consists of neutrons and protons, resulting always in a positive net charge. Moreover, specific atomic nuclei such as the hydrogen nucleus are characterized by an effect known as 'spin'. Conceptually, the nucleus is spinning around its axis inducing a magnetic moment that results in a local magnetic field (see Figure 2.1a). However, the magnetic moment of a single nucleus is small and undetectable, and the spinning directions of the hydrogen nuclei are considered to be random in the absence of an external

magnetic field.

When a strong, external magnetic field (B_0) is applied, the protons of the hydrogen nuclei align either in parallel or perpendicular to this field. Typically, the external static magnetic field is produced by a large electromagnet (1.5 to 7 Tesla) that is part of the MRI machine. The nuclei alignment, along the direction of B_0, results in a detectable net magnetization (M_0) in the tissue (see Figure 2.1b). Furthermore, the aligned protons precess about the external magnetic field, at random phases, with an angular frequency according to the Larmor frequency (Larmor, 1897). The angular frequency is proportional to the strength of the external magnetic field (B_0). Next, RF transmitter coils are used to excite the aligned net magnetization (M_0) in the tissue, by transmitting an RF pulse (B_1) that is perpendicular to the external static magnetic field (B_0). This procedure is known as 'RF excitation' and involves the 'flipping' of the net magnetization away from the longitudinal axis i.e., the axis that is parallel to B_0, to the transverse plane, which is orthogonal to B_0 (Grover et al., 2015; Bolas, 2016) (see Figure 2.1c).

When the net magnetization is tipped to the transverse plane, it can be detected by another hardware part of the machine, the receiver coil. In more detail, when the RF excitation is over, the magnetization starts to return to its thermal equilibrium through two processes: the transverse relaxation (i.e., the transverse magnetization begins to diminish, described by the time constant T_2) and the longitudinal relaxation (i.e., the longitudinal magnetization is returning to its original position, parallel to B_0, described by the time constant T_1) (Bolas, 2016; Soher et al., 2007). T_2 is defined as a time constant for the decay of transverse magnetization due to natural spin-spin interactions however, in reality, the transverse magnetization decays faster and this effect is denoted as T_2^*. T_2^* is a product of inhomogeneities in the main magnetic field due to susceptibility-induced field distortions produced by the tissue or the magnet. Finally, during the relaxation procedures, a measurable current is induced in the receiver coil (Free induction decay, see Figure 2.1d). This current corresponds to the raw MR signal (Crooks and Hylton, 1994).

Moreover, another important aspect of the NMR signal acquisition is its spatial encoding. Magnetic field gradients, positioned in three dimensions within the MR system, are used to perturb the external, static magnetic field (B_0) in a linear way. Thus, the gradients control the spatial inhomogeneity of the magnetic field (Brown and Semelka, 2011) and nuclei at different positions will have different resonance frequencies. This property allows the image reconstruction using the inverse Fourier transform (see Figure 2.1e) in three dimensions with a spatial resolution of 1 to 3 mm (Plewes and Kucharczyk, 2012; Paschal and Morris, 2004).

Finally, different types of MRI images can be acquired by altering the repetition (TR) and echo time (TE). TR refers to the time interval between consecutive RF pulse excitations while TE is the time between the RF pulse application and maximum MR signal in the receiver coil. In a typical neuroscience experiment, depending on the choice of these two parameters, the output MRI images will emphasize different tissues such as the grey, white matter, or cerebrospinal fluid (CSF). The most common types of MRI images include the T1-weighted
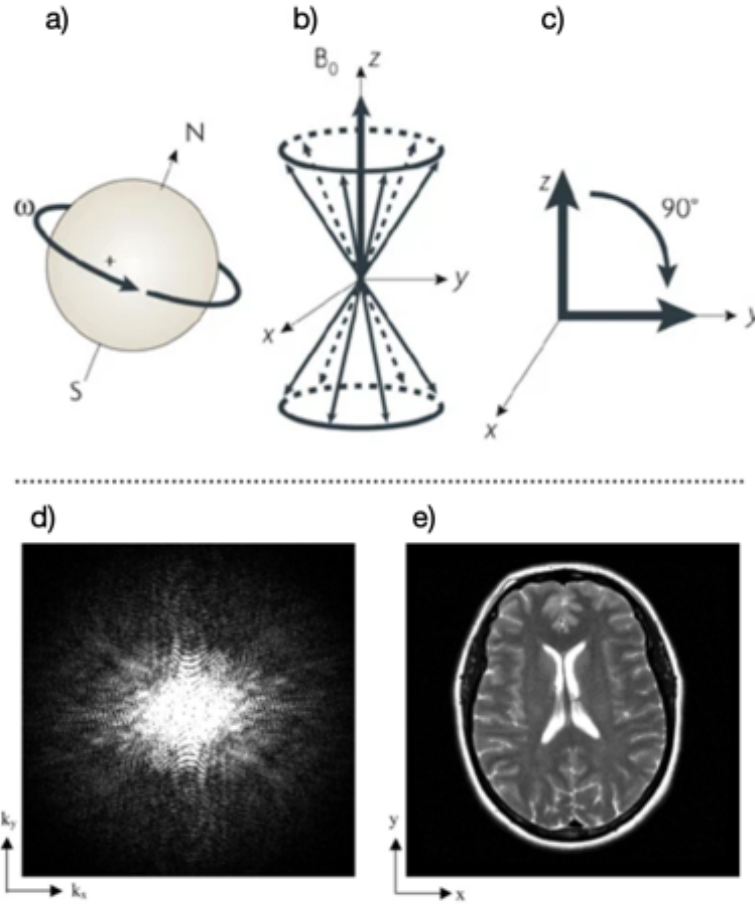
Figure 2.1 – **a)** The spin of a nucleus. **b)** Under an external magnetic field (B_0) these nuclei align with the field and precess around it at a specific angular frequency. **c)** An RF pulse, that is perpendicular to the main field (B_0), is applied to flip the net magnetization from the z into the xy plane. Magnetization in this plane induces a detectable signal in the receiver coil. **a), b)** and **c)** were adapted with permission from Brindle (2008). **d)** The magnitude of the raw (k-space) MR data in an array format and **e)** the magnitude of the Fourier transform of the raw data in the image space. **d)** and **e)** were adapted with permission from Paschal and Morris (2004).

and T2-weighted images. T1-weighted images are used to characterize anatomic structures whereas T2-weighted images are useful for identifying underlying pathological processes. The anatomical images used in this work were obtained based on these aforementioned principles. The exact parameters of the MRI sequence are reported within each study.

2.1.1 Structural connectivity

In the previous section (section 2.1), an overview of the main MRI principles that enable the acquisition of three-dimensional anatomical brain images was provided. Based upon those principles, brain images that reflect microstructural properties of the brain can be obtained.

Recent advances in magnetic resonance imaging (MRI) such as the Diffusion-weighted Imaging (DWI) technique, have allowed the non-invasive assessment of the microstructural properties and organization within the brain tissue based upon the dispersion of water molecules (Fink and Fink, 2018; Bodini and Ciccarelli, 2014; Bihan, 2014). DWI was first developed aiming to detect, in vivo, acute ischemic stroke (Baird and Warach, 1998), as well as brain tumors and multiple sclerosis (Larsson et al., 1992; Kono et al., 2001).

Diffusion-weighted imaging (DWI) enables the non-invasive, in vivo, quantification of water molecule movement in the brain. The main principle underlying DWI is that molecular diffusion follows the Brownian motion (or pedesis) rules. In more detail, when the water molecules are unconstrained (in terms of physical boundaries) their movement is expected to be random and equally probable to occur across all possible directions in space. This random, unconstrained movement is often described as 'isotropic' or 'gaussian' diffusion process. However, the motion of water molecules in structured environments such as the brain is constrained due to the physical boundaries of the underlying medium (Pandit et al., 2013). In the brain, the microstructure of the white (WM) and grey matter (GM) brain tissues (i.e., the presence of axons, neuronal cell bodies, glial cells, etc.) comprises a heterogeneous environment and constrains the diffusion of the water molecules. It has been shown that the diffusion in the white matter tends, in principle, to be parallel to the white matter tracts instead of perpendicular (Doran et al., 1990; Pandit et al., 2013). Thus, the diffusion of the water molecules within the WM is constrained and not equal to all directions. This phenomenon is termed as 'anisotropic' or 'non-gaussian' diffusion process (Chenevert et al., 1990; Doran et al., 1990).

To mathematically model the anisotropic diffusion in the brain, Basser and colleagues proposed the use of diffusion tensors (Basser et al., 1994; Basser and Jones, 2002). The diffusion tensor describes the properties of a three-dimensional ellipsoid and the tensor's definition requires the acquisition of diffusion neuroimaging data in at least six non-collinear directions (Jones and Leemans, 2010). This acquisition procedure is known as Diffusion Tensor Imaging (DTI) (Basser et al., 1994). More specifically, a tensor is fitted at each brain voxel, producing a brain diffusion map. This map encodes the magnitude and dominant direction of the underlying diffusion process. Thus, by tracking across voxels, the dominant directions form fiber tracts (streamlines of the WM fibers) along the most likely direction that the diffusion occurred. This technique is known as tractography (Pandit et al., 2013; Grover et al., 2015).

An example of isotropic and anisotropic diffusion in the brain modeled by diffusion tensors is shown in Figure 2.2. The eigenvalues and eigenvectors of the fitted tensor define the shape (magnitude) and orientation (direction) of the ellipsoid planes, respectively (Mori and van Zijl,
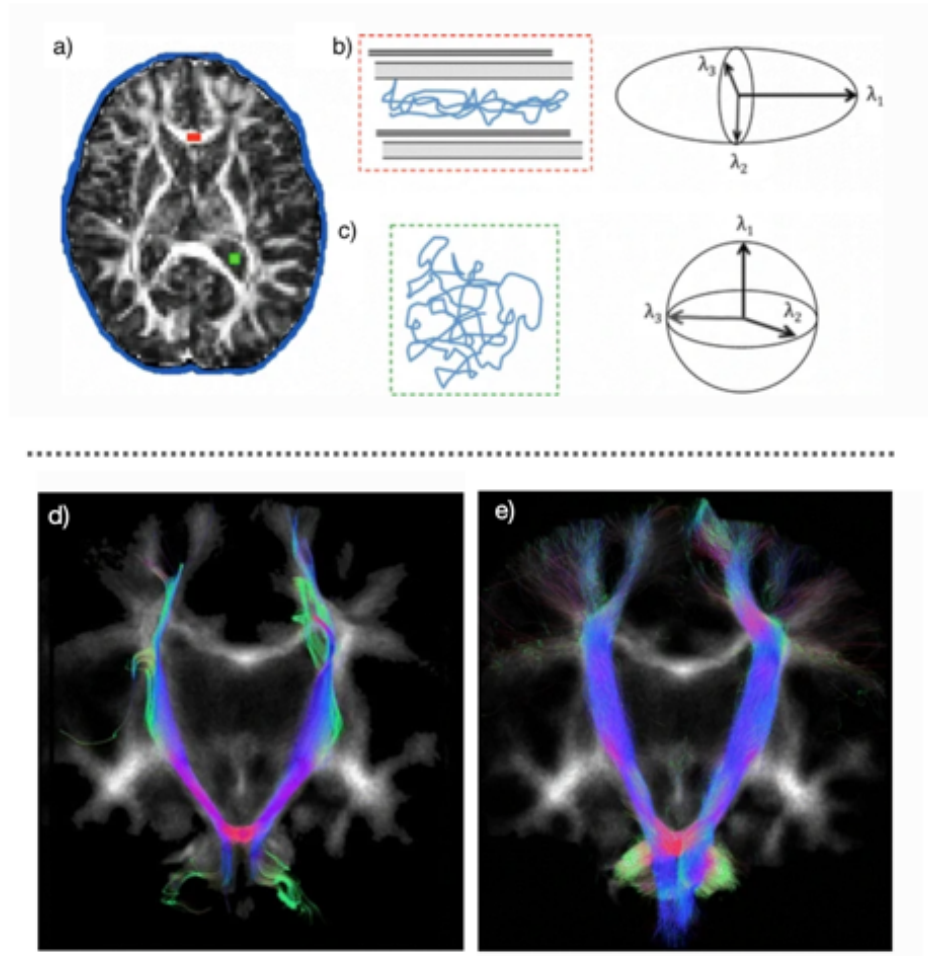
Figure 2.2 – **a)** Two brain regions: white matter (red) and CSF (green). **b)** The diffusion in the WM (corpus callosum; red spot) is anisotropic occurring along the axonal fibers whereas, the diffusion in the ventricular CSF (green spot) is unrestricted and thus, isotropic **c)**. The diffusion tensor ellipsoids that model the anisotropic and isotropic diffusions are shown in **b)** and **c)**, respectively. Each tensor is characterized by three eigenvectors with corresponding eigenvalues λ_1, λ_3 and λ_3, and in the case of anisotropic diffusion the long axis of the ellipsoid is aligned with the white matter tract. **d)** and **e)** show the tractography results of the cortico-spinal tract using a deterministic and probabilistic algorithm, respectively. Figures adapted with permission from Pandit et al. (2013).

2005). The isotropic diffusion is modeled by a 3-dimensional sphere whereas, the anisotropic diffusion is modeled by a three-dimensional ellipsoid where the long axis of the ellipsoid is aligned with the white matter tract (Figure 2.2 c & b).

The main two tractography algorithms are the deterministic and probabilistic techniques (see Figure 2.2 d & e). Deterministic algorithms are based on the propagation of the WM tracts

from seed regions along with the principal orientation of the ellipsoid in a voxel by voxel manner until a criterion is met (Conturo et al., 1999). This family of algorithms provides high accuracy in terms of WM streamline reconstruction however, it is very limited when WM fiber tracts are crossing in some brain regions. To overcome this important limitation, probabilistic tractography algorithms have been introduced that take into account the intra-voxel crossing of WM tracts and estimate the probability that a WM fiber will cross through any other voxel in the brain (Behrens et al., 2007; Pandit et al., 2013).

Finally, DTI provides a plethora of metrics about the microstructure of the brain such as the mean diffusivity (i.e., a measure of the displacement of water molecules), the apparent diffusion coefficient (i.e., a measure of tissue water diffusivity), and the fractional anisotropy (i.e., a measure of the degree of anisotropy of the fibers) (Curran et al., 2016). Brain maps based on these metrics can be constructed and explored to better characterize and understand the underlying brain *structural connectivity*.

2.1.2   Functional connectivity

Advances in magnetic resonance imaging (MRI) have not only allowed us to acquire brain scans that reflect anatomical and microstructural properties of the brain (as described in the previous section 2.1) but also brain scans that reflect brain function across time. To this end, a sequence of brain volumes is acquired by repeating the steps described in Section (2.1) at a fixed time interval and using a different acquisition protocol. The time interval corresponds to the difference in the acquisition time of two consecutive brain scans and it is known as Repetition Time (TR). Moreover, for the acquisition of the sequence of brain scans, echo-planar imaging (EPI) (Mansfield, 1984) is commonly used and the TR is usually set to 2 or 3s (but can fall to ms scale). This technique is known as functional Magnetic Resonance Imaging (fMRI).

fMRI can be used to either study intrinsic brain activity, in the absence of external stimuli (resting-state fMRI, see section 2.2.2), or brain response (i.e., activation/deactivation) to external stimuli (task-based fMRI, see section 2.2.1). Since its introduction in 1990, fMRI has provided valuable insights in cognitive and clinical neuroscience allowing us to better characterize and understand brain function.

Principles of fMRI

Functional magnetic resonance imaging (fMRI) is a non-invasive, neuroimaging technique that is able to measure indirect neural activity by detecting blood flow-related changes in the brain. fMRI relies on the coupling between cerebral blood flow and neuronal activation, in the sense that when a brain region is active, the blood flow in this region increases. In more detail, when neurons are active they consume oxygenated hemoglobin (Gore, 2003). To compensate for this oxygen consumption, an inflow of oxygenated hemoglobin is delivered to the active brain region, via the blood. This phenomenon is known as 'neurovascular coupling'.

As a result, a regional imbalance occurs where the concentration of oxyhemoglobin (oxy-Hb) is higher compared to this of deoxyhemoglobin (deoxy-Hb) (see Figure 2.3a). Oxy-Hb is diamagnetic whereas deoxy-Hb is paramagnetic leading to the suppression of the MR signal (Gore, 2003). Thus, this imbalance reduces the net "susceptibility effect" of deoxy-Hb which significantly affects the T2- and T2*-weighted images (Fink, 2007). Increased neuronal activity is represented (with a time delay) by an increase in the BOLD signal. The size of the BOLD effect varies between approximately 1% and 3% (Huettel, 2010; Gore, 2003).
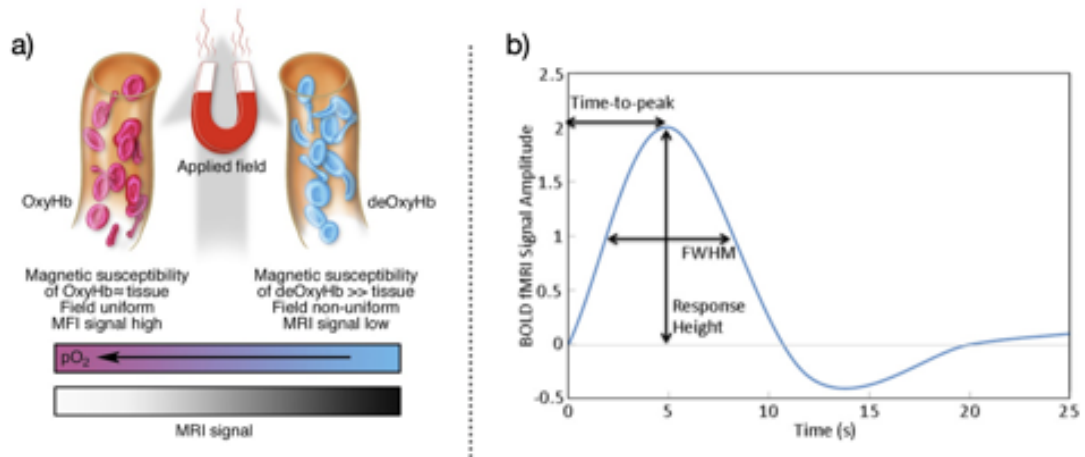
Figure 2.3 – **a)** A visual representation of the principles underlying the BOLD signal in fMRI. Deoxy-Hb is paramagnetic inducing inhomogeneities in the magnetic field. The BOLD signal from active brain regions increases as newly oxy-Hb is delivered via the blood and due to the imbalance in the concentration of oxy-Hb and deoxy-Hb. **b)** The canonical HRF. Figures adapted with permission from Gore (2003) and Rangaprakash et al. (2018), respectively.

As discussed previously, the acquired BOLD signal is an indirect measure of the underlying neural activity. Every neural activation is followed by a hemodynamic response. This is typically referred to as the hemodynamic response function (HRF) and it is modeled as a combination of two gamma functions. Following the neural activity, the peak of the HRF occurs, on average, after a 5s time lag (Logothetis et al., 2001; Friston et al., 1998). Briefly, the neurovascular coupling evolves as follows. Some seconds upon neural activity (t=0) the measured signal starts to increase and the peak appears around five seconds (t=5-6s). Next, the BOLD signal decreases below the baseline (post-stimulus undershoot) and finally it returns to the initial baseline (t=20s) (see Figure 2.3 b). The post-stimulus undershoot is observed since blood flow decreases more rapidly than blood volume allowing a higher concentration of deoxy-Hb (Friston et al., 1998). Moreover, it is worth pointing out that the accurate modeling of the HRF can massively affect the fMRI data analysis and that variability in the HRF across different populations (e.g. adults vs neonates, see Arichi et al. (2012)) exists and needs to be considered.

Finally, fMRI enables us to explore and study brain function, by acquiring multiple functional brain scans and then tracking across time the measured activity of the underlying brain regions,

resulting in brain activity time-series (after first applying some pre-processing steps such as realignment, co-registration, normalization and spatial smoothing of the brain volumes). Methods and experimental designs for the analysis of *functional connectivity* are described in the next sections (see section 2.2).

2.1.3 Brain tissue volumes

In the previous sections, the acquisition procedure of functional and structural brain images was described. Functional MRI allows us to study brain function while DWI enables the exploration of microstructural properties of the brain. To study *anatomical* features of the brain such as tissue volumes, anatomical images (as described in section 2.1) can be used.

Advances in the MRI processing tools have allowed the extraction and quantification of tissue brain volumes from anatomical MRI images. This has prompted research into the possible contribution of such information to better understand and characterize possible brain damage as well as brain anatomical abnormalities (discussed in the next sections). Brain volumetric segmentation algorithms aim to segment a 3D anatomical image of the brain into different tissue types. These typically include the grey matter, white matter, CSF, as well as subcortical regions, such as amygdala, thalamus, putamen, caudate, etc. An example of brain tissue segmentation is presented in Figure 2.4.

The analysis of brain volumetric data using magnetic resonance imaging (MRI) has provided valuable insights into pathology and it is considered a valuable neuroimaging tool to support diagnosis and evaluate neurodegenerative disease progression (Maclaren et al., 2014).

Figure 2.4 – The automatic segmentation of a T1-weighted scan. Different colors correspond to different brain tissue types. Figure adapted with permission from Puonti et al. (2016).

2.2 Data analysis tools

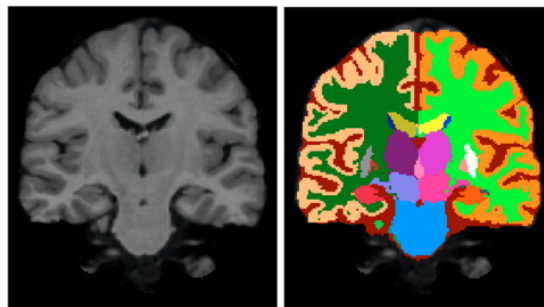In this section, the state-of-the-art methodological tools and frameworks for the analysis of the different brain neuroimaging modalities are presented.

2.2.1 Task-based fMRI for brain function

To study the functional activity of the brain during externally-induced stimuli, the task-based fMRI (t-fMRI) experimental design has been widely used in most t-fMRI studies. As opposed to the task-free resting-state fMRI (see section 2.2.2), t-fMRI studies aim to explore how the brain responds to external stimuli that are presented during acquisition. The presentation of the stimuli is usually performed in a block design where the different stimuli (tasks or conditions on time) are grouped into extended time intervals forming what we call 'blocks'. Blocks of stimuli (e.g., visual or auditory stimuli) are usually followed by blocks of rest (e.g., fixation cross on a black screen) and this pattern is repeated several times to form the experimental time horizon. Finally, the main advantage of the block design is the high statistical power for brain activity localization and robustness to different shapes of HRFs, as opposed to the event-based designs (Lindquist, 2008). In this dissertation, block design was used for the t-fMRI studies.

The most common approach to analyze fMRI data and to localize task-dependent brain activity is the General Linear Model (GLM). GLM is a confirmatory method aiming to separate stimulus-induced signals from noise. It models the observed BOLD time-series as a linear combination of different components that contribute to the signal (known as regressors) and tests (hypothesis testing) whether brain activity is related to the know input functions (conditions or tasks) that represent/model neural response. GLM is very flexible allowing the inclusion of several regressors in the design matrix such as motion parameters or clinical data (e.g., age, IQ) allowing this way the modeling of confound factors. Hypothesis testing of the GLM model's estimates (beta estimates) reflects how well the model fits the experimental observation (BOLD signals) (Friston et al., 1995a; Friston, 2005; Monti, 2011). The model's estimates represent the magnitude of the effect of the corresponding regressor. To reveal brain activity differences between tasks, a comparison (known as contrast) of the task-specific *responses* is usually performed (e.g., task music - task silence). The results of the GLM analysis are typically reported in the form of statistical parametric maps (SPMs) that show the brain response differences between the task responses (Lindquist, 2008).

Formally, the theoretical GLM model for a single voxel time-course sampled T times is defined as $\mathbf{y} = \mathbf{X}\boldsymbol{\beta} + \boldsymbol{\varepsilon}$, where $\mathbf{y}$ is an $T \times 1$ column vector representing the measured BOLD signal time-series of a single voxel, $\mathbf{X}$ is the $T \times p$ design matrix with each column representing a different regressor (i.e., predictor variable), and $\boldsymbol{\varepsilon}$ is the error term. The design matrix ($\mathbf{X}$) models all available knowledge about experimentally controlled factors and potential confounds such as motion parameters or clinical data (Friston et al., 1995b). To solve for beta, the ordinary least-squares estimator (OLS) is a minimum variance linear unbiased estimate (MVUE) of $\boldsymbol{\beta}$ under the assumption that the noise ($\boldsymbol{\varepsilon}$) is normally distributed as $\mathcal{N}\left(0, \sigma^2 \boldsymbol{I}\right)$. The unknown model parameter (betas) and the variance are estimated as $\hat{\boldsymbol{\beta}} = \left(\mathbf{X^T X}\right)^{-1} \mathbf{X^T y}$ and $\text{var}(\hat{\boldsymbol{\beta}}) = \sigma^2 \left(\mathbf{X^T X}\right)^{-1}$ (Monti, 2011; Pernet, 2014). The $t - value$, for a specific contrast of interest ($\mathbf{c}$), is estimated as $t = (\boldsymbol{c}^T \hat{\boldsymbol{\beta}}) / \hat{\sigma} \sqrt{\boldsymbol{c}^T \left(\boldsymbol{X}^T \boldsymbol{X}\right)^{-1} \boldsymbol{c}}$, where $\hat{\sigma}^2 = (\hat{\mathbf{e}}^T \hat{\mathbf{e}}) / (T - \text{rank}(\mathbf{X}))$ is the variance estimate and the $t - value$ follows the student t-distribution with $T - p$ degrees of freedom.

GLM is powerful but has three main disadvantages. First, it is strongly model-based and thus extremely sensitive to the design matrix construction and setup. Second, GLM is a confirmatory, hypothesis-driven approach based on mass-univariate testing (50-100k voxels) and false-positives need to be controlled. Third, the GLM ignores voxel interactions and assumes independent responses among voxels which might not always hold.

Several extensions of the GLM have been proposed, with one being the Psychophysiological Interaction (PPI) confirmatory analysis that has been employed in the context of the present dissertation (Friston et al., 1997). PPI estimates context-specific changes in coupling (known as *effective connectivity*) between a seed region and the rest of the brain. In more detail, PPI can capture interactions between brain voxels that enhance their relationship with a predefined seed region in a particular 'context' such as during the execution of a high cognitive demand task. The main principle underlying PPI is that the BOLD activity of two interacting brain regions will correlate over time suggesting that the activity in one region may be driven by the activity of the other. To capture this context-specific association, the task time-course, the seed time-course, and the PPI interaction term (i.e., the element by element product of the seed activity with the task time-course), can be included as regressors in the design matrix ($\mathbf{X}$) in a standard GLM analysis as previously described. Thus, voxels that were correlated with the seed during the task blocks will be captured by the PPI regressor (McLaren et al., 2012; O'Reilly et al., 2012). Finally, one important thing to mention is that PPI cannot infer the direction of causality, as opposed to other causal models such as the dynamic causal modeling (DCM) that assumes that the brain is a deterministic nonlinear dynamic system that is subject to inputs producing outputs (Friston et al., 2003).

Brain activity is characterized by spatio-temporal dependencies that cannot be accurately modeled a priori (Bowman, 2005). This fact prevents their evaluation by confirmatory methods such as the GLM, PPI, or DCM. To address this limitation, several data-driven or exploratory methods for the analysis of fMRI data exist. These are usually multivariate and model-free methods that are capable of revealing the underlying structure in the data. Some of the most widely used exploratory models for t-fMRI analysis include the principal component analysis (PCA) (Zhong et al., 2009) and clustering methods (Aljobouri et al., 2018; Venkataraman et al., 2009). PCA is usually used to reduce the high dimensionality of the t-fMRI data (100k voxels), before further analysis, by decomposing and projecting the data into a reduced space where the variance is maximized. Finally, clustering analysis can be used to detect brain active regions by grouping brain scans, forming clusters of activity (known as co-activation patterns) usually based on a similarity or distance metric, without the need for strict assumptions.

2.2.2 Resting-state functional connectivity

Resting-state fMRI (rs-fMRI) refers to the acquisition of fMRI data in the absence of external stimuli (task-free paradigm). During the rs-fMRI acquisition, participants are usually instructed to mind wander with their eyes closed. The main difference between t-fMRI and

rs-fMRI is that in the case of rs-fMRI there is no explicit demand for cognitive, motor, or perceptual tasks. The origin of rs-fMRI dates back to 1995 when Barat Biswal and colleagues reported that fluctuations in BOLD rs-fMRI signals of the motor cortex revealed spatial correlation patterns of neuronal origin (Biswal et al., 1995). These patterns were observed in the absence of any explicit motor task. Based upon these observations, similar findings for the auditory, visual cortex, and default mode network (DMN) have been reported (Hampson et al., 2004; Greicius et al., 2002). Thus, when accounting for confounding effects (e.g., head motion (Power et al., 2018), respiratory and cardiac rate (Yoshikawa et al., 2020) etc.), these low-frequency fluctuations in rs-fMRI reflect neuronal-originated aspects of the brain functional organization. For a review of the historical context of these rs-fMRI studies refer to Lowe (2010).

The main advantages of rs-fMRI include, first of all, the simplicity of the experimental design and the short acquisition time needed (usually around 15 min but even 5 to 7 min provide enough statistical power and reliability, Dijk et al. (2010)) make it an ideal way to study brain function at rest. Second, rs-fMRI allows the acquisition of data for participants that are incapable to perform fMRI tasks such as sedated, paralyzed, cognitively impaired patients as well as neonates and preterm infants (O'Connor and Zeffiro, 2019). Third, rs-fMRI can also be used to accurately detect individual differences (functional fingerprinting, (Finn et al., 2015)) as well as brain function alterations.

The spontaneous fluctuations of brain activity during rest have been shown to be organized in terms of consistent large-scale functional networks across healthy subjects (Damoiseaux et al., 2006). To explore these functional networks, graph and network-based frameworks have been widely used. These networks are also known as 'connectomes', a representation of the brain wiring, which holds important information related to brain organization and functioning (Sporns et al., 2005; Fornito et al., 2015). Moreover, disease propagation patterns are constrained by the highly organized topology of the underlying neural architecture i.e., the connectome and therefore, a connectomics approach can be essential to understand neuropathology (Fornito et al., 2015). Each vertex (node) in these networks represents a brain region while each edge (weight) reflects the interdependence of two nodes. In the case of rs-fMRI data, the edge weights between brain regions are defined as the functional connectivity that is often measured as the Pearson correlation between the regionally averaged voxel time-courses (Sporns, 2011; Bullmore and Sporns, 2009). This network representation is known as 'functional connectome'. However, alternative functional connectivity measures have been recently introduced, such as accordance and discordance measures that are based on the activation-deactivation modeling of the brain activity (Meskaldji et al., 2015a,b). In the case of diffusion-weighted imaging data, the edge weights between brain regions are usually defined as the number of streamlines that connect the brain regions. The streamlines are estimated using tractography algorithms (as discussed in section 2.1.1). This is known as 'structural connectome'.

Network-based measures can be used to characterize several aspects of global and local

brain connectivity that reflect functional integration and segregation, as well as quantify the importance of individual brain nodes (Rubinov and Sporns, 2010). A widely used measure of segregation is the network's clustering coefficient ($C = (1/N)C_i$, N: number of nodes). For an undirected, weighted graph, the clustering coefficient of node i is defined as $C_i = e_i/(k_i(k_i - 1)/2)$, where e_i is the sum of weight edges in neighborhood of node i and k_i is its strength (Watts and Strogatz, 1998). The C measure reflects the fraction of triangles around an individual node (Rubinov and Sporns, 2010). On the other hand, the most commonly used measures of network integration is the characteristic path length of the network i.e., the average shortest path length between all pairs of nodes, defined as $L = (1/n)\sum_{i \in N} L_i = (1/n)\sum_{i \in N} \frac{\sum_{j \in N, j \neq i} d_{ij}}{n-1}$, where L_i is the average distance between node i and all other connected nodes (Watts and Strogatz, 1998). Finally, the importance of an individual brain node can be measured by the strength of the node defined as $k_i = \sum_{j=1}^{N} a_{i,j}$, where A is the adjacency matrix. The investigation of brain connectomes has revealed interesting and important network-related characteristics such as small-world (high clustering coefficient and short path length) (Bassett and Bullmore, 2016), rich-hub (van den Heuvel and Sporns, 2011), scale-free (power-law degree distribution) (Eguíluz et al., 2005) and modular (community structure) (Kabbara et al., 2019; Betzel et al., 2017; Zhigalov et al., 2017; Sporns and Betzel, 2016) underlying organization. The latter has allowed the natural, data-driven grouping of brain regions, exploiting the modular nature of the brain (Sporns and Betzel, 2016; Akiki and Abdallah, 2019; Diez et al., 2015). However, one major limitation of most connectomics analyses is the fact that the full dimensionality of the data is not exploited. Instead, the brain is parcellated into brain regions based on a predefined parcellation atlas. This is done due to the high-dimensionality nature of the data (spatial resolution) that is prohibitive as it does not allow the explicit estimation of the connectomes at the voxel level. Thus, a network-based analysis at the voxel level is not feasible. In this dissertation, we attempt to fill this gap by proposing a method that enables the estimation of modularity at the voxel level enabling, for the first time, the fine-grained modularity mapping of voxel-wise connectivity.

Alternative methods to connectomics, such as the independent component analysis (ICA), can be used to analyze rs-fMRI data and reveal brain functional networks. ICA is a blind source separation method that assumes statistical independence of the input sources. The term 'blind' refers to the fact that the method aims to recover signal source from mixtures with unknown mixing coefficients (Brown et al., 2001; McKeown, 2003). The assumption, when applied to rs-fMRI data, is that the measured data is a product of different neuronal sources and therefore, by applying ICA, we can separate these input sources and recover isolated brain networks. ICA has been able to successfully identify several reproducible resting-state functional networks (e.g. DMN network) and broaden our knowledge on how brain networks emerge at rest but also during task (Smith et al., 2009).

Finally, techniques that quantify the strength of the relationship between different modalities have provided valuable insights into the neuroimaging field. One such method is the partial least squares (PLS) analysis that maximizes the covariance between two different modalities (McIntosh and Lobaugh, 2004). For example, using PLS we can associate fMRI-based features

(e.g., nodal strength, brain activity, etc.) to cognitive or behavioural data (e.g., intervention dose, IQ, age, etc.), unveiling the neural correlates of the observed cognitive or behavioural outcome (Krishnan et al., 2011).

2.2.3 Brain volumetric data for brain abnormalities

Tissue brain volumes obtained from anatomical MRI images using segmentation algorithms (see section 2.1.3) enable us to unveil disease-related brain anatomical abnormalities and evaluate disease progression and its relation to adverse outcomes (Hoogman et al., 2017; Alexander et al., 2019; Peterson, 2000; Veijola et al., 2014).

Recently the number of studies employing machine learning techniques on brain tissue volumes, instead of traditional linear regression and correlation models, has increased. The main advantage of machine learning models such as Support vector machines (SVMs), Linear discriminant analysis (LDA), and others, is that the modeling of the data is performed in a multivariate way (Ion-Margineanu, 2018) enabling the modeling of multivariate relationships in the data. An SVM model is a supervised machine learning model that finds the best separating hyperplane between two classes (Hearst et al., 1998). On the other hand, LDA projects the data into a reduced space where the intra-class separation is maximized (Tharwat et al., 2017). Thus, multivariate models can model the underlying structure of the data as a whole, taking into account the relationship among the variables, than simply looking at a single variable at the time. (Formisano et al., 2008; Chen et al., 2014). By investigating the learned/fitted model functions, we can relate brain tissue abnormalities to the observed adverse outcomes. In the context of the present thesis, both SVM and LDA models were used aiming to investigate the relationship between brain tissue volumes and cognitive as well as behavioural adverse neurodevelopmental outcomes in preterm infants (see section 4.1 and 4.2).

2.3 Preterm birth

Preterm birth is defined as the birth that occurs prior to 37 weeks of gestation and it constitutes a major pediatric public health problem. Approximately 15 million babies are born preterm every year and this number has been rising (Blencowe et al., 2013). Based on the birth gestational age (GA), three subcategories exist: a) extremely preterm (EP; less than 28 weeks), b) very preterm (VPT; 28 to 32 weeks) and c) moderate/late preterm (LP; 32 to 37 weeks). Preterm-born infants (PT) have an increased risk of suffering from chronic health issues, infections, asthma, and feeding problems. Furthermore, complications due to prematurity have been reported to be the leading cause of death in children under 5 years of age (Liu et al., 2016). Most importantly, preterm birth has been strongly associated with adverse neurodevelopmental outcomes that may persist even into adulthood (Delobel-Ayoub et al., 2009; Marlow et al., 2005; Arpino et al., 2010; Doyle and Anderson, 2010). Thus, understanding the underlying neuronal mechanisms of preterm birth may allow more targeted and individualized early

therapeutic interventions aiming to prevent the observed adverse outcomes.

In this section, an overview of the poor neurodevelopmental outcomes linked to preterm birth is first provided. Next, the functional and structural brain alterations underpinning preterm birth are presented followed by a summary of the early interventions that are usually administrated to preterm populations. This dissertation aims to provide novel knowledge about the effect of early musical interventions on brain function in preterm infants as well as to investigate the association of brain tissue volumes and clinical data with neurodevelopmental outcomes later in life.

2.3.1 Preterm birth and adverse outcome

Recent advances in the neonatal intensive care units (NICU) have increased the survival rates of preterm infants (Arpino et al., 2010). However, the incidence of preterm birth is rising worldwide and remains strongly associated with persistent long-term neurodevelopmental disabilities such as cognitive, motor, and behavioural adverse outcomes (Delobel-Ayoub et al., 2009; Marlow et al., 2005; Arpino et al., 2010; Doyle and Anderson, 2010). Cognitive problems include thinking and learning disabilities while motor development problems refer mainly to crawling and walking problems and finally, behavioural deficits include attention deficits and poor social skills. Importantly, these adverse outcomes may persist into school age and even adulthood (Soleimani et al., 2014). Additionally, it has been reported that only 61% of infants born at 24–32 weeks of gestational age were free of disabilities at 5 years of age (Larroque et al., 2008) and that preterm infants have three times odds of developing a psychiatric disorder, compared to full-term born infants (Treyvaud et al., 2013; Chung et al., 2020).

Early identification of infants at high risk of neurodevelopmental impairments can thus be extremely valuable since it would allow better decision making about appropriate early intervention aiming to prevent these adverse neurodevelopmental consequences through resilience (Sutton and Darmstadt, 2013; Silveira et al., 2018; Spittle and Treyvaud, 2016; Puthussery et al., 2018).

2.3.2 Preterm birth and brain alterations

The impact of preterm birth on the brain can be heterogeneous, ranging from specific focal injuries to a more general alteration of cerebral development resulting in the disruption of the typical child's development and finally leading to functional consequences.

While the main mechanisms and processes underlying preterm birth have not yet been fully understood, magnetic resonance imaging (MRI) has provided valuable insights and has played a central role in studying the preterm developing brain and identifying relevant neuroimaging biomarkers. Using this non-invasive imaging technique, a plethora of studies has focused on the understanding of the consequences of prematurity on brain structure. In more detail, it has been shown that preterm-born children have smaller cortical grey matter,

cortical white matter, basal ganglia, amygdala, hippocampus, and cerebellum brain volumes compared to control children born at term (Lodygensky et al., 2008; Cismaru et al., 2016; Inder, 2005; Hüppi et al., 1998; Counsell and Boardman, 2005). Additionally, reduced volumes in brain areas involved in high executive functions such as sensorimotor, parieto-occipital, and fronto-temporal regions have been reported by several studies (Peterson et al., 2003; Gimenez et al., 2006). Moreover, the reduction of white matter, cerebellum and basal ganglia volumes has been linked to poor neurodevelopmental outcome (Ment et al., 2009; Padilla et al., 2014) whereas cortical grey matter (CGM) volume was found to be negatively correlated with motor and cognitive outcome at 2 years old, reflecting potential neuronal migration disturbance at the UWM-CGM boundary (Keunen et al., 2016). Neonatal brain abnormalities in the white matter, cerebellar, cortical, and deep grey matter have been linked to psychiatric and socio-emotional disorders in school-aged preterm-born children (Treyvaud et al., 2013). Finally, lower hippocampal volume was associated with a higher prevalence of hyperactivity, inattention, and socio-emotional problems in VPT school-aged children while reduced volume in frontal regions was associated with poorer prosocial skills (Rogers et al., 2012).

Resting-state functional connectivity studies have also revealed alterations in functional connectivity related to preterm birth. Ball and colleagues identified alterations to a complex set of interactions between functional nodes in subcortical and cortical grey matter. The most dominant sets of altered connections were found between basal ganglia and frontal cortex confirming that functional connectivity in the preterm brain is significantly altered by term-equivalent age in higher-level association regions (Ball et al., 2016). Moreover, Lordier and colleagues reported decreased resting-state functional connectivity in preterm infants between the salience network with the superior frontal, auditory, and sensorimotor regions, and the salience network with the thalamus and precuneus regions, compared to full-terms (Lordier et al., 2019). Furthermore, Papini and colleagues reported alterations in resting-state functional connectivity between the amygdala, parietal and temporal cortices that could be linked to the deficits in emotion processing observed in preterm-born children (Papini et al., 2016). Functional connectivity alterations of the sensorimotor and higher cognitive networks have been shown to be the most affected in VPT-born children and were associated with poorer executive functions (Wehrle et al., 2018). Moreover, motor deficits have been linked to altered functional connectivity in the thalamus-motor, basal ganglia-motor, and dorsal attention-default mode network in VPT-born children (Wheelock et al., 2018). Finally, altered resting-state functional connectivity in emotion processing brain regions was reported in a cohort of VPT-born adults (Papini et al., 2016).

Taking all these into account, we can highlight the vulnerability of the brain following preterm birth and the importance of developing better clinical tools for the early prediction of long-term neurodevelopmental outcomes in preterm infants. This would enable the early identification of infants at risk and the development of more focused interventions. However, this is a challenging task due to the complexity of the developing infant brain and to potential other factors (such as the socioeconomic status of the parents, SES) that influence neurodevelopment (Christensen et al., 2014; ElHassan et al., 2018).

Moreover, there is conflicting evidence concerning the predictive utility of brain volumes acquired early in life (e.g., at birth or TEA). A number of studies have verified the predictive utility of the brain volumetric data (as described above, for a review see Anderson et al. (2015)), whereas others not (Morsing et al., 2018). A clear consensus about the predictive utility of neuroimaging brain data for the prediction of long-term neurodevelopmental outcome has yet to be established (Keunen et al., 2012; Anderson et al., 2015). Thus, more studies aiming to investigate the predictive power of volumetric and clinical as well as perinatal data are needed. This thesis aims to provide more evidence on this dispute.

Finally, although functional, structural, and volumetric brain alterations due to prematurity have been previously extensively studied (Dewey et al., 2019; Karolis et al., 2017; Alexander et al., 2019; Gui et al., 2019; de Almeida et al., 2021; Inder, 2005), the exact sequence of brain abnormality underlying preterm birth has never been investigated. Understanding the sequence of biological events along the course of prematurity provides valuable insights into the underlying pathophysiology and can help intervention development. The present thesis aims to fill this gap in knowledge by attempting to unveil the sequence of abnormality of prematurity.

2.3.3 Early interventions

Preterm infants spend the first weeks of their life in the neonatal intensive care unit (NICU). NICU provides a special environment designed to support life and assure the survival of these infants. During their hospitalization, preterm infants undergo interventions aiming to boost brain maturation and development. These early developmental interventions have been traditionally provided in the clinical setting usually during hospitalization but also post-hospital discharge focusing on the improvement of neurodevelopmental outcomes.

Spittle et al., recently explored the effectiveness of early developmental interventions provided either during the primary hospitalization or post-hospital discharge on the motor and cognitive development, concluding that early interventions have a significant impact on cognitive development up to preschool age (Spittle et al., 2015). In another study, researchers reported that developmental care interventions during hospitalization in the NICU improved short-term growth, feeding outcomes, decreased respiratory support, decreased length of hospitalization as well as improved neurodevelopmental outcomes at 2 years old age (Symington and Pinelli, 2006). Finally, several authors have reported stabilizing effects on heart and respiratory rates, reduction of apnea or bradycardia, improved feeding, better weight gain, and more mature sleep patterns (Filippa et al., 2017; Anderson and Patel, 2018; Pineda et al., 2017; Haslbeck, 2012; Filippa et al., 2015).

Interestingly, new promising ways to enrich NICU's environment have been recently introduced such as music therapy among other sensory stimuli (Allen, 2014; van der Heijden et al., 2016). However, there is a gap in our knowledge about the basic music processing in the brain of preterm infants. Cortical processing of the music, as well as the effect of the

musical intervention of the brain functional connectivity, is an important question to address before supporting the enrichment of the neonatal environment with music. This highlights the importance of this dissertation to fill this gap.

2.4 Challenges in neonatal neuroimaging research

MRI has provided valuable insights into the brain development and abnormality characterizing preterm birth. Due to its non-invasive nature and sensitivity to detect and quantify brain damage, MRI is the preferred imaging modality for neonatal populations. Thanks to MRI, new findings of the brain structural and functional connectivity as well as morphology and microstructural architecture of the neonatal brain have been reported. Additionally, the association of these brain alterations with neurodevelopmental outcome has played a central role in the development of early interventions aiming to avoid long-term disabilities (Dubois et al., 2020). However, some methodological aspects need to be cautiously considered when performing MRI neuroimaging studies in neonatal populations.

First of all, the acquisition of fMRI or rs-fMRI data requires the subjects to lay still on a motorized table that is moved into the interior of the MRI scanner. Depending on the experimental design and task paradigm, the duration of the MRI scan can vary between 10 and 40 minutes (Murphy et al., 2007). An important difference between MRI studies in adults compared to neonatal populations is that infants cannot be sedated for research purposes, but only for clinical indications. Additionally, it is impossible to explicitly instruct the infants to stay still. This can be a major problem given that MRI images are very susceptible to head motion (for an example see Figure 2.5 b). To reduce this artefact, neonates usually receive breast or formula feeding before the MRI acquisition. Next, they are swaddled in a blanket, placed in a vacuum pillow for immobilization, and finally scanned while resting quietly in the scanner. Moreover, MR-compatible headphones are used for noise protection. To deal with motion-corrupted brain scans, motion scrubbing has been an acceptable solution (Power et al., 2018, 2014) for this hard-to-image population (Dubois et al., 2020; Cusack et al., 2018) however, it is worth mentioning that often the percentage of motion-corrupted scans is large enough and thus, the subject needs to be discarded. This eventually leads to reduced sample sizes and less statistical power, a common characteristic of most neonatal neuroimaging studies.

Another important consideration is the hemodynamic response. fMRI measures indirect neural activity via the blood-oxygen-level-dependent (BOLD) response (as described previously in section 2.1.2). The measured BOLD signal is considered to be the result of the convolution of neural response with the HRF (the temporal model of the hemodynamic response). In adults, the peak of the (canonical) HRF occurs around 5-6s following the neural response (t=0s, see Figure 2.3). On the other hand, the brain develops dramatically in the third trimester of pregnancy (see Figure 2.5 a for an illustration) and it has been shown that the neonatal HRF differs from this of adults in terms of temporal characteristics (Arichi et al., 2012). Thus, the accurate modeling of fMRI data requires the precise definition of the HRF since this can

massively affect the fMRI results and their interpretation however, a consensus on the exact form of the HRF in neonates has yet to be established.
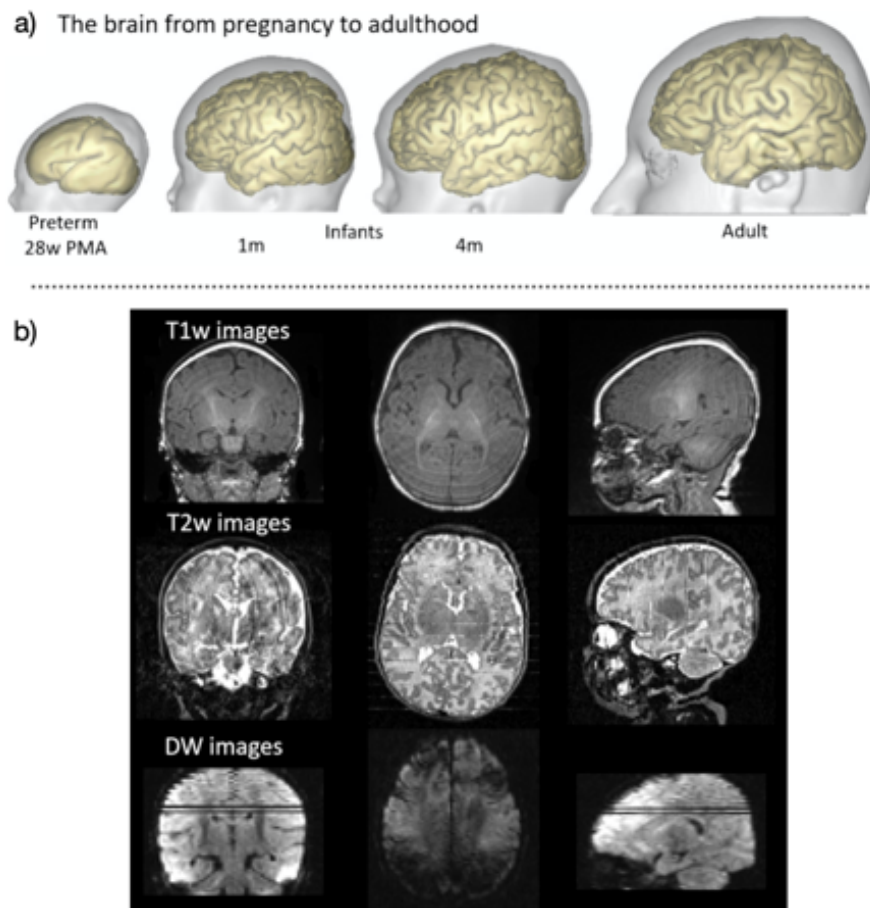
Figure 2.5 – **a)** Cortical surface changes from pregnancy to adulthood. **b)** Common motion artifacts on neonatal MRI images. Figures adapted with permission from Dubois et al. (2020).

Moreover, another important consideration that needs to be taken into account is the use of an appropriate template or atlas. Most of the state-of-the-art brain atlases and templates have been developed for adult populations (Glasser et al., 2016; Yeo et al., 2011; Brodmann, 1994; Eickhoff et al., 2018). For adult fMRI studies, the gold standard stereotaxic space is considered to be the Montreal Neuroimaging Institute (MNI) space that allows the normalization of multiple subjects into the same space, enabling the direct comparison of brain features across different subjects. On the other hand, the neonatal brain is much smaller than an adult-sized brain and thus, normalization algorithms using MNI templates fail to provide acceptable results. In the context of this thesis, the fMRI analysis of the preterm and full-term populations was performed using a custom-made group-specific template allowing the normalization of the infants into a common 'neonatal' space. Furthermore, for the connectome-based studies

included in this thesis, the UNC neonatal brain atlas was used to construct the neonatal functional connectomes (Shi et al., 2011). Finally, it should be noted that different parcellation schemes can impact notably the brain network structure and connectomics-based statistics, and thus affect the analyses and results (Bellec et al., 2015; Wang et al., 2009; de Reus and van den Heuvel, 2013) however, at the same time, there is no consensus on this potent issue. The present dissertation aims to provide new tools enabling the spectral graph theory analysis at the voxel level. The proposed framework could be also used to create data-driven, functional atlases providing a potential solution to the aforementioned problem.

3 Unveiling the effects of intervention in preterm infants with task-based and resting-state fMRI

Preterm birth is often characterized by the presence of subtle alterations of cerebral structures, leading to the potential disruption of the infant's brain development. Additionally, preterm birth has been associated with persistent long-term neurodevelopmental disabilities such as cognitive, motor, and behavioural problems (Delobel-Ayoub et al., 2009; Doyle and Anderson, 2010). To support life, preterm infants spent their first weeks of life in the neonatal intensive care unit. During their hospitalization, early developmental interventions are administrated aiming to restore development and prevent adverse outcomes. Recently, musical interventions have been introduced in the clinical setting but little is known about their effectiveness and how the preterm brain processes this type of stimulus. To the best of our knowledge, at the time of publication, no previous study has investigated the effect of musical intervention on brain functional connectivity and how music affects brain functional connectivity in preterm infants using fMRI.

The first article included in this chapter has been published in the peer-reviewed NeuroImage journal. Its goal is to investigate the neural processes underlying music processing in preterm infants as well as the effect of music exposure during hospitalization on brain functional connectivity. Lara Lordier and Serafeim Loukas are joint first-authors for the paper having contributed equally to the writing and editing of the article. Lara Lordier acquired the neuroimaging data and Serafeim Loukas performed all formal analysis including the pre-processing, statistical analysis, and visualization of the results. Andreas Vollenweider composed the music used for the intervention. The remaining authors participated in different stages including conceptualization, supervision, review and/or funding acquisition.

The second article has been submitted to Human Brain Mapping peer-reviewed journal. In this study, we explore the resting-state brain connectivity changes following the presentation of the same music used for the intervention, unveiling the beneficial effects of the early interventions. The authors' contribution statement is the same as in the previous article.

3.1 Journal Article: Music processing in preterm and full-term newborns: A psychophysiological interaction (PPI) approach in neonatal fMRI

Lara Lordier[a,b,*], Serafeim Loukas[a,c,*], Frédéric Grouiller[d], Andreas Vollenweider [a], Lana Vasung[a], Djalel-Eddine Meskaldji[a,e], Fleur Lejeune[f], Marie Pascale Pittet[a], Cristina Borradori-Tolsa[a], François Lazeyras[g], Didier Grandjean[b,d], Dimitri Van De Ville[c,g], and Petra S. Hüppi[a]

[a] Division of Development and Growth, Department of Pediatrics, University Hospital of Geneva, Geneva, Switzerland

[b] Neuroscience of Emotion and Affective Dynamics Lab, Department of psychology and educational sciences, University of Geneva, Switzerland

[c] Institute of Bioengineering, Ecole Polytechnique Fédérale de Lausanne, Lausanne, Switzerland

[d] Swiss Center for Affective Neurosciences, University of Geneva, Geneva, Switzerland

[e] Institute of Mathematics, Ecole Polytechnique Fédérale de Lausanne, Lausanne, Switzerland

[f] Child Clinical Neuropsychology Unit, FPSE, University of Geneva, Switzerland

[g] Department of Radiology and Medical Informatics, University of Geneva, Geneva, Switzerland

* These authors contributed equally and are considered joint-first authors.

Abstract

Neonatal Intensive Care Units (NICU) provide special equipment designed to give life support for the increasing number of prematurely born infants and assure their survival. More recently NICU's strive to include developmentally oriented care and modulate sensory input for preterm infants. Music, among other sensory stimuli, has been introduced into NICUs, but without knowledge on the basic music processing in the brain of preterm infants. In this study, we explored the cortico-subcortical music processing of different types of conditions (Original music, Tempo modification, Key transposition) in newborns shortly after birth to assess the effective connectivity of the primary auditory cortex with the entire newborn brain. Additionally, we investigated if early exposure during NICU stay modulates brain processing of music in preterm infants at term equivalent age. We approached these two questions using Psychophysiological Interaction (PPI) analyses. A group of preterm infants listened to music (Original music) starting from 33 weeks postconceptional age until term equivalent age and were compared to two additional groups without music intervention; preterm infants and full-term newborns. Auditory cortex functional connectivity with cerebral regions known to be implicated in tempo and familiarity processing were identified only for preterm infants

with music training in the NICU. Increased connectivity between auditory cortices and thalamus and dorsal striatum may not only reflect their sensitivity to the known music and the processing of its tempo as familiar, but these results are also compatible with the hypothesis that the previously listened music induces a more arousing and pleasant state. Our results suggest that music exposure in NICU's environment can induce brain functional connectivity changes that are associated with music processing.

Keywords: *Preterm newborns, Psychophysiological interaction analysis, Music intervention, Auditory cortex, Functional connectivity, fMRI*

3.1.1 Introduction

Music is the art of combining and organizing sounds to obtain a harmonious combination of frequencies and thus, a pleasant melody, which positively influences physiological and behavioral states (e.g. Panteleeva et al. (2017)). Music listening involves auditory, cognitive, motor, and emotional functions across cortical and subcortical brain regions (Koelsch, 2014). Thus, music listening, because of its beneficial effects, has been used in post-stroke rehabilitation and in patients with aging related neurological disorders (Johansson, 2011; Särkämö, 2017; Särkämö et al., 2014). In adult intensive care units, music listening has been shown to have an impact on anxiety states, physiological indices, and sleep duration of critically ill patients (Hu et al., 2015; Lee et al., 2017). Therefore, there has been an increased interest in introducing music interventions in neonatal intensive care units (NICU). A number of authors have considered the effects of music listening in preterm infants and many have shown stabilizing effects on heart and respiratory rates, reduction of apnea or bradycardia, improved resting energy expenditure, improved feeding, better weight gain and more mature sleep patterns; and most of them report a beneficial effect on at least one of these outcomes (Haslbeck, 2012; Filippa et al., 2017; Pineda et al., 2016; Anderson and Patel, 2018). Nevertheless, these music interventions have been proposed for enhancing neonatal intensive care environments without knowing the preterm brains ability to process music. Perani et al. (2010) using functional magnetic resonance imaging (fMRI) observed a differential processing of altered (music acoustic structure alteration: dissonance; and music-syntactic structure modification: key shift) versus consonant music in full-term newborns. Furthermore, a right lateralized auditory cortex activity in response to consonant music was observed in these newborns. In contrast, two other studies performed in few days old newborns, one using fMRI (Dehaene-Lambertz et al., 2010) and one using near-infrared spectroscopy (Kotilahti et al., 2010), showed no lateralization during music processing in newborns and mainly primary auditory cortex activation.

The ability to process music may therefore already be present in full-term newborns either be innate or learned by sound and tissue vibrations exposure in the womb, which may provide experience for the fundamental temporal organization of music elements; i.e., detection of regular patterns as is present in rhythm and meter (mothers' heart and respiratory sounds)

and pitch and melody (mothers' voice) (Teie, 2016).

The ability to mirror musical tempo by rhythmic movements has been shown in infants between 5 and 24 month of age (Zentner and Eerola, 2010). Similarly, listening to a 15% tempo change, faster or slower than spontaneous non-nutritive sucking tempo has been found to slow down sucking tempo in newborns and two month-old infants (Bobin-Bègue et al., 2006). In addition, a number of authors reported an ability of two to six months old infants to remember a tempo and perceive tempo modifications using a head-turn paradigm (Baruch and Drake, 1997; Trehub and Hannon, 2009; Trainor et al., 2004). Thus, these early behavioral responses speak for an ability to detect rhythm and tempo and violation of these temporal patterns have been detected by electroencephalogram studies in two month-old infants (Otte et al., 2013) and in newborns (Háden et al., 2015). Recently, using magnetoencephalography in 9-month-old infants, (Zhao and Kuhl, 2016) showed that a music intervention in a social environment for one month (12 sessions of 15 minutes) increased mismatch responses in auditory and prefrontal cortical regions to temporal violation in music and speech. Thus, the authors suggested that repeated music intervention might modify not only music processing abilities, but also speech processing.

In addition to tempo and rhythm, pitch cues are key elements for music processing. Using a head-turn preference testing Plantinga and Trainor (2005) observed no difference in 6 month-old infants responses to a familiar music and the same melody transposed (absolute pitch modification). This absence of preference suggested either that infants did not process the absolute pitch of the music or that they remembered the melody, but not the absolute pitch of it. Opposing to this, another study from (Volkova et al., 2006) using a similar behavioral assessment showed a preference for transposed music in 7 month-old infants after 14 days of exposure, assuming a processing of and a memory for absolute pitch. These divergent findings between the two studies could be explained by a longer exposure in the latter or by differences of the age of the participants.

Lastly, even exposure to music during fetal life (during the 35th 36th and 37th weeks of gestation) was shown to reduce heart rate in the newborn when listening to the music, played to the fetus antenatally, one month after birth. Authors suggested that this cardiac response may be linked to memory for the melody heard during the last weeks of pregnancy (Granier-Deferre et al., 2011). Furthermore, full-term newborns that have been exposed to a specific melody during the last weeks of pregnancy presented larger brain event-related responses when hearing the known music than newborns without music intervention (Partanen et al., 2013b). Also, middle-syllable raise of pitch (relative pitch modification) within pseudo-words of three syllables (e.g. [tatata]) elicited larger mismatch response amplitudes in newborns with fetal exposure to these pseudo words than in newborns without fetal exposure (Partanen et al., 2013a). Furthermore, mismatch responses for alteration of the middle-syllable duration of the pseudo word were also observed. Thus fetal exposure to music or pseudo words seems to induce learning for the processing of some features of words and music such as relative pitch processing and duration of the stimuli.

However, for preterm infants, sound exposure is different and exposure to voices, noise and potentially music happens earlier and non-attenuated by surrounding fluid. Brain networks implicated in processing and remembering tempo and in the processing of absolute pitch in newborns remain to be explored, as well as the effect of music exposure during NICU stay on this processing.

How music introduction to preterm infants contributes to cortical processing of the listened music is an important question to ask, before promoting enrichment of the neonatal environment by music. We hypothesize that prematurely born newborns have existing music processing abilities that could be enhanced by enrichment of NICUs' environment with repetitive music listening. To test for this hypothesis, we have used functional MRI to observe tempo and absolute pitch processing in full-term newborns at birth and preterm newborns with or without early music intervention at term equivalent age (TEA) using an effective connectivity approach; i.e., a psychophysiological interaction (PPI) analysis.

3.1.2 Methods

3.1.2.1 Participants

Preterm and full-term newborns were recruited from the University Hospital of Geneva neonatal units. Ethical review board approval of the study and parental informed consent was obtained for each newborn prior to participation in the study. 35 preterm infants (GA at birth <32 weeks) were randomized to either music intervention or control condition (without music). The Preterm-Music group consisted of eighteen preterm newborns who were exposed to music with closed headphones (isolating from noise) during the hospitalization in the NICU. The Preterm-Control group consisted of seventeen preterm newborns, who had open headphones (which do not isolate babies from noise around them) without music five times per week during the hospitalization. At term equivalent age all preterm infants underwent magnetic resonance imaging including a fMRI music exposure paradigm. The Full-term group consisted of twenty-one full-term newborns scanned in the first days of life with the same fMRI music paradigm protocol. Few infants were excluded from further analysis because of major brain lesions or large-scale movement on MR-Imaging. Infants with no auditory cortex activation to sound were also excluded (see 2.4 Image Processing). The final sample of infants used for further analysis was as follow: 9 Preterm-Music (4 females/ 5males, mean GA at birth: 28.70 ± 2.46 weeks, mean GA at MRI: 40.25 ± 0.51 weeks), 9 Preterm-Control (5 females/4 males, mean GA at birth: 28.7 ± 2.01 weeks, mean GA at MRI: 40.4 ± 0.77 weeks) and 9 Full-term infants (4 females/5males, mean GA at birth: 39.32 ± 1.03 weeks, mean GA at MRI: 39.63 ± 1.02 weeks). No significant difference between the Preterm-Music and the Preterm-Control groups was found in demographic and perinatal variables: gestational age at birth; weight, height and head circumference at birth; gender; neonatal asphyxia; bronco-pulmonary dysplasia; intraventricular hemorrhages grade 1 and 2; sepsis (positive blood culture); mean number of music/no-music intervention; gestational age at MRI and socio-economic parental status

([Largo et al.](), [1989]()) (see Table [A.1]() in Appendix [A]()).

3.1.2.2   Music intervention

Infants were randomly assigned to either the Preterm-Music or the Preterm-Control group. Parents, music intervention providers and caregivers were blind to group assignment.

The Music group listened to 8 minutes of a music especially created by Andreas Vollenweider ([http://vollenweider.com/en]()), composed of a background, bells, harp and punji (charming snake flute), five times per weeks, from 33 weeks gestational age until TEA. This music was chosen based on behavioral and physiological responses of preterm newborns to the instruments (for more details see Table [A.2]() in Appendix [A]()). The music was either presented on B (4 infants) or Eb key (5 infants).

Preterm-Control group followed the exact same protocol but had headphones placed without music. Preterm-Music infants listened to music about 5 times per week (mean: 4.96 ± 1.54) and Preterm-Control infants had the headphones put on without music at the same frequency (mean: 4.91 ± 2.60).

3.1.2.3   MRI acquisition

All infants received breast or formula feeding before the MRI and were swaddled in a blanket and set up in a vacuum pillow for immobilization. No sedation was used; infants were scanned while resting quietly in the scanner or sleeping. Infants were monitored (heart rate and oxygen saturation) during imaging. To protect infants from the noise of the scanner and to deliver the music, MR-compatible headphones were used (MR confon, Magdeburg, Germany).

A Siemens 3T scanner (Siemens Trio: 11 out of 18 Preterm-Music, 9/17 Preterm-Control, 15/21 Full-term infants and Siemens Prisma) was used to acquire T2*-weighted gradient-echo EPI images (260 images, TR= 1600 ms, TE= 30 ms, 30 slices, voxel size= 2.5x2.5x3.0 mm^3, flip angle = 90°, Matrix size 64x52) as well as T2-weighted structural image for anatomical reference (113 coronal slices, TR= 4990ms, TE=151ms, flip angle=150°, Matrix size=256x164; voxel size =0.78x0.78x1.2 mm^3).

During the EPI sequence, music stimuli were presented in a pseudo-random block design protocol of 5 conditions: Silence, Original music, Tempo music, Transposed music and Background music. Each block lasted 8 seconds and each condition was repeated ten times. Original music stimuli consisted of 10 different extracts, lasting 8 seconds, of the music heard during NICU stay (known music). All contained background music as well as at least one of the instruments (bells, harp and/or punji) and all instruments were represented in the 10 extracts. Tempo music stimuli were composed of these same extracts played 40% faster, and transposed music were the same extracts but transposed on a different key (B/Eb).

3.1.2.4 Image Processing

Functional MRI sequences were preprocessed and analyzed using Statistical Parametric Mapping software SPM8 [Wellcome Department of Imaging Neuroscience, London (www.fil.ion. ucl.ac.uk/spm/software/spm8/), including: (i) realignment; (ii) slice-timing; (iii) rigid body coregistration with the T2 structural image; (iv) normalization of the T2 structural image ($1x1x1mm^3$) and the EPI ($2x2x2mm^3$) using a newborn template (N=20 term and preterm at TEA newborns); and (v) smoothing with a Gaussian kernel of 6-mm full-width at half-maximum. To correct for motion, 24 motion-related parameters (the 6 realignment parameters and their Volterra expansion) (Friston et al., 1996) were reduced into 6 components using Singular Value Decomposition (SVD) and included in the model as covariates to remove any residual motion-related variance. First, infants with brain lesions were excluded. Next, only infants with absolute motion (framewise displacement) under 1 mm for more than 180 consecutive images (70% of the total run) were used for subsequent analyses. Finally, all subsequent analyses were performed only on infants showing activations induced by the overall sound > silence contrast, at p<0.05 uncorrected in auditory regions. The final number of infants per group was 9.

3.1.2.5 Data Analysis

In order to define the long-range connectivity during music processing a PPI analysis was used to determine which voxels in the brain alter their relationship (connectivity) with a seed region of interest (the auditory cortex) in a given context, such as during music listening. After defining the contrasts of interest (e.g., Original versus Tempo Modification music and Original versus Transposed (key modification) music), BOLD signals were extracted from each seed region of interest (Left and Right Primary Auditory cortex, anatomically defined) for each participant (see Figure 3.1).
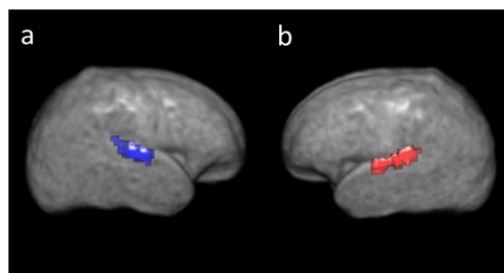
Figure 3.1 – Seeds (regions of interest) anatomically defined on T2 template: (a) Right and (b) Left Primary Auditory Cortex.

These BOLD signals were used for putting together the PPI design matrix that contains the seed region's time course, the task time course, and the interaction term. The latter is the element-by-element product of the seed time course (physiological variable) with the task time course (psychological variable), which is a vector coding for a specific task (e.g. Original music vs Tempo), convolved with the HRF.

Next, two standard psychophysiological (PPI) analyses were carried out (one for each seed region, respectively) for each subject using the Generalized PPI toolbox that also supports standard PPI analysis (McLaren et al., 2012), in order to detect task-specific changes in the relationship between the seed regions and different brain areas (Friston et al., 1997). A task-specific increase in the relationship between brain regions suggests an increase in the exchange of information. Subject-specific contrast images using the contrast (0 1 0), where the second column in the design matrix represented the psychophysiological interaction (PPI) term, were then entered into second-level analyses to identify clusters of voxels for which the PPI effect was significantly present.

In more detail, two sample t-tests, one for each seed region (right and left primary auditory cortex anatomically defined), were performed for each pair of groups (Preterm-Music versus Preterm-Control, Preterm-Music versus Full-Term and Preterm-Control versus Full-Term).

3.1.2.6   Multiple comparisons correction at cluster level

For corrections of multiple testing at 0.05 FWE of each statistical map, the individual voxel threshold was set at $p < 0.005$ and the corresponding threshold of cluster size was set based on the Random Field Theory (RFT).

RFT corrections attempt to control the FWE rate by assuming that the data follow certain specified patterns of spatial variance so that the distributions of statistics mimic a smoothly varying random field. RFT corrections work by calculating the smoothness of the data in a given statistic image and estimating how unlikely it is that cluster with particular statistic levels would appear by chance in data of that local smoothness. Finally, RFT methods are computationally extremely efficient and offered by SPM.

In more detail, the corresponding thresholds defined by the RFT corrections were: FWEc: 171 for the one-sample t-test and FWEc: 257, FWEc: 207 and FWEc: 474 for Music vs Non-music group for right primary auditory cortex (A1), Music vs Full-Term group for left A1 and Music vs Full-Term group for right A1, respectively. Therefore, all the identified clusters were significant at cluster level with p<0.05 FWE (for more details see Table A.3, A.4, and A.5 in Appendix A).

3.1.3   Results

The present results explore the effective connectivity of the primary auditory cortex (seed regions) with the entire newborn brain; i.e., how is connectivity modulated by music processing studied by different types of musical conditions (Original music, Tempo modification, Key modulation, Background music, see below) in preterm infants at term equivalent age and full-term infants.

A group of preterm infants had listened to the Original music for several weeks during their NICU stay prior to term age and another group of preterm infants received a caregiver blinded

intervention with headphones but without music.

Brain network based music processing as a function of music exposure: We examined between-group differences across the following experimental conditions: Original-music, Tempo-Modification music (same melody played 40% faster) and Transposed-music (same melody key transposed: B/Eb).

3.1.3.1 Original music versus Tempo-Modification

A stronger connectivity between the right primary auditory cortex and right thalamus ($p <$ 0.009 FWE at cluster level), left middle cingulate cortex (MCC) ($p < 0.01$ FWE at cluster level) as well as with the left caudate nucleus ($p < 0.01$ FWE at cluster level) was observed during Original > Tempo modified music condition for the Preterm-Music group compared to the Preterm-Control group.

When comparing the Preterm-Music group to the Full-term group, during the Original > Tempo-Modification condition, the connectivity between the left primary auditory cortex region and the left superior temporal gyrus (STG) ($p < 0.03$ FWE at cluster level) and the left MCC ($p < 0.01$ FWE at cluster level) was stronger for the Preterm-Music group. In the same way, the connectivity between the right primary auditory cortex and left MCC and putamen ($p < 0.001$ FWE at cluster level) was increased (See Figure 3.2) for the Preterm Music-group.

To further explore this stronger connectivity when listening to the Original music compared to the Tempo modified music condition, we explored the PPI data for each group separately. We found significant PPI effects (Original > Tempo-Modification condition) for the Preterm-Music, but not for the Preterm-Control and Full-term infants. In more detail, during the Original > Tempo-modified condition, the connectivity between the left primary auditory cortex and left MCC ($p < 0.007$ FWE at cluster level), right caudate nucleus and putamen ($p < 0.01$ FWE at cluster level) was increased in Preterm-Music group (See Figure 3.3). A similar trend was observed between the right auditory cortex and left MCC, right caudate nucleus and putamen but failed to pass the statistical significance test based on the corrected p-values ($p = 0.275$ FWE) (See Figure 3.3).

The connectivity between the primary auditory cortices and the rest of the brain for the Tempo-Modification > Original music conditions was not increased in any comparison (e.g., Preterm-Music compared to Preterm-Control or to Full-term). Furthermore, Preterm-Control and Full-term groups did not show increased connectivity between the primary auditory cortices and the rest of the brain in any condition when compared to the Preterm-Music group.
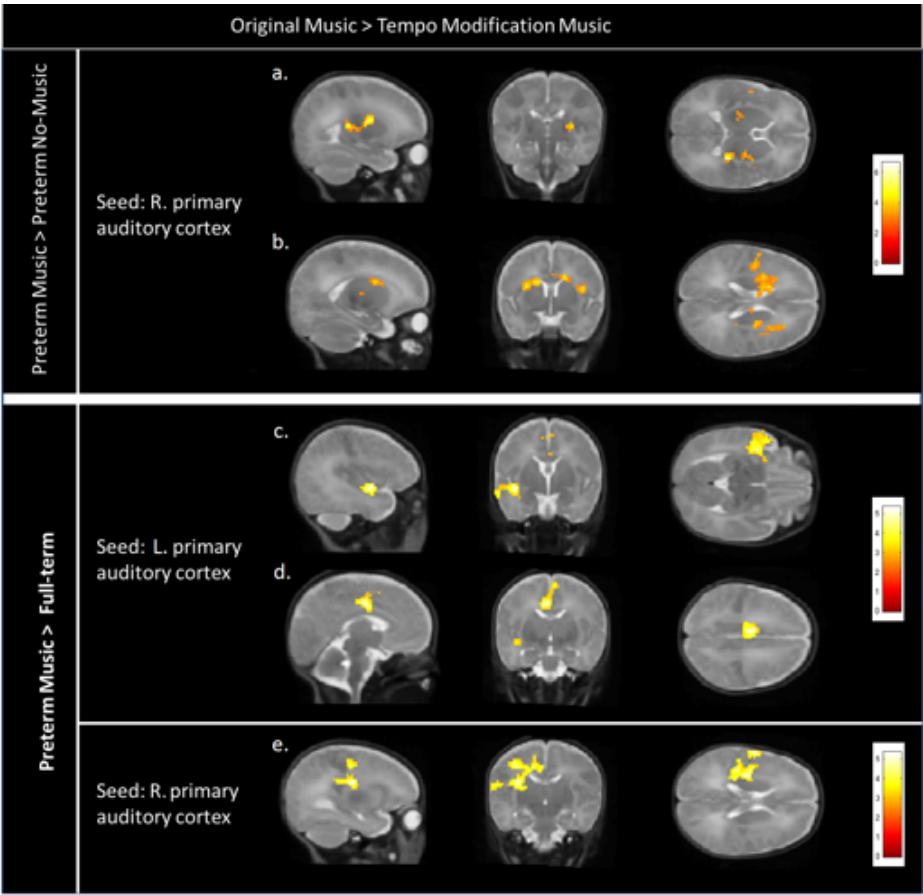
Figure 3.2 – Each row shows in a sagittal, coronal, and axial plane, results of the PPI analysis for Original > Tempo-Modification conditions (p < 0.05 FWE at cluster level): (a-b) Enhanced connectivity in Preterm-Music compared to Preterm-Control group between right primary auditory cortex (seed) and (a) the right thalamus and (b) the left caudate nucleus and middle cingulate cortex (MCC; p < 0.01 FWE at cluster level). (c-d) Enhanced connectivity in Preterm-Music compared to Full-Term group between left primary auditory cortex (seed) and (c) the left superior temporal gyrus and (d) the MCC. (e) Enhanced connectivity in Preterm-Music compared to Full-Term group between right primary auditory cortex (seed) and (e) the left MCC cortex and left putamen.

3.1.3.2 Original music versus Key-Transposition (absolute pitch)

Finally, we compared the connectivity between left and right primary auditory cortex and the rest of the newborn brain during Original versus Key-Transposed music conditions. In this case, no difference was found in any group (one sample t-test) and no difference was found between groups (two-sample t-test).
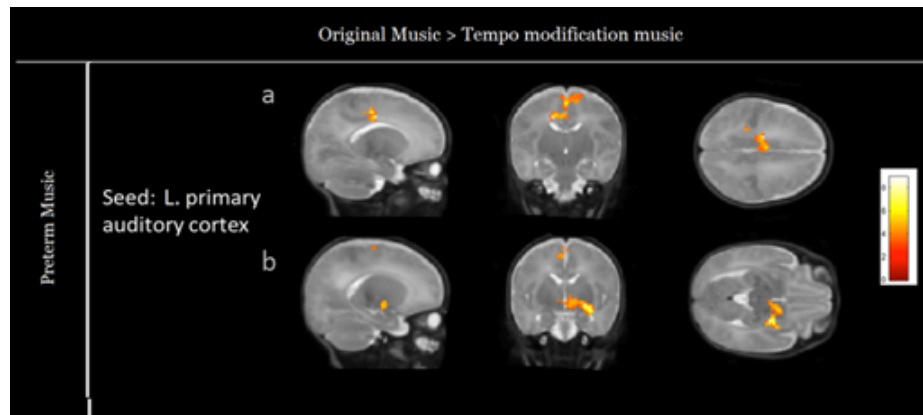
Figure 3.3 – PPI results for Original > Tempo-Modification conditions (p < 0.05 FWE at cluster level): enhanced connectivity in Preterm-Music infant between left primary auditory cortex (seed) and (a) the left MCC and (b) the right caudate nucleus and putamen. No significant activations were found for Preterm-Control and Full-Term groups.

3.1.3.3 Background music versus Silence

We did not observe any difference between background condition and silence condition. We suppose that this absence of difference may be linked to the lower sound level of the background stimuli and that babies did not hear the background stimuli due to the high noise level in the MRI. The background only results are thus not presented in a figure.

3.1.4 Discussion

The aim of the current study was to explore cortico-subcortical music processing in the newborn and assess if early music exposure during NICU stay modulates brain processing of music in preterm infants at term equivalent age so that they can recognize the melody, differentiate its tempo and its absolute pitch at term equivalent age.

We hypothesized that music intervention would change effective connectivity between primary auditory cortex and brain regions implicated in music temporal processing (e.g. basal ganglia) when listening to known or Tempo modified music (Original versus Tempo-Modification). Thus, we used music played 40% faster (Tempo-Modification music) meaning we modified its tempo, but not the melody. Preterm-Control and Full-term infants (both groups without previous music exposure) did not modify connectivity of their auditory cortices for either Original or Tempo-Modification conditions. It has previously been observed by EEG recordings that full-term newborns may detect sudden rhythm change (Winkler et al., 2009) and modification of temporal relations within a train of sounds (Háden et al., 2015). Nevertheless, in our study the entire stimulus was presented faster meaning there is no violation or temporal difference within the music piece. Thus, this absence of difference in processing between the two tempi in our two control groups may be explained by the fact that they processed

the unknown musical structure independently of the different tempi because they were not exposed to previous specific tempo.

In contrast the Preterm-Music group, showed stronger connectivity between the left primary auditory cortex and right dorsal striatum (caudate nucleus and putamen) during Original music (compared to Tempo-modification) (Figure 3.3 b.). Furthermore, between group comparisons indicated a higher connectivity in Preterm-Music newborns between right primary auditory cortex and left caudate nucleus (Preterm-Music > Preterm-Control; Figure 3.2 b.) and between primary auditory cortices and left putamen and superior temporal gyrus (Preterm-Music > Full-term; Figure 3.2 c. & e.) when listening to Original music (compared to Tempo-modification). These findings are in line with an important corpus of literature about the role of the basal ganglia and its connectivity with cortical areas in temporal structure processing (for a review see: (Péron et al., 2013), an enhanced functional connectivity between putamen and superior temporal gyrus observed in adults during perception of beat rhythms compared to non-beat rhythms (Grahn and Rowe, 2009) and brain lesions in the striatum having been found to impair tempo detection (Schwartze et al., 2011). Taken all together, our results indicate that Preterm-Music infants, unlike Preterm-Control and Full-term newborns, processed the Original music differently from the Tempo-modified music, and that specific cortical and subcortical networks are involved in the detection of tempo variation at early age. However, increased activity was seen only for the Original music (compared to Tempo-Modification) and not for Tempo modification music (compared to Original). Thus, the increased functional connectivity observed during Original music compared to Tempo-modification music in preterm infants with the music intervention might reflect either an increased cortico-subcortical processing of known temporal features or to specific tempo recognition. These findings can also be interpreted in the context of the infants' abilities to extract regularities during specific dynamic pattern exposures (here music) creating thus a kind of early perceptual habit as defined by Graybiel (2008). Furthermore, extensive research has shown that noise levels in NICUs are often higher than general recommendations (White et al., 2013; Lahav, 2015). This loud noise has a negative effect on the stability of the cardio-respiratory system, behavior and sleep of the preterm infants (Aly and Ahmed, 2016; Joshi and Tada, 2017) and is presumed to have long lasting effects in preterm infants language and behavioral development (Lahav and Skoe, 2014). Our results support the view that preterm infants can learn from their auditory environment and that preterm infants could have memory also for auditory dis-stimulation and thus warrant for ambient noise reduction in NICU.

By comparing connectivity between primary auditory cortices and the rest of the brain during Original versus Key-Transposed music conditions we have tested if (ii) music intervention can increase functional connectivity between primary auditory cortex and regions implicated in absolute pitch processing. We did not find differences in connectivity within or between groups. Prior studies using ERP's reported that pitch processing is already present in full-term newborns (Háden et al., 2009), and that newborn process differently music with key shifts inside the music piece (Perani et al., 2010). However, in these previous studies, key modulations were presented either as deviant or as alteration of the melody. In contrast,

in our study, the entire music excerpt was transposed to a different key and melody was preserved. Thus, Preterm-Control and Full-term infants process equally both Original and Key-Transposed music conditions, which might be due to preserved melody.

Lastly, preterm newborns with music intervention did not show any difference in Original and Key-Transposed music processing either. Therefore, our findings suggest that music exposure did not enhance cortical processing of absolute pitch. However, the lack of difference in cortical processing in Preterm-Music group could also be explained by a learning of the melody (relative pitch information) they heard during music intervention independently of absolute pitch information. In line with this finding, Plantinga and Trainor (2005) showed that key transposition do not affect melody recognition in 6 month-old infants.

A final question that can be addressed is to what extent music processing presents familiarity concerning memory for listened music. As mentioned before, increased functional connectivity was found in favor of the Preterm-Music infants at group level (one sample t-test) when listening to known tempo (Original > Tempo-Modification) (Figure 3.3 a. & b.). Similarly, higher connectivity was found at second level analysis (two-sample t-tests) in Preterm-Music compared to either Preterm-Control (Figure 3.2 a. & b. and Figure 3.2 . d. & e.) or Full-term (Figure 3.2 d. & e.) when listening to Original music (compared to Tempo-modification). However, no difference of connectivity between the primary auditory cortices and the rest of the brain was observed under the Tempo-Modification-Music > Original music condition in the Preterm-Music group (compared either to Preterm-Control or to Full-term groups), suggesting that this effect does not rely on simple tempo detection ability but rather on memory for the tempo. Putamen and thalamus have been shown to be activated more for familiar than for unfamiliar music (Pereira et al., 2011). Moreover, dorsal striatum has been shown to activate more for beat prediction than beat detection (Grahn and Rowe, 2013). Thus, our findings are in line with previously published work in adults showing higher activity in putamen when listening to the known beat than to a new beat. Thus, putamen activity may be dependent on the familiarity of the perceived rhythm. In our study, faster tempo music activated the dorsal striatum less than the original music, indicating that Tempo-Modification rhythm may be perceived as less familiar by the Preterm-music infants. Also, activation of MCC and superior temporal areas for familiar music has been shown to be dependent on musical expertise (Groussard et al., 2010a). It can thus be suggested that preterm-infants probably acquired specific tempo processing expertise during these weeks of music exposure. Furthermore, it is known that familiar music is perceived as more pleasant (Schellenberg et al., 2008). In adults, thalamus activity correlates to chills intensity when listening to pleasurable music (Blood and Zatorre, 2001). It has further been shown that consonant (Trost et al., 2014), pleasant (Koelsch and Skouras, 2014) and emotional arousing music (Trost et al., 2011) activates dorsal striatum. Thus, increased connectivity between auditory cortices and thalamus and dorsal striatum in Preterm-Music infants may not only reflect their sensitivity to the known music and the processing of its tempo as familiar but these results are also compatible with the hypothesis that this specific known music tempo induces a more arousing and pleasant state.

3.1.5 Conclusion and future implications

In conclusion, this study addresses important basic questions of music processing in preterm and full-term newborns relevant for designing music interventions for NICU patients. The study shows that music can have lasting learning effects on music processing with an increased effective connectivity between primary auditory cortex and brain regions implicated in tempo, familiarity and pleasant music processing. One can argue that, based on our results, preterm newborns are able to implicitly recognize a known musical temporal structure at a specific tempo and that listening to this known music evokes brain modulations of regions known to be involved in perceptual habits and related emotional aspects. Our findings bring new insights for supporting music exposure to preterm infants in the NICU. Rhythm processing has further been shown to be especially important for language processing and recognition. Here, we showed that early postnatal music intervention increases neural responses related to tempo processing and recognition in music. This might be relevant for language processing and recognition later in life. Based on these results, it is interesting to mention that future musical interventions in NICU should target tempo and rhythms aspects rather than absolute pitch processing because the sensitivity of these kinds of information at this stage of development seem more important compared to the one related to absolute pitch processing. However, additional studies are also needed to explore if the increased connectivity between regions implicated in tempo processing and recognition have an impact on the processing of other stimuli such as speech and singing. Lastly, we hope that longitudinal follow-up of these infants might reveal the impact of early music exposure on neurodevelopmental outcome.

Acknowledgments

3.2 Journal Article: Musical memories in newborns: A resting-state functional connectivity study

(This article has been submitted to Human Brain Mapping peer-reviewed journal)

Serafeim Loukas[a,c,d,*], Lara Lordier[a,*], Djalel-Eddine Meskaldji[a,c], Manuela Filippa[a], Joana Sa de Almeida[a], Dimitri Van De Ville[b,d], and Petra S. Hüppi[a]

[a] Division of Development and Growth, Department of Pediatrics, University Hospital of Geneva, Geneva, Switzerland
[b] Institute of Bioengineering, Ecole Polytechnique Fédérale de Lausanne, Lausanne, Switzerland
[c] Institute of Mathematics, Ecole Polytechnique Fédérale de Lausanne, Lausanne, Switzerland
[d] Department of Radiology and Medical Informatics, University of Geneva, Geneva, Switzerland

* These authors contributed equally and are considered joint-first authors.

Abstract

Music is known to induce emotions and activate associated memories, including musical memories. In adults, it is well known that music activates both working memory and limbic networks. We have recently discovered that as early as during the newborn period, familiar music is processed differently from unfamiliar music. The present study evaluates music listening effects at the brain level in newborns, by exploring the impact of familiar or first-time music listening on the subsequent resting-state functional connectivity in the brain. Using a connectome-based framework, we describe resting-state functional connectivity (RS-fc) modulation after music listening in three groups of newborn infants, in preterm infants exposed to music during their Neonatal-Intensive-Care-Unit stay, in control preterm, and full-term infants. We observed a modulation of the RS-fc between brain regions known to be implicated in music and emotions processing, immediately following music listening in all newborn infants. In the music exposed group, we found increased RS-fc between brain regions known to be implicated in familiar and emotionally arousing music and multisensory processing, and therefore implying memory retrieval and associative memory. Finally, we demonstrate a positive correlation between the occurrence of the prior music exposure and increased RS-fc in brain regions implicated in multisensory and emotional processing, indicating strong engagement of musical memories; and a negative correlation with the Default Mode Network, indicating disengagement due to the aforementioned cognitive processing. Our results describe the modulatory effect of music listening on subsequent brain resting-state functional connectivity in newborns that can be linked to brain correlates of musical memory engrams in preterm infants.

Chapter 3. Unveiling the effects of intervention in preterm infants with task-based and resting-state fMRI

Keywords: Prematurity, Resting-state fMRI, Connectomics, Engrams, Brain networks, Functional connectivity, Musical memories

3.2.1   Introduction

Understanding the preterm infants' brain maturity and its functional integrity is pivotal for developing new individually oriented care interventions, such as music for preterm infants in the neonatal intensive care unit (NICU). Resting-state functional magnetic resonance imaging allows the assessment of functional connectivity (RS-FC) between resting-state networks (RSNs), and is an ideal way to study the functional networks of the preterm infants' brain. In fact, functional connectivity at rest has been shown to provide information about basic brain processing, brain maturity and integrity (Bäuml et al., 2015; Dosenbach et al., 2010; Pruett et al., 2015). Consistent RSNs are found across healthy adults, and most of these networks are also observed in children, infants, and neonates (Doria et al., 2010; Lordier et al., 2019; Thornburgh et al., 2017). These RSNs have been linked to brain functions, such as sensorimotor, visual, auditory, as well as higher-order cognitive processes (Doucet et al., 2011; Reineberg et al., 2015; van den Heuvel and Pol, 2010).

Even if RSNs are consistently present in healthy adults, a variation of the functional connectivity within and across them has been previously observed. Cognitive, motor, or music expertise has been linked to an increased RS-FC between regions involved in the processing of the aforementioned expertise (for a review see Cantou et al. (2018)). A number of previous studies have compared RS-FC in musicians and non-musicians and found RS-FC connectivity between limbic, sensorimotor, and auditory regions to be correlated with the number of years of practice (Palomar-García et al., 2017; Zamorano et al., 2017). Recently, we have shown that even a session of receptive music listening in the NICU can provoke a functional network reorganization at term-equivalent age (TEA) (Lordier et al., 2019). Higher RS-FC was found in the music intervention group both in sensory functional networks and in networks implicated in higher-level functions, namely between auditory, sensorimotor, thalamus, salience network, superior frontal, and precuneus networks. Hence, past musical experience has effects on brain RS-FC development that can be observed at 40 weeks of gestational age in preterm infants.

In adults, RS-FC is also influenced by a particular state of mind, mood, and preceding stimulus-induced brain activity. It has been shown that hypnosis (Demertzi et al., 2011), acupuncture (Dhond et al., 2008), sad mood induction (Bernat and Stępień, 2010; Harrison et al., 2008), stress (van Marle et al., 2010), anxiety (Simpson et al., 2001), emotion induction (Eryilmaz et al., 2011), and attention tasks (Elton and Gao, 2015) induce a variation on the subsequent RS-FC in adults. Furthermore, modification of RS-FC has also been observed after music listening in adults. Additionally, pleasant and relaxing music was used to reduce pain perception in fibromyalgia patients (Garza-Villarreal et al., 2015). To this end, patients were asked to listen to their preferred relaxing music. When comparing RS-FC before and after the musical stimuli, a modulation of RS-FC between brain regions related to music, pain, and analgesia processing

was observed. The RS-FC of the angular gyrus was especially modified after music listening, a region which is connected to parietal, temporal, and frontal regions, representing networks implicated in multisensory information integration (Seghier, 2013) and in memory, allowing the recognition of the music as familiar (Platel et al., 2003). Listening to familiar, pleasant and soothing music may thus impact brain states and subsequent RS-FC. Furthermore, in the present study, preterm infants had listened to the same musical composition during their entire stay in the NICU, and this music was presented prior to waking-up or falling asleep and in moments of alertness to interact with the environment, which are considered to be meaningful salient events for these newborns. Indeed, when preterm infants listen to this same music during an fMRI experiment, brain regions implicated in emotionally arousing and familiar music processing, are activated (Lordier* et al., 2018).

In this recent task-based fMRI study, we observed brain functional connectivity modulation during music listening in newborns. We used Psychophysiological Interaction Analysis (PPI), which estimates context-specific changes in coupling between a seed region and the rest of the brain, to argue that music listening during NICU stay improves music processing in preterm newborns (Lordier* et al., 2018). When preterm infants listened to the known music (heard previously in the neonatology) compared to the same music played 40% faster (changing the tempo), the functional connectivity of the auditory cortex with putamen caudate and thalamus was increased. We interpreted this increased connectivity both in terms of tempo processing expertise and of familiar music processing since these brain regions have been shown in adults to be activated more for familiar than for unfamiliar music (Freitas et al., 2018; Pereira et al., 2011) and for beat prediction than beat detection (Grahn and Rowe, 2013). We concluded that, due to the early music intervention, preterm newborns acquired expertise in music feature processing, and the music they heard during their hospitalization had become familiar to them (Lordier* et al., 2018). Furthermore, familiarity is considered as a semantic memory process, i.e. a long-term storage of music (Groussard et al., 2010b), and an implicit memory phenomenon dependent on the integrity of pitch and rhythm perception (Peretz et al., 1998). Also, adult musicians, compared to non-musicians, have larger auditory working memory (Parbery-Clark et al., 2009). The familiarity effect that we observed in this previous experience may thus therefore be directly linked to an auditory memory effect.

Finally, learning tasks induce changes in subsequent resting-state functional connectivity, which have been shown to be correlated with improvements in later task performance (Gregory et al., 2014). It is also worth noting that subsequent RS-FC may not be increased only between brain regions activated during encoding, but also between these brain regions and regions implicated in later retrieval. Increased functional connectivity after a memory task has been observed between the hippocampus and cortical regions involved both in encoding and retrieval, and this RS-FC predicted later memory performance (Tambini et al., 2010). Additionally, after a memory task, Risius and colleagues (Risius et al., 2019) showed increased subsequent RS-FC between brain regions activated during the task (including inferior occipital and fusiform gyri) and the middle temporal gyri, which was found to mediate later retrieval.

The question now being addressed is how music listening modifies the distributed brain networks in preterm and full-term newborns, measured by the subsequent RS-FC. We additionally hypothesize that preterm infants who were already exposed to music listening during their NICU stay would increase their RS-FC between brain regions implicated in the formation and retrieval of musical memories. To this end, we used connectomic and multivariate techniques on the MRI based functional connectomes (Fornito et al., 2015; Sporns et al., 2005).

3.2.2 Methods

3.2.2.1 Population

The present study was approved by the Research and Ethics Committees of the University Hospital of Geneva and informed written consent was obtained from the parents before participating in the study. Thirty-nine preterm and twenty-four full-term infants (FT) were recruited at Geneva University Hospital neonatal units. The preterm newborns were randomly assigned to either music intervention (PM: n=20) or standard of care group (PC: n=19). All infants underwent magnetic resonance imaging at 40 weeks gestational age (GA).

Inclusion criteria for full-term newborns were birth after a GA of 37 weeks, an appropriate height, weight, and head circumference (above the 10th and below the 90th percentiles). Exclusion criteria for all babies were major brain lesions, such as high-grade intraventricular hemorrhage or leukomalacia (1 PC and 2 FT were excluded). Four preterm and three full-term infants dropped out of the study before completion of the MRI (3 PM, 1 PC, and 3 FT). Technical problems during the MRI prevented us from acquiring the necessary data for 1 preterm infant (1 PC). Furthermore, of due to high levels of motion, RS-fMRI data from six infants were not used in subsequent analyses (2 PM, 1 PC, and 3 FT) – see Figure A.1 in Supplementary Material Section.

The final analysis, after removal of motion corrupted MRI volumes, was performed on 15 premature babies in the PM group (8 girls, mean GA at birth: 29.16 weeks) scanned at TEA (mean GA at scan: 40.28 weeks), 15 premature newborns in the PC group (8 girls, mean GA at birth: 28.95 weeks) scanned at TEA (mean GA at scan: 40.50 weeks) ,and 16 FT (9 girls, mean GA: 39.51 weeks) scanned in the first 4 days of life (mean GA at scan: 39.83 weeks). No statistically significant differences (using ANOVA for numerical and chi-squared test for categorical variables) in gender, GA at birth, birth weight, birth height, head circumference at birth, neonatal asphyxia, chorioamnionitis, sepsis (positive blood culture) ,bronco-pulmonary dysplasia (Jobe and Bancalari, 2001), intraventricular hemorrhages grade 1 and 2 (Papile et al., 1983), and mean number of music/no-music intervention sessions were observed between the two preterm groups. Furthermore, no differences in gender, GA at scan and parental socioeconomic status (SES) were observed across the three groups. The population characteristics and the results of the aforementioned statistical tests are presented in Table A.6 and Table A.10 in the "Statistical tests for clinical variables" subparagraph in Appendix A.

3.2.2.2 MRI Acquisition

Before the MRI, all infants received breast or formula feeding, were swaddled in a blanket, and set up in a vacuum pillow for immobilization. No sedation was used and the infants were scanned while resting quietly in the scanner. To protect infants from the noise of the scanner and to deliver the music, MR-compatible headphones were used (MR confon, Magdeburg, Germany).

Two RS-fMRI runs (run 1, run 2) of eight-minute duration were acquired resulting in 300 volumes using an EPI sequence with TR=1600 ms, TE=30 ms, slice thickness = 3mm on a Siemens 3-T scanner. Between these two RS-fMRI runs, the music used for the musical intervention during the hospitalization was presented to all infants (3 groups) in a task-based fMRI run of eight minutes. The musical stimulus was thus, familiar only to the Preterm-Music group (PM). The two resting-state sequences were acquired immediately before and after music listening and infants stayed in the scanner during the entire protocol. Also, T2*-weighted structural images were acquired for anatomical reference (113 coronal slices, TR=4990 ms, TE=151 ms, voxel size=0.78x0.78x1.2 mm^3). The acquisition protocol was identical for all three groups.
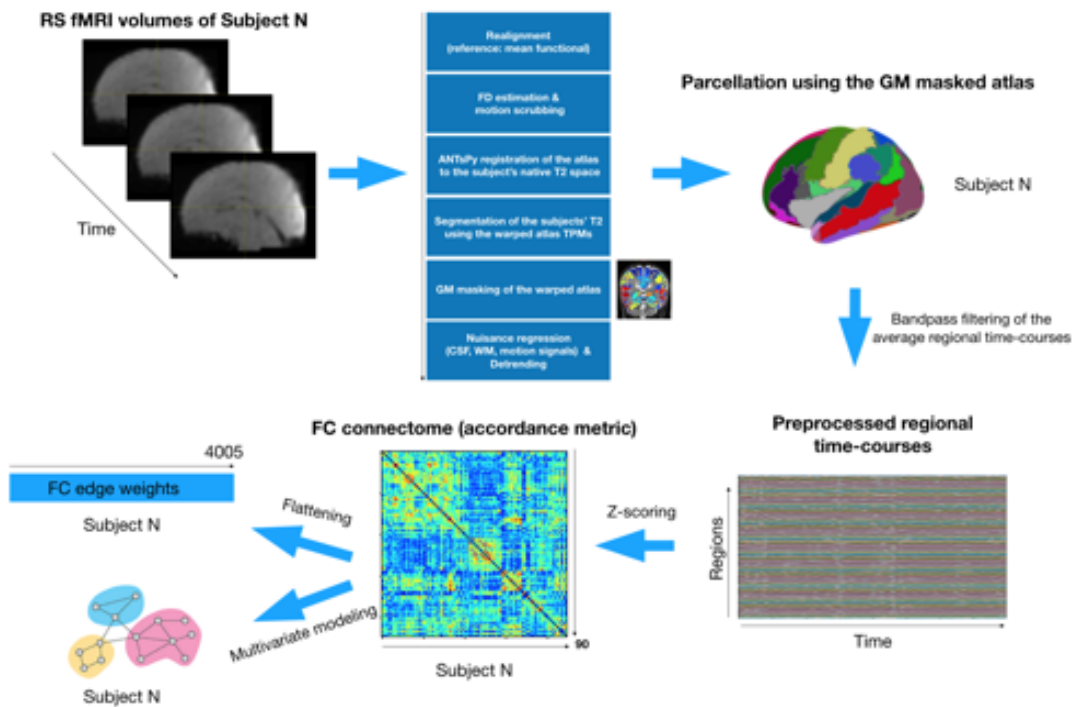
Figure 3.4 – Flowchart showing the preprocessing and network construction pipeline. This procedure was repeated for each subject and each run.

3.2.2.3 Music

The music was especially created by Andreas Vollenweider composed of a soothing background, bells, harp, and punji (charming snake flute) tones (http://vollenweider.com). This

music was chosen based on behavioral responses of preterm newborns to the instruments (observed by a nurse specialized in developmental care) and its duration was eight minutes. Extracts of this music were played to all groups between the two RS-fMRI acquisitions. The PM group underwent musical intervention during the hospitalization using headphones, five times per week (mean number: 25 ± 8.92, range: 7 to 35), from 33 weeks GA until the MRI scan (see Table S2 in Supplementary Material Section for more details). The control group had the same handling as the intervention group (namely putting headphones) but the headphones were made open to environmental sounds, as such representing an active control group. Music and no-music sessions were administrated once a day, five days per week. For more details see (Lordier et al., 2019).

3.2.2.4 Data Preprocessing

For each subject, the functional data were first realigned to the mean functional volume and then co-registered to the structural image using Statistical Parametric Mapping software SPM12 [Wellcome Department of Imaging Neuroscience, (www.fil.ion.ucl.ac.uk/spm/software/spm12/)]. All volumes with a frame-wise displacement (Power et al., 2014) greater than 0.5 mm or with a rate of BOLD signal changes across the entire brain (DVARS) greater than 3% were removed, along with the previous and the two successive images. The remaining images were included for further analysis. Six babies were excluded from subsequent analyses due to high levels of motion in data from run 1 and/or run 2. The above steps are summarized in the flowchart presented in Figure 1. Finally, the three groups were balanced in terms of remaining MRI scans for both sessions.

3.2.2.5 Functional Connectome Construction

To extract regional time-series from the RS-fMRI data, the UNC neonatal AAL atlas (Shi et al., 2011) consisting of 90 regions was used. First, the atlas was registered to each subject's native (T2) space using Advanced Normalization Tools (ANTs, Avants et al. (2011)) with Symmetric normalization algorithm with cross-correlation as optimization metric algorithm (SyNCC cost function). To do so, the fixed and moving images were chosen to be the T2 and the atlas intensity model images, respectively, so that the original volumes are not altered.

After obtaining the forward deformation field (i.e., going from the atlas space to the native space), the deformation was applied to the UNC tissue probability maps of Gray, White matter, and CSF (TMPs), as well as to the 90 regions atlas (label image). The output of this step is the UNC atlas and the three TPMs in the native subject's T2 space. Next, using these TPMs, the subject's T2 image is segmented using SPM8 and the subject-specific GM, WM and CSF probability maps are obtained in the T2 space.

Furthermore, to ensure that we extract BOLD signals only from GM voxels, the UNC atlas in the native space was masked using the subject-specific tissue probability maps obtained by

the segmentation step. If the probability of one voxel being GM was less than the probability of this voxel being WM or CSF (P(GM) < P(WM) or P(GM) < P(CSF)), then this voxel was not considered as GM and it was excluded from the atlas. The output GM-masked UNC atlas in the T2 subject space for one subject is shown in Figure 2, where the color coding corresponds to the atlas labeling.
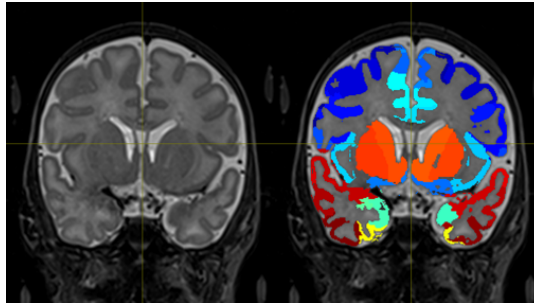
Figure 3.5 – Example of the final GM-masked atlas of one subject. Only BOLD signals from GM voxels are considered. Color coding corresponds to the atlas labeling.

The GM-masked atlas was then resliced to the functional (BOLD) space and the average regional BOLD time-courses were extracted, after performing voxel-wise nuisance regression (CSF, WM, motion signals) and detrending, yielding a matrix with dimensions [number of volumes, 90] for each subject and each RS-fMRI run (before and after the musical stimulus presentation). The average regional time-courses were finally bandpass filtered ([0.01Hz – 0.1Hz]) to discard noise components.

Lastly, the functional connectome of each subject was constructed based on the accordance measure (Meskaldji et al., 2015c) that captures coupling between brain regions. This resulted in a 90 by 90 functional connectome (with 4005 unique connections) per run for each subject represented by a 90 by 90 symmetric weighted matrix (see Figure 3.5), which can be used for connectome-based statistical analysis and multivariate modeling.

3.2.2.6 Statistical Connectome-based analysis

Investigating the short-term effect of music listening on subsequent RS-FC

To investigate whether the functional connectivity was altered after the presentation of a musical stimulus, connection-wise (using the upper triangle part of the functional connectomes) one-sided paired t-tests (between run 2 and run 1) were performed for each group, separately. Additionally, the Cohen's d metric was calculated for each test to characterize the effect size and to complement the statistical analysis given that the statistical power is limited due to the small sample sizes. The statistical tests were employed to address the scientific question of interest (run 2 > run 1). A positive t-value would indicate increased connectivity for that specific connection in run 2 (after the presentation of the musical stimuli) compared to run 1 (before the stimuli).

Chapter 3. Unveiling the effects of intervention in preterm infants with task-based and resting-state fMRI

Investigating the brain trace of a familiar musical stimulation in the Preterm-Music group

To unveil changes in the functional connectivity evoked by the familiar musical stimuli (presented between the RS-fMRI runs) in the PM group, the group-specific p-value vectors, resulted from the previous step (see first paragraph in Statistical Connectome-based analysis section) were used. First, we converted the p-values obtained in the previous step into z-scores (Z_{PM}, Z_{PC}) encoding the effect of interest (increased functional connectivity in run 2 compared to run 1). The conversion (p-values to z-scores) was performed using the quantile function of the normal distribution and thus, the z-scores follow the standard normal distribution under the null hypothesis. Next, to explore the short-term effects of the intervention on the functional connectivity of the Preterm-Music group (the effect of listening to the same music), we accounted for the effect that the Preterm-Control group experienced (i.e., listening to music for the first time during the MRI scan) by subtracting the z-score of the PC group from the one of the PM group. We then made the resulted vector of differences normally distributed under the null:

$$\frac{Z_{PM} - Z_{PC}}{\sqrt{2}} \sim N(0, 1) \tag{3.1}$$

Here, we divided by $\sqrt{2}$ to obtain valid z-scores with zero mean and unit standard deviation (based on the Variance Sum/Difference Law we have):

$$var(Z_{PM} - Z_{PC}) = var(Z_{PM}) + var(Z_{PC}) - 2cov(Z_{PM}, Z_{PC}) = 2,$$

assuming that $2cov(Z_{PM}, Z_{PC}) = 0$ under statistical independence of the group-specific z-score vectors that holds in this case (independent groups).

This enables us to define a z-score threshold that correspond to a specific p-value under the null (e.g., z-threshold of 2.58 corresponds to a p-value of 0.005) and to obtain significant results at the specific alpha level.

Multivariate modeling: Exploring the dosage effect of prior music listening on the functional connectivity

To further investigate neural correlates of the music intervention effect on the brain's functional connectivity, multivariate brain-outcome associations for the Preterm-Music (PM) group, were explored using Partial Least Squares Correlation (PLSC) (Krishnan et al., 2011; McIntosh and Lobaugh, 2004). In this study, the outcome variable was chosen to be the actual number of times that each PM infant listened to the musical stimuli during the hospitalization i.e., the occurrence of the prior musical intervention - dosage (see Table A.7 in Appendix A for more details). The imaging variables for the PLSC analysis were brain network-based features. For each subject in the Preterm-Music group, a brain graph was created by treating the FC connectome as a weighted, undirected, symmetric adjacency matrix. Next, the nodal strength of all 90 vertices of the graph (brain regions) were estimated. The procedure was repeated for each run (run 1 & run 2), resulting in two vectors of nodal strengths per run for each PM

infant.

Since our goal was to relate RS-FC changes (imaging variables), induced by the musical stimulus, to the actual number of music listening episodes during hospitalization (outcome variable), the difference (delta) of the two nodal strength vectors (estimated as described above) was computed (run 2 - run 1). If we would only use the brain nodal measures of run 2 (i.e., using only the post musical stimulus presentation nodal strength) then we would not ensure that we focus on pure stimuli-induced connectivity changes. By doing so, we ensure that the outcome variable is going to be related to the actual change of brain connectivity induced by the musical stimulus. A positive delta nodal strength value indicates increased nodal strength of the corresponding brain region in run 2 compared to run 1, i.e., following the musical presentation. The subject-specific delta vectors were used as imaging variables for the PLSC analysis.

PLSC details

The core of the PLSC method is the singular value decomposition (SVD) of the cross-covariance matrix $\mathbf{R} = \mathbf{U}\mathbf{S}\mathbf{V}^{\mathbf{T}}$ defined as $\mathbf{R} = \mathbf{Y}^{\mathbf{T}}$, $\mathbf{X} \in \mathbb{R}^{N_{outcomes} \times N_{imaging}}$, where $\mathbf{Y}$ is a matrix storing the outcome variables (one outcome variable in this study) for each subject as rows and $\mathbf{X}$ is a matrix storing the imaging variables ($\mathbf{Y} \in \mathbb{R}^{N_{subjects} \times N_{outcomes}}$, $\mathbf{X} \in \mathbb{R}^{N_{subjects} \times N_{imaging}}$). In this study, the matrices $\mathbf{X}$ (dimension [15 x 1]) and $\mathbf{Y}$ (dimension [15 x 90]) were z-scored across subjects prior to the construction of matrix $\mathbf{R}$. Given that we only have one outcome variable, the estimated cross-covariance matrix $\mathbf{R}$ has dimension [1 x 90].

The SVD of $\mathbf{R}$ results in correlation components composed of a set of outcomes (column of $\mathbf{U}$) and brain salience weights (columns of $\mathbf{V}$). In the present study we only have one PLSC component considering $\mathbf{R}$ has dimension [1 x 90]. This component is associated with a singular value (value in $\mathbf{S}$) that specifies the explained cross-correlation along this dimension similarly to the explained variance in a Principal Components Analysis (PCA) analysis. Outcome and brain imaging salience weights ($\mathbf{U}$, $\mathbf{V}$) indicate how strongly each input variable contributes to the multivariate outcome-brain correlation in this component.

To assess the statistical significance of the PLSC component, permutation testing was performed and finally, to evaluate the stability and importance of the brain and behavior saliences, bootstrapping with replacement was used as in Krishnan et al., and Zöller et al. Krishnan et al. (2011); Zöller et al. (2019). These two steps provide complementary information about the statistical significance of the component (permutation testing) and the stability of regional contributions (elements of the saliences) to the multivariate pattern (bootstrap resampling, McLaren et al. (2012)), (see "PLSC Details" in Appendix A, Section A.2 for more details). Significant PLSC results (salience weights) are reported in terms of bootstrapping mean and standard deviations for the statistically significant component (as assessed by the permutation testing).

3.2.3 Results

3.2.3.1 Short term effect of music listening on subsequent RS-FC

All three groups showed distinct effects of music listening on subsequent RS-FC. In Table 3.1, 3.2 and 3.3, we report and present the connections with higher connectivity (accordance) in run 2 compared to run 1 for each group separately (FT, PC, PM). We only kept connection differences with corresponding p-values less than 0.001 (uncorrected) due to the reduced statistical power (small sample size; n=15). However, we also report the Cohen's d metric that characterizes the effect size (magnitude of the effect) to accompany the p-values. In Figure 3.6, 3.7 and 3.8 we present these connections in a brain glass surface using BrainNet plotting toolbox.
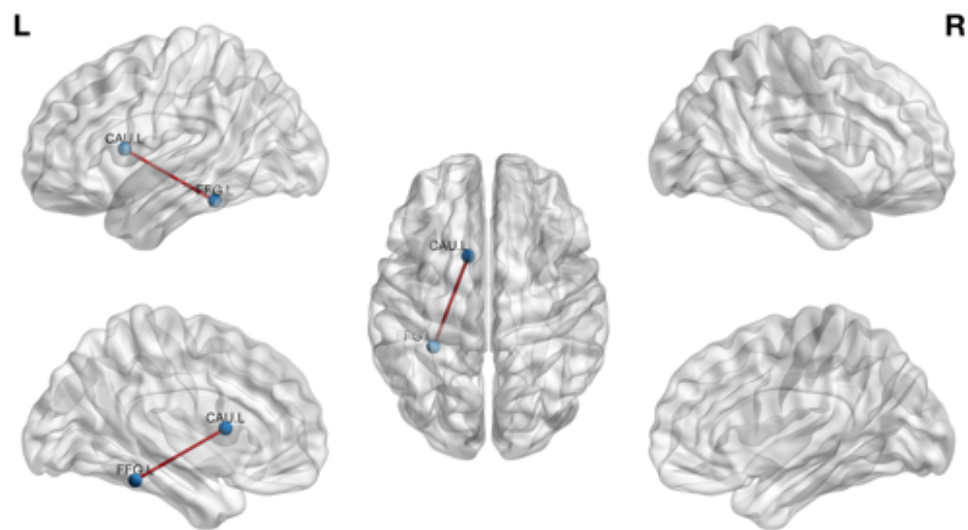
Figure 3.6 – Full-Term group run 2 vs. run 1 differences. Edges represent connections that were increased in run 2 compared to run 1 (see Table 3.1).

Table 3.1 – FT group: Increased functional connectivity between brain regions in run 2 compared to run 1.

Region	Region	p-value	Cohen's d
Left Fusiform gyrus	Left Caudate nucleus	0.00021	0.861
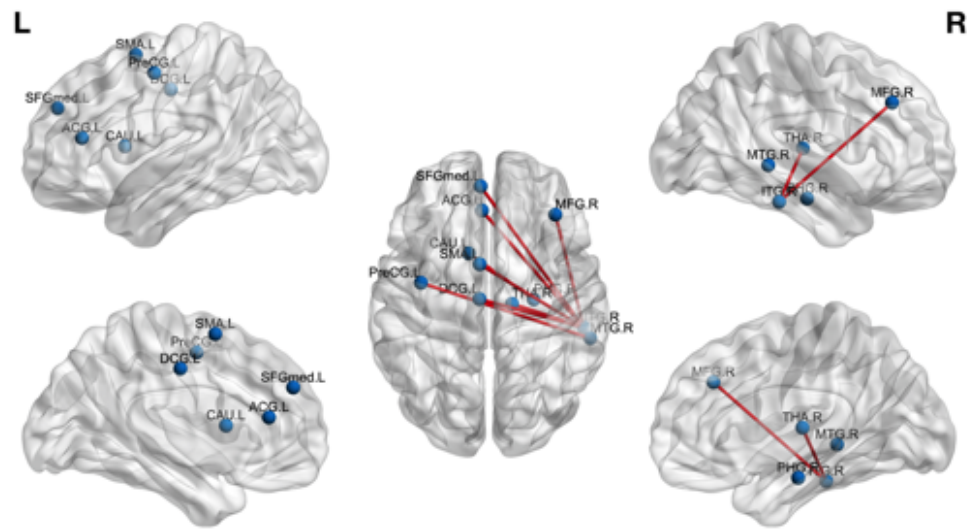
Figure 3.7 – PC group: run 2 vs. run 1 differences. Edges represent connections that were increased in run 2 compared to run 1 (see Table 3.2).

Table 3.2 – PC group: Increased functional connectivity between brain regions in run 2 compared to run 1.

Region	Region	p-value	Cohen's d
Right Thalamus	Right Inferior temporal gyrus	4.45E-05	1.1744
Left Superior frontal gyrus, medial	Right Inferior temporal gyrus	0.00015	1.2131
Left Median cingulate and paracingulate gyri	Right Inferior temporal gyrus	0.00038	1.3858
Left Precentral gyrus	Right Middle temporal gyrus	0.00042	0.9495
Left Supplementary motor area	Right Inferior temporal gyrus	0.00049	1.5041
Right Parahippocampal gyrus	Left Caudate nucleus	0.00079	1.0203
Left Anterior cingulate and paracingulate gyri	Right Inferior temporal gyrus	0.00079	0.9439
Right Middle frontal gyrus	Right Inferior temporal gyrus	0.00083	1.036
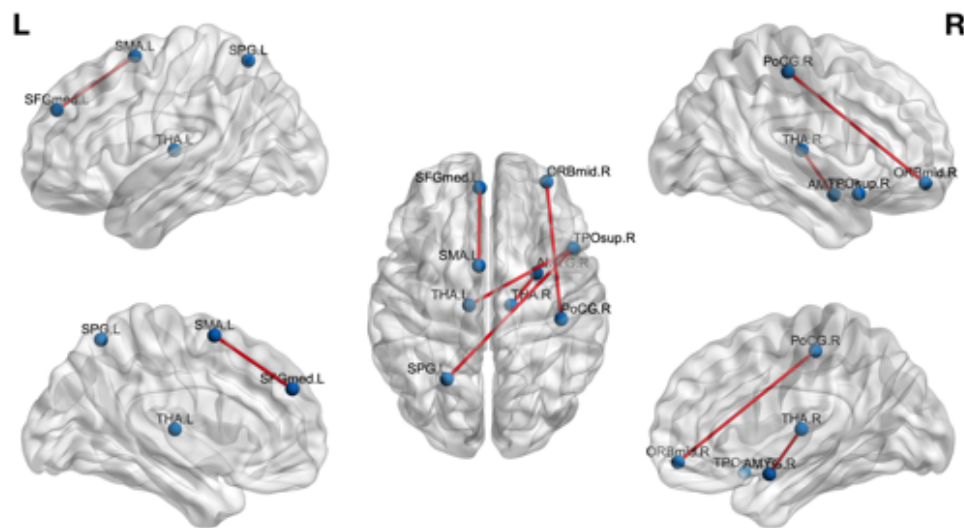
Figure 3.8 – Preterm Music (PM) group run 2 vs. run 1 differences. Edges represent connections that were increased in run 2 compared to run 1 (see Table 3.3).

Table 3.3 – PM group: Increased functional connectivity between brain regions in run 2 compared to run 1.

Region	Region	p-value	Cohen's d
Left Superior parietal gyrus	Right Temporal pole: superior temporal gyrus	0.000009	1.217
Left Thalamus	Right Temporal pole: superior temporal gyrus	0.00036	1.331
Right Middle frontal gyrus, orbital part	Right Postcentral gyrus	0.00071	1.513
Left Supplementary motor area	Left Superior frontal gyrus, medial	0.00074	0.833
Right Amygdala	Right Thalamus	0.00087	0.922

3.2.3.2 Brain trace of a familiar musical stimulus on the Preterm-Music group

In this section, we report the short-term effects of the intervention on the PM group, after accounting for the effect that the PC group experienced (see the second paragraph in Statistical Connectome-based analysis section for more details). The results were thresholded using a z-value 2.58 that corresponds to a p-value 0.005 for the normal distribution.

Table 3.4 – The short-term effects of intervention on the PM group after accounting for the effect that PC experienced: Increased functional connectivity between brain regions in run 2 compared to run 1.

Region	Region	z-score difference
Right Middle frontal gyrus orbital part	Right Calcarine fissure and surrounding cortex	3.341
Left Thalamus	Right Temporal pole: superior temporal gyrus	2.918
Left Middle frontal gyrus orbital part	Right Calcarine fissure and surrounding cortex	2.803
Right Olfactory cortex	Right Angular gyrus	2.672
Left Superior frontal gyrus medial orbital	Right Calcarine fissure and surrounding cortex	2.665
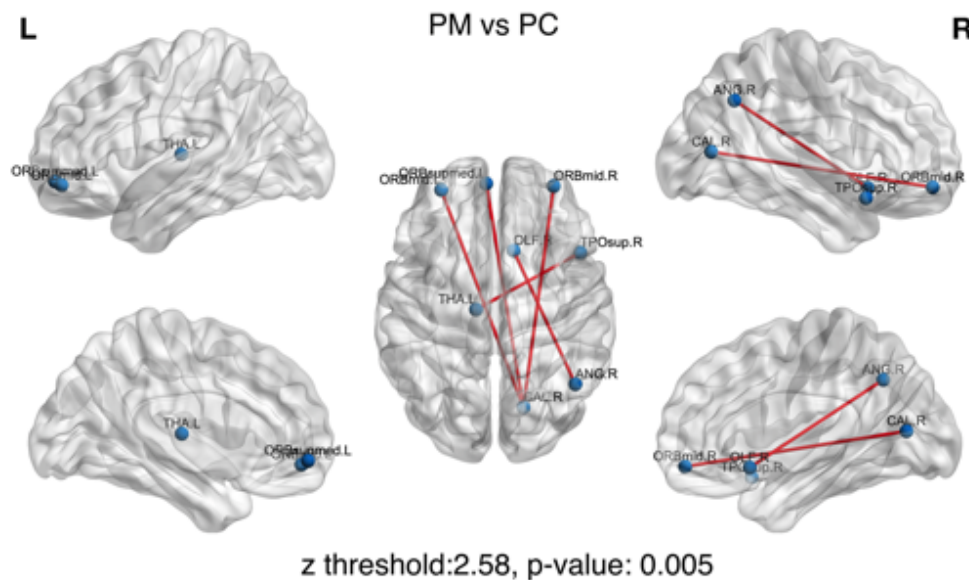
Figure 3.9 – The short-term effects of intervention on the PM group after accounting for the effect that the PC group experienced. Increased functional connectivity between brain regions in run 2 compared to run 1.

3.2.3.3   Dose effect of prior music listening on the functional connectivity

To assess the statistical significance of the computed PLSC component, 5000 permutation tests were performed. The p-value was estimated from the permutation null distribution by counting the number of times that the permuted singular values (Sp) were above the observed true singular value (S) of the PLSC component. The permutation null distribution is shown in Figure S2. The PLSC component was found to be statistically significant based on the permutation testing (p=0.043).

The outcome (bottom left) and brain imaging (top) saliences (elements of **U,V**, respectively) of the aforementioned significant component are shown in the top of Figure 3.10 (x-axis: index of brain region, y-axis: salience weight). To assess which of these weights are robust, we used 200 bootstrapping samples and we considered stable salience weights in terms of bootstrapping mean and standard deviation. These robust brain salience weights (highlighted with yellow in Figure 3.10 (top), green dots represent the bootstrapped brain salience values) can be interpreted similarly to correlation values. Error bars indicate bootstrapping 5th to 95th percentiles and bar heights correspond to the mean bootstrapped salience weights.

Moreover, the correlation plot of the brain scores and music experience (intervention dosage) is shown in Figure 3.10 (bottom right). The set of outcomes and brain imaging salience weights (U, V) indicate how strongly each input variable contributes to the multivariate outcome-brain correlation for the corresponding component. Multivariate associations between the outcome variable (the intervention frequency, i.e., number of music listening during the hospitalization) and brain imaging variables (delta of nodal strengths; run2>run1) were revealed. Significant PLSC salience weights are reported in terms of bootstrapping mean and standard deviations as in Zöller et al. 2019 (Zöller et al., 2019). The exact values of bootstrap mean and 5th to 95th percentiles are reported in Table A.9 in Appendix A.

We observe a significant positive correlation of the intervention occurrence (i.e., the number of music listening during hospitalization – dosage) with the positive increase of nodal strength (delta: run 2 > run1) of L Amygdala, R putamen and L temporal pole (middle temporal gyrus). On the other hand, there is a significant negative correlation of the intervention frequency with the positive delta nodal strength (delta: run 2 > run1) in R middle frontal, L Inferior frontal (triangular part), R superior frontal, L superior frontal (medial orbital), R posterior Cingulate gyrus, R hippocampus, R parahippocampal, L Inferior Occipital, R Fusiform, L Inferior parietal, R Inferior parietal, L paracentral lobule, L thalamus, and R middle temporal. These results are also presented in Figure 3.11 on a brain glass surface using the BrainNet plotting toolbox.

Figure 3.10 – Partial least squares correlation (PLSC) results for the effect of the intervention in PM group (number of listening to the musical stimulus during the hospitalization). The outcome (weight in U; bottom left) and brain imaging saliences (weights in V; top) of the significant PLSC component (p=0.043, 5000 permutations) are presented. Error bars indicate bootstrapping 5th to 95th percentiles and robust results are indicated by a yellow background. Bar heights correspond to the mean bootstrapped salience weights of the significant PLSC component. Each bar corresponds to one brain region (n=90 in the UNC atlas) and depicts the brain regional contributions (saliences weights) to the multivariate pattern/correlation. Bottom right: The correlation plot of the latent variables i.e., the brain scores and outcome scores, are shown (bottom right, r=0.776, p=0.001). Points represent the PM subjects (n=15).

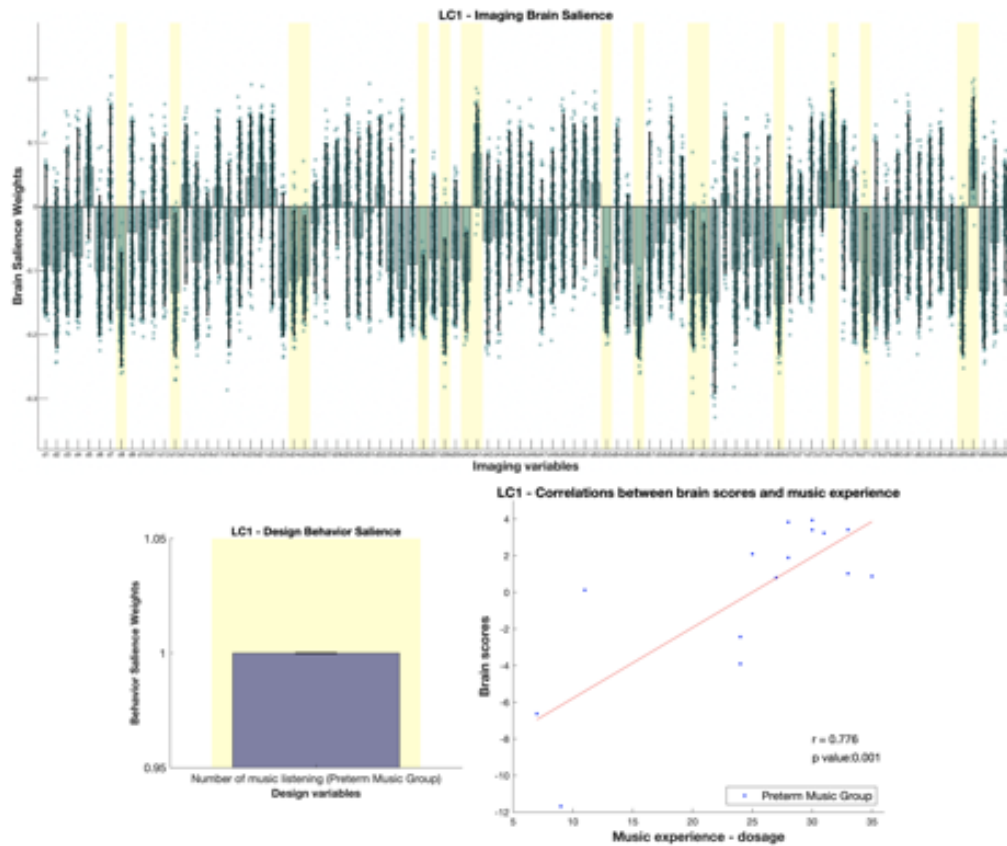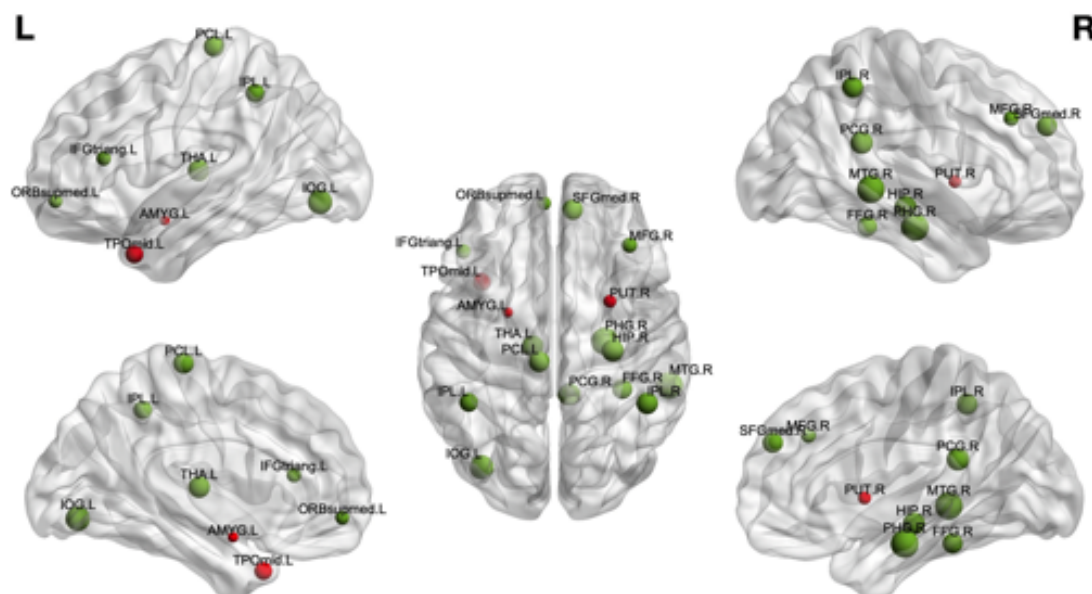Figure 3.11 – Brain glass-surface representation of the Partial least squares correlation (PLSC) results for the effect of the intervention in PM group (number of listening to the musical stimulus during the hospitalization). Red color: nodes with significant positive brain-outcome correlation. Green color: nodes with significant negative brain-outcome correlation. The size of the nodes is proportional to the salience weights.

3.2.4 Discussion

Music is known to induce emotions and associated musical memories. In adults, it is well known that complex auditory sound streams such as music, activate both working memory networks and limbic networks. We have recently shown that a familiar music is processed differently from unfamiliar music already in the newborn period. Musical memories are thought to go beyond the immediate processing of a musical stimulus. The present study aims to evaluate the effects of familiar and first-time music listening on the subsequent RS-FC in the brain and to assess the dose effect of prior music intervention.

Modulation of functional connectivity at rest after music listening

Our findings show that music listening can induce modulation of the RS-FC in both hemispheres as early as TEA in preterm and full-term newborns. Even if lateralization tendency has previously been observed in adults, music processing engages auditory pathways in both left and right hemispheres (Schirmer et al., 2012). It is thus not surprising to observe increased functional connectivity between brain regions in both hemispheres as well as between the two hemispheres after music listening in our newborns. We describe the effect of music listening on subsequent RS-FC between regions implicated in sensory functions, higher cognitive functions and emotional processing. Listening to music is a complex process for the brain, known to trigger cognitive and emotional responses with distinct neural substrates. The present findings suggest that music perception cannot be summarized only by acoustic analysis, since it also involves auditory memory, processing of interval relations and of musical syntax and semantics, as well as emotions (Koelsch, 2014).

It is also worth noting that we observed much fewer modifications by music listening of brain RS-FC in full-term compared to preterm newborns, which confirms prior studies in which preterm infants, due to earlier extrauterine experience, modify their brain capacity of sensory and auditory processing (Baroncelli et al., 2010). It has been shown that premature infants can process auditory stimuli and even possess the ability to process subtle changes of sounds as early as 29 weeks of gestational age (Mahmoudzadeh et al., 2013). Recent work from our research group on voice processing in preterm infants shows that preterm infants show additional cortical regions involved in voice processing in fMRI and a late mismatch response for maternal voice, considered as the first trace of a recognition process based on memory representation. This indicates an experience-dependent maturation of brain networks in preterm infants with the early postnatal exposure to voices (Adam-Darque et al., 2020).

Furthermore, the brain does not develop normally in the absence of external stimuli and activity of its neuronal system during the respective critical period of development (Morishita et al., 2010). Deprivation of sounds and specific auditory stimuli, such as vocal sounds, have been shown to prevent the auditory cortex from maturing and developing normally (Pineda et al., 2014). Additionally, preterm babies with higher endogenous spontaneous brain activity in the first 72 hours of life show subsequently better brain growth at term age (Benders et al.,

2015). The current results, with a significantly higher number of RS-FC modulations after listening to music in preterm controls infants compared to full-term infants, can be viewed as an enhanced development, based on sensory stimulation in the neonatal period, and especially sound processing.

Moreover, when comparing RS-FC immediately before and after music listening, we observed modulation of RS-FC in different brain regions in preterm and full-term infants. In FT control newborns, a higher RS-FC was observed between the left fusiform gyrus and the left caudate nucleus. The caudate nucleus is highly involved in music listening processing. Furthermore, increased activity of the caudate nucleus has been observed during rhythmic information processing (Bengtsson and Ullén, 2006) and consonant (Trost et al., 2014), pleasant (Koelsch and Skouras, 2014) and emotional arousing music processing (Mitterschiffthaler et al., 2007; Trost et al., 2011). The caudate nucleus is further thought to be involved in sensorimotor behavior, such as experiencing chills during music listening (Koelsch, 2014). Therefore, the caudate nucleus is not only implicated in music processing but also in multisensory response to music listening. In the present study, full-term newborns, after listening to music, displayed increased functional connectivity between the caudate nucleus and the fusiform gyrus, another region known to be highly implicated in visual and multisensory processing (Zhang et al., 2016). It has been shown in adult populations, that the fusiform area is activated conjointly, and increases its functional connectivity, with emotional brain regions (amygdala and insula) when music is used to enhance the emotional experience during picture or film presentation (Baumgartner et al., 2006; Pehrs et al., 2014). The fusiform gyrus thus has a crucial role in the processing of emotional multisensory stimuli. Music listening, therefore, engages multisensory processes and it is thus not surprising to observe higher functional connectivity after music listening between brain regions implicated in music and multisensory processing.

In PC infants, we observed an increase in RS-FC between the right inferior temporal gyrus and right thalamus, right middle frontal gyrus, medial part of the left superior frontal gyrus, left middle cingulate gyrus (MCC) and anterior cingulate gyrus (ACC), left supplementary motor area (SMA), and between right middle temporal gyrus and left precentral gyrus, as well as between right parahippocampal gyrus and left caudate nucleus. As in FT, but to a greater extent, listening to music modulates post-listening RS-FC in PC between brain regions implicated in music and multisensory stimuli processing. We observed, in both groups, a modulation of caudate nucleus RS-FC, known, as discussed earlier, to be a multisensory processing hub network. Interestingly, we also found RS-FC modulation in PC, but not in FT immediately after music listening between regions known to be implicated in direct music processing and linked, in adults, to previous music practice, including ACC, MCC, SMA, inferior temporal gyrus, middle frontal gyrus and superior frontal cortex. Functional connectivity in ACC and MCC has been shown to be more developed in musicians when compared to non-musicians (Zamorano et al., 2017). Also, Hou and colleagues (Hou et al., 2015) observed a higher RS-FC between numerous brain regions, including motor areas and inferior temporal gyrus, middle frontal gyrus, and superior medial frontal cortex in adult non-musician depending on previous music practice. As previously reported, unlike full-term

newborns, preterm infants are exposed to higher variability of ex-utero auditory stimulations earlier, including different and unfamiliar adult voices and potentially lullabies or songs. We assumed that due to this variability in auditory extra-uterine stimulations, they developed specific abilities to process sounds and streams of sounds, such as music, and thus activate more specific brain regions implicated in such processing during music listening.

Furthermore, we did not only observe modulations of RS-FC between brain regions implicated in music processing, but also in regions linked to novel stimulus processing. In adults, watching novel visual stimuli (Blackford et al., 2010; Wright et al., 2003), as well as listening to an unfamiliar language (Karmonik et al., 2016), induces an increased activation in the inferior temporal cortex. In this study, we observed an increase in the RS-FC between the inferior temporal cortex and numerous other brain regions after listening to this unknown music. We thus assume that this increased RS-FC reflects the further processing of the unknown music that was just heard. Moreover, we observed an increased RS-FC of the inferior temporal cortex with regions implicated both in music processing and emotional music processing. More specifically, in adults, the supplementary motor area, ACC, thalamus, middle frontal gyrus, parahippocampal gyrus, middle temporal gyrus, and caudate nucleus, are activated in response to the emotion evoked by music (Bogert et al., 2016; Bravo et al., 2019; Brown et al., 2004; Koelsch, 2014) and to music processing (Alluri et al., 2012; Peretz and Zatorre, 2005). Also, a recent meta-analysis showed that ACC is more activated during unfamiliar music listening (Freitas et al., 2018).

We therefore conclude that in PC, novel music listening increased subsequent RS-FC between brain regions implicated in music, novelty, and emotional processing.

Brain trace of a familiar musical stimulus in the Preterm Music group

In the PM group, listening to music modulated subsequent brain RS-FC between brain regions implicated in music and multisensory processing, but also between brain regions known to be linked to processing of familiar music and processing of emotional content. In more detail, RS-FC between the right temporal pole and the left superior parietal gyrus and left thalamus, as well as between the right orbitofrontal region (orbital part of the middle frontal gyrus) and the right postcentral gyrus; left superior motor area and left superior medial frontal gyrus; and between the right amygdala and the right thalamus was increased after music listening in the PM group. As mentioned previously, music processing activates motor and sensorimotor brain regions, including supplementary motor and postcentral gyrus (Gordon et al., 2018), as well as limbic and paralimbic regions, including amygdala, orbitofrontal (OFC) regions, thalamus, and temporal pole (Koelsch, 2014). However, RS-FC modulations between the amygdala and OFC regions were only found in PM group and not in PC or FT groups. Since the music presented between the two resting-state runs were the same as the one used during the hospitalization of the PM infants, we infer that modulation of RS-FC between these regions is not only due to immediate effects of music listening, but also because this music is familiar to the infants and evokes emotional memories. In adults, music familiarity increases the "liking"

rate (Ali and Peynircioğğlu, 2010), and electrodermal activity (van den Bosch et al., 2013). Thus, music familiarity may play a role in modulating the emotional response of the listener. Furthermore, compared to unfamiliar music, familiar music activates more emotion-related regions, including the amygdala, thalamus, supplementary motor area, temporal poles and orbitofrontal regions (Pereira et al., 2011), as well as memory-related regions such as superior frontal and superior parietal regions (Sikka et al., 2015). Also, the superior frontal gyrus and thalamus have been shown, in a recent meta-analysis, to have the highest likelihood of being activated when listening to familiar music (Freitas et al., 2018). Thus, the increased RS-FC observed here between auditory, familiar and emotional brain regions, may reflect musical memories evoking brain activations similar to familiar music listening.

These results are strengthened by the comparison of the modulation of RS-FC connectivity immediately after music listening between the two preterm groups (PM group > PC group). Based on our findings, we observed a greater increase in RS-FC between OFC regions (orbital part of the right middle frontal gyrus and orbital part of the left middle and superior frontal gyrus) and right calcarine fissure, and between left thalamus and right temporal pole, as well as between right olfactory cortex and the right angular gyrus in the PM group. All these regions can be linked to the multisensory processing induced by music listening, and to familiar and emotionally arousing music processing, and therefore to associative memory and memory retrieval of the earlier experienced music (Bonnici et al., 2016). More specifically, listening to music, in the PM group, led to a greater increase of subsequent RS-FC between the angular gyrus (a region known to participate in memory retrieval, multisensory integration and implicated in attention to relevant information (Seghier, 2013)), and brain regions implicated in visual, olfactory, cognitive and emotional processing. When comparing the PM to the PC group, PM showed a higher modulation of RS-FC in visual brain regions (calcarine fissure and surrounding cortex) with numerous other brain regions. In animal models, early tactile interventions from birth contribute to the acceleration of the visual system development in rodents, both at behavioral and electrophysiological levels (Cancedda, 2004; Landi et al., 2007). Another preliminary study on early massage intervention in a preterm population showed a difference in the maturation of visual function in infants who received massages in comparison to those who received standard care (Guzzetta et al., 2009). Music exposure during early ex-utero life may thus have left multisensory brain traces that are reactivated by familiar music listening through musical memory retrieval. These results are also in line with the increased RS-FC of the angular gyrus in adults after listening to pleasant, soothing, and familiar music (Garza-Villarreal et al., 2015). Furthermore, we also found a greater increase of RS-FC between brain regions known to be linked to familiarity and pleasantness (including thalamus, orbitofrontal, and superior frontal regions), which is consistent with the fact that these infants already knew the music (Freitas et al., 2018; Pereira et al., 2011). Previously, using a Psychophysiological Interaction Analysis, we observed an increased functional connectivity in preterm infants' brain between regions implicated in music processing, familiarity and pleasantness during known music listening (Lordier* et al., 2018). Here, we further show that increased functional connectivity linked to this familiar and pleasant music listening

is present at rest, minutes after music listening, indicating the presence of an associative memory process for the familiar music (Platel et al., 2003).

Preterm infants with early music intervention listened to a music that was especially composed for them during their hospitalization. During weeks, this music was used to punctuate the day of these preterm infants. It is now well known that events, and even more repeated and meaningful events, leave a trace on brain structure and function. Memory encoding and retrieval processes, including musical memories, lead to the joint activation of different populations of neurons. This eventually results in an increase in the synaptic strength between this ensemble of neurons which then finally leads to the formation of an engram cell ensemble, an old theory of memory formation and retrieval that still has value today in neuroscience (Josselyn and Tonegawa, 2020). Any percept, or emotional memory formation, is represented by a specific group of engram cells (or memory associative cells). i.e., a special cell ensemble. Emotional associate memories have been shown to be processed through such ensembles or engrams of specific groups of neurons (Bocchio et al., 2017). Retrieval of memories involves cues, external sensory (e.g., in our experiment, musical tones) or internally generated stimuli (e.g., in our experiment, associate emotions to music listening), and reawakening specific neuronal engrams (Frankland et al., 2019). The associated engram cells or memory associative cells in this special group are distributed over broad cortical and subcortical areas rather than in a special brain region, (Josselyn et al., 2015) making it possible to capture such functional brain states using in vivo approaches of functional MRI. Supporting this, Richiardi and colleagues (Richiardi et al., 2015) showed a correlation of functional resting-state dynamics and synaptic gene expression, while Canals and colleagues (Canals et al., 2009) showed recruitment of neocortical and limbic circuits after hippocampal changes in synaptic strengths. Activity in engram cells is persistent and it is still observed during subsequent sleep or wakeful rest. Resting-state fMRI may be used to observe the re-occurrence of neural activity patterns between engram cells, produced by previous experience. For instance, Hamano and colleagues recently studied the motor engram as a dynamic change of the cortical network during learning as assessed by fMRI (Hamano et al., 2020).

Thus, experience leads to traces in neuronal plasticity, an engram (Josselyn et al., 2015), as well as in psychological traces (Ansermet and Magistretti, 2019; Escobar et al., 2017). Early music intervention during the first weeks of life may leave both psychic and neuronal traces in PM infants. However, if the modulation of subsequent RS-FC observed here is the reflection of traces left by music exposure (training) during hospitalization, intervention dose effects should be observed.

Dose effect of prior music listening on the functional connectivity

To further study the brain traces of the previous music exposure, we used Partial Least Squares Correlation (PLSC), a well-known method for the investigation of multivariate relationships between outcome measures and brain imaging data (Krishnan et al., 2011; McIntosh and Lobaugh, 2004).

Based on the revealed multivariate relationships, we observed a significant positive correlation of the occurrence of the prior music intervention during hospitalization (i.e., the frequency of the intervention - the dosage), with the delta nodal strength of run 2 vs run1 of left amygdala, right putamen and left temporal gyrus. This means that following the presentation of the musical stimuli, the higher the intervention occurrence (during the NICU stay) is, the higher the delta change in RS-FC (delta nodal strength: run 2 - run1) in these brain regions. These results are in line with previously reported results where we showed that music listening during NICU hospitalization improves music processing in preterm newborns (Lordier* et al., 2018), observing an increased functional connectivity in preterm infants that underwent an early musical intervention between the auditory cortex and brain regions involved in music features processing (caudate, putamen, superior temporal gyrus), as well as in musical expertise (superior temporal gyrus and middle cingulate cortex). Furthermore, the amygdala and temporal cortices have been characterized as the brain correlates of music-evoked emotions (Koelsch, 2014). Thus, the present results suggest that in PM infants, a higher dose of prior music listening correlates positively with an increase in RS-FC between brain regions implicated in multisensory and emotion processing (following the musical stimulus). Along this line, an increased intervention frequency during hospitalization (dose of musical training) may have reinforced the effects of music listening both in terms of expertise in music features processing and in terms of forming associative memories including emotions. During hospitalization, the music intervention was put immediately before or after interaction with their parents or nurses, accompanying meaningful emotional events. So, the music intervention left neuronal traces in the preterm infants' brain, and listening again to this familiar music reactivated engram cells, leading to a modulation of functional connectivity we observed during subsequent rest.

On the other hand, we also observed a negative correlation between the occurrence of the prior musical intervention (dose) and the delta nodal strength (run 2 - run1) in right medial frontal, left inferior frontal (triangular part), right superior frontal, left superior frontal (medial orbital), right posterior cingulate gyrus, right hippocampus, right parahippocampal, left inferior occipital, right fusiform, left inferior parietal, right inferior parietal, left paracentral lobule, left thalamus, and right middle temporal. This indicates that the higher the musical intervention occurrence, the lower the delta RS-FC change (delta nodal strength: run 2 - run1) in these regions, following the presentation of the musical stimuli. Interestingly, most of these regions, such as the posterior cingulate cortex, inferior parietal, prefrontal, middle/superior frontal, hippocampal, and temporal areas are part of the well-known "Default Mode Network" (DMN) (Koshino et al., 2014). In adults, it has been reported that the DMN shows low intra-subject variability (Mueller et al., 2013) and tends to remain stable in terms of connectivity changes. Moreover, the DMN is stable and mainly engaged under internal thought processes, mind wandering (Mason et al., 2007), and even during receptive music listening (Kay et al., 2012). DMN is thought to have an important role in the performance of these tasks because it deactivates during cognitively demanding tasks (Raichle et al., 2001). At rest, the posterior cingulate cortex shows functional connectivity with both central executive network (CEN)

and DMN. But during a cognitively demanding task, ventral and dorsal posterior cingulate functional connectivity are modulated in opposite directions with the dorsal part becoming more integrated with the DMN and more anticorrelated with CEN (Leech et al., 2011). The posterior cingulate cortex is hence thought to be implicated in the switching between CEN and DMN. Along these lines, we assume that this downregulation of the regions of the DMN, as the occurrence of the prior musical intervention (dosage) increases, is linked to the fact that music exposure has led to neuronal and psychic traces, and repeatedly listening to this music may have reactivated cognitive brain processes associated with the retrieval of familiarity, memory, and emotions. In other words, the more the PM infants listened to the music during the NICU stay, the more they engage cognitive brain processes and disengage regions of the DMN.

3.2.5 Conclusion

To the best of our knowledge, this study is the first to assess both the effect of music listening on the subsequent RS-fc in preterm and full-term newborns and musical memories through RS-FC modulation. First, we showed that all infants experienced changes in their RS-FC after music listening, mostly between brain regions implicated in music perception, including multisensory processing and emotion. Also, we showed that preterm infants who were previously repeatedly exposed to music increased their RS-FC between brain regions known to be involved in associative memory and multisensory processing. We assume that modulation of subsequent RS-FC reflects reactivation of memory associative cells, an ensemble of neurons with increased synaptic connections due to previous exposure to a repeated, pleasant and salient piece of music.

The study further indicates a brain correlate of musical memory engrams in preterm infants that listened to music during the hospital stay with a dose-dependent effect on this modulation. These last findings confirm and extend our previous results on the preterm infant's ability to process, recognize, and activate brain regions associated with memory and familiar music processing.

Limitations

The main limitation of this study is the small sample size. As a consequence, the statistical power is limited and the connection-wise comparisons were not corrected for multiplicity. However, a strict uncorrected p-value threshold was applied in all cases (i.e., p=0.001). To accompany the p-values, we also estimated the Cohen's d to quantify the effect size and complement our findings. P-values are indicative of the presence of an effect, whereas Cohen's d informs us about the presence of thus effect. All effect sizes were above 0.8, meaning that there is a large impact on all reported cases. Furthermore, multiplicity correction on a small sample size could potentially lead to the absence of some important underlying clinically relevant effects due to the lack of statistical power. We recognize that this is a weakness of the

study, however, this is an exploratory analysis and not a confirmatory analysis. Finally, the reported PLCS results were statistically significant (p<0.05 based on permutation testing).

Acknowledgments

4 Predictive utility of brain volumes for cognitive and behavioural long-term outcomes

While functional MRI studies provide insightful information on brain activity and function, volumetric studies are essential for the characterization of brain tissue abnormalities following preterm birth. Several studies have reported associations between brain volumetric abnormalities and long-term adverse outcomes (Peterson et al., 2003; Beauchamp et al., 2008) while others contradicted these findings (Lee et al., 2016). Moreover, recent reviews (Keunen et al., 2012; Anderson et al., 2015) concluded that up to date there is limited evidence regarding the value of neonatal brain volumes in predicting long-term neurodevelopmental outcome. Thus, a clear consensus about the predictive utility of neuroimaging brain data for the prediction of long-term neurodevelopmental outcomes has yet to be established.

The first article in this section has been published in the peer-reviewed NeuroImage journal. The main goal of this publication is to investigate longitudinal brain development between birth and TEA in a cohort of preterm infants as well as to identify potential predictive biomarkers for the long-term outcome. In his study, as a second author, I performed the multivariate classification modeling of the data as well as produced most of the main figures of the article. Moreover, I contributed significantly to the writing/editing and review of the article as well as to its conceptualization. Laura Gui performed the data preprocessing and contributed to the formal statistical analysis and writing/editing of the article. The remaining authors participated in different stages including conceptualization, supervision, review and/or funding acquisition.

The second article is a preprint aiming to disentangle, for the first time, the association between brain volumes measured at TEA and behavioural outcomes assessed through parental questionnaires in the preterm population. Maria Chiara Liverani and Serafeim Loukas are joint first-authors of the paper having contributed equally to the writing and editing of the article. Maria Chiara Liverani acquired the data while Serafeim Loukas performed all formal statistical and multivariate analysis, and produced all visualizations. The remaining authors participated in different stages including conceptualization, supervision, review and/or funding acquisition.

4.1   Journal Article: Longitudinal study of neonatal brain tissue volumes in preterm infants and their ability to predict neurodevelopmental outcome

Laura Gui[a], Serafeim Loukas[a,b], François Lazeyras[c], Petra S. Hüppi[a], Djalel-Eddine Meskaldji[a], and Cristina Borradori Tolsa[a]

[a] Division of Development and Growth, Department of Pediatrics, University Hospital, Geneva, Switzerland
[b] Institute of Bioengineering, Ecole Polytechnique Fédérale de Lausanne, Lausanne, Switzerland
[c] Department of Radiology and Medical Informatics, University Hospital, Geneva, Switzerland

Abstract

Premature birth has been associated with poor neurodevelopmental outcomes. However, the relation between such outcomes and brain growth in the neonatal period has not yet been fully elucidated. This study investigates longitudinal brain development between birth and term-equivalent age (TEA) by quantitative imaging in a cohort of premature infants born between 26 and 36 weeks gestational age (GA), to provide insight into the relation of brain growth with later neurodevelopmental outcomes.

Longitudinal T2-weighted magnetic resonance images (MRI) of 84 prematurely born infants acquired shortly after birth and TEA were automatically segmented into cortical gray matter (CGM), unmyelinated white matter (UWM), subcortical gray matter (SGM), cerebellum (CB) and cerebrospinal fluid (CSF). General linear models and correlation analysis were used to study the relation between brain volumes and their growth, and perinatal variables. To investigate the ability of the brain volumes to predict children's neurodevelopmental outcome at 18–24 months and at 5 years of age, a linear discriminant analysis classifier was tested and several general linear models were fitted and compared by statistical tests.

From birth to TEA, relative volumes of CGM, CB and CSF with respect to total intracranial volume increased, while relative volumes of UWM and SGM decreased. The fastest growing tissues between birth and TEA were found to be the CB and the CGM. Lower GA at birth was associated with lower growth rates of CGM, CB and total tissue. Among perinatal factors, persistent ductus arteriosus was associated with lower SGM, CB and IC growth rates, while sepsis was associated with lower CSF and intracranial volume growth rates.

Model comparisons showed that brain tissue volumes at birth and at TEA contributed to the prediction of motor outcomes at 18–24 months, while volumes at TEA and volume growth

rates contributed to the prediction of cognitive scores at 5 years of age. The family socio-economic status (SES) was not correlated with brain volumes at birth or at TEA, but was strongly associated with the cognitive outcomes at 18–24 months and 5 years of age. This study provides information about brain growth between birth and TEA in premature children with no focal brain lesions, and investigates their association with subsequent neurodevelopmental outcome. Parental SES was found to be a major determinant of neurodevelopmental outcome, unrelated to brain growth. However, further research is necessary in order to fully explain the variability of neurodevelopmental outcomes in this population.

Keywords: *Preterm infants, Neurodevelopmental outcome, Machine learning, Classification, Volumetric brain data, MRI*

Abbreviations

TEA   term-equivalent age

MRI   magnetic resonance imaging

CSF   cerebrospinal fluid

UWM inmyelinated white matter

CGM   cortical gray matter

SGM   subcortical gray matter

IC   intracranial

MDI   mental developmental index

PDI   psychomotor developmental index

MPC   mental processing index

SES   socioeconomic status

LDA   Linear Discriminant Analysis

GLMs General Linear Models

4.1.1   Introduction

The last trimester of pregnancy is the stage of major brain growth and development (Volpe, 2008). Prematurely born children spend a part of this crucial period outside the womb, making them vulnerable to a multitude of risk factors susceptible to perturb their brain growth and development, and affect their motor and cognitive outcomes. Indeed, preterm (PT) birth has been associated with adverse neurodevelopmental outcomes, such as motor impairment, cognitive and language difficulties, and behavioural or attention problems (Larroque, 2004; Aarnoudse-Moens et al., 2009; Moore et al., 2012). Such adverse outcomes can occur even in the absence of significant brain lesions and can be related to subtle alterations in brain development (Wood, 2005; Ment et al., 2009). For some PT children, these difficulties may

persist throughout childhood and adolescence and therefore have a significant impact on their school achievements and quality of life (Aarnoudse-Moens et al., 2009; Mulder et al., 2009; Lindstrom et al., 2011; Jaekel et al., 2013; Wilson-Ching et al., 2013). In addition, these morbidities have important public health and economic implications. A key responsible for such poor outcomes seems to be a combination of antenatal conditions leading to PT birth, postnatal brain injury and impaired brain maturation (Ment et al., 2009; Volpe, 2009; Xiong et al., 2012). In order to better understand and prevent these impairments, neonatologists need tools to help them identify the most vulnerable PT infants, and better prognosticate neurodevelopmental outcomes.

Recent advances in magnetic resonance imaging (MRI) have allowed the acquisition of good quality images of the newborn brain, which, together with the emergence of adequate post-processing tools, has allowed the extraction of global and regional tissue brain volumes. In turn, this has prompted research into the possible contribution of such information to understanding the relationship between impairments in brain development and the poor outcomes associated with prematurity. Several studies have shown that, in comparison with their term-born peers, PT born infants have altered brain tissue volumes at term-equivalent age (TEA) (Peterson et al., 2003; Inder, 2005; Mewes et al., 2006; Thompson et al., 2007; Keunen et al., 2012; Padilla et al., 2015) and also in childhood and adolescence (Peterson, 2000; de KIEVIET et al., 2012). Additionally, several authors reported associations between neurodevelopmental outcomes and global and regional tissue volumes at TEA (Peterson et al., 2003; Inder, 2005; Woodward et al., 2005; Beauchamp et al., 2008; Lodygensky et al., 2008; Thompson et al., 2008; Van Kooij et al., 2012; Keunen et al., 2016; Monson et al., 2016). However, others did not find evidence of such associations, or found that the associations were weakened or not significant after adjustment for perinatal variables (Shah et al., 2006; Lind et al., 2010; Cheong et al., 2016; Lee et al., 2016). To improve our understanding of the brain maturation after PT birth, some authors performed longitudinal studies of volumetric brain tissue growth between birth and TEA (Mewes et al., 2006; Kersbergen et al., 2016a,b; Makropoulos et al., 2016), but only few investigated possible relationships between neonatal brain volumes and later neurodevelopmental outcomes (Kapellou et al., 2006; Rathbone et al., 2011; Kersbergen et al., 2016a,b; Lee et al., 2016; Moeskops et al., 2017). Furthermore, studies looking at associations between neonatal brain volumes and outcomes beyond 24 months of age are scarce (Thompson et al., 2008; Lind et al., 2010; Keunen et al., 2016; Lee et al., 2016; Monson et al., 2016). Therefore, recent reviews (Keunen et al., 2012; Anderson et al., 2015) concluded that up to date there is limited evidence regarding the value of neonatal brain volumetric information in predicting neurodevelopmental outcome in childhood.

In order to provide early prediction of neurodevelopmental outcome, it is crucial to be able to identify early perinatal markers of neurodevelopmental outcomes. In this context, the first objective of this study was to investigate longitudinal brain development between birth and TEA in a cohort of relatively healthy PT infants. Additionally, we also investigated whether brain asymmetries are already present at birth or at TEA. The second objective of this study was to investigate the ability of brain volumetric data to predict cognitive/motor outcomes at

18-24 months of corrected age and at 5 years of age.

4.1.2 Methods

4.1.2.1 Participants

The participants to our study were infants born PT before 36 weeks gestational age (GA) at the University Hospitals of Geneva between 2000 and 2011, who had undergone two MRI exams – one as soon as possible after birth and one at TEA. Exclusion criteria were the presence of congenital or chromosomal abnormalities, or major brain pathology such as intraventricular hemorrhage (grade 3 or higher) and/or parenchymal hemorrhagic infarction on early cerebral ultrasound. Infants who developed major lesions on MRI at TEA were also excluded from the study. Out of 125 infants who had two MRI scans, 41 were excluded because they did not fulfill inclusion criteria, or because image quality in one or both scans was not sufficient to enable automatic tissue segmentation. The remaining 84 infants born between 25 and 36 weeks GA (mean ± SD: 30.15 ± 2.5 weeks) were included in the study.

Perinatal data known from the literature to be associated with neurodevelopmental outcome was taken from the infants' medical records. GA was based on the last menstrual period or pre-natal ultrasound. Birth weight z-scores were calculated based on the growth curves by (Voigt et al., 2006). Persistent ductus arteriosus (PDA) was defined as a ductus arteriosus requiring medical or surgical closure. Birth asphyxia was diagnosed based on an Apgar score less than 6 at 5 minutes after birth, and umbilical cord blood pH less than 7.0. Presence of proven sepsis was defined as at least one positive blood culture during the hospital stay. Bronchopulmonary dysplasia (BPD) was defined as a need for supplemental oxygen or ventilatory support at 36 weeks postmenstrual age (Jobe and Bancalari, 2001).

Parental socioeconomic status (SES) was rated according to (Largo et al., 1989), based on recorded mother's education and father's occupation. The scores are distributed from 2 to 12, with 2 indicating higher SES.

4.1.2.2 MRI acquisition and processing

A first MRI examination of all PT infants was performed as soon as possible after birth (GA at scan = 31.78 ± 2.55 weeks, range: 26.6 to 36.1 weeks) and a second longitudinal scan was acquired at TEA (GA at scan = 40.35 ± 1.03 weeks, range: 38.4 to 44.4 weeks). Both scans were acquired without sedation, during infants' natural sleep. Infants were positioned inside the scanner wrapped in a vacuum pillow and monitored with electrocardiography and pulse oximetry. Earmuffs were used for noise attenuation. The scans were performed on four different machines because of scanner upgrades throughout the study period: Philips Eclipse (1.5T), Philips Achieva (1.5T), Siemens Avanto (1.5T), and Siemens Trio Tim (3T). Adequate signal-to-noise ratio (SNR) and absence of geometric distortions were verified on each scanner using regular phantom-based quality control programs provided by the vendors. To obtain

comparable images, scanning protocols were harmonized among the machines during the study period. Since infant cortex can be as thin as 1-2 mm in some areas, we used the smallest slice thickness possible in order to capture and allow the segmentation of such fine anatomical details (1.5 mm for the older scanners, and 1.2 mm for the more recent scanners). In-plane resolution was set so as to obtain similar voxel volumes, and thus similar SNR among scanners, namely to 0.7 mm x 0.7 mm on the older scanners, and 0.8 mm x 0.8 mm on the more recent scanners, yielding voxel volumes of 0.735 mm^3, and 0.768 mm^3 respectively. To obtain similar contrast on all scanners, the values of echo times, repetition times, and echo train lengths were chosen to be as close as possible among scanners. Acquisition parameters and number of infants scanned on each of the MRI scanners are presented in the Appendix B, Table B.1.

All scans were automatically segmented into cortical gray matter (CGM), unmyelinated white matter (UWM), subcortical gray matter (SGM), cerebellum (CB), brainstem, and cerebrospinal fluid (CSF) with the method of Gui et al. (2012) which is a segmentation pipeline based on mathematical morphology. The SGM segmentation step of the method was modified by employing a multi-atlas label fusion method (Heckemann et al., 2006) which provided more accurate segmentation. The atlases consisted of SGM segmentations obtained with the original method of (Gui et al., 2012) and manually corrected where necessary. A total of 20 atlases were used (10 for each MRI examination), and they were chosen to represent all scanner types from the study. All segmentations were visually inspected and small manual corrections were applied where necessary (Figure 4.1). The automatic phase of the segmentation took about 90 minutes on an iMac computer (3.4 GHz Intel Core i7, 32 GB RAM) and the manual corrections required an average of 15 minutes per exam. This allowed the automatic extraction of global and hemispheric tissue volumes. The volume of the brainstem was not considered for statistical analysis since imaged brainstem length varied among scans because of differences in image plane positioning. The volume growth rate (GR) between the birth and TEA scans was calculated as the ratio of the volume difference and the age difference between the two scans. Total brain tissue volume was computed as the sum of all brain tissue volumes, and total intracranial (IC) brain volume was computed as the sum between the total brain tissue volume and the volume of CSF.

4.1.2.3   Neurodevelopmental outcome data

Children underwent structured neurological and developmental assessments at 18-24 months of age (corrected for the prematurity) and at 5 years of age. The standardized neurological examination was completed by a developmental pediatrician and the developmental assessment was performed by a developmental psychologist, both blinded to children's clinical details as well as possible in a clinical situation. All children had normal neurologic examinations at both time points. Developmental outcomes at 18-24 months were the mental and psychomotor developmental indices (MDI and PDI, respectively) of the Bayley Scales of Infant Development II (Bayley, 1993). Cognitive outcome at 5 years of age was assessed with the French version of the Kaufman Assessment Battery for Children (K-ABC) (Kaufman and Kaufman, 1983), yield-
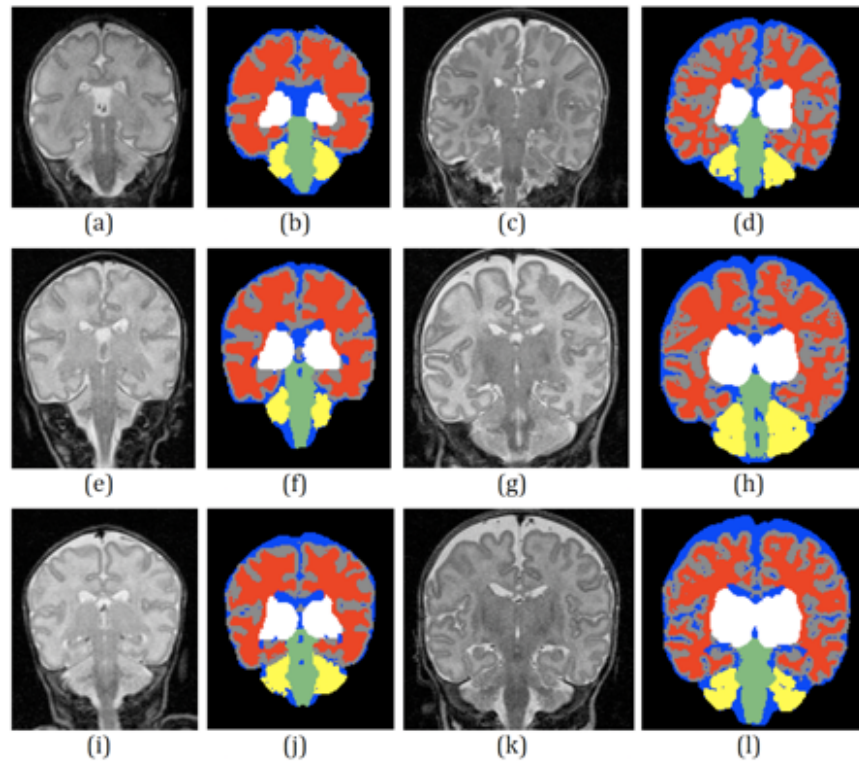
Figure 4.1 – Automatic segmentation of longitudinal T2-weighted images acquired at birth and TEA of three infants, each corresponding to one line. Gestational ages at acquisition were 30 4/7 GW and 41 3/7 GW for the first infant (a, c), 33 5/7 GW and 39 5/7 GW for the second infant (e, g), and 32 6/7 GW and 40 6/7 GW for the third infant (i, k). Image acquisition was performed on the following scanners: Siemens Avanto (a), Siemens Trio (c), Philips Eclipse (e, g), Philips Achieva (i, k). Segmented tissues: CGM (gray), UWM (red), SGM (white), CB (yellow), brainstem (green), and CSF (blue).

ing a cognitive score, the mental processing composite (MPC), comparable to the one found in general intelligence tests. All these scores have an expected mean of 100 and a standard deviation (SD) of 15. Thus, at 18-24 months of age, delayed mental development was defined as a MDI score < 85, and delayed motor development was defined as a PDI score < 85. Normal development was defined as a MDI/PDI score ≥ 85. At 5 years of age, low cognitive outcome was defined as an MPC score < 85, and good cognitive outcome was defined as an MPC score ≥ 85. Mental/motor outcome at 18-24 months of age was assessed in 74 out of the 84 children (88.1%) included in the study (5 children moved, 3 refused and 2 were unable to be tracked), whereas cognitive outcome at 5 years of age was available for 56 out of the 84 children (66.7%) included in the study (4 children moved, 7 refused to come back for the follow up, 1 was ill the day of the assessment and 6 were unable to be tracked).

Data collection and evaluation for this study were approved by the Ethics Committee of the Geneva University Hospitals and written consent was obtained from all participating families.

4.1.2.4 Statistical analysis

Differences between the children included and excluded from the study, as well as between the children who had and those who did not have a cognitive assessment at 5 years of age were evaluated using Student t-tests for continuous variables, and chi-square tests or Fisher exact tests, as appropriate, for categorical variables. Analysis of covariance revealed no significant effects of scanner type on tissue volumes controlled for GA at birth (Appendix B, Table B.2); therefore, scanner type was not included as a covariate in the following analyzes. Moreover, since correlation analysis showed that none of the volumes or volumes GR was significantly correlated with the SES, we did not adjust the volumetric analyses for SES.

Correlation analysis was used to investigate associations between GA at birth and tissue volumes (absolute and relative to the total intracranial volume) at birth and at TEA, as well as between absolute tissue volumes at birth and at TEA. Correlations of tissue volumes at birth with GA at birth were adjusted for gender, while correlations of tissue volumes at TEA with GA at birth were adjusted for gender and GA at the TEA MRI. Correlations between tissue volumes at birth and at TEA were adjusted for gender, GA at birth and GA at the TEA MRI.

Since factors such as asphyxia, BPD, sepsis and PDA are expected to have an impact on brain development, we evaluated their associations with tissues GR. Thus, multiple general linear models (GLMs) were used to study the associations between tissue volumes GR and the presence of asphyxia, BPD, sepsis and PDA, adjusting for gender and GA at birth, according to the following equation: *Volume GR=Asphyxia+BPD+Sepsis+PDA+Gender+GA birth*. Inter-hemispheric asymmetries of CGM, UWM, SGM and CB were assessed at birth and at TEA using paired t-tests.

Furthermore, we investigated the predictive ability of brain volumetric data for the identification of infants with normal or low mental/motor outcome at 18-24 months and normal or low cognitive outcome at 5 years of age, using Linear Discriminant Analysis (LDA) (implemented via R software). In order to build a classifier for the two groups, the brain volumes at birth and at TEA were normalized by birth weight. Then, LDA was applied on the normalized longitudinal volumetric data (CGM, UWM, SGM, CSF, CB, total IC and total brain tissue volume) to classify children into two classes: those with scores < 85 and those with scores ≥ 85. Classifications were performed using the following sets of features: (i) volumetric data at birth, (ii) volumetric data at TEA, (iii) volumetric data at birth and TEA, and (iv) brain volume GR. All cases were considered with and without the addition of GA at birth and SES as features. Leave-one-out cross-validation (LOOCV) was considered in order to avoid overfitting issues. The prediction power of classifiers was assessed by receiver operating characteristic (ROC) curves and evaluated by the area under the curve (AUC) of ROC curves. The same procedure was repeated using different normalization schemes (normalization by brain volume or without normalization).

In order to better understand the ability of brain tissue volumes (at birth or TEA), or GR to predict the developmental outcomes at 18-24 months or 5 years of age, we compared (via

Table 4.1 – Comparison between children included and excluded from the study. Group characteristics were compared using independent sample t-tests for continuous variables, and chi-square or Fisher's exact test for categorical variables, as appropriate.

Variables	Children included in the study	Children excluded from the study	P-value *
Perinatal data	**N = 84**	**N = 41**	
Male gender, No. (%)	38 (45.2)	22 (53.7)	0.783
GA, weeks, mean (± SD), range	30.16 (2.56), [25.57, 35.57]	31.02 (2.82), [24.71, 36.57]	0.092
Birth Weight, g, mean (± SD)	1305.77 (405.45), [510, 2730]	1422.56 (485.42), [580, 2680]	0.159
BW z-score, mean (± SD), range	-0.37 (1.13), [-3.06, 2.06]	-0.57 (1.01) [-2.11, 2.38]	0.346
Birth height, cm, mean (± SD), range	38.83 (3.34), [29, 47.5]	39.59 (4.36), [31, 48]	0.301
Birth head circumference, cm, mean (± SD), range	26.93 (2.57), [21.5, 33.6]	27.34 (3.03), [20.5, 32.5]	0.431
Asphyxia, No. (%)	9 (10.7)	5 (12.2)	0.061
BPD, No. (%)	14 (16.7)	9 (22)	0.512
Sepsis, No. (%)	14 (16.7)	1 (2.4)	0.021
PDA, No. (%)	16 (19)	7 (17.1)	0.072
Mental/motor development at 18-24 months	**N = 74**	**N = 34**	
MDI, mean (± SD), range	92.22 (14.88), [50, 119]	87.09 (14.93), [57, 128]	0.100
MDI <85, No. (%)	20 (27)	11 (32.4)	0.570
PDI, mean (± SD), range	85.61 (14.80), [50, 121]	81.68 (18.64), [50, 113]	0.284
PDI <85, No. (%)	27 (36.5)	14 (41.2)	0.641
Cognitive outcome at 5 years	**N = 56**	**N = 26**	
MPC, mean (± SD), range	100.07 (15.38), [50, 133]	98.11 (15.66), [64, 126]	0.585
MPC <85, No. (%)	6 (10.7)	3 (10.7)	1.000
Parental socioeconomic status			
SES, mean (± SD), range	5.88 (3.23), [2, 12]	5.85 (2.8), [2, 11]	0.961

F-tests) adjusted R2 values of different GLMs of the outcomes with either gender, GA at birth, and SES as independent variables or with models obtained by adding volumes (at birth and TEA) and tissue GR. The R2, which indicates the variance explained by a model increases as long as we add more variables in the model and hence, it is not a good indicator of a better model. However, the adjusted R2 takes into account the number of variables in the model and favors ease of interpretability. We therefore used this indicator to compare different models.

Statistical analysis was performed with SPSS Statistics and R software. A two-tailed p-value ≤ 0.05 was considered significant for all analyses.

4.1.3 Results

4.1.3.1 Cohort characteristics

GA at birth, birth weight, birth weight z-score and parental SES were similar between the 84 infants included in the study and the 41 infants not included in the study (Table 4.1). Moreover, there were no significant differences in gender distribution, rates of BPD, asphyxia and PDA between the two groups. The incidence of sepsis was significantly higher in infants included in the study compared to the infants excluded from the study (16.7% versus 2.4%, p-value = 0.021). No significant differences between neurodevelopmental outcomes at 18-24 months corrected age and 5 years of age were found between groups.

Among children included in the study, there were no significant differences in perinatal characteristics, nor in mental/motor development at 18-24 months, between children who

Table 4.2 – Comparison between children who had and those who did not have cognitive assessment at 5 years of age. Group characteristics were compared using independent sample t-tests for continuous variables, and chi-square or Fisher's exact test for categorical variables, as appropriate.

Variables	Children assessed at 5 years N = 56	Children not assessed at 5 years N = 28	P-value*
Perinatal data			
Male gender, No. (%)	24 (42.9)	14 (50)	0.535
GA, weeks, mean (± SD)	30.18 (2.60)	30.11 (2.5)	0.905
Birth Weight, g, mean (± SD)	1282.95 (432.98)	1351.43 (346.73)	0.469
BW z-score, mean (± SD)	-0.45 (1.16)	-0.23 (1.09)	0.401
Birth height, cm, mean (± SD)	38.61 (3.63)	39.29 (2.64)	0.392
Birth head circumference, cm, mean (± SD)	26.9 (2.66)	26.97 (2.41)	0.912
Asphyxia, No. (%)	6 (10.7)	3 (10.7)	1.000
BPD, No. (%)	9 (16.1)	5 (17.9)	1.000
Sepsis, No. (%)	7 (12.5)	7 (25)	0.213
PDA, No. (%)	10 (17.9)	6 (21.4)	0.694
Mental/motor development at 18-24 months			
MDI, mean (± SD)	92.66 (15.89)	90.95 (11.79)	0.669
PDI, mean (± SD)	86.1 (15.01)	84.21 (14.51)	0.636
Parental socioeconomic status			
SES, mean (± SD)	5.93 (3.17)	5.75 (3.46)	0.835

had and those who did not have a cognitive assessment at 5 years of age (Table 4.2).

4.1.3.2   Brain development between birth and TEA

Absolute and relative tissue volumes

Figure 4.2 illustrates infant's absolute and relative tissue volumes at birth and TEA. Absolute volumes of all tissue classes increase between the two scans. While the relative volumes of CGM, CB and CSF increase from birth to TEA, we observe a reduction of the relative volumes of UWM (which was found to be the most prominent brain tissue at birth) and of SGM from birth to TEA.
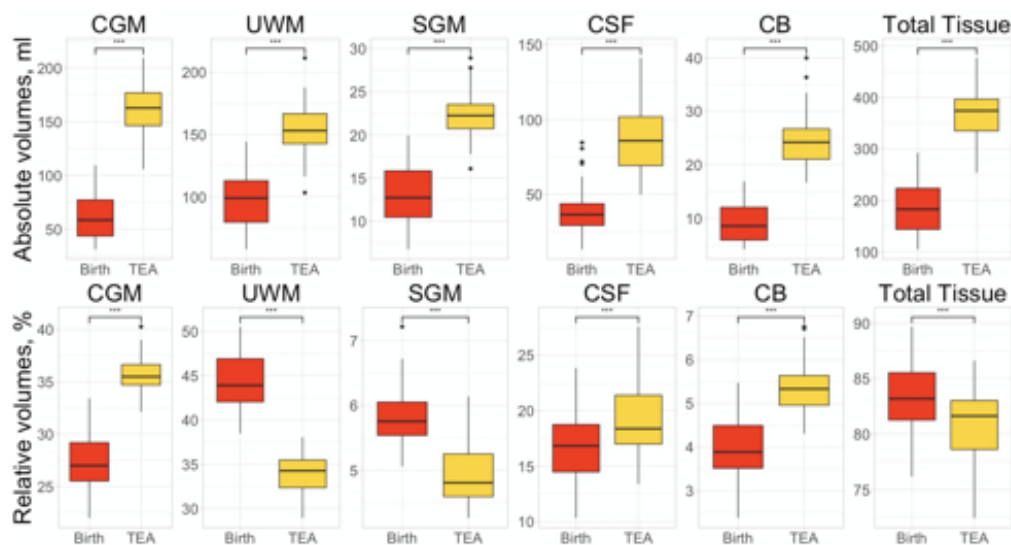
Figure 4.2 – Absolute and relative cerebral tissue volumes measured at birth and at TEA (expressed as medians with 25/75 centile box, 10th/90th centile error bars, and outliers).

Absolute tissue volumes at birth adjusted for gender showed a significant positive association of all brain tissues with GA at birth (Table 4.3). The repetition of the analysis using relative tissue volumes at birth (in percentages of IC volumes at birth) showed that only CGM and CB volumes at birth were significantly positively associated with GA at birth, while relative UWM at birth was significantly negatively associated with GA at birth. Associations with GA at birth were no longer significant for relative SGM, CSF and total tissue volumes.

Correlations between GA at birth and absolute volumes at TEA adjusted for gender and GA at 2nd MRI showed that only CSF volumes were significantly negatively correlated with GA at birth (Table 4.3). The repetition of the analysis using relative tissue volumes (in percentages of IC volumes) at TEA showed positive correlations of relative volumes of UWM and total tissue with GA at birth, and negative correlations of relative CSF volumes with GA at birth. There was no significant correlation between the relative volumes of CGM, SGM and CB and GA at birth.

Table 4.3 – Correlations between GA at birth and absolute/relative tissue volumes at birth on one hand and between GA and absolute/relative tissue volumes at TEA on the other hand.

Tissue type	Birth				TEA			
	Absolute volume		Relative volume		Absolute volume		Relative volume	
	r	P-value[1]	r	P-value[1]	r	P-value[2]	r	P-value[2]
CGM	.884	<.001	.765	<.001	-.041	.718	.037	.738
UWM	.796	<.001	-.678	<.001	.103	.356	.322	.003
SGM	.845	<.001	.058	.601	-.008	.940	.089	.424
CB	.863	<.001	.730	<.001	-.002	.984	.045	.688
CSF	.543	<.001	-.075	.500	-.235	.034	-.277	.012
Total tissue	.855	<.001	.075	.500	.026	.816	.277	.012
IC	.825	<.001			-.066	.558		

[1] Correlations between absolute and relative tissue volumes at birth and GA at birth were adjusted for gender.

[2] Correlations between absolute and relative tissue volumes at TEA and GA at birth were adjusted for gender and for GA at 2nd MRI.

Moreover, our cohort presented moderate to strong positive correlations between absolute tissue volumes at birth and absolute tissue volumes at TEA, adjusted for gender, GA at birth and GA at the 2nd MRI: CGM: r .526, p<.001; UWM: r .707, p<.001; SGM: r .452, p<.001; CB: r .629, p<.001; CSF: r .489, p<.001; total tissue: r .662, p<.001; IC: r .655, p<.001).

Tissue volume GR

Table 4.4 presents average absolute tissue GR, and tissue GR relative to birth volumes, the latter allowing the comparison of growth rates among tissues. We observe that the fastest growing tissues are the CB (22 ± 7 % of its birth volume / week) and the CGM (21 ± 5 % of its birth volume / week), followed by the CSF (17 ± 9 % of its birth volume / week).

Table 4.4 – Averages of tissue absolute and relative GRs.

Variable	Tissue type						
	CGM	UWM	SGM	CB	CSF	Total tissue	IC
Absolute GR, mean (SD, ml / week)[1]	11.94 (2.1)	6.51 (1.3)	1.05 (0.2)	1.76 (0.3)	5.77 (1.9)	21.44 (3)	27.22 (3.7)
Relative GR, mean (SD, % / week)[2]	21 (5)	7 (2)	9 (3)	22 (7)	17 (9)	12 (3)	13 (3)

[1] Tissue absolute growth rates were computed as: (TEA volume – birth volume) / (GA TEA – GA birth).
[2] Tissue relative growth rates were computed as: absolute growth rates x 100 / birth volume.

In Figure 4.3 we display individual tissue volume trajectories from birth to TEA in our PT born children. Line colors indicate relative tissue growth rates, with red lines depicting faster growth, and blue lines – slower growth.
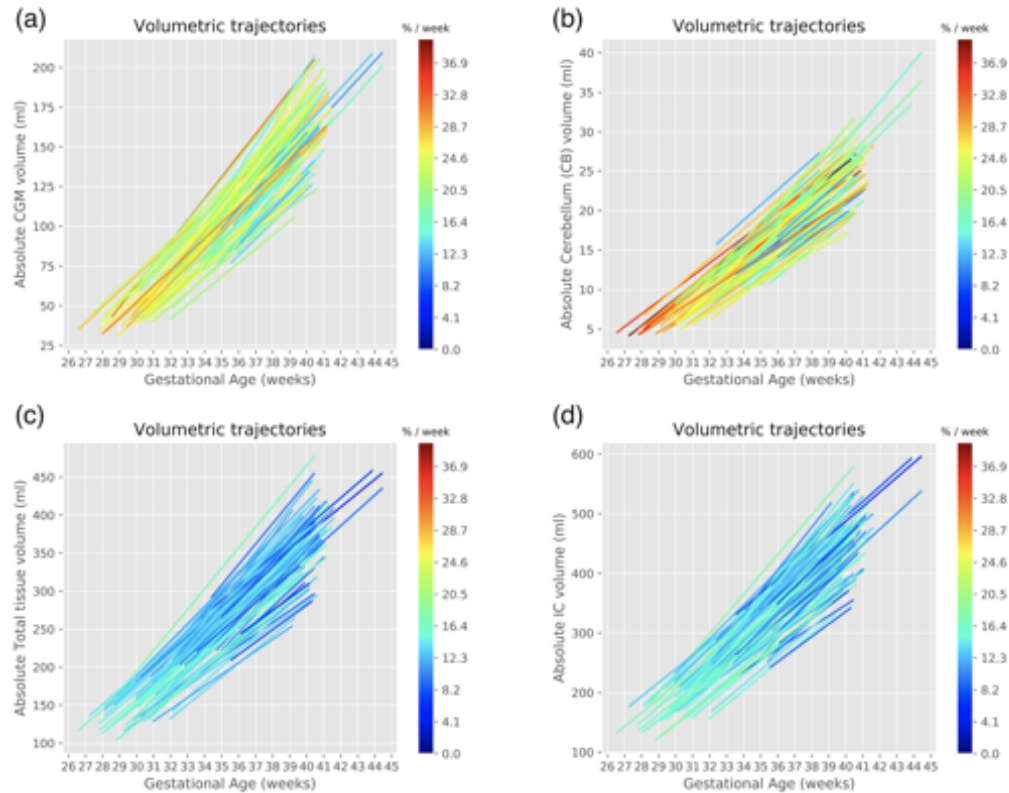
Figure 4.3 – Individual volume growth trajectories from birth to TEA: (a) CGM volume; (b) CB volume; (c) Total tissue volume; (d) Total IC volume. Line colors indicate tissue growth rates relative to birth volumes (faster and slower growth are represented by red and blue colors, respectively).

GLM analysis of tissue volume GR showed a significant positive association of CGM, CB, and total brain tissue GR with GA at birth (Table 4.5). On the other hand, SGM volume GR was negatively associated with GA at birth. Infants that had suffered from sepsis had significantly lower CSF (mean difference [MD] 1.55 ml/week, 95% CI, 0.26 – 2.84) and IC GR (MD 3.01 ml/week, 95% CI, 0.64 – 5.39) than infants who did not suffer from sepsis. Neither BPD nor asphyxia had significant effects on volumes GR. Infants that were suffering from PDA had significantly lower SGM (MD 0.21 ml/week, 95% CI, 0.07 – 0.35), CB (MD 0.30 ml/week, 95% CI, 0.13 – 0.47) and IC GR (MD 2.54 ml/week, 95% CI, 0.18 – 4.89) compared to infants who did not suffer from PDA. Finally, males had significantly higher CB GR (MD 0.21 ml/week, 95% CI, 0.10 – 0.32) than females.

Volume asymmetries

The comparison of tissue volumes between hemispheres (Table 4.6) revealed that at birth, CGM and SGM volumes were significantly higher in the left hemisphere than in the right hemisphere (MD 0.42 ml for CGM, 0.06 ml for SGM), while UWM volumes were significantly lower in the left hemisphere than in the right hemisphere (MD 0.28 ml). At TEA only the UWM

Table 4.5 – General linear model analysis of tissue volume GR and perinatal factors.

Dependent variables	Model R2	B (95% CI)	P-value
CGM GR			
Gender		-.63 (-1.50, .23)	.149
GA		.33 (.14, .52)	.001
BPD	.281	.83 (-.40, 2.06)	.183
Asphyxia		-.65 (-1.96, .67)	.330
Sepsis		-1.05 (-2.37, .27)	.116
PDA		-.82 (-2.12, .49)	.215
UWM GR			
Gender		-.18 (-.77, .42)	.553
GA		-.04 (-.17, .09)	.573
BPD	.091	.38 (-.46, 1.22)	.374
Asphyxia		-.90 (-1.80, .004)	.051
Sepsis		-.49 (-1.49, .41)	280
PDA		-.42 (-1.32, .48)	.353
SGM GR			
Gender		-.05 (-.14, .05)	.338
GA		-.03 (-.05, -.01)	.005
BPD	.202	.087 (-.044, .217)	.191
Asphyxia		-.02 (-.16, .12)	.769
Sepsis		.02 (-.12, .16)	.804
PDA		-.21 (-.35, -.07)	.004
CSF GR			
Gender		-.19 (-1.04, .66)	.659
GA		-.06 (-.24, .13)	.538
BPD	.155	.49 (-.72, 1.69)	.423
Asphyxia		.91 (-.38, 2.20)	.162
Sepsis		-1.55 (-2.84, -.26)	.019
PDA		-.73 (-2.01, .55)	.258
CB GR			
Gender GA		-.21 (-.32, -.10)	.000
BPD		.04 (.02, .06)	.002
Asphyxia	.313	.15 (-.004, .31)	.056
Sepsis		-.01 (-.18, .16)	.931
PDA		.07 (-.10, .24)	.424
		-.30 (-.47, -.13)	.001
Total tissue GR			
Gender		-1.07 (-2.34, .21)	.099
GA		.30 (.01, .58)	.040
BPD	.226	1.47 (-.35, 3.28)	.111
Asphyxia		-1.58 (-3.51, .36)	.110
Sepsis		-1.47 (-3.41, .48)	.137
PDA		-1.81 (-3.73, .12)	065
Total IC GR			
Gender		-1.26 (-2.82, .30)	.113
GA		.24 (-.11, .58)	.173
BPD	.270	1.95 (-.26, 4.17)	.083
Asphyxia		-.66 (-3.03, 1.71)	.579
Sepsis		-3.01 (-5.39, -.64)	.014
PDA		-2.54 (-4.89, -.18)	.035

Table 4.6 – Volume asymmetries. Paired samples t-test.

Tissue volume difference	Mean (ml) (95% CI)	SD	P-value
CGM birth left – CGM birth right	.42 (.24, .60)	.83	<.001
UWM birth left – UWM birth right	-.28 (-.46, -.10)	.84	.003
SGM birth left – SGM birth right	.06 (.03, .09)	.14	<.001
CB birth left – CB birth right	-.03 (-.09, .03)	.28	.396
CGM TEA left – CGM TEA right	.42 (-.24, 1.08)	3.05	.206
UWM TEA left – UWM TEA right	-.61 (-1.04, -.18)	2.00	.006
SGM TEA left – SGM TEA right	.004 (-.04, .05)	.22	.883
CB TEA left – CB TEA right	.14 (-.03, .31)	.77	.097

asymmetry was maintained, with UWM volumes significantly lower in the left hemisphere than in the right hemisphere (MD 0.61 ml).

4.1.3.3 Neurodevelopmental outcome in relation with neonatal brain volumes

Neurodevelopmental outcome was assessed in 74 of the 84 PT children (88.1 %) at 18-24 months of corrected age (Table 4.1). At 18-24 months of age, mean mental scores were 92 ± 15 for MDI and 86 ± 15 for PDI. Of these children, 20 (27%) exhibited mental delay (MDI < 85) and 27 (36%) exhibited motor delay (PDI < 85). At 5 years of age, cognitive development was assessed in 56 out of 84 children (66.7%). Mean MPC scores were 100 ± 15; 6 children (11%) had cognitive MPC scores below the normal range.

Classification of neurodevelopmental outcomes

Figure 4.4 presents the ROC curves of the LDA classification of the children into two classes: those with outcome scores < 85 and those with outcome scores ≥ 85 at 18-24 months and 5 years of age using the four sets of birth weight normalized features, as well as the GA at birth and the SES. Among the three outcome scores (MDI, PDI and MPC), the classification of MDI scores at 18-24 months had the highest predictive power evaluated by the AUC (AUC = 0.77 using the birth volumetric data, AUC = 0.73 using TEA volumetric data, AUC = 0.7 using the combination of birth and TEA data, and AUC = 0.72 using volume GR). However, this predictive power may be influenced by the inclusion of GA and SES as features, since the predictive power for GA and SES alone were similar (AUC = 0.78). For the PDI score at 18-24 months, the predictive performance was lower than in the MDI case (AUC = 0.63, 0.64, 0.6 and 0.62 for birth, TEA, birth and TEA, and GR, respectively), however GA and SES seem to contribute less in this case (AUC = 0.57 for the prediction based solely on GA and SES). Finally, for predicting the MPC outcome at 5 years of age, the highest AUC was obtained by using only GA and SES as features (AUC = 0.77), while the addition of volumetric features did not improve the performance of the classifier (AUC = 0.63, 0.71, 0.64, and 0.76, for birth, TEA, birth and TEA, and volume GR, respectively). Classification performance was not changed when the data was not normalized, or normalized by the total IC volume (instead of the birth weight).

Table 4.7 – General linear model analysis of neurodevelopmental outcomes.

Variables	MDI 18-24 months		PDI 18-24 months		MPC 5 years	
	B (95% CI)	P-value	B (95% CI)	P-value	B (95% CI)	P-value
SES	-2.15 (-3.11, -1.19)	<.001	-.34 (-1.40, .71)	.519	-2.07 (-3.31, -.83)	.001
GA at birth	.72 (-1.97, .52)	.251	-1.18 (-2.56, .19)	.092	.27 (-1.23, 1.77)	.718
Gender	2.96 (-3.44, 9.36)	.360	7.74 (.66, 14.83)	.033	1.82 (-6.08, 9.73)	.646

Lower classification performance was obtained when using only brain volumes as features (without GA at birth or SES); corresponding ROC curves are shown in the Appendix B, Figure B.1.

The classification suffers from the small number of subjects in the abnormal group, especially for the MPC score, with only 6 abnormal scores vs. 50 normal scores. This is one of the limitations of this study that we will discuss later. Furthermore, the classification may have suffered from over fitting and low rank issues in some cases. For these reasons, we explored the ability of volumetric data to predict neurodevelopmental outcomes by using GLMs and F-tests, whose results are presented in the next section.
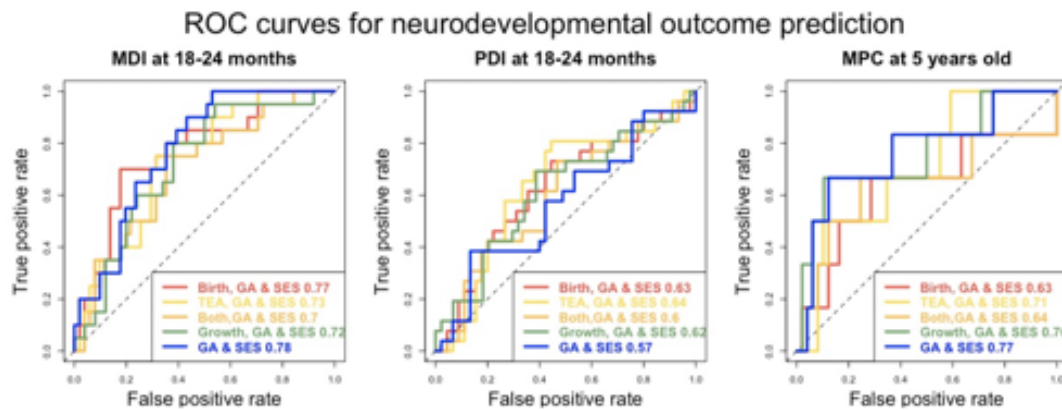
Figure 4.4 – Individual volume growth trajectories from birth to TEA: (a) CGM volume; (b) CB volume; (c) Total tissue volume; (d) Total IC volume. Line colors indicate tissue growth rates relative to birth volumes (faster and slower growth are represented by red and blue colors, respectively).

General linear models for the prediction of the neurodevelopmental outcome

The analysis of outcomes by GLM with gender, GA at birth and SES showed that low parental SES was associated with poorer cognitive development at 18-24 months and 5 years of age, reflected by lower MDI and MPC scores, but not with motor development (PDI score) at 18-24 months of age (Table 4.7). At that age, males had significantly lower motor scores compared to females (PDI score: mean ± SD: 82 ± 16 versus 89 ± 13, p .043). GA at birth was not significantly associated with outcome in our cohort.

Associations between neurodevelopmental outcome and perinatal factors, tissue volumes and GR were investigated by comparing (F-test) R2 values of six GLMs. Table 4.8 shows that the MDI score at 18-24 months is predicted mainly by model 1 (GA, Gender and SES) (adjusted-R2 = 0.22). Adding the perinatal data (model 2) in the analysis does not improve the prediction of outcomes (p = 0.45, 0.23, 0.57 for MDI, PDI and MPC, respectively). MRI volumetric data (either at birth, at TEA, both at birth and at TEA, or volume GR) do not contribute to the prediction power of the MDI score (p = 0.73, 0.43, 0.53, 0.38, respectively). For the PDI score, model 1 has a lower predictive power (adjusted-R2 = 0.055) compared to MDI outcome. This lack of predictive power is compensated by the volumetric data, especially at birth (p = 0.0029) (model 3). The combination of birth volumetric data and TEA volumetric data also contributes to the predictive power for the motor outcome (adjusted-R2 = 0.25, p = 0.0026) (model 5). However, volumetric data at TEA only (model 4) seems to contribute more to the predictive power of the MPC (p=0.037) at 5 years. The best model for predicting the cognitive outcome at 5 years of age is achieved when the volume GR (model 6) is added to model 1 (adjusted-R2 = 0.27, p=0.021). Over all, the models do not have a high predictive power as the adjusted-R2 is lower than 0.3 in all cases. Finally, the adjusted-R2 cannot be negative in theory, but it can be in practice, in which case it is an indication of a badly fitted model.

Table 4.8 – Predictive power and model comparison for MDI, PDI, MPC scores.

Model	MDI 18-24 month	PDI 18-24 months	MPC 5 years
Model /Model comparison	R2 /R2 adjusted p value	R2 /R2 adjusted p value	R2 /R2 adjusted p value
1	0.2543/0.2209	0.09631/0.05585	0.1899/0.1422
1 + 2	0.319/0.2185	0.2032/0.08562	.268/0.1216
1 + 2/ 1 (2 contribution)	0.4461	0.2251	0.5695
3	0.04103/-0.04888	0.2296/0.1574	0.05961/-0.05794
1 + 3	0.2964/0.1926	0.3187/0.2181	0.2823/0.1388
1 + 3/ 1 (3 contribution)	0.723	0.002878 **	0.4464
1 + 3/ 3 (1 contribution)	6.083e-05 ***	0.04664 *	0.002954 **
4	0.1053/0.02137	0.1473/0.06732	0.202/0.1023
1 + 4	0.3208/0.2206	0.2226/0.1079	0.3757/0.2508
1 + 4/ 1 (4 contribution)	0.4263	0.1285	0.03721 *
1 + 4/ 4 (1 contribution)	0.0002309 ***	0.116	0.005806 **
5	0.1458/-0.03094	0.3194/0.1785	0.4444/0.2308
1 + 5	0.3789/0.2095	0.4167/0.2576	0.2349/0.02142
1 + 5/ 1 (5 contribution)	0.526	0.002602 **	0.1197
1 + 5/ 5 (1 contribution)	0.0001251 ***	0.02706 *	0.001712 **
6	0.06175/-0.02621	0.09551/0.01071	0.2107/0.1121
1 + 6	0.3252/0.2256	0.2125/0.09633	0.3909/0.269
1 + 6/ 1 (6 contribution)	0.3789	0.1735	0.02148 *
1 + 6/ 6 (1 contribution)	2.735e-05 ***	0.02845 *	0.004018 **

1 Gender, GA birth, SES

2 Asphyxia, BPD, Sepsis, PDA

3 Absolute volumes at birth: CGM, UWM, SGM, CB, CSF, Total IC

4 Absolute volumes at TEA: CGM, UWM, SGM, CB, CSF, Total IC

5 Absolute volumes at birth + Absolute volumes at TEA: CGM, UWM, SGM, CB, CSF, Total IC

6 Absolute volumes GR: CGM, UWM, SGM, CB, CSF, Total IC

4.1.4 Discussion

There are currently only few studies that investigated longitudinal brain tissue volume growth in PT infants in the neonatal period and its association with later neurodevelopmental outcomes (Kapellou et al., 2006; Rathbone et al., 2011; Kersbergen et al., 2016a,b; Lee et al., 2016), and even fewer such studies that considered outcomes beyond 24 months of age (Lee et al., 2016). This study evaluated longitudinal brain tissue growth between birth and TEA, and its relation with perinatal factors and neurodevelopmental outcomes at 18-24 months of corrected age, and at five years of age, in a cohort of PT children free of major brain injury.

Relative volumes of CGM and CB were found to increase with GA at birth, while relative volumes of UWM decreased with GA at birth. The trend continued in the longitudinal evolution of the cohort, with higher relative volumes of CGM, CB and CSF at TEA compared to birth, and lower relative volumes of UWM and SGM at TEA than at birth. Increasing prematurity at birth was associated with lower relative volumes of UWM and total brain tissue at TEA, as well as higher absolute and relative volumes of CSF at TEA. Moreover, increasing prematurity was associated with lower growth rates of CGM, CB and total tissue. Among perinatal factors, neither BPD nor asphyxia had significant effects on tissue GR; PDA was associated with lower SGM, CB and IC GR, while sepsis was associated with lower CSF and IC GR. The fastest growing tissues were found to be the CB and the CGM (22 % of birth volume / week, and 21 % of birth volume / week, respectively).

An exploratory analysis was performed using LDA for the classification of children's neurodevelopmental outcome into normal and abnormal, based on perinatal brain volumes and their growth. Cognitive outcome at 18-24 months (MDI) and at 5 years of age (MPC) were best predicted by the LDA based solely on GA and SES, while the addition of volumetric features did not improve the performance of the classifier. Motor outcome at 18-24 months (PDI) was best predicted by combining GA and SES with volumetric data measured at birth and at TEA.

To analyze the contributions of either perinatal factors, parental SES and brain volumetric factors to the prediction of neurodevelopmental outcomes, statistical models comparison was performed, showing again that cognitive outcome at 18-24 months and 5 years of age is predicted mainly by GA at birth and SE. Brain volumetric data at birth and at TEA contributed significantly to the variability of motor outcome at 18-24 months, whereas brain tissue volumes at TEA and tissue volume GR significantly influenced cognitive outcome at 5 years of age.

Longitudinal brain tissue volumes growth and volumes asymmetry

Several studies performed in PT born infants have demonstrated reductions in brain volumes at TEA in comparison with their term-born peers, (Peterson et al., 2003; Inder, 2005; Mewes et al., 2006; Thompson et al., 2007; Keunen et al., 2012; Padilla et al., 2015), but only few authors performed longitudinal studies of volumetric brain tissue growth between birth and TEA (Mewes et al., 2006; Kersbergen et al., 2016a,b; Makropoulos et al., 2016). Our data shows

an effect of GA at birth on all cerebral tissue volumes measured early after birth. Relative volumes of CGM and CB as percentages of total IC were positively correlated with GA at birth, while relative UWM at birth was significantly negatively associated with GA at birth. At TEA, only UWM and relative total brain tissue volume were positively associated with GA at birth, while relative CSF was negatively correlated with GA at birth. Regarding tissue volume changes between birth and TEA, we observed an increase of the relative volume of CGM as percentage of total IC volume and, on the other hand, a decrease in relative volume of UWM, which is consistent with the cross-sectional study of Hüppi et al. (1998). Moreover, the increase of relative CGM, CB and CSF volumes, and decrease of relative UWM and SGM volumes between birth and TEA demonstrated in our cohort confirm the findings of Mewes et al. (2006); Makropoulos et al. (2016). The increase in relative CSF between birth and TEA revealed by our study and corroborated by Makropoulos et al. (2016) explains the slight decrease in relative total brain tissue between birth and TEA indicated by our data. Furthermore, in line with Dubois et al. (2008) our data revealed moderate to strong correlations between tissue volumes at TEA and tissue volumes at birth (after adjustment for gender, GA at birth and GA at 2nd MRI), suggesting that structural measurements at birth contribute to explaining brain development at TEA.

Additionally, tissue volumes GR of CGM, SGM, CB, adjusted for gender, also showed a significant positive association with GA at birth. This is in line with other studies that found that gestational age at birth is a major predictor of cerebral volume growth rates (Inder, 2005) meaning that the longitudinal brain growth trajectory is influenced by GA at birth. In the absence of major cerebral lesions, this may suggest delayed or impaired cerebral development, either due to postnatal factors after PT birth, or as a consequence of the processes leading to PT birth. Huppi and colleagues (Hüppi et al., 1998) were the first to quantitatively assess in vivo of early human brain development using 3D-MRI and tissue segmentation techniques. This cross-sectional study showed a fourfold increase in CGM and a five-fold increase in myelinated white matter in 78 prematurely born infants from 29 to 41 weeks GA. In line with these findings, our longitudinal study showed a relatively rapid increase of CGM between birth and TEA, of 21% per week relative to birth volume (almost 12 ml/week in absolute volume). UWM, which accounts for nearly 98% of the total WM during this period of brain development, was shown to increase with 7% per week relative to birth volume (6.5 ml/week in absolute volume), while CSF volumes were shown to increase with 17% per week relative to birth volume (5.7 ml/week in absolute volume). SGM, which represents the volume of basal ganglia and thalamus together, showed a growth rate of 9% per week relative to birth volume (1 ml/week in absolute volume). In line with other studies (Mewes et al., 2006; Kersbergen et al., 2016a,b), we found that the CB displayed the fastest growth between birth and TEA of 22% per week relative to birth volume (1.76 ml/week in absolute volume. Considering the rapid evolution of brain differentiation in this critical period of development, a neonatal intensive care unit (NICU) environment might negatively impact the vulnerable PT brain, causing abnormal development.

When looking at the individual growth trajectories of brain tissue volumes, we observed a

great inter-individual variability, which reflects the fact that, even in the absence of brain injury, tissue volume growth from birth to TEA might be influenced by various clinical factors, such as gender, intrauterine growth restriction, asphyxia, BPD, neonatal sepsis and PDA (Tolsa et al., 2004; Boardman et al., 2007; Thompson et al., 2007; Keunen et al., 2012; Skiöld et al., 2014; Bouyssi-Kobar et al., 2016). In our study, the effect of several perinatal risk factors on brain volumes growth was modest. Males had significantly higher CB GR (MD 0.21 ml/week, 95% CI, 0.10 – 0.32) than females. In this study, sepsis was associated with lower CSF and IC GR. (Lee et al., 2014) found infants suffering from necrotizing enterocolitis with sepsis to have reduced trans-cerebellar diameter and increased left ventricles, while Padilla et al. (2015) did not find significant differences in global or regional brain volumes between infants with and without sepsis. Differently from the report of Thompson et al. (2007), in our study BPD had no significant effect on brain tissue volume growth. PDA on the other hand was associated with lower GR of SGM and CB. Indeed, it has been shown that PDA can affect perfusion and oxygenation in the premature brain (Lemmers et al., 2016), which might lead to impaired growth in rapidly growing brain structures. Moreover, PDA has been shown to be associated with reduced volumes of the CB (Limperopoulos, 2005; Padilla et al., 2015) and several gray matter areas (Padilla et al., 2015), while others (Kersbergen et al., 2016a,b) reported that surgery (including PDA-related surgery) was associated with volume reductions in several brain areas, but not the CB. As also confirmed by our results, the CB has been shown to be one of the fastest growing tissues in the last trimester of pregnancy (Limperopoulos, 2005; Volpe, 2009; Andescavage et al., 2016; Kersbergen et al., 2016a,b), which could explain its greater vulnerability to a lack of oxygenation caused by PDA.

Regarding brain asymmetry, we found small but statistically significant inter-hemispheric differences: CGM and SGM volumes were higher, and UWM lower in the left hemisphere at birth, while at TEA only the UWM asymmetry was maintained. In a study of the fetal brain, Andescavage et al. (2016) also reported larger volumes of left hemisphere CGM and SGM in early gestation, followed by left-right volume equalization by TEA. However, in their study white matter asymmetries were not significant. Gilmore et al. (2007) studied infants born at term in the first few weeks after birth, and found left-greater-than-right asymmetries in the CGM, SGM and UWM, with gray matter asymmetries more pronounced. Thus, our study confirms the accumulating evidence that brain asymmetry evolves during lifespan, and that the well-known rightwards asymmetry of the adult brain is not yet present at birth, but develops later in life.

Relationship to Neurodevelopmental Outcome

Of the 84 children who had 2 MRI scans, 74 children were evaluated for mental and motor development with the BSID II (MDI and PDI scores respectively) at 18-24 months of corrected age and 56 children were assessed for cognitive development with the K-ABC (MPC score) at 5 years of age. These follow-up rates with some dropouts are mostly due to high migration rates in the area. In this cohort of relatively healthy children, with no major cerebral lesions,

spanning a wide range of GA from extreme to late prematurity, mean MDI, PDI and MPC scores were all in the normal range.

To study the relationship between brain tissue volumes measured in the neonatal period and subsequent neurodevelopmental outcome, we first performed an exploratory analysis using LDA to classify neurodevelopmental outcomes of PT children into normal and abnormal as defined by standardized tests. Cognitive outcomes (MDI scores) at 18-24 months and at 5 years of age (MPC scores) were predicted with highest AUC by the LDA based solely on GA and SES (AUC = 0.78 for MDI and AUC = 0.77 for MPC). The addition of tissue volumes at birth, TEA or tissue GR as features of the classifier did not improve its performance. Motor outcome (PDI scores) at 18-24 months was predicted with lower AUC values than the cognitive scores (MDI and MPC), with the highest AUC obtained by combining GA and SES with brain volumes at TEA (AUC = 0.64). For the prediction of the PDI and MPC scores, the specificity was found to be very high vs. the sensitivity due to the small number of subjects considered as having abnormal scores (< 85) was low. Interestingly, the classification performance increased when using the GA at birth and SES as features when predicting MDI and MPC scores, but not for the PDI score. This is in line with Moeskops et al. (2017), who also performed classification of PT children's neurodevelopmental scores based on brain structural features (including volumes) and reported that the GA at birth improves their classification performance. Furthermore, in our study the prediction of PDI and MPC outcomes suffered from the small number of subjects in the abnormal range, which yielded low prediction ability for these two scores. This corroborates the results of Moeskops et al. (2017), whose ROC curves indicated that high specificity was achieved by paying the price of a large false discovery rate, and therefore a reduced ability to predict abnormal neurodevelopmental outcomes.

In order to better understand and prognosticate neurodevelopmental outcome associated with preterm birth, we then used a GLM of outcomes including the parent SES, gender and GA at birth (model 1). The main finding of this simple model was that cognitive scores (MDI and MPC) at 18-24 months of corrected age and at 5 years old were associated with the SES of the family, which confirms evidence from the literature. High-risk environments have been shown to negatively impact the cognitive trajectories of both PT and term born children (Wong and Edwards, 2013; Bradley and Corwyn, 2002a). Child SES, characterized by parental educational attainment and parental occupation, has been shown to be strongly associated with global cognitive development (Farah et al., 2006), but also with language and memory (Fluss et al., 2009; Jednoróg et al., 2012; Noble et al., 2015), executive functions development (Stevens et al., 2009) and school achievement. Mangin et al. (2017), who performed a longitudinal analysis describing cognitive development of very PT children over time, reported that the combination of PT birth and family high social risk is particularly detrimental, resulting in PT children to have the poorest developmental trajectory from early age to 12 years. There are also several recent studies looking at brain structural relations with SES in childhood. Jednoróg et al. (2012) examined the influence of the family SES on brain anatomy through MRI in a group of 10-year-old children. They found that unfavorable environmental conditions were associated with smaller hippocampal volume and with smaller volumes of CGM in regions related to

language and executive function development. Recent data from the large "Pediatric Imaging, Neurocognition and Genetics" (PING) study has confirmed the effect of SES on childhood cortical thickness changes, which in turn are associated with cognitive performance (Piccolo et al., 2016). Our analyses in the newborn period did not yield any association between tissue volumes measured at birth or at TEA and parental SES. These results suggest that the effects of SES are related to environmental factors postnatally, rather than genetically influenced and present at birth.

Furthermore, we investigated whether the addition to this model of perinatal factors, brain tissue volumes or growth rates significantly increases the R2 of the model. A variety of neonatal risk factors have been associated with adverse outcome in PT children, such as BPD (Short et al., 2003; Anderson and Doyle, 2006), PDA (Bourgoin et al., 2016) and sepsis (Miller et al., 2005a; Lee et al., 2014). Although in the literature alterations in brain tissue volumes and several perinatal morbidities associated with preterm birth seem to be related to later neurodevelopmental impairments, in this study perinatal risk factors such as asphyxia, sepsis, BPD and PDA do not consistently improve the prediction of outcomes until 5 years of age.

Concerning possible associations between reduced neonatal brain volumes and unfavorable neurodevelopmental outcomes, the evidence in the literature is mixed, with several authors reporting such associations (Peterson et al., 2003; Inder, 2005; Woodward et al., 2005; Beauchamp et al., 2008; Lodygensky et al., 2008; Thompson et al., 2008; Van Kooij et al., 2012; Keunen et al., 2016; Monson et al., 2016), and a few reporting the lack of significant associations, or a weakening of such associations after adjustment for perinatal variables (Shah et al., 2006; Lind et al., 2010, 2011; Cheong et al., 2016; Lee et al., 2016). In our subset of preterm born children with no brain lesions, adding the MRI volumetric data (either at birth, at TEA, both at birth and at TEA, or volume GR) does not contribute to the prediction power for the mental outcome at 18-24 months of corrected age. However, model 1 has a lower predictive power for the motor outcome at 18-24 months, compared to mental outcome. This lack of predictive power is compensated by adding tissue volumes segmented at birth. The prediction of the motor outcomes is further improved by using the combination of brain volumes measured at birth and TEA. At 5 years of age, volumetric measurements at TEA contributed to the predictive power of the cognitive outcome. The best model was achieved by adding volumes GR to model 1. These results suggest that the volumetric assessments at birth and TEA contribute to the prediction of outcomes, but their relevance is limited, as the adjusted-R2 is lower than 0.3. However, this lack of evidence needs to be carefully considered in the light of its possible explanations. First of all, our cohort was a relatively healthy one, exhibiting no major brain injury, spanning a wide range of gestational ages from extreme to late prematurity, and with few children whose outcomes indicated neurodevelopmental delay. The cohorts investigated in most studies reporting significant associations between neonatal tissue volumes and later outcomes had lower mean GA-s than our cohort, and several included cases of moderate to severe brain injury, factor not always adjusted for in statistical tests (Inder, 2005; Woodward et al., 2005; Beauchamp et al., 2008; Thompson et al., 2008; Van Kooij et al., 2012; Keunen et al., 2016; Monson et al., 2016). The other differences to be mentioned between our study and the

others were related to MRI parameters, volume extraction methodologies or the use of more specific neuropsychological assessment tools for outcome evaluation. Limitations

A few limitations of this study need to be mentioned. First, the MRI scans were performed on four different scanners because of scanner upgrades throughout the study period. Despite the fact that protocols were harmonized in order to obtain similar quality images, subtle differences might subsist among images acquired on different machines, and these might be reflected in the positioning of segmentation boundaries, and thus also in the final extracted tissue volumes. In order to mitigate this limitation, systematic visual inspection and manual correction of visible segmentation errors was performed. Moreover, analysis of covariance showed no effect of scanner type on brain tissue volumes corrected for GA at birth.

Secondly, we evaluated global tissue volumes, while several other studies looked at finer divisions of the brain, by performing parcellations (Peterson et al., 2003; Woodward et al., 2005), or studying specific structures, such as the hippocampus (Isaacs et al., 2000; Beauchamp et al., 2008; Lodygensky et al., 2008; Thompson et al., 2008). Indeed, we speculate that segmentations into finer anatomical divisions might improve our understanding of associations between early brain structure and later outcomes, and envisage performing such segmentations in our future work. In the same line of thought, it seems that investigations of brain cortical surface and folding (Kapellou et al., 2006; Dubois et al., 2008; Rathbone et al., 2011; Kersbergen et al., 2016a,b), structural connectivity (Thompson et al., 2016), and functional connectivity (Rogers et al., 2017)constitute promising investigation paths for the detection of MRI neonatal biomarkers associated with future outcomes.

Thirdly, dropout rates of our cohort were quite high, especially for the 5 years examination, where only 56 out of 84 children (66.7%) could be evaluated, thus limiting the power available for statistical testing. Furthermore, the groups where unbalanced for the LDA classification, which resulted in high specificity vs. low sensitivity. Finally, we could not perform a comparison with term-born neonates, since such data was not available.

4.1.5 Conclusion

This is one of the few longitudinal studies of premature infants from a wide spectrum of gestational ages, looking at neonatal brain structure and growth between birth and TEA, and their relation to neurodevelopmental outcomes at 18-24 months of corrected age and 5 years of age.

Increasing prematurity, as well as several perinatal risk factors were found to have an impact on brain tissue volumes and their growth between birth and TEA. By fitting and comparing several GLMs and testing an LDA classifier, we demonstrated that children's cognitive outcomes at 18-24 months and 5 years of age were strongly associated with parental SES – a well-known potent modifier of childhood brain development. Moreover, volumetric data at birth and at TEA contributed to explaining the variability of children's motor outcomes at 18-24 months,

while brain volumes at TEA and tissue growth rates between birth and TEA contributed to explaining the variability of children's cognitive outcome at 5 years of age. These results suggest that perinatal brain characteristics in PT infants may influence later functional development. However, since the overall predictive power of our models was relatively low, further research is required to elucidate the factors that affect brain development after premature birth.

Promising directions for future research include investigations of finer regional brain divisions, brain cortical surface, structural and functional brain connectivity as other possible biomarkers for neurodevelopmental outcomes.

Acknowledgments

4.2   Journal Preprint: Behavioral outcome of very preterm children at five years of age: Prognostic utility of brain tissue volumes at TEA and perinatal factors

(Preprint version of the article to be submitted to NeuroImage)

Maria Chiara Liverani[a,b,*], Serafeim Loukas[a,c,*], Laura Gui[a], Marie-Pascale Pittet[a], Maricé Pereira[a], Myriam Bickle-Graz[d], Anita Carmen Truttmann[d], Petra S. Hüppi[a], Djalel-Eddine Meskaldji[a,e,**], and Cristina Borradori Tolsa[a,**]

[a] Division of Development and Growth, Department of Pediatrics, University Hospital, Geneva, Switzerland

[b] Sensorimotor, Affective and Social Development Laboratory, Faculty of Psychology and Educational Sciences, University of Geneva, Geneva, Switzerland

[c] Institute of Bioengineering, Ecole Polytechnique Fédérale de Lausanne, Lausanne, Switzerland

[d] Clinic of Neonatology, Department of Women Mother Child, University Center Hospital and University of Lausanne, Vaud, Switzerland

[e] Institute of Mathematics, Ecole Polytechnique Fédérale de Lausanne (EPFL), Lausanne, Switzerland

* These authors contributed equally and are considered joint-first authors.

** These authors contributed equally and are considered joint-last authors.

Abstract

Objective: Prematurity is associated with a higher risk of developing behavioral problems in the long term. However, the association between these negative outcomes, brain development, and neonatal characteristics at birth has never been investigated. This study aimed to assess the prognostic utility of volumetric brain data at term-equivalent age (TEA), perinatal data, and socio-economic status (SES) in the prediction of the behavioral outcome at five years in a cohort of very preterm infants (VPT).

Methods: T2-weighted magnetic resonance brain images (MRI) of 86 VPT children were acquired at TEA and automatically segmented into cortical grey matter, deep subcortical gray matter, white matter, cerebellum, and cerebrospinal fluid. Amygdala was manually segmented by a medical doctor experienced in amygdala segmentation. Children were followed up at five years of age with a behavioral assessment, using the Strengths and Difficulties Questionnaire (SDQ). The utility of TEA brain volumes, clinical data and SES for the prediction of behavioral outcome at five years was investigated using support vector machine classifiers (SVC) and permutation feature importance and PCA was used to assess redundancy in the SDQ.

Results: PCA analysis revealed that the SDQ is a valid clinical tool for separating normal from

at risk, for behavioral problems, subjects. Moreover, the predictive modeling of the volumetric data showed that the white matter, amygdala and cerebellum volumes are the top predictors of the emotional subscale of the SDQ. From the clinical data, gender, sepsis and BPD were found to be the most important predictors for the hyperactivity subscale. When combining all three sets of variables (volumes, clinical, SES), the volumetric and clinical sets were the most informative for the prediction of the emotional outcome. Finally, the SES was positively correlated with the conduct and peer-relations outcomes.

Conclusions: This study provides evidence for the association between volumes at TEA, clinical and SES variables, and behavioral outcomes at five years of age. We showed that MRI at TEA could potentially be a good predictor of long-term emotional problems, since altered volumes of amygdala, white matter and cerebellum at TEA were linked to emotional symptoms at 5yo in VPT. Moreover, clinical variables such as sepsis, BPD and gender are good predictors of long-term hyperactivity-related problems. Finally, lower SES scores were associated with poorer conduct and peer-relations outcomes.

***Keywords**: Preterm infants, Neurodevelopmental outcome, Behavioral outcome, Machine learning, Classification, Volumetric brain data, MRI.*

Abbreviations

VPT	very preterm
GA	gestational age
TEA	term-equivalent age
MRI	magnetic resonance imaging
BW	birth weight
BPD	bronchopulmonary dysplasia
CSF	cerebrospinal fluid
WM	white matter
CGM	cortical gray matter
SDQ	Strengths and difficulties questionnaire
SES	socioeconomic status
SVM	Support vector machine
MDA	Mean decrease accuracy

4.2.1 Introduction

In the last decades, the incidence of preterm births and the survival rate among very preterm (VPT, birth before 32 weeks of gestation) newborns have increased due to improved assistance

during high-risk pregnancies and to the progress in medical techniques. As survival rates have improved, concern about the long-term outcome of the survivors of VPT birth has risen.

To improve outcome for VPT infants, it is crucial to understand both the nature of the cerebral abnormalities that underlie the wide range of adverse outcomes documented in this population, as well as any modifiable perinatal factors involved in pathogenesis. The ability to better predict outcome in the infant period could enable interventions that improve prognosis. Prematurity is associated with a high rate of long-term morbidities and a broad spectrum of neurodevelopmental impairments. These include motor disorders, speech and articulation problems, learning disorders, intellectual delay, as well as cognitive difficulties (Spittle and Orton, 2014; Twilhaar et al., 2018; Woodward et al., 2009).

Additionally, premature children show a higher rate of behavioral difficulties and psychiatric disorders compared to term-born children (Johnson and Marlow, 2014; Bhutta et al., 2002; Delobel-Ayoub, 2006; Delobel-Ayoub et al., 2009). By childhood, behavioral symptoms become more specific and can be summarized into a "preterm behavioral phenotype" described by S. Johnson and coll. and characterized by inattention/hyperactivity, social problems and emotional symptoms (Johnson and Marlow, 2011).

Several studies have shown that prematurity could have an impact on the ability to regulate emotions, tolerate frustration, and modulate behavior according to different situations (Bora et al., 2011; Gardner, 2004; Lejeune et al., 2015; Witt et al., 2014; Woodward et al., 2017). These problems can lead to weaker social competencies (Peralta-Carcelen et al., 2017), lower cognitive outcome and educational underachievement (Burnett et al., 2019; Indredavik et al., 2005), together with psychiatric disorders such as attention deficit hyperactivity disorder (ADHD), emotional disorders and autism spectrum disorders (ASD) (Indredavik et al., 2005; Johnson et al., 2010; Johnson and Marlow, 2011; Limperopoulos et al., 2008; Treyvaud et al., 2013).

Behavioral problems in children and adolescents are often assessed through questionnaires (Delobel-Ayoub et al., 2009; Gardner, 2004; Indredavik et al., 2005; Samara et al., 2008). According to studies using screening questionnaires, the prevalence of behavioral problems ranges from 13 to 46% for VPT children (Johnson and Marlow, 2011) and these rates have been reported to remain stable over time (Gray, 2004a).

The Strength and Difficulties Questionnaire (SDQ, (Goodman, 1997)) is the most frequently used and well-validated screening tool when investigating behavioral problems in subjects aged from 4 to 16. It is short to fill in by parents or teachers, allowing a multi-informant approach, and has excellent psychometric properties in detecting mental health problems. Behavioral problems are organized on 4 scales (conduct disorder, hyperactivity/inattention, relationship problems with peers and emotional symptoms) and a fifth scale assesses prosocial behavior. Several studies have used the SDQ to investigate the behavioral profile of preterm or low birth weight populations (Graz et al., 2015; Burnett et al., 2019; Delobel-Ayoub et al., 2009; Fevang et al., 2017; Gardner, 2004; Indredavik et al., 2005; Johnson et al., 2014; Samara et al.,

2008; van Houdt et al., 2020), confirming the increased risk for symptoms related to the triad described by Johnson and Marlow ((Johnson and Marlow, 2011)).

Recently, a retrospective multicenter cohort study investigated the prevalence of behavioral symptoms in VPT children at preschool age (Bartal et al., 2020). Compared to a control group of fullterm-born children, the rate of overall behavioral problems and symptoms linked to hyperactivity and inattention was not significantly higher in VTP children. Nevertheless, a greater prevalence of emotional symptoms has been found in VPT participants, together with a higher rate of prosocial behavior.

Even in the absence of clear brain injury, PT birth is often characterized by the presence of subtle alterations of cerebral structures, leading to potential disruption in the typical progression of child's development and to subsequent functional consequences. The impact of preterm birth on the brain can be heterogeneous, ranging from specific focal injuries (Ment et al., 2009; Volpe, 2009) to a more general alteration of cerebral development (Inder, 2005). Compared to children born at term, premature children show abnormal tissue volumes at term equivalent age (Inder, 2005; Keunen et al., 2012; Padilla et al., 2015; Peterson et al., 2003). Moreover, these alterations are observed even in the absence of severe neonatal complications, seem to be more pronounced in infants with the lower gestational age and can persist until childhood and adolescence (de KIEVIET et al., 2012; Inder, 2005; Mewes et al., 2006; Peterson, 2000; Thompson et al., 2007). Several studies in preterm born children have focused on the relationship between structural brain alterations at TEA and neurodevelopmental outcome later on, some of them showing an impact of brain abnormalities on cognitive, motor and neurosensory development (Peterson, 2000; Peterson et al., 2003; Soria-Pastor et al., 2009; Thompson et al., 2008; Woodward et al., 2006). In addition, neonatal brain abnormalities have been shown to be associated with psychiatric diagnoses and with the presence of socio-emotional problems in school-aged VPT children. Treyevaud and colleagues showed that white matter, cerebellar, cortical and deep gray matter abnormalities in the neonatal period were associated with a higher risk of psychiatric problems in a group of VPT children aged 7 year old (Treyvaud et al., 2013). Similarly, Rogers et al. found associations between lower hippocampal volume and higher prevalence of hyperactivity, inattention and socio-emotional problems in VPT female preschoolers, while reduced volume in the frontal region was associated with lower prosocial scores in males (Rogers et al., 2012). These findings are in line with a study assessing developmental outcome in VPT children aged 4 years old, in which white matter injury at TEA contributed significantly to internalizing behaviors, behavioral symptoms and executive functions deficits (Young et al., 2016).

Such studies might offer indications as to what extent neonatal brain MRI can represent a valuable instrument for prediction of developmental outcomes in this vulnerable population. Nevertheless, a clear consensus about the importance of neuroimaging brain data at TEA to predict the neurodevelopmental outcome in the long term is still missing (Linsell et al., 2015).

In the attempt to investigate the association between brain volumes in the neonatal period

and cognitive outcomes during early childhood, Gui and colleagues showed that brain tissue volumes at birth and at TEA contributed to the prediction of motor outcomes at 18-24 months, while volumes at TEA and volume growth rates contributed to the prediction of cognitive outcome at 5 years of age (Gui et al., 2019). Other studies confirmed these findings, since the predictive ability of volumetric data was not significant after the adjustment for neonatal variables (Cheong et al., 2016; Lind et al., 2010).

To our knowledge, no previous studies have tried to disentangle the association between brain volumes measured at TEA and behavioral outcomes assessed through parental questionnaires in the preterm population. The main objective of the present research was to evaluate the ability of brain volumetric data at TEA to predict behavioral outcome at 5 years of age in VPT infants. Additionally, we also investigated the contributions of either perinatal factors and parental socioeconomic status to the prediction of behavioral outcome at 5 years of age.

4.2.2 Methods

4.2.2.1 Participants

In the present retrospective cohort study, eighty-six (86) very preterm (VPT) infants born below 32 gestational weeks (mean $\pm$ SD: 28.17 $\pm$ 1.65 weeks) at the University Hospitals of Geneva (HUG) and Lausanne (CHUV) between 2007 and 2013 were included. All participants underwent a Magnetic Resonance Imaging (MRI) exam at term-equivalent age (TEA). As part of the standard follow-up of very preterm infants in both hospitals, participants in this study were given cognitive assessment and behavioral screening at 5 years of age.

Exclusion criteria included severe physical or sensory disabilities, chromosomal abnormalities and the presence of severe intraventricular hemorrhage (grade 3 or higher) on early cerebral ultrasounds. Out of the eighty-six (86) infants who had MRI scans at TEA and cognitive assessment at 5 years, MRI quality was not acceptable for six (6) participants. Therefore, these children were excluded from subsequent analysis that involved volumetric measures, but were included in the analysis of the clinical data (see Table B.3 in Appendix B).

Gestational age (GA) was based on the last menstrual period or the best estimation from a prenatal ultrasound. Birth weight (BW) z-scores were calculated based on the growth curves by Voigt, Fusch et al. (Voigt et al., 2006). The presence of proven sepsis was defined as at least one positive blood culture during the hospital stay. Bronchopulmonary dysplasia (BPD) was defined as a need for supplemental oxygen or ventilatory support at 36 weeks postmenstrual age (Jobe and Bancalari, 2001). Parental socio-economic status (SES) was estimated using the Largo scale, which results in a score based on maternal education and paternal occupation (score range 2–12). Higher SES scores reflect lower socio-economic level (Largo et al., 1989).

4.2.2.2 MRI acquisition

The MRI examination of the VPT infants was performed at TEA (GA at scan = 40.1 ± 0.8 weeks, range: 38.3 to 41.9 weeks). The acquisition was performed without the use of sedation, during infants' natural sleep. Infants were positioned inside the scanner wrapped in a vacuum pillow and monitored with electrocardiography and pulse oximetry. In addition, earmuffs were used for noise attenuation. Imaging data were acquired at both sites (HUG and CHUV) using identical Siemens Trio Tim (3T) MRI scanners. T2 -weighted images were acquired using the same protocol at both sites, namely a turbo spin echo sequence (TSE) with parameters: TE = 150 ms, TR = 4600 ms, 113 coronal slices, voxel size: 0.8 x 0.8 x1.2mm^3.

4.2.2.3 Image Processing

The automatic segmentation method of Gui, Lisowski et al. (Gui et al., 2012), was employed to segment all scans into cortical gray matter (CGM), white matter (WM), deep subcortical gray matter (DSGM), cerebellum (CB), and cerebrospinal fluid (CSF). The segmentation of the DSGM was improved by using a multi-atlas label fusion method (Heckemann et al., 2006). The atlases consisted of manually-corrected DSGM segmentations obtained with the method of Gui et al. (Gui et al., 2012). The DSGM comprised the following brain structures and nuclei: thalamus, hypothalamus, globus pallidus, dorsal striatum (putamen, caudate), ventral striatum (nucleus accumbens), and subthalamic nucleus. The resulting segmentations were visually examined, and small manual corrections were performed when necessary. Global and hemispheric tissue volumes were then automatically extracted from the final segmentations.

Amygdala was manually segmented in each scan, and its volume was calculated using ITK-SNAP software (Yushkevich et al., 2006). The segmentation was performed on T2-weighted MR cerebral images by a medical doctor who was trained in the manual segmentation of the amygdala for 6 months. The anatomical delineation was based on guidelines for the localization of the amygdala (Mai and Paxinos, 2012). Bayer and Altman's histological atlases were used for the validation and correction of anatomical landmarks (Bayer, 2003). Amygdala segmentations were performed using the same delineator and the same methodology for all scans.

4.2.2.4 Behavioral and cognitive outcome data

All children were followed-up around their fifth birthday at the developmental Units of Lausanne and Geneva with a neurological assessment completed by a developmental pediatrician, and an assessment of cognitive outcomes performed by a developmental psychologist. Behavior was rated by the parents using the SDQ.

The behavioral outcome was assessed using the Strengths and Difficulties Questionnaire (SDQ), parent version (Goodman, 1997). SDQ is a 25-item questionnaire composed of 5 subscales assessing emotional symptoms, conduct problems, hyperactivity/inattention, peer

problems, and prosocial behavior. For each item, parents are asked to answer on a 3-point scale (0 = not true, 1 = somewhat true, 2 = certainly true). The score for each subscale is computed by summing up the related items. Higher scores reflect more serious difficulties in the domain, except for the prosocial behavior, for which a high score means positive behavior. A total difficulties score (ranging from 0 to 40 points) is calculated by adding all the subscales scores except the prosocial behavior one. The official scoring guidelines (see http://www.sdqinfo.org) classify the total difficulties score and each subscale as "normal", "borderline", or "abnormal". Given that most of our participants scored in the normal range (normal group), we decided to pool together children with borderline and abnormal scores ("at risk" group).

Intelligence was assessed with the French version of the Kaufman Assessment Battery for Children (K-ABC I and II, Kaufman and Kaufman (1983)). This psychological diagnostic test allows the calculation of a cognitive score (IQ) which has an expected mean of 100 and a standard deviation (SD) of 15.

Data collection was approved by the Ethics Committee of the Canton of Geneva/of the Geneva University Hospitals. Parents were informed about the modalities and aims of the research according to the guidelines of the ethics committees of the two hospitals and signed an informed consent form. The research was carried out according to the Declaration of Helsinki.

4.2.2.5 Statistical analysis

Exploratory analysis: Principal Components Analysis

To first explore and visualize the encoded information and potential relatedness and redundancy of the five SDQ subscales, we employed a Principal Components Analysis (PCA).

PCA is a well-known unsupervised dimensionality reduction technique that constructs relevant features summarizing the original variables via linear combinations. The construction of these features is achieved by linearly transforming correlated variables (e.g., the five SDQ subscales) into a set of uncorrelated variables i.e., into the principal components (PCs), which can be ordered according to how much variance of the original data they explain. The first PCs capture most of the variance in the data (Jolliffe, 1986; Mourão-Miranda et al., 2005; Zhu et al., 2005). Before performing the PCA, we z-scored the original input variables to have zero mean and unit standard deviation and then, constructed and eigen-decomposed the correlation matrix. Eigenvalues are sorted in a decreasing order representing decreasing captured variance in the data. Finally, the projection of the original normalized data onto the reduced PCA space is obtained by projecting the originally normalized data onto the leading eigenvectors of the covariance matrix. The new reduced PCA space maximizes the variance of the original data.

Predictive modeling of behavioral outcome

The present study includes three categories/sets of variables: a) the volumetric data (brain tis-

sue volumes) for n=80 subjects (DSGM, CGM, WM, CB, CSF, Amygdala), b) the perinatal factors for n=86 subjects (GA, BW z-score, Gender, BPD, Sepsis) and c) the parents' socioeconomic status (SES) for n=86 subjects.

To investigate the predictive ability and prognostic utility of these sets of variables for the identification of infants with normal or at risk behavioral outcomes (i.e., Emotional symptoms, Conduct problem, Hyperactivity/inattention and Peer problems subscales of the SDQ) at five years of age, we employed Support Vector Classifier (SVC) models (linear-SVC, default parameters, implemented in scikit-learn using Python 3.8) (Hearst et al., 1998; Varoquaux et al., 2015). The Prosocial subscale of the SDQ was not used, since all participants were categorized into the normal group.

Classifications were performed using different combinations of the three aforementioned sets of features: (i) using only the volumetric data (ii) using only the perinatal factors and (iii) using all the three sets together, i.e., volumetric, perinatal factors and SES. The SES was considered separately to unveil its contribution to the perinatal factors variables in terms of predictive power. Stratified K-Folds cross-validation (K=5) was considered to avoid overfitting issues and deal with the unbalanced dataset (Poldrack et al., 2020). The folds were created by preserving the proportion of samples for each class. Furthermore, variables measured at different scales do not contribute equally to the analysis and might create a bias. Thus, to deal with this potential problem, the training set variables were standardized ($\mu = 0$, $\sigma = 1$) within each fold. Then, the standardization parameters estimated on the training set were applied to the test set before the model predictions. Finally, the classifiers' prediction ability was assessed by receiver operating characteristic (ROC) curves, and the corresponding area under the curve (AUC) was evaluated.

Feature importance

To quantify the feature importance of the input variables, we employed a permutation-based method known as Mean Decrease Accuracy (MDA) analysis (Breiman, 2001). This technique assesses the feature importance of a variable by evaluating the decrease in the model's accuracy when its values are shuffled. We estimated and reported the MDA across permutations, that is, the decrease in accuracy when a specific feature is shuffled, which is expected to be a positive value if the underlying feature is important in terms of classification power and separability. However, negative values of MDA can be observed in practice. In those cases, the predictions on the shuffled, noisy data happen to be more accurate than the real data. This might happen when the feature is not essential, but random chance can also cause the predictions on shuffled data to be more accurate. Finally, to evaluate the feature importance of each of the three sets of variables as a whole (i.e., volumetric, perinatal factors, and SES), we shuffled the values of all the variables contained in each subset. In all cases, the number of shuffles (permutations) was set to 1000.

Linear models and Analysis of Variance

Chapter 4. Predictive utility of brain volumes for cognitive and behavioural long-term outcomes

We completed the statistical analysis by associating the socioeconomic status (SES) variable with the behavioral outcomes. Additionally, to investigate the predictive utility of the SES variable, we constructed General Linear Models (GLMs) and we conducted an ANOVA. We compared the models to explore the contribution of the SES to the prediction of the behavioral outcomes at five years of age.

4.2.3 Results

4.2.3.1 Cohort characteristics & brain tissue volumes at TEA

Table 4.9 – Cohort characteristics: The perinatal data were available for 86 subjects whereas the absolute tissue brain volumes at TEA for 80 subjects.

Participants N = 86	
Perinatal data	
Male gender, n (%)	41 (47.67)
GA, weeks, mean (SD), range	27.82 (1.65) 23.86-32
Birthweight, g, mean (SD), range	992.15 (240.71) 600-1730
Birth weight z-score, mean (SD)	-0.41 (0.70)
BPD, n (%)	31 (36.04)
Sepsis, n (%)	24 (27.90)
PVL, n (%)	4 (4.65)
Parental socio-economic status	
SES score, mean (SD), range	6.43 (3.00) 2-12
Participants N = 80	
Absolute tissue volumes, ml	
CGM, mean (SD)	165.78 (23.59)
DSGM, mean (SD)	21.13 (1.97)
WM, mean (SD)	147.80 (15.94)
Amygdala, mean (SD)	0.82 (0.15)
CB, mean (SD)	22.71 (3.61)
CSF, mean (SD)	100.89 (25.51)

Table 4.9 illustrates the perinatal characteristics of our cohort, together with the means of the absolute brain volumes at TEA.

4.2.3.2 Outcome at 5 years of age

All participants had a normal neurological examination. Overall, 80% of participants had an IQ in the normal range (i.e., score higher than 85, as assessed by the K-ABC battery), 13% between 70 and 85, and 7% below 70. Table 4.10 shows the scores of the SDQ questionnaire for the total difficulties score and each subscale. Based on statistical t-tests, no significant differences were found between the two groups of children with and without volumetric data measured at TEA (n=80 and n=86). The majority of the participants had a normal total score (87% of the whole

sample). The behavioral problems that are mostly represented in our population are conduct problems and emotional symptoms (23% and 20%, respectively), followed by a relatively low rate of peer problems and hyperactivity/inattention symptoms (17% and 16%, respectively). Concerning the prosocial behavior score, all participants scored within the normal range.

Table 4.10 – Behavioral outcome at 5 years of age using the SDQ Questionnaire

Strengths and Difficulties Questionnaire	Participants (MRI at TEA) n = 80	Participants (No MRI at TEA) n = 86	P-value
Total Difficulties Score			
Normal (range 0-13)	69 (86%)	75 (87%)	0.861
At risk (range 14-40)	11 (14%)	11 (13%)	0.586
Emotional symptoms score			
Normal (range 0-3)	63 (79%)	69 (80%)	0.938
At risk (range 4-10)	17 (21%)	17 (20%)	0.998
Conduct problems score			
Normal (range 0-2)	61 (76%)	66 (77%)	0.856
At risk (range 3-10)	19 (24%)	20 (23%)	0.897
Hyperactivity/inattention score			
Normal (range 0-5)	66 (83%)	72 (84%)	0.989
At risk (range 6-10)	14 (17%)	14 (16%)	0.998
Peer problems score			
Normal (range 0-2)	66 (83%)	71 (83%)	0.935
At risk (range 3-10)	14 (17%)	15 (17%)	0.890
Prosocial behavior score			
Normal (range 6-10)	80 (100%)	86 (100%)	0.883
At risk (range 5-0)	0 (0%)	0 (0%)	-

No significant differences were observed for any of the brain absolute tissue volumes (CGM, DSGM, CB, WM, CSF, Amygdala) between the normal and at risk SDQ groups (see Figure B.2 and Table B.4 in Appendix B).

4.2.3.3   Exploratory analysis of the SDQ subscales using PCA

To visualize the projected data, as well as the contribution of the original variables in the same plot, we created a biplot. Figure 4.5 shows the biplot of the five SDQ subscales projected into the subspace spanned by the first two principal components. PC1 captures 50% of the variance of the data, and it is mostly influenced by the Conduct problems, Emotional symptoms, and

Prosocial behavior SDQ subscales. PC2 captures 20% of the variance of the data and captures the contrast between the Hyperactivity/inattention & Peer problems SDQ subscales. The scree plot of the PCA analysis is shown in Figure B.3 in Appendix B. We also plot the SDQ Total Difficulties score values for all subjects on the biplot. Red points represent the subjects at risk that belong to the group, whereas green points represent the normal ones based on the SDQ total Difficulties score. We observe that, in the PCA reduced space, a clear separation between normal and subjects at risk can be achieved by projecting the subjects (points) onto the first principal component (PC1).
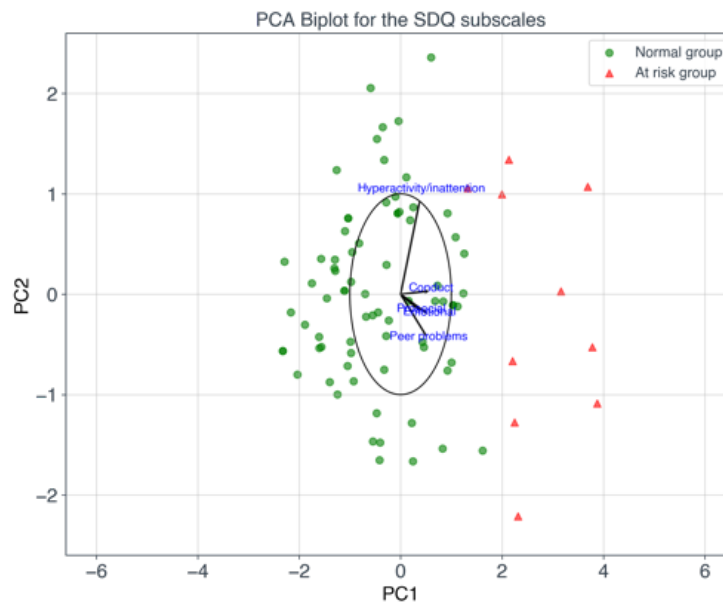
Figure 4.5 – The PCA biplots following the PCA analysis on the five SDQ subscales (Emotional, Prosocial, Conduct, Hyperactivity/inattention and Peer problems). Green and red points represent subjects in the normal (total difficulties scores normal) and at-risk group (total difficulties scores at risk = borderline scores & abnormal scores), respectively.

4.2.3.4 Predictive modeling: Classification of the behavioral outcomes

I. Using only volumetric data (brain tissue volumes measured at TEA)

The top panel of Figure 4.6 shows the classification ROC curves with cross-validation for the case where only the volumetric data were used as features. Only the performance of the model predicting the Emotional symptoms subscale is reliable, with an average AUC 0.74 (0.06) across all the stratified folds. The bottom panel of Figure 4.6 indicates that based on this model (Emotional symptoms), the most informative features (according to the MDA), in decreasing order, are the WM, Amygdala, CB, DSGM, CGM, CSF volumes. The remaining models have an average AUC around chance, indicating that those models are not reliable.

II.Using the perinatal factors
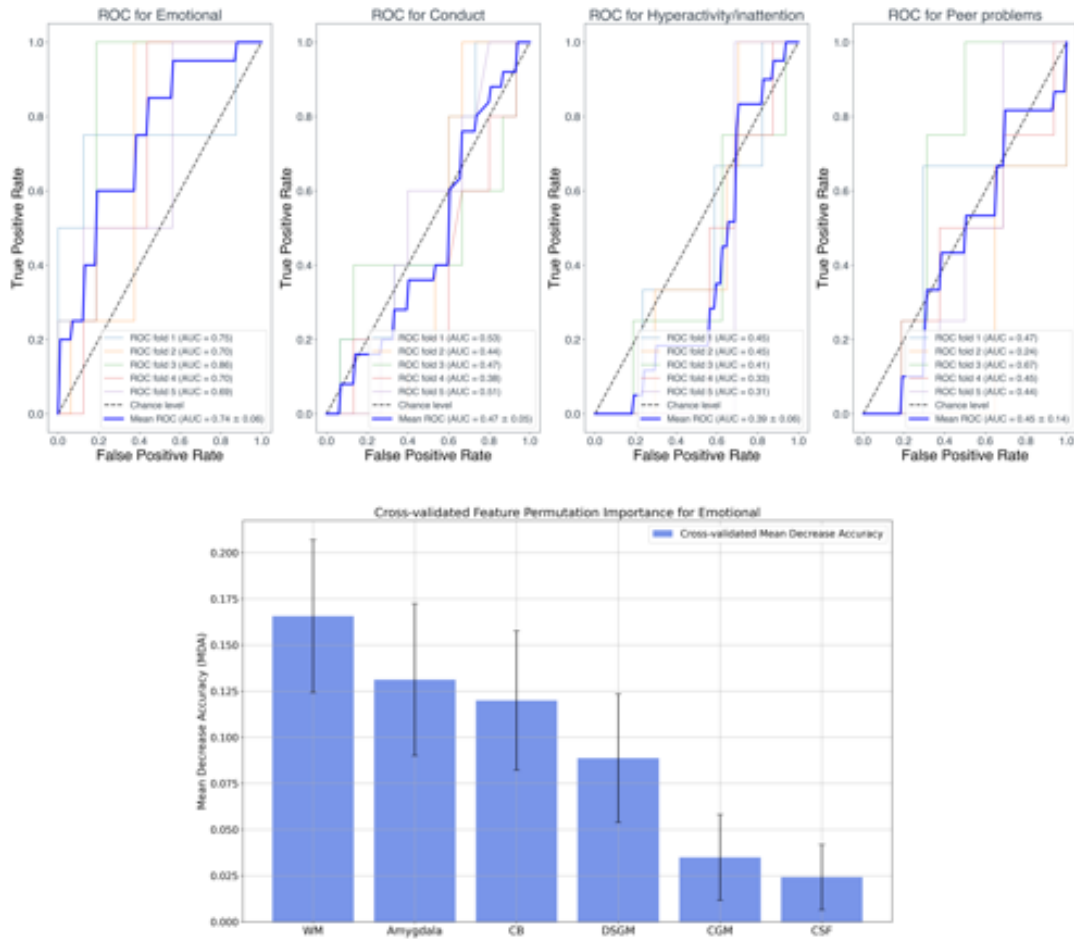
Figure 4.6 – Top panel: Classification ROC curves using only the volumetric data and, as target variables, the four SDQ subscales (i.e., Emotional, Conduct, Hyperactivity/inattention and Peer problems). Bottom panel: The Mean Decrease Accuracy (MDA) using 1000 permutations of the individual volumetric variables. Bar height represents the average across permutations MDA value, and the error bars show the standard deviation of these MDA values.

Figure 4.7 shows the classification ROC curves with cross-validation for the case where only the perinatal factors were used as features. Only the performance of the model predicting the Hyperactivity/inattention subscale is reliable, with an average AUC 0.75 (0.08) across all stratified folds. The bottom panel of Figure 4.7 indicates that the most informative features in terms of classification performance for this specific model (Hyperactivity/inattention) are, in decreasing order, the Gender, Sepsis and BPD. On the other hand, the BW z-score and GA variables are not considered as important in terms of predictions, given that the range of the standard deviation of the MDA values includes negative values. Furthermore, it is worth pointing out that the MDA values are small, meaning that the influence on the model's predictive power is limited. Post-hoc analysis showed that females tend to have slightly higher levels of hyperactivity/inattention, although the difference is not statistically significant

(p = .59). Similarly, children with sepsis showed higher levels of hyperactivity/inattention compared to children without sepsis, even if the comparison felt short of significance (p = .29).
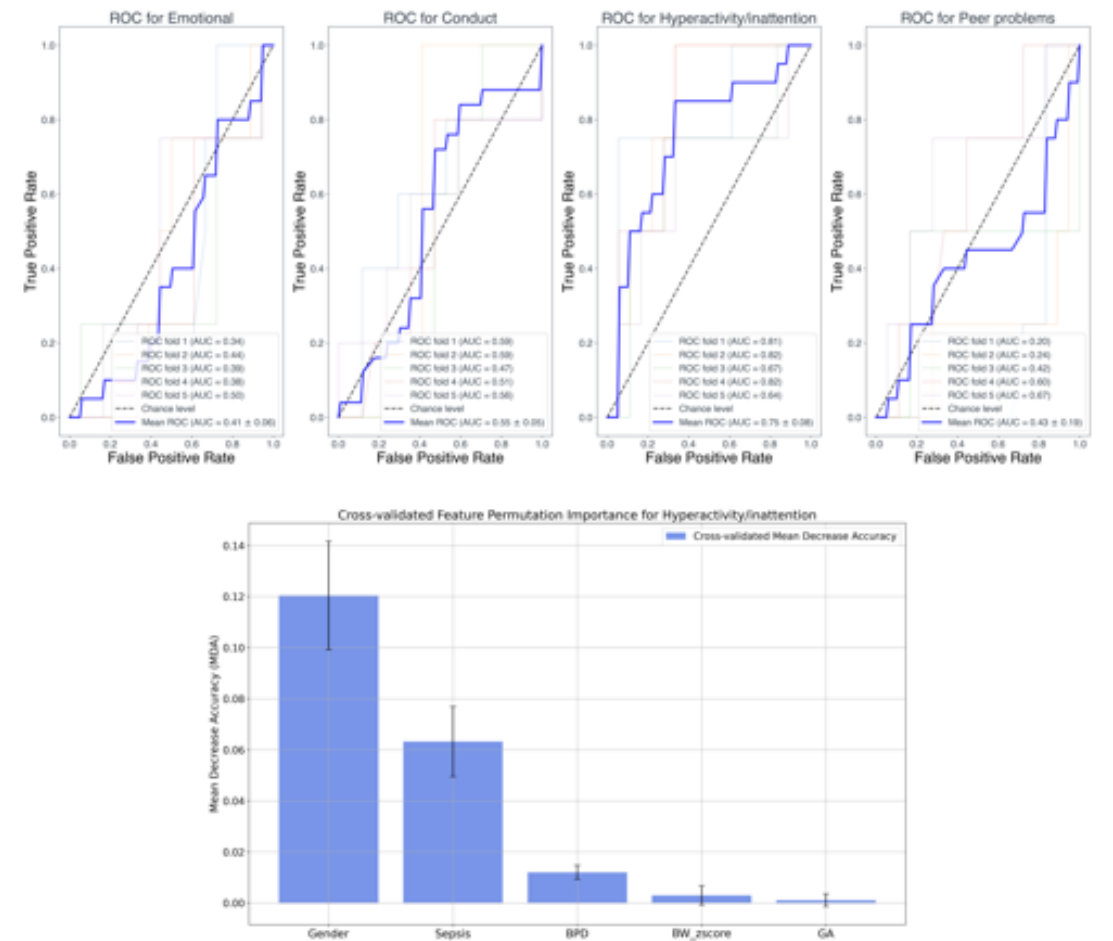
Figure 4.7 – Top panel: Classification ROC curves using only the perinatal factors and, as target variables, the four SDQ subscales (i.e., Emotional, Conduct, Hyperactivity/inattention, and Peer-problems). Bottom panel: The Mean Decrease Accuracy (MDA) using 1000 permutations of the clinical variables, individually. Bar height represents the average across permutations MDA value, and the error bars show the standard deviation of these MDA values.

III.Using all three sets of variables: volumetric data, perinatal factors and socioeconomic status (SES)

The top panel of Figure 4.8 shows the classification ROC curves with cross-validation for the case where all three sets of variables were used as features (volumetric, perinatal and SES). The performance of the models predicting the Emotional symptoms subscale is reliable, with an average AUC of 0.76. The bottom panel of Figure 4.8 indicates that the most informative set of features in terms of classification performance for the Emotional symptoms subscale model is the volumetric set of variables. Note that variable sets with a standard deviation of

the MDA values below zero cannot be considered as important. The remaining models have an average AUC around or below chance level, indicating that those models are not reliable and thus, not further explored.
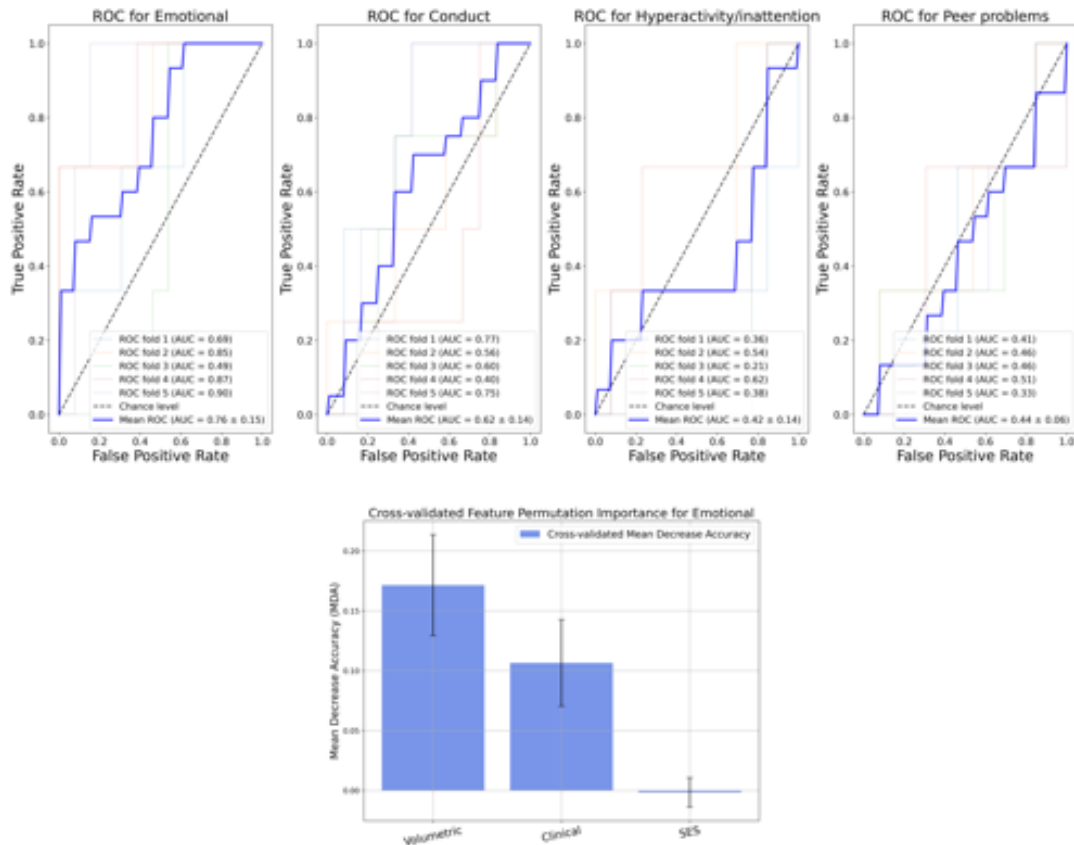
Figure 4.8 – Top panel: Classification ROC curves using all three sets of variables (volumetric, perinatal and SES) and, as target variables, the four SDQ subscales (i.e., Emotional, Conduct, Hyperactivity/inattention, and Peer problems). Bottom panel: The Mean Decrease Accuracy (MDA) using 1000 permutations of the individual sets of variables. Bar height represents the average across permutations MDA value for the specific set of variables, and the error bars show the standard deviation of these MDA values.

4.2.3.5 Linear models for the prediction of the behavioral outcome

Associations between SES and behavior outcomes

The analysis of outcomes by linear models showed that high SES score (i.e., low parenal SES) was associated with higher the conduct problems score (r=0.155, p=0.0015), as well as with higher peer problems score (r=0.156, p=0.0098), but not with any other behavioral scores.

Model comparisons

Table 4.11 shows the ANOVA p-values table of the different model comparisons. Based on these comparisons, the SES variable, when added to the volumetric and perinatal factors sets, does not contribute significantly to the prediction of the SDQ subscales scores, except for the conduct problems scores (first column, Table 4.11). Furthermore, the SES adds significant information when added in the linear model of the volumetric data in terms of predictions of the peer problems, conduct problems and hyperactivity/inattention scores (second column, Table 4.11). Finally, the SES adds weaker information when added to the linear model of the perinatal factors set of variables and only contributes to the prediction of the conduct problems score (third column, Table 4.11). This contribution is expected since the SES is significantly positively correlated with the conduct problems score.

Table 4.11 – ANOVA table showing the p-values of different models' comparisons. For each SDQ subscales score, we report the p-value of comparing predictive models with and without an additional variable or set of variables.

	SES to Volumetric + perinatal factors	SES to Volumetric	SES to perinatal factors
Peer problems	0.1231	0.0236	0.0605
Conduct problems	0.0096	0.0008	0.0063
Emotional symptoms	0.2756	0.2924	0.2442
Hyperactivity/inattention	0.1210	0.0285	0.1431

4.2.4 Discussion

In this study, we investigated the ability of either brain volumetric data measured at TEA, perinatal factors and parents' SES to predict behavioral outcome at 5 years of age in children born VPT. A growing body of research has focused on the utility of brain volumetric data in the predictability of neurodevelopmental outcome. Nevertheless, there is still no consensus on the prognostic value of brain volumes measured by MRI at TEA for predicting neurodevelopmental outcomes in childhood, especially concerning the behavioral and emotional aspects of children development (Linsell et al., 2015).

The SDQ is one of the most popular questionnaires used to assess behavioral problems in children born both at term and prematurely, showing very high reliability and acceptance

among parents (Bartal et al., 2020; Johnson et al., 2014). In our sample, 87% of children showed a total difficulties score in the normal range. Abnormal scores were mainly found in the conduct problems subscale (23%), followed by emotional symptoms (20%). Finally, a relatively low rate of peer problems and hyperactivity/inattention symptoms have been found in our sample (17 and 16%, respectively). These results are partly consistent with those of a recent paper on a Swiss cohort of preterm-born children of the same age (Bartal et al., 2020), where emotional problems were reported to occur more frequently compared to term-born children, and hyperactivity was not a prominent symptom. Other studies using the SDQ found a higher occurrence of conduct problems and emotional symptoms in this clinical population (Fevang et al., 2017; Johnson et al., 2014). Nevertheless, it is worth noting that these studies also reported a higher rate of hyperactivity/inattention symptoms and peer problems, findings that are not in line with ours.

Exploratory analysis

As a first exploratory step in our analysis, we investigated the information encoded by the SDQ questionnaire in order to unveil potential information redundancies of the different subscales of the questionnaire. Principal Component Analysis (PCA) of the SDQ subscales revealed that a large amount of variance (50%) was explained by the combination of conduct problems, emotional symptoms and prosocial behavior subscales. Additionally, all these three variables were highly correlated as revealed by the PCA biplot. A smaller amount of variance (20%) was explained by the contrast (i.e., variables pointing in opposite direction in the biplot) of the hyperactivity/inattention with the peer problems subscales. Therefore, we can conclude that the SDQ Total Difficulties score is mainly influenced by conduct problems, emotional symptoms and prosocial behavior scores, while hyperactivity/inattention and peer problems scores are less represented. These results underline the importance of carefully considering each of the subscales of the questionnaire in a clinical setting, in order to avoid losing important information on the behavioral outcome of the children. Studies on the screening efficiency of the SDQ questionnaire revealed that this tool can predict conduct-oppositional disorders, hyperactivity disorders and depression with relatively few false negatives (Goodman et al., 2000a, 2003). Based on our PCA analysis, conduct problems, emotional symptoms and prosocial behavior scores are strongly correlated. This result suggests the presence of high comorbidity between these symptoms, which is confirmed by longitudinal studies highlighting the co-occurrence of mood disorders such as depression and conduct problems in children and early adolescents, leading to worsened social competencies and low academic performance (Capaldi, 1992; Ingoldsby et al., 2006; Olsson, 2009). Finally, we observed that a clear separation between normal and at-risk subjects can be achieved in the PCA reduced space when projecting the subjects onto the first principal component (PC1). This suggests that the information encoded in the correlated variables that influence the most PC1 (i.e., conduct problems, emotional symptoms and peer problems), is sufficient for abnormality detection in terms of SDQ total difficulties score categorization.

Predictive modeling

To study the relationship between brain tissue volumes measured in the neonatal period (TEA) and subsequent neurodevelopmental long-term outcome, we performed a predictive analysis using SVM to classify the behavioral outcomes of VPT children into normal and at risk.

Using the volumetric dataset, we were able to predict the emotional symptoms' score with a satisfying AUC (AUC = .74). Permutation importance analysis revealed that the most important variables in terms of classification accuracy of the model were the white matter, the amygdala and the cerebellum absolute volumes. An association between white matter abnormalities and emotional disorders has already been proven in adults (de Groot et al., 2000; Skellern et al., 2001; Spittle et al., 2009). Recent studies confirmed this link in a younger population, showing microstructural abnormalities in cingulum-callosal white matter pathways and uncinate fasciculus in children with emotional dysregulation (Hung et al., 2020; Stephens et al., 2020; Versace et al., 2015). Furthermore, the amygdala is a key region in the neural circuit involved in emotional competencies, and it is particularly vulnerable in case of premature birth (Rutherford, 2002). Cismaru and colleagues (Cismaru et al., 2016) showed that amygdala volumes at TEA were significantly smaller in VPT children compared to term children, and that this reduction was associated with poorer fear-processing ability. Additionally, altered amygdala connectivity in preterm children has been associated with social functioning deficits and emotional difficulties (Johns et al., 2019). Finally, the cerebellum is another brain region that is particularly at risk in preterm children (Gano and Ferriero, 2017; Limperopoulos et al., 2014; Volpe, 2009) and cerebellar abnormalities have been linked to affective problems such as socialization deficits and mood abnormalities (Tavano et al., 2007).

When using the clinical dataset, we were able to predict the hyperactivity problems score with an AUC = .75. In that case, permutation importance analysis revealed that the most important variables in terms of classification accuracy of the model were gender and the presence of sepsis and bronchopulmonary dysplasia (BPD). Concerning the link between gender and hyperactivity/inattention problems, post-hoc analysis (see Figure B.4) showed that females tend to have slightly higher levels of hyperactivity/inattention score, although the difference is not statistically significant. This is in line with several studies indicating that the male predominance of hyperactivity disorders in the general population is missing in preterm children (Elgen, 2002; Indredavik, 2004; Johnson and Marlow, 2011). The impact of BPD on premature infants long-term outcomes covers a broad spectrum of consequences, ranging from neurosensory problems to cognitive functioning, language, memory, visuo-spatial skills, memory and behavioral problems (Doyle and Anderson, 2009). Our results suggest an association between BPD and hyperactivity/inattention symptoms. This corroborates previous studies that showed impaired sustained attention in BPD children compared to controls and reported a double rate of attention deficit-hyperactivity disorder in premature BPD children compared to premature non-BPD children at 8 years (Cheong and Doyle, 2018; Short et al., 2003). Moreover, perinatal risk factors such as sepsis has been associated with adverse outcome in PT children (Miller et al., 2005b). Kavas and colleagues (Kavas et al., 2017) found

that postnatal sepsis is a risk factor for the development of minor neurological dysfunctions, leading to lower IQ and significantly increased incidence of hyperactivity in children born with very low birth weight, which is in line with our results, as the post hoc analysis showed a tendency for more hyperactivity problems in subjects with sepsis, compared to subjects without sepsis. However, the statistical difference was not significant. Consistent with our results, Delobel-Ayoub and the EPIPAGE study group (Delobel-Ayoub, 2006) did not find any significant relationship between behavioral problems and the degree of gestational age or birth weight, a result found in other studies (Gray, 2004b; Graz et al., 2015; Yang et al., 2011).

Finally, when combining parental socio-economic status (SES), with the volumetric and perinatal data (all three sets of variables combined), we were able to accurately predict the emotional symptoms score (AUC = 0.76). Permutation importance analysis unveiled that the volumetric and perinatal datasets were the most important in terms of the model's accuracy improvement. This is in line with the results of the analysis where only the volumetric data were used, which showed a good prediction for the emotional symptoms score. However, it is worth pointing out that in this case, where all three datasets were combined, the predictive ability of the model was slightly higher (AUC = 0.76 for all three datasets, compared to AUC = 0.74 for the volumetric dataset alone). This is expected, since the addition of more variables provides more information in terms of classification power. Moreover, it is important to note that the SES is the least important factor that predicts the presence of emotional symptoms at 5 years. This is quite surprising since the impact of SES on the prevalence of behavioral, and more specifically emotional problems is well documented in typical children (Bøe et al., 2011; Hosokawa and Katsura, 2018) and also in preterm populations (de Laat et al., 2016). However, Conrad and colleagues (Conrad et al., 2010) showed that biological factors (such as birth weight) account for more variance in parent behavioral ratings than factors associated with SES in preterm children. In this study, biological factors such as brain tissue volumes at TEA and perinatal factors are more important in predicting long-term emotional outcome than parental socio-economic status (SES).

Linear Models

In order to better understand and prognosticate behavioral outcomes associated with preterm birth, we then used a LM of outcomes including the parent SES, the volumetric data and the perinatal risk factors.

Child SES, characterized by parental educational attainment and parental occupation, has been shown to be strongly associated with cognitive development in PT children (Mangin et al., 2016; Gui et al., 2019). Associations between behavioral problems and environmental factors, have also been reported (Bradley and Corwyn, 2002b; Nicholson et al., 2010; Girouard et al., 1998; McCormick et al., 1996) and this is in line with the current findings, which provide evidence of the influential role of the SES on long-term *bevarioural* outcome. Indeed, when we explored the associations of the SES variable with the behavioral outcomes in our cohort using linear models, we found a significantly positive correlation between the SES and the

conduct problems score (r=0.155, p=0.0015), as well as between SES and the peer problems score (r=0.156, p=0.0098), but not with any other behavioral score. Therefore, our results show that the lower the socio-economic status of the family (i.e., higher SES scores) is, the higher the conduct and peer problems in these children at five years of age are.

Concerning the predictive utility of SES, ANOVA results showed when it is added to the volumetric and clinical combined sets, it does not contribute significantly to the prediction of the behavioral outcomes, except for the conduct problems score. This is in line with the classification results of the last case where all three sets of variables were used for the prediction of the emotional outcome and SES was shown not to be contributing to the model. However, based on the model comparisons, the SES adds significant information in terms of predictions of the peer problems, conduct problems and hyperactivity/inattention scores, when added in the linear model of the volumetric data. Finally, the SES adds weaker information when added to the linear model of the perinatal variables and contributes only to the prediction of the conduct problems score. This is expected since SES is significantly positively correlated with the conduct problems score.

Taking into account all these findings we could argue that the prediction of long-term behavioural outcome is a complex task and that different influential factors contribute to the prediction of different behavioural subscales. These results suggest that the volumetric assessments at birth and TEA contribute to the prediction of outcomes, but their relevance is limited. This could be due to the fact that our cohort was a relatively healthy one, exhibiting no major brain injury, and with few children whose outcomes indicated neurodevelopmental delay. Moreover, the inclusion of SES into the volumetric dataset improves performance indicating that SES is an informative factor but, the perinatal variables appear to conceal the value of SES given that we did not find a significant contribution of SES when added to the combined volumetric and perinatal sets.

4.2.4.1 Limitations

The present study has two main limitations. First, here we used the parent form of the SDQ, which might not be sensitive enough. Indeed, multi-informant SDQs (based on parents and teachers) were found to be much more sensitive in identifying of behavior problems in children that need psychological intervention (Goodman et al., 2000b). Unfortunately, no multi-informant SDQ was available in this study. Second, the classification performance might be influenced by the unbalanced nature of the two groups. However, to deal with the high specificity vs. low sensitivity problem, stratified K-Fold cross-validation was employed and we report results in terms of cross-validated outcomes. Moreover, in the present study we studied the relation of global tissue volumes with neurodevelopmental outcome however, there are several studies that have explored these associations using finer brain segmentation volumes, providing more fine-grained information on these associations. This constitutes a feasible extension of our work for the near future.

4.2.5 Conclusion

This is one of the few studies of VPT children looking at brain structure measured at TEA, and their relation to behavioural outcomes at 5 years of age. This study provides evidence for the association between volumes at TEA, perinatal risk factors and SES, and behavioral outcomes at five years of age. We showed that brain volumes at TEA, specifically, volumes of amygdala, white matter and cerebellum contributed to explaining the variability of children's emotional symptoms at 5 years of age. Moreover, gender and perinatal variables such as sepsis and BPD were shown to predict long-term hyperactivity-related problems. Finally, SES was positively correlated with the conduct and peer-relations outcomes, and seems to add predictive power for the detection of behavioral problems such as conduct problems, peer problems and hyperactivity/inattention symptoms when added to the volumetric variables measured at TEA.

5 Advanced models for neurodevelopment

Although, brain alterations due to prematurity have been previously extensively investigated (Dewey et al., 2019; Karolis et al., 2017; Alexander et al., 2019; de Almeida et al., 2021; Inder, 2005), the exact sequence of brain abnormality underlying preterm birth has never been explored. Neurodevelopment is a dynamic process characterized by large macroscopic changes where brain abnormality compensation mechanisms are highly present (Young et al., 2020; de Silva et al., 2020). Conditions such a preterm birth may change the dynamic process of neurodevelopment and lead to developmental delay, similar to disease progression. Thus, understanding the sequence of biological events of the encephalopathy of prematurity can provide valuable insights into the underlying pathophysiology and can help develop more targeted interventions aiming to prevent severe delay through resilience.

The first article in this chapter is a preprint aiming to unveil, for the first time, the disease progression of prematurity using advanced models that have been previously used to successfully characterize other diseases' progression (Fonteijn et al., 2012; Young et al., 2014). Preterm birth leads to developmental delay similar to disease progression and thus, disease progression models might be of potential clinical use in prematurity.

In the second section of this chapter, we introduce a novel, data-driven framework that enables the spectral graph theory analysis of the functional connectome at the voxel level. The proposed framework is able to characterize, for the first time, the brain's fundamental organizational principles, without the use of a parcellation scheme. We validate and illustrate the importance of the proposed method using 40 subjects from the Human Connectome Project (HCP). Our results indicate the presence of both functional gradients and community structure at the voxel level revealing fine-grained, dominant connectivity eigenmodes. The code developed to perform the analysis is available at https://github.com/seralouk/Voxel_wise_Laplace_Modularity.

5.1 Journal Preprint: Fine-grained, image-based disease progression characterization of prematurity

(Preprint with preliminary results)

Serafeim Loukas[a,b,c], Neil Oxtoby[d], Djalel-Eddine Meskaldji[a,e], Laura Gui[a], Dimitri Van De Ville[b,c], Petra S. Hüppi[a] and Daniel C. Alexander[d]

[a] Division of Development and Growth, Department of Pediatrics, University of Geneva, Switzerland
[b] Institute of Bioengineering, Ecole Polytechnique Fédérale de Lausanne (EPFL), Switzerland
[c] Department of Radiology and Medical Informatics, University of Geneva, Switzerland
[d] Centre for Medical Image Computing, Department of Computer Science, University College London, United Kingdom
[e] Institute of Mathematics, Ecole Polytechnique Fédérale de Lausanne (EPFL), Switzerland
[f] Department of Radiology and Medical Informatics, University of Geneva, Switzerland

Corresponding author at serafeim.loukas@epfl.ch

Abstract

Preterm birth has been strongly associated with adverse cognitive, behavioural and motor outcomes that may persist into school age and even into adulthood. Understanding the underlying brain mechanisms as well as the sequence of the disease progression may allow more targeted and individualized early therapeutic interventions aiming to prevent the observed adverse outcomes. Using Magnetic Resonance Imaging (MRI), several studies have explored the brain abnormalities associated with preterm birth. However, no previous study has tried to unveil the disease progression of prematurity. In this study, we use a data-driven approach, the event-based modeling (EBM) method, to explore the disease progression of prematurity, producing a fine-grained estimation of the sequence of brain volumetric abnormality changes in prematurely-born infants at term-equivalent-age (TEA). We hypothesized that prematurity can change the process of neurodevelopment similar to disease progression and thus, models such as the EBM that have been previously employed to characterize other diseases' progression, might be of potential clinical use in prematurity as well. Event sequences obtained with EBM showed that the first biomarkers to become abnormal were the brainstem and white matter whereas the last biomarkers were found to be the cerebellum and the subcortical gray matter. This is the first study to unveil and characterize the progression of encephalopathy of prematurity using a data-driven approach.

Keywords: *Premature birth, Neurodevelopment, Progression model, Event-based model, Disease progression, Brain volumes*

5.1.1 Introduction

Preterm birth is defined as the birth before 37 weeks of gestation and it is a major pediatric public health problem. According to the World Health Organization (WHO), approximately 15 million babies are born preterm every year. Premature infants are likely to suffer from chronic health issues with infections, asthma and feeding problems being the most probable to develop or persist. Additionally, complications due to prematurity have been reported to be the leading cause of death in children under 5 years of age (Liu et al., 2016).

Furthermore, converging evidence suggests that preterm birth disturbs the genetically determined program of corticogenesis in the developing brain. Recent advances and improvements in the perinatal care units have led to increased survival rates of these preterm infants. However, despite the decreasing mortality rates, the incidence of preterm birth is increasing world-wide and has been strongly associated with persistent neurodevelopmental disabilities such as cognitive, motor and behavioural adverse outcomes (Delobel-Ayoub et al., 2009; Marlow et al., 2005; Arpino et al., 2010; Doyle and Anderson, 2010). Cognitive problems refer to thinking and learning abilities, motor development problems refer to the ways children move, such as by crawling and walking, while behavioural deficits refer to attention and poor social/interactive skills inabilities. Worryingly, the aforementioned adverse outcomes may also persist into school age and adulthood (Soleimani et al., 2014). Larroque et al., highlighted that only 61% of infants born at 24–32 weeks of gestational age were free of mild, moderate, or severe disabilities at 5 years of age (Larroque et al., 2008). Additionally, compared to full-term born children, preterm infants have a three times odds of developing a psychiatric disorder (Treyvaud et al., 2013). It is thus evident that early identification of infants at high risk of neurodevelopmental impairments as well as a better characterization of the underlying brain abnormalities can be extremely valuable since it will allow a more targeted early intervention aiming to improve and even prevent these adverse neurodevelopmental deficits through resilience (Sutton and Darmstadt, 2013). Principally, early developmental interventions have been provided in the clinical setting either during hospitalization or post-hospital discharge focusing on the improvement of overall outcomes for these infants.

While the main underlying mechanisms and processes of these brain development alterations have not yet fully unveiled, magnetic resonance imaging (MRI) provides a non-invasive, in vivo technique to study the developing brain. Over the past decade, MRI has provided valuable insights and has played a central role in studying the preterm brain and identifying relevant neuroimaging altered biomarkers. It has been reported that preterm-born children have smaller cortical grey matter, cortical white matter, basal ganglia and cerebellum brain volumes compared to control children born at term (Counsell and Boardman, 2005). Additionally, reduced brain volumes, following preterm birth, in important brain areas for high executive functions such as sensorimotor, parieto-occipital and fronto-temporal regions have been reported by several studies (Peterson et al., 2003; Gimenez et al., 2006). Moreover, it has been shown that preterm-born children have decreased structural connectivity in cortico-basal ganglia-thalamocortical loop connections compared to full-term born children providing

evidence for impaired networks relevant for higher-order cognitive skills and social cognition (Fischi-Gómez et al., 2015). Finally, resting-state functional connectivity alterations between the amygdala, parietal and temporal cortices, that could be linked to the deficits in emotion processing, have been observed in preterm-born adults (Papini et al., 2016).

Although functional, structural and volumetric brain alterations due to prematurity have been previously studied (Dewey et al., 2019; Karolis et al., 2017; Alexander et al., 2019; Gui et al., 2019; de Almeida et al., 2021; Inder, 2005), the exact sequence of brain abnormality underlying preterm birth has never been investigated. Understanding the sequence of biological events along the course of prematurity provides valuable insights into the underlying pathophysiology and can help intervention selection and setup.

In this study, we employ a data-driven approach to unveil the disease progression of pre-maturity, producing a fine-grained estimation of brain volumetric abnormality changes in prematurely-born infants at term-equivalent-age (TEA). We hypothesize that preterm birth alters the dynamic process of neurodevelopment and leads to developmental delay similar to disease progression. Thus, advanced statistical models, such as the event-based model (EBM) (Fonteijn et al., 2012; Young et al., 2014), that have been previously used to successfully characterize other diseases' progression, might be of potential clinical use in prematurity.

Previous works have demonstrated the EBM is able to accurately order biomarkers with a fine-grained ability in separation of Cognitively normal (CN) and AD subjects as well as to distinguish between Mild Cognitive Impairment (MCI) to AD or from CN to MCI (Fonteijn et al., 2012; Young et al., 2014). The EBM is a probabilistic data-driven method developed to explore the evolution of biomarkers as the disease develops and progresses (Oxtoby et al., 2018). To the best of our knowledge, this is the first study to unveil and characterize the timeline of encephalopathy of prematurity using a generative, probabilistic, data-driven method.

5.1.2 Methods

5.1.2.1 Participants

A total of seventy-five (n=75) full-term (FT) infants born after 37 gestational weeks (mean ± SD: 39.614 ± 1.105 weeks) and one-hundred-eighty-one (n=181) preterm infants born before 32 gestational weeks (mean ± SD: 28.526 ± 1.746 weeks) from different cohorts were selected and consisted the final cohort for this study. All cohorts were analyzed using the same methodology (see 5.1.2.3). Analysis of covariance revealed no significant effects of the scanner type on brain volumes controlled for GA at birth (Table C.1 in Appendix C). The population characteristics are reported in Table 5.1. Furthermore, there was no statistically significant difference in gender between the two groups (Fisher's exact test; p-value = .885).

Each study was approved by the local medical ethics committee. All infants were born either at the University Hospital of Geneva (HUG) or at the University Hospital of Lausanne (CHUV).

5.1. Journal Preprint: Fine-grained, image-based disease progression characterization of prematurity

Gestational age (GA) was estimated based on the last menstrual period or via based on a prenatal ultrasound. All infants underwent a Magnetic Resonance Imaging (MRI) session at term-equivalent-age (TEA). The exclusion criteria for this study included the presence of intraventricular hemorrhage (≥ grade 3) and hemorrhagic parenchymal infarction, as assessed by an early cerebral ultrasound, as well as physical or sensory disabilities and chromosomal abnormalities.

Table 5.1 – Population characteristics for the full-term and preterm infants. Student t-tests were performed for continuous variables and Fisher's exact tests for categorical variables.

	PT (n=181)	FT (n=75)	P-value
GA at birth; mean (SD)	28.526 (1.746)	39.614 (1.105)	$p < .001$
GA at MRI; mean (SD)	40.231 (.757)	40.372 (1.787)	$p = .376$
Birth weight (g); mean (SD)	1105.076 (302.16)	3357.237 (376.004)	$p < .001$
Gender (M/F)	87 / 94	35 / 40	$p = .885$

5.1.2.2 Data Acquisition

For all infants, the MRI examination was performed at term-equivalent-age (TEA) (GA at MRI scan; mean ± SD; PT group: 40.231 ± .757, FT group: 40.372 ± 1.787). There was no statistically significant difference in the gestation age (GA) at the MRI scan between the two groups of infants (p-value = .376, GA at MRI; mean ± SD; PT: 40.231 ± .757, FT: 40.372 ± 1.787). All infants were positioned inside the scanner wrapped in a vacuum pillow. Monitoring was performed using electrocardiography and pulse oximetry. Furthermore, the acquisition was performed without the use of sedatives and during infants' natural sleep. Finally, to protect the infants from noise, earmuffs were used.

5.1.2.3 Image preprocessing

Brain volumetric data (tissue volumes) were extracted for each infant. All neuroimaging brain scans were segmented into cortical gray matter (CGM), white matter (WM), subcortical gray matter (SGM), cerebellum (CB), cerebrospinal fluid (CSF), and brainstem volumes using an automatic segmentation method (Gui et al., 2012). The segmentation of the subcortical gray matter was further improved using a multi-atlas label fusion method (Heckemann et al., 2006). Moreover, the atlases consisted of manually-corrected SGM segmentations. The SGM consisted of the following brain structures: thalamus, hypothalamus, globus pallidus, dorsal striatum (including putamen & caudate), ventral striatum (including nucleus accumbens) and subthalamic nucleus. The resulting segmentations were visually inspected and manually corrected if needed. Global and hemispheric tissue volumes were then automatically extracted from the final segmentations.

5.1.2.4   The Event-based model

The event-based model (EBM) is a generative, probabilistic, data-driven method that was first developed to explore the evolution of biomarkers, as disease unfolds (Fonteijn et al., 2012; Young et al., 2014; Oxtoby et al., 2018), using cross-sectional data. The underlying assumption of the model is that the disease is characterized by a monotonic change of biomarkers towards abnormality, which represents the disease progression. This change is also assumed to be irreversible.

Each biomarker is treated by the model as either "normal" or "abnormal". The biomarker's probabilistic transition from the normal to the abnormal state is defined as an "event". In other words, an event is a statistical deviation from normality (as defined by controls' data) toward abnormality/disease (as defined by patients' data). The EBM estimates the probabilistic "sequence of events" that describes the most likely ordering of events that characterize the transition of a subject from the healthy to disease state (Young et al., 2014) and the uncertainty (positional variance diagram) in the sequence. Conceptually, higher prevalence corresponds to an earlier position in the estimated sequence. The positional variance diagram depicts the posterior distribution on S and is essentially a histogram (confusion matrix) of the position in the ordering of each event over the set of MCMC samples.

Formally, the likelihood of an ordered sequence S, assuming independent observations and biomarkers, is defined as

$$\Pr(X \mid S) = \prod_{j=1}^{N} \left[\sum_{m=0}^{M} \left\{ \prod_{i=1}^{m} \Pr\left(x_{ij} \mid E_i\right) \prod_{i=m+1}^{M} \Pr\left(x_{ij} \mid \neg E_i\right) \right\} \right] \tag{5.1}$$

with $x \in X$ being observations of $i \in M$ biomarkers and $j \in N$ being the subjects in the cohort (Fonteijn et al., 2012).

The characteristic ordering (S) is the sequence that maximizes the likelihood $Pr(X|S)$ in Eq. 5.1. Event probability of each biomarker is a function of the likelihood of an event having occurred i.e. $Pr(x_{ij}|E_i)$ or not having occurred i.e. $Pr(x_{ij}|\neg E_i)$, modeled by a two-component univariate mixture model (Fonteijn et al., 2012). In the present study, we use a recent version of the EBM that is based on a non-parametric mixture modeling approach allowing the modeling of biomarkers that do not necessarily follow a parametric distribution (Firth et al., 2020). The probability of an event for each biomarker is determined by a Kernel Density Estimation mixture model (KDE-EBM) where the normal (controls) and abnormal (patients) components are KDE components (with Gaussian kernels). The model output is the average maximum-likelihood sequence over all individuals providing inference at the group-level.

5.1.2.5   Biomarkers

The brain tissue volumes of the preterm (PT) and full-term (FT) groups were used as input biomarkers for the KDE-EBM model including cortical gray matter (CGM), white matter (WM),

subcortical gray matter (SGM), cerebellum (CB), cerebrospinal fluid (CSF) and brainstem volume.

All brain tissue volumes were normalized by the intracranial brain volume prior to any subsequent analysis. Figure C.1 in Appendix C shows the boxplots of the brain development at TEA for the two groups. Statistically significant differences between the two groups (PM, FT) were only observed for the white matter, CSF and Brainstem brain volumes. The p-values of the t-tests are reported in Table C.2 in Appendix C.

Following the model fitting, the estimated model sequence of events defines the disease progression of prematurity i.e., a fine-grained estimation of the sequence of the brain volumetric abnormality changes in prematurely-born infants at term-equivalent-age (TEA).

5.1.2.6 Cross-validation

To quantify the robustness of the sequence we performed Stratified K-Folds cross-validation. We repeated the estimation of the model (including the event distributions and maximum likelihood sequence) using 10 Stratified K-Folds, preserving the percentage of samples for each group. Sequence robustness was quantified based on the cross-validated similarity of the sequence defined in terms of the average Hellinger distance between folds.

5.1.3 Results

5.1.3.1 Events ordering

In this section, we report the results of the event-based model (KDE-EBM).

Figure 5.1 shows the model-estimated fine-grained sequence as well as the uncertainty in the sequence, corresponding to cumulative deficits in imaging-based brain volumetric data at term-equivalent-age (TEA). We present event-based model results as positional density heat maps (positional variance diagrams). A positional density heat map shows the posterior distribution of events and their position in the most likely sequence (Fonteijn et al., 2012). In these heat maps, regions with high density correspond to high confidence in the ordering, appearing as a dark diagonal pattern. On the other hand, regions with lower density correspond to lower confidence in the ordering meaning that some events are likely to occur concurrently as far as the model can infer from the input data. Lower confidence corresponds to the off-diagonal blocks/elements of the heat maps.
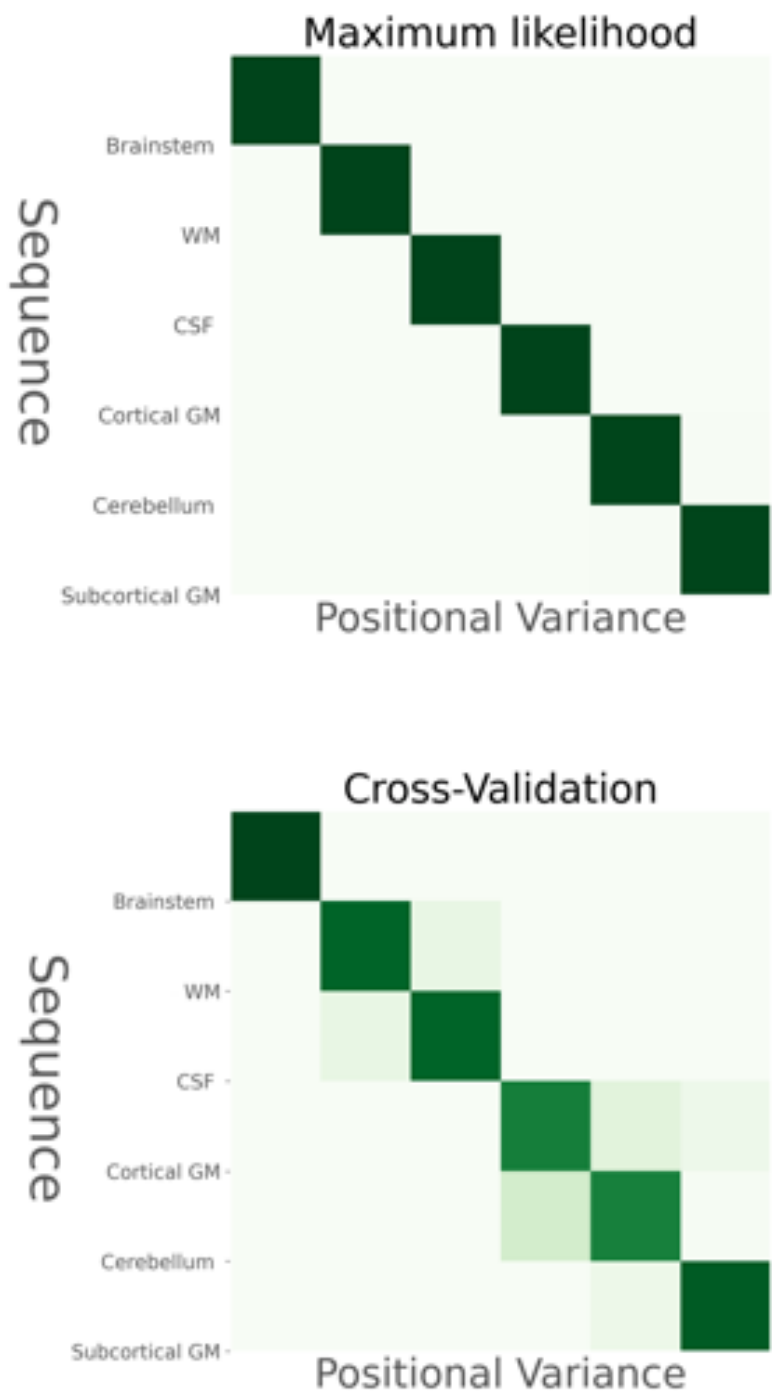
Figure 5.1 – Positional variance diagrams of the event orderings obtained with KDE-EBM. Top: The estimated maximum likelihood sequence of the disease progression in prematurity. Bottom: The cross-validated sequence using 10 stratified folds. Green-white intensity represents the proportion (0 in white, 1 in dark green) of the posterior samples in which events (y-axis) appear in a particular position (x-axis) in the sequence.

We are confident in the robustness of our findings due to the high cross-validation similarity
of the event sequence (CVS = 0.90) as shown in Figure 5.2. Our results suggest that the
tissue volume abnormalities of the white matter (WM) and CSF occur first followed by the
cortical gray matter (cortical GM) and cerebellum, and finally by the subcortical gray matter
(subcortical GM). Additionally, we observe a slight uncertainty in the ordering between cortical
GM and cerebellum, and WM and CSF volumes as shown in Figure 5.1.

To quantify the robustness of the sequence (Figure 5.1), we repeated the estimation of the
model using 10 Stratified K-Folds preserving the percentage of samples (subjects) for each
group. The sequence robustness is shown in Figure 5.2 and it is quantified using the cross-
validated similarity of the sequence defined as the average Hellinger distance between folds,
per event i.e. row of positional variance diagram.

Finally, the individual event probabilities of each input biomarker are presented in the Supple-
mentary Material (see Figure C.2 in Appendix C).

Figure 5.2 – The cross-validation similarity (CVS) of the sequence quantifying the robustness
of the estimated sequence. CVS is defined in terms of the average Hellinger distance ($CVS =
1 - H^2$) across folds per event (row of the position variance heat map).

5.1.4 Discussion

Neurodevelopment is a dynamic process, that can be related to disease progression, charac-
terized by large macroscopic changes where brain abnormality compensation mechanisms
are highly present (brain resilience) (Young et al., 2020; de Silva et al., 2020; Taylor et al., 2019).
Conditions such a preterm birth may change the dynamic process of neurodevelopment and
lead to adverse neurodevelopmental outcomes. In fact, several studies have reported motor,

cognitive, and language difficulties as well as behavioural or attention problems, related to preterm birth (Aarnoudse-Moens et al., 2009; Moore et al., 2012; Larroque, 2004; Barnes-Davis et al., 2020). Furthermore, these deficits may persist throughout childhood and even adolescence and therefore can significantly impact the quality of life of these preterm infants (Mulder et al., 2009; Favrais and Saliba, 2019; Lindstrom et al., 2011). Although cerebral cortex alterations due to prematurity have been previously extensively studied (Dewey et al., 2019; Karolis et al., 2017; Alexander et al., 2019; Gui et al., 2019; de Almeida et al., 2021; Inder, 2005), the exact sequence of brain abnormality underlying preterm birth has never been investigated. Understanding the sequence of biological events along the course of prematurity provides insights into the underlying pathophysiology and can help intervention selection and setup. Thus, early characterization of prematurity progression is extremely important for parent counseling and early intervention to prevent severe delay through resilience.

To our knowledge, this is the first study to characterize the progression signatures of prematurity using a generative, probabilistic, data-driven method. The estimated model sequence of events defines the disease progression of prematurity that is, the fine-grained estimation of brain volumetric abnormality sequence in prematurely-born infants at term-equivalent-age (TEA). The event sequence obtained with the KDE-EBM algorithm showed that brainstem biomarker became abnormal first. The abnormalities of the white matter (WM) and CSF are the next events to occur followed by the cortical gray matter (cortical GM) and cerebellum, and finally by the subcortical gray matter (subcortical GM) biomarker. Moreover, there is a small uncertainty in the ordering between cortical GM and cerebellum, and WM and CSF volumes as shown in Figure 5.1. However, we are confident about our findings given that the estimated sequence is robust as assessed by the cross-validated similarity measure ($CSV = 0.90$).

Higher prevalence corresponds to an earlier position in the estimated sequence. Thus, our findings suggest that the first brain volumetric alterations occur in the brainstem and WM (early events) whereas, volumetric alterations in the cerebellum and subcortical gray matter volumes come last (last events). CSF and cortical GM volumetric alteration are estimated to occur in the middle of the prematurity sequence (between early and last events). A recent study explored the role of cerebellar and brainstem dysfunction in preterm infants compared to full-term newborns. It was reported that premature infants had smaller left and right cerebellar hemispheres and impaired growth of the brainstem compared to the control infants. Furthermore, these alterations in cerebellar and brainstem development persisted at term-equivalent-age. It was thus concluded that prematurity alters the development of the cerebellum and brainstem following early extrauterine exposure (Wu et al., 2020). The brainstem is almost entirely mature at the end of the second / beginning of the third trimester and is responsible for the regulation of heart rate, breathing, sleeping, and eating. It also plays an important role in cardiovascular system control, respiratory control, pain sensitivity control, alertness, awareness, and consciousness (Machado and Brody, 1988; Ikeda et al., 2016; Benarroch, 2018; Fernández-Gil et al., 2010). On the other hand, the cerebellum grows rapidly during late gestation and its surface area is increased 30-fold during the last 15 weeks of gestation. Furthermore, the cerebellum is responsible for the coordination of voluntary movement

(Manto et al., 2011) and abnormalities in this region have been linked to behavioral and social dysfunctions in premature infants survivors (Limperopoulos et al., 2007). Thus, alterations in these key brain regions may lead to adverse behavioural and motor outcomes. Furthermore, larger cortical grey and white matter volumes (CGM, WM) have been associated with better cognitive and language developmental outcomes at 2 years of age in preterm-born children (Kelly et al., 2020) and white matter microstructural alterations have been associated with adverse neurological and behavioural performance at TEA in infants born preterm (Kelly et al., 2018). Moreover, WM, cortical GM, and cerebellum have been shown to be good indicators of neurodevelopmental outcome in preterm infants (Keunen et al., 2016). Therefore, early volumetric alterations of brain regions may contribute to the developmental deficits observed later in life in premature-born children.

The model recovered meaningful progression signatures of prematurity that might be of clinical use allowing more targeted early interventions aiming to restore or even prevent the adverse outcomes observed in preterm-born populations.

5.1.5 Conclusion

In this study, we employed a probabilistic model to unveil, for the first time, the disease progression of prematurity. The estimated ordering of events (sequence) suggested that the first biomarker to become abnormal is the brainstem and white matter whereas the last biomarkers are the cerebellum and the subcortical gray matter. Individually, all these brain volumes have been shown to be altered by prematurity however, there has not been any study that has previously tried to characterize the ordering/sequence (in a probabilistic sense) of these abnormalities. Finally, future research needs to address the reproducibility of the findings in a population of preterm-born children or adults to investigate whether the specific event ordering (disease progression) persists into childhood and/or adulthood, or whether brain resilience and compensation mechanisms have reversed the damage.

Limitations

Modeling neurodevelopment comes with challenges, such as the rapid and diverse changes that occur in early-life brain development as well prematurity brain compensation mechanisms such as brain resilience. This constitutes a major limitation of this study given that there are two underlying assumptions of the model. First, the disease progression is assumed to be monotonic meaning that the change of biomarkers can only be towards abnormality, which represents the disease progression. However, in reality, prematurity is also characterized by brain compensation mechanisms that restore or persist brain damage and abnormality. Second, the disease progression direction is also assumed to be irreversible which again might not be completely true since brain resilience provides a natural way for reversing abnormality. Taken all these into account, the interpretation of these novel findings should be performed with caution.

Supportive Information

All codes used in this study for the disease progression modeling is available on the following repository: https://github.com/seralouk/preterm_ebms_open.

Acknowledgments

5.2 Journal Preprint: A new framework for high-resolution spectral analysis of resting-state fMRI functional connectivity

(Preprint with preliminary results)

Serafeim Loukas[a,b,d], Djalel-Eddine Meskaldji[a,c], Petra S. Hüppi[a], and Dimitri Van De Ville[b,d]

[a] Division of Development and Growth, Department of Pediatrics, University of Geneva, Switzerland
[b] Institute of Bioengineering, Ecole Polytechnique Fédérale de Lausanne (EPFL), Switzerland
[c] Institute of Mathematics, Ecole Polytechnique Fédérale de Lausanne (EPFL), Switzerland
[d] Department of Radiology and Medical Informatics, University of Geneva, Switzerland

Corresponding author at serafeim.loukas@epfl.ch

Abstract

Spectral graph theory has been widely used to explore network characteristics of the functional connectomes at the system level providing novel insights into brain functioning and organization. Recent studies have shown that the human brain is characterized by a large-scale modular and cortical gradient-based organization. However, in most cases, the functional connectome is constructed based on a subjective, non-trivial choice of a predefined brain parcellation scheme due to the high dimensionality of the fMRI data that prohibits the connectomic analysis at the voxel level. In this work, we introduce a framework for the estimation of the Laplacian and the modularity spectrum at the voxel level. We validate our framework on 40 subjects from the Human Connectome Project. Our results indicate the presence of both functional gradients and community structure at the voxel level revealing fine-grained, dominant connectivity patterns (eigenmodes). We show that the spatial configuration of known intrinsic RSNs is not random but instead a natural spatial ordering for these networks is provided by the leading eigenvectors of the Laplacian and modularity matrices. Finally, the proposed framework enables the characterization of the brain's fundamental organizational principles at the voxel level, without the need for a parcellation scheme.

Keywords: *Network science, Modularity, Functional connectivity, Laplacian, Connectomics*

List of notations:

- **A**: matrix, bold capital letter.
- **x**: column vector, bold small letter.
- m or N: scalar, small or capital letter.

5.2.1 Introduction

Resting-state functional magnetic resonance imaging (rs-fMRI) enables the measurement of spontaneous fluctuations of brain activity during rest. These fluctuations are organized in terms of consistent large-scale functional networks across healthy subjects (Damoiseaux et al., 2006). To explore these functional networks, graph and network-based approaches have been traditionally employed. These networks are also known as "connectomes", a representation of the brain wiring, which holds important information related to brain organization and functioning (Sporns et al., 2005; Fornito et al., 2015). Disease propagation patterns are constrained by the highly organized topology of the underlying neural architecture, i.e. the connectome. Therefore, a connectomic approach can be essential to understand neuropathology (Fornito et al., 2015) as well as to explore the topological properties of the underlying network. Each vertex in these networks represents a brain region while each edge reflects the statistical interdependence of two vertices, i.e., the functional connectivity between the brain regions (Sporns, 2011; Bullmore and Sporns, 2009). This interdependence is often measured as the Pearson correlation between the regionally averaged voxel blood-oxygen-level-dependent (BOLD) signals, however, alternative functional connectivity measures such as the cross-correlation, coherence, and accordance/discordance have been also introduced (Mohanty et al., 2020; Meskaldji et al., 2015b).

Over the past decade, the investigation of graph theoretical metrics of the functional connectomes has revealed interesting and important network-related global characteristics of the human brain. The most common local graph metrics that characterize the properties of the individual nodes include the local clustering coefficient, nodal degree, global/local network efficiency, and characteristic average path length (Rubinov and Sporns, 2010). To explore global aspects of the network organization, such as small-world (high clustering coefficient and short path length) (Watts and Strogatz, 1998; Bassett and Bullmore, 2016), rich-hub (van den Heuvel and Sporns, 2011) and scale-free (Eguíluz et al., 2005) underlying organization, averaging of these nodal metrics is often performed to characterize the network as a whole.

Recently, the number of studies employing spectral graph theory in order to explore global brain network characteristics at the system level, and to complement the aforementioned standard graph theoretical metrics, has increased. Spectral graph theory provides novel insights into brain functioning capturing global network aspects that would not have been detected by conventional graph theoretical metrics (Atay et al., 2006). This information is often expressed on the basis of the eigenvectors of fundamental matrices of the underlying network. One such spectral measure is the eigenvector centrality, a measure of the influence

of a node in a network that is based on the leading eigenvector of the adjacency matrix (**A**) (Lohmann et al., 2010; Joyce et al., 2010; Markett et al., 2015). Moreover, the eigenvectors of the graph Laplacian or the modularity matrix have been widely used for graph partitioning and community detection purposes (Newman, 2004; Fortunato, 2010). Graph partitioning refers to the division of the nodes of a network into several groups while keeping the number of edges running between the groups minimal (Newman, 2004). Two widely used methods for graph partitioning is the spectral bisection method (Fiedler, 1973; Chung, 1996; Pothen et al., 1990), which is based on the eigenvectors of the graph Laplacian (**L**) and the modularity-based community detection that is based on the leading eigenvectors of the modularity matrix (**B**) (Newman, 2006b,a). Interestingly, using spectral graph theory approaches, novel insights into the brain topography and function have been reported such as its modular structure (Mahon and Cantlon, 2011; Yeo et al., 2014; Kabbara et al., 2019; Zhigalov et al., 2017; Sporns and Betzel, 2016), its large-scale cortical gradient organization (Margulies et al., 2016) and the existence of connectome harmonics that emerge from the brain's structural connectivity and constrain the functional connectivity of the brain (Atasoy et al., 2016; Naze et al., 2021; Das et al., 2014).

While these studies have provided valuable insights into brain topological organization and function, in most of them, the full dimension of the fMRI data is not exploited due to the high spatial resolution of the fMRI data that prohibits the connectomics analysis at the voxel level ($\sim 10^{10}$ matrix entries considering only brain gray matter voxels $\sim 10^5$). Thus, a whole-brain network-based analysis at the voxel level is usually not feasible. To overcome this limitation, the brain is usually parcellated into a set of regions based on a predefined atlas, or the high dimensional fMRI data are reduced using dimensionality reduction or sampling techniques. However, it should be noted that there is no gold standard solution to this issue and that different parcellations can impact notably the brain network structure and connectome-based metrics (Bellec et al., 2015; Wang et al., 2009; de Reus and van den Heuvel, 2013).

Due to the aforementioned limitations, only a small number of studies have tried to explore the functional connectivity at the voxel level using spectral graph theory approaches. First, Wink and colleagues introduced a framework for the fast computation of the eigenvector centrality (EC) measure of functional networks, enabling the fine-grained analysis of brain hubs (measured by functional connectivity) at the voxel level (Wink et al., 2012). The EC reflects the influence of a node and is defined on the basis of the leading eigenvector of the adjacency matrix. Similarly, other studies have explored the EC of the functional networks at the voxel level, opening a new research window in the neuroscience field (Markett et al., 2015; Lohmann et al., 2010; Joyce et al., 2010). Interestingly, voxel-level eigenvector centrality studies have revealed disease-related changes of functional network properties (McCarthy et al., 2014), and alterations in the known resting-state networks (Buckner et al., 2009). Furthermore, based on the fast eigenvector centrality framework at the voxel level (Wink et al., 2012), Preti et colleagues (Preti and Van De Ville, 2017) provided a technical solution for data-driven analysis of dynamic functional connectivity (dFC) at the voxel level, revealing dFC long-range interactions and fine-scale organization in terms of meaningful brain subdivisions. Therefore, spectral graph theory and connectomics analysis at the voxel level can provide valuable

insights into brain function and organization however, up to date, no study has proposed a solution for the estimation of the laplacian and modularity spectra at the voxel level using resting-state fMRI data.

In this paper, we introduce a novel framework that enables the fast, implicit estimation of the laplacian and modularity spectra at the voxel level exploiting the full dimension of the resting-state fMRI data. To obtain a valid adjacency matrix, we split the resting-state BOLD signals into their positive and negative parts, and we then build two adjacency matrices by individually estimating the covariance of these parts. This is closely related to the accordance and discordance measures that are based on the modeling of the extreme activation-deactivation events/intervals of the brain activity (Meskaldji et al., 2015b).

The present paper is organized as follows. First, we provide a brief overview of the graph partitioning concept using the graph Laplacian (**L**) and modularity matrix (**B**). Next, we describe and formulate our proposed framework for the implicit estimation of both Laplacian and modularity spectra at the voxel level. Furthermore, we validate our framework on a cohort consisting of 40 subjects from the publicly available Human Connectome Project (Human Connectome Project, 2020). Finally, we illustrate that the Laplacian and modularity eigenmodes unveil topological properties of the human brain confirming the presence of both modular and functional gradient organization at the voxel level.

5.2.2   Methods

5.2.2.1   Graph partitioning

The problem of graph partitioning refers to the division of a network's nodes into c groups of approximately equal size, while minimizing the cut size (R) that is, the number of edges that run between nodes of different groups. Traditionally, most graph partitioning approaches are based on iterative bisection i.e., first finding the best division of the network into two groups and then further subdividing those groups until the desired number of groups is reached. One of the most widely used methods for the graph partitioning problem is the spectral bisection method that is based on the eigenvectors of the graph Laplacian matrix (Fiedler, 1973; Barnes, 1982).

The mathematical formulation of the spectral bisection method is derived as follows. Given an undirected network G (graph) with n nodes (vertices), the graph Laplacian matrix is a real, symmetric matrix defined as $\mathbf{L} = \mathbf{D} - \mathbf{A}$ where $\mathbf{A}$ is the adjacency of the network and $\mathbf{D}$ is the degree matrix. We consider a specific partition of the network into two groups encoded by the index vector $\mathbf{s}$ such as $s_i = 1$ and $s_i = -1$ if node i belongs to the first or second group, respectively. The index vector is satisfies the normalization condition $\mathbf{s^T s} = n$. The cut size R

of the partition of the graph can be therefore expressed as (Newman, 2006a; Fortunato, 2010)

$$R = \frac{1}{2} \sum_{\substack{i,j \\ s_i \neq s_j}} a_{i,j} = \frac{1}{2} \sum_{i,j} \left(\frac{1 - s_i s_j}{2} \right) a_{i,j} = \frac{1}{4} \mathbf{s}^\top \mathbf{L} \mathbf{s} \tag{5.2}$$

By expressing the vector $\mathbf{s}$ as a linear combination of the normalized eigenvectors $\mathbf{u_i}$ of $\mathbf{L}$ so that $\mathbf{s} = \sum_{i=1}^{n} w_i \mathbf{u}_i$ with $w_i = \mathbf{u}_i^T \mathbf{s}$, Equation 5.2 becomes

$$R = \sum_{i=1}^{n} w_i^2 \lambda_i, \tag{5.3}$$

where λ_i is the eigenvalue corresponding to eigenvector $\mathbf{u}_i$ of the graph Laplacian matrix ($\mathbf{L}$).

Minimizing the cut size

The minimization of the cut size (R) is equivalent to the minimization of the sum term of the equation 5.3 however, this is a NP-hard problem (Fortunato, 2010). A relaxed solution is provided by the smallest non-zero eigenvector of the graph Laplacian matrix. In more detail, the minimum cut can be achieved by choosing $\mathbf{s}$ to be parallel to the smallest non-zero eigenvector ($\mathbf{u_2}$) which is known as the Fiedler vector (Fiedler, 1973) however, the index vector $\mathbf{s}$ cannot be perfectly parallel to $\mathbf{u_2}$. Instead, by setting $s_i = +1$ if the corresponding element of $\mathbf{u_2}$ is positive and $s_i = -1$ otherwise, the index vector becomes proportional to the Fiedler vector minimizing the sum term (Fortunato, 2010). Finally, the relaxed solution of the minimization problem in the case of k arbitrary groups of nodes is given by choosing the first k eigenvectors of $\mathbf{L}$ that correspond to the smallest non-zero eigenvalues (von Luxburg, 2007).

5.2.2.2 Modularity and Community structure

The main limitation of the spectral bisection method is that it does not provide information about the number of groups/communities that the underlying network should be split into. To overcome this limitation Newman and Girvan (Newman and Girvan, 2004; Newman, 2004) proposed a subdivision method that is based on the quantification of how good a particular division is. A way to quantify the true community structure in a network is the modularity measure (Q) that reflects the number of edges falling within groups minus the expected number in an equivalent network with edges placed at random (Newman and Girvan, 2004; Newman, 2006b). Q can be either positive or negative reflecting the presence of community structure or not, respectively (Newman, 2006b).

The mathematical formulation of modularity is derived in the following way. Given a network G (graph) with n nodes (vertices) and a specific partition of the network into two groups, let $s_i = 1$ and $s_i = -1$ if node i belongs to the first group or to the second group, respectively. Furthermore, the observed number of edges between two nodes i, j is given by the element A_{ij} of the adjacency matrix $\mathbf{A}$ of the network and, at the same time, the expected number

of edges between node i and j is $k_i k_j / 2m$, where $m = \frac{1}{2}\sum_i k_i$ is the total number of unique edges in the network and k_i is the degree of node i (or the strength in the case of a weighted network) (Newman, 2006b). Observing that $\delta(g_i, g_j) = \frac{1}{2}(s_i s_j + 1)$ is equal to 1, if i, j belong to the same group and 0 otherwise, the modularity measure Q is defined as (Newman, 2006b)

$$Q = \frac{1}{4m}\sum_{ij}\left(A_{ij} - \frac{k_i k_j}{2m}\right)(s_i s_j + 1) = \frac{1}{4m}\sum_{ij}\left(A_{ij} - \frac{k_i k_j}{2m}\right)s_i s_j, \qquad (5.4)$$

where $\sum_{ij} A_{ij} = \sum_i k_i = 2m$ and $m = \frac{1}{2}\sum_i k_i$.

The matrix form of the modularity measure (Q) is defined as

$$Q = \frac{1}{4m}\mathbf{s}^T \mathbf{B}\mathbf{s}, \qquad (5.5)$$

where $\mathbf{s}$ is an index vector encoding the grouping information of node s_i for $i = 1,\dots,n$ and $\mathbf{B}$ is the real, symmetric modularity matrix defined as

$$B_{ij} = A_{ij} - \frac{k_i k_j}{M}, \qquad (5.6)$$

where $M = 2m = \sum_{ij} A_{ij}$ is a scalar.

One important property of the modularity matrix $\mathbf{B}$ is that it always has a zero eigenvalue with corresponding eigenvector $\mathbf{1} \in \mathbb{R}^{N\times 1}$ since the elements of each row and column of $\mathbf{B}$ sum to zero (Newman, 2006b). This is also a well-known property of the graph Laplacian matrix.

Finally, by expressing $\mathbf{s}$ as a linear combination of the normalized eigenvectors u_i of $\mathbf{B}$ so that $\mathbf{s} = \sum_{i=1}^{n} w_i \mathbf{u}_i$ with $w_i = \mathbf{u}_i^T \mathbf{s}$, the modularity measure (Q) can be written as

$$Q = \frac{1}{4m}\sum_i w_i \mathbf{u}_i^T \mathbf{B}\sum_j w_j \mathbf{u}_j = \frac{1}{4m}\sum_{i=1}^{N}\left(\mathbf{u}_i^T \mathbf{s}\right)^2 \lambda_i, \qquad (5.7)$$

where $\lambda_i = \frac{\mathbf{u}_i^T \mathbf{B}\mathbf{u}_i}{\mathbf{u}_i^T \mathbf{u}_i}$ is the eigenvalue of modularity matrix $\mathbf{B}$ corresponding to the eigenvector $\mathbf{u}_i$. Note that, assuming normalized eigenvectors, we have $\lambda_i = \mathbf{u}_i^T \mathbf{B}\mathbf{u}_i$.

Maximizing the modularity

The maximization of the modularity Q of a given network as defined in Eq. 5.7, involves the selection of the largest (most positive) eigenvalue λ_1 of $\mathbf{B}$ and the maximization of the dot product $\mathbf{u}_1^T \mathbf{s}$ where $\mathbf{u}_1$ is the leading eigenvector of $\mathbf{B}$ with corresponding eigenvalue λ_1. It should be noted that the index vector $\mathbf{s}$ cannot be constructed to be parallel to $\mathbf{u}_1$ but the maximum is achieved by setting $s_i = +1$ if the corresponding element of $\mathbf{u}_1$ is positive and $s_i = -1$ otherwise (when $\mathbf{s}$ is proportional to $\mathbf{u}_1$). Thus, by estimating the leading eigenvector of the modularity matrix $\mathbf{B}$, the signs of its elements provide a nodal grouping (network split)

that maximizes the modularity measure Q. Finally, the presence of positive eigenvalues of **B** signifies community structure in the underlying network (Newman, 2006b).

More than two communities

The previous section refers to the case where the modularity Q is maximized for a given split of the network into two groups of nodes however, real-world networks are often characterized by more than two communities. In that case, given an index matrix **S** with dimension $[N, C]$ where each column contains an index vector with elements in $[0, 1]$ range such as $s_{ij} = 1$ if vertex i belongs to community j or 0 otherwise, the kronecker δ is now defined as $\delta\left(g_i, g_j\right) = \sum_{k=1}^{c} S_{ik} S_{jk}$ and the modularity Q for a specific division of the network is

$$Q = \frac{1}{2m} \sum_{i,j=1}^{N} \sum_{k=1}^{C} B_{ij} S_{ik} S_{jk} = \frac{1}{2m} \operatorname{tr}\left(\mathbf{S}^T \mathbf{B} \mathbf{S}\right) = \frac{1}{2m} \sum_{j=1}^{N} \sum_{k=1}^{C} \left(\mathbf{u}_j^T \mathbf{s}_k\right)^2 \lambda_j, \tag{5.8}$$

where $\mathbf{u_j}$ is an eigenvector of the modularity matrix **B** with corresponding eigenvalue λ_j (Newman, 2006a).

The maximization of Q is achieved by spectral clustering using the eigenvectors of the **B** with the largest positive eigenvalues (Newman, 2006a).

5.2.2.3 Proposed framework & mathematical formulation

Functional connectome definition

Previous fMRI studies employed spectral graph theory approaches at the voxel level exploiting the fact that the functional connectivity (FC) matrix (adjacency matrix) can be expressed in a matrix form using the Pearson correlation as $\mathbf{C} = \mathbf{X}\mathbf{X}^\mathbf{T}/(T-1)$ with T being the number of time-points and assuming z-scored voxel time-series stored in the rows of **X** (Wink et al., 2012; Preti and Van De Ville, 2017). This enables the fast spectral estimation of the adjacency matrix using iterative power methods and by performing the operations from right to left, avoiding the explicit matrix multiplication that would generate **C**. However, such an approach would not be valid for the laplacian and modularity spectral estimation since the adjacency matrix (i.e. the FC matrix) would include both positive and negative values and thresholding procedures cannot be performed without explicitly constructing the FC matrix, which cannot be done due to the high dimension of the data. To overcome this problem, we propose to split the resting-state BOLD signals into their positive and negative parts, and we define (implicitly) two adjacency matrices by estimating the covariance of these parts.

Formally, let $\mathbf{X} \in \mathbb{R}^{N \times T}$ be a set of normalized ($\mu = 0, \sigma = 1$) voxel time-courses, where N is the number of brain gray matter voxels and T is the length of the time-course (time-points). We first define two new matrices $\mathbf{X_u} \in \mathbb{R}^{N \times T}$ and $\mathbf{X_l} \in \mathbb{R}^{N \times T}$ with row vectors defined as $\mathbf{x^u} = \{x_t^u, t = 1, \dots, T, x_t^u = x_t \text{ if } x_t \geq 0\}$ and $\mathbf{x^l} = \{x_t^l, t = 1, \dots, T, x_t^l = x_t \text{ if } x_t < 0\}$ being the upper and

lower thresholded vectors of the normalized time-course $\mathbf{x}$ of length T. Thus, it holds that $\mathbf{X} = \mathbf{X_u} + \mathbf{X_l}$.

We express the functional connectome by splitting the Pearson correlation as follows

$$
\begin{aligned}
\mathbf{C} = \frac{\mathbf{X}\mathbf{X}^T}{T-1} &= \frac{(\mathbf{X_u} + \mathbf{X_l})(\mathbf{X_u} + \mathbf{X_l})^T}{T-1} \\
&= \frac{(\mathbf{X_u}\mathbf{X_u}^T + \mathbf{X_l}\mathbf{X_l}^T + \mathbf{X_u}\mathbf{X_l}^T + \mathbf{X_l}\mathbf{X_u}^T)}{T-1} \\
&= \frac{(\mathbf{X_u}\mathbf{X_u}^T + \mathbf{X_l}\mathbf{X_l}^T)}{T-1} + \frac{(\mathbf{X_u}\mathbf{X_l}^T + \mathbf{X_l}\mathbf{X_u}^T)}{T-1} = \mathbf{A_{cc}} + \mathbf{D_{isc}}.
\end{aligned}
\tag{5.9}
$$

The accordance matrix ($\mathbf{A_{cc}}$) reflects co-activations/co-deactivations between the brain regions, contributing to the positive correlations in FC, whereas the discordance matrix ($\mathbf{D_{isc}}$) reflects opposition in co-activation and co-deactivation, contributing to negative correlations in FC. These two matrices disentangling coupling and anti-coupling events, respectively and are used as undirected, weighted adjacency matrices as described in the following sections.

The range of the values of the $\mathbf{A_{cc}}$ and $\mathbf{D_{isc}}$ matrices are $[0, 1]$ and $[-1, 0]$, respectively, and the signs of $\mathbf{D_{isc}}$ can be flipped using $-\mathbf{D_{isc}}$. Additionally, the two matrices can be written in a matrix form as expressed in equation 5.9 allowing fast, non-explicit computations as described in the following section. Finally, this approach is closed related to the accordance and discordance measures that are based on the modeling of extreme activation-deactivations of the brain activity (Meskaldji et al., 2015b,a).

Laplacian and Modularity definition at the voxel level

Laplacian

The symmetric, normalized Laplacian ($\mathbf{L}_{sym}$) matrix using $\mathbf{A_{cc}}$ as adjacency matrix is defined as

$$
\mathbf{L}_{sym} = \mathbf{D}^{-\frac{1}{2}}\mathbf{L}\mathbf{D}^{-\frac{1}{2}} = \mathbf{I} - \mathbf{D}^{-\frac{1}{2}}\mathbf{A_{cc}}\mathbf{D}^{-\frac{1}{2}},
\tag{5.10}
$$

where $\mathbf{A_{cc}}$ is the accordance matrix defined in Eq. 5.9 and $\mathbf{D}$ is the strength diagonal matrix defined as

$$
diag(\mathbf{D}) = \mathbf{A_{cc}}\mathbf{1} = \frac{\mathbf{X_u}\mathbf{X_u}^T}{T-1}\mathbf{1} + \frac{\mathbf{X_l}\mathbf{X_l}^T}{T-1}\mathbf{1}.
\tag{5.11}
$$

Similarly, the graph Laplacian matrix ($\mathbf{L}_{sym}$) using $\mathbf{D_{isc}}$ as adjacency matrix (see Eq. 5.9) can be formulated.

Modularity

The modularity matrix ($\mathbf{B}$) using $\mathbf{A_{cc}}$ as adjacency matrix is defined as

$$
\mathbf{B} = \mathbf{A_{cc}} - \frac{\mathbf{k}\mathbf{k}^T}{M},
\tag{5.12}
$$

where $M = 2m = \sum_i k_i = \sum(\mathbf{A_{cc}} \mathbf{1})$ is a scalar, and $\mathbf{k}$ is the strength vector defined as

$$\mathbf{k} = \mathbf{A_{cc}} \mathbf{1} = \frac{\mathbf{X_u X_u}^T}{T-1} \mathbf{1} + \frac{\mathbf{X_l X_l}^T}{T-1} \mathbf{1}, \tag{5.13}$$

with $\mathbf{1}$ being a column vector with all ones.

Using Eq. 5.9 and Eq. 5.13, the modularity matrix $\mathbf{B}$ using accordance matrix as adjacency can be expressed as

$$\mathbf{B} = (\frac{\mathbf{X_u X_u}^T}{T-1} + \frac{\mathbf{X_l X_l}^T}{T-1}) - \frac{(\frac{\mathbf{X_u X_u}^T}{T-1} \mathbf{1} + \frac{\mathbf{X_l X_l}^T}{T-1} \mathbf{1})(\frac{\mathbf{X_u X_u}^T}{T-1} \mathbf{1} + \frac{\mathbf{X_l X_l}^T}{T-1} \mathbf{1})^T}{M}. \tag{5.14}$$

Similarly, the modularity matrix ($\mathbf{B}$) using $\mathbf{D_{isc}}$ as adjacency matrix (see Eq. 5.9) can be formulated.

Estimation of the spectra

Laplacian

To estimate the spectrum (eigenvalues λ and eigenvectors $\mathbf{v}$) of the symmetric, normalized Laplacian matrix ($\mathbf{L}_{sym}$) we express the eigendecomposition problem as follows

$$\begin{aligned} \mathbf{L}_{sym}\mathbf{v} &= \lambda\mathbf{v}, \\ (\mathbf{I} - \mathbf{D}^{-\frac{1}{2}}\mathbf{A_{cc}}\mathbf{D}^{-\frac{1}{2}})\mathbf{v} &= \lambda\mathbf{v}, \\ \mathbf{Iv} - \mathbf{D}^{-\frac{1}{2}}\mathbf{A_{cc}}\mathbf{D}^{-\frac{1}{2}}\mathbf{v} &= \lambda\mathbf{v}, \end{aligned} \tag{5.15}$$

with $\mathbf{A_{cc}}$ being the accordance matrix as defined in Eq. 5.9.

The operations are performed from right to left, avoiding matrix multiplications. Thus, only matrix-vector products are involved in the estimation. Note that $\mathbf{D}^{-\frac{1}{2}}$ is a diagonal matrix and thus, the dot product $\mathbf{D}^{-\frac{1}{2}}\mathbf{v}$ in Eq. 5.15 is equivalent to a vector-vector multiplication. Thus, we express $\mathbf{D}^{-\frac{1}{2}}$ as a column vector by first estimating the strength vector (see Eq. 5.11) and then taking the square root and inverting it. Next, the product $\mathbf{D}^{-\frac{1}{2}}\mathbf{v}$ results in a vector that is going then to be multiplied by $\mathbf{A_{cc}}$ (see Eq. 5.9) performing the operations from right to left. Finally, it is trivial that $\mathbf{Iv} = \mathbf{v}$.

The eigendecomposition problem of the normalized Laplacian matrix using $-\mathbf{D_{isc}}$ as the adjacency matrix can be formulated similarly.

Modularity

Similarly, to estimate the spectrum (eigenvalues λ and eigenvectors $\mathbf{v}$) of the modularity matrix

(**B**) we express the eigendecomposition problem as follows

$$\mathbf{B}\mathbf{v} = \lambda\mathbf{v},$$

$$(\mathbf{A_{cc}} - \frac{\mathbf{k}\mathbf{k}^T}{M})\mathbf{v} = \lambda\mathbf{v}, \tag{5.16}$$

$$\mathbf{A_{cc}}\mathbf{v} - \frac{\mathbf{k}\mathbf{k}^T}{M}\mathbf{v} = \lambda\mathbf{v},$$

with

$$\mathbf{A_{cc}}\mathbf{v} = \frac{\mathbf{X_u}\mathbf{X_u}^T}{T-1}\mathbf{v} + \frac{\mathbf{X_l}\mathbf{X_l}^T}{T-1}\mathbf{v}. \tag{5.17}$$

and

$$\frac{\mathbf{k}\mathbf{k}^T}{M}\mathbf{v} = \frac{(\frac{\mathbf{X_u}\mathbf{X_u}^T}{T-1}\mathbf{1} + \frac{\mathbf{X_l}\mathbf{X_l}^T}{T-1}\mathbf{1})(\frac{\mathbf{X_u}\mathbf{X_u}^T}{T-1}\mathbf{1} + \frac{\mathbf{X_l}\mathbf{X_l}^T}{T-1}\mathbf{1})^T}{M}\mathbf{v}. \tag{5.18}$$

All the terms in Eq. 5.17 and Eq. 5.18 are computed from right to left avoiding matrix multiplications. For instance, in Eq. 5.18 we start with $\mathbf{k}$ (see also Eq. 5.13) by first estimating the term $\mathbf{X_l^T}\mathbf{1}$ which results in a vector and we then continue performing the operations from right to left, to eventually obtain the strength vector $\mathbf{k}$. Having estimated $\mathbf{k}$, the operation $\mathbf{k^T}\mathbf{v}$ results in a scalar and $\mathbf{k}(\mathbf{k^T}\mathbf{v})$ is a multiplication of a vector with a scalar. Similarly, to estimate the term $\mathbf{A_{cc}}\mathbf{v}$ in Eq. 5.17 we first start by estimating the term $\mathbf{X_l^T}\mathbf{v}$ which is a matrix-vector multiplication resulting in a vector and we then proceed with $\mathbf{X_l}(\mathbf{X_l^T}\mathbf{v})$ etc.

Finally, the eigendecomposition problem of the modularity matrix (**B**) using $\mathbf{D_{isc}}$ as the adjacency matrix can be formulated similarly.

In this study we used the ARPACK library in Python 3.8 to estimate a subset of the spectra in a fast, iterative way; we chose $M = 1000$ (ARPACK Software, 2020).

5.2.2.4 Framework validation

To validate the proposed framework we used data from the publicly accessible Human Connectome Project data release.

Subjects and fMRI Acquisition

In the present study we included $n = 40$ healthy subjects from the Human Connectome Project (Essen et al., 2013) 900 subjects release (S900, HCP, Human Connectome Project (2020)). All experiments were reviewed and approved by the local institutional ethical committee (Swiss Ethics Committee of human research). Informed consent forms, including consent to share anonymized data, were collected for all subjects (within the HCP project) and were approved by the Washington University institutional review board. All methods were carried out in accordance with relevant guidelines and regulations. Subjects were selected from the HCP S900 data release based on the following criteria: Age between 31 and 35 years old, cognitive MMSE status >28 and image reconstruction information = 3T MR r227.

Both runs of the two resting-state gradient-echo EPI sequences (1200 frames per run, TR = 720 ms, TE = 3.31 ms, flip angle = 52 deg, FOV = 208 × 180 mm, voxel size = 2 mm isotropic, multiband factor = 8) (Moeller et al., 2010; Feinberg et al., 2010; Setsompop et al., 2011) as well as the structural 3D MPRAGE T1-weighted sequence (TR = 2400 ms, TE = 2.14 ms, TI = 1000, flip angle = 8 deg, FOV = 224 × 224 mm, voxel size = 0.7 mm isotropic) were included in the analysis presented in this paper.

Preprocessing

The HCP public data release includes neuroimaging data that are already minimally pre-processed. In more detail, the data have been aligned across modalities (functional and structural) and have been wrapped across all subjects to the Montreal Neurological Institute (MNI) standard space using appropriate volume-based and surface-based registration methods. Spatial distortions were also minimized (Glasser et al., 2013). Additionally, we applied spatial smoothing on the functional volumes (using a Gaussian kernel of FWHM = 5 mm) using SPM12 (Statistical Parametric Mapping, 2020). The first ten volumes were discarded to ensure steady-state magnetization of the fMRI signals, resulting in T = 1190 time-points (functional volumes) per run for further analysis.

Voxel-wise time-courses were detrended (by removing linear and quadratic trends) and nuisance variables were regressed out using the DPARSF toolbox (Yan, 2010). The nuisance regression procedure included the six motion parameters (3 for rotation and translation, respectively) and the average white matter (WM) and cerebrospinal fluid (CSF) signals, obtained from standard white matter and ventricular masks mapped to the subjects' fMRI space and masked with the individual segmentation maps (Leonardi et al., 2013). The voxel-wise time-courses were finally band-pass filtered (range [0.015–0.15 Hz]) to preserve resting-state related fluctuations and discard noise components. Finally, to restrict the analysis to brain voxels that belong exclusively to the gray matter (GM), the SPM12 GM tissue probability map (TPM) was first thresholded by removing voxels with low probability belonging to the GM tissue (P(GM voxel) <0.25) ensuring a fine-grained GM coverage of the brain. Next, the GM mask was resliced to the fMRI BOLD space resolution in order to extract GM voxel-wise time-courses for each subject. The GM mask used in the present study is shown in Fig. 5.3. In this study, the number of GM voxels is $N = 159'459$. The aforementioned preprocessing procedure was identical for both resting-state runs.

Group-level spectral estimation at the voxel level

Having obtained the preprocessed, z-scored, time-courses at the voxel level for each subject and run, a group-level matrix $\mathbf{X_G}$ was constructed by concatenating the voxel-wise time-courses across subjects and runs. The group-level matrix, $\mathbf{X_G} \in \mathbb{R}^{N \times T}$ (with $N = 159'459$ voxels and $T = n \times 2 \times$ run's timepoints $= 40 \times 2 \times 1190$) was used to construct the matrices $\mathbf{X_u}, \mathbf{X_l}$ as described in Section 5.2.2.3. Fig. 5.4 summarizes the whole procedure. Finally, the dimension of these two matrices is the same as $\mathbf{X_G}$.
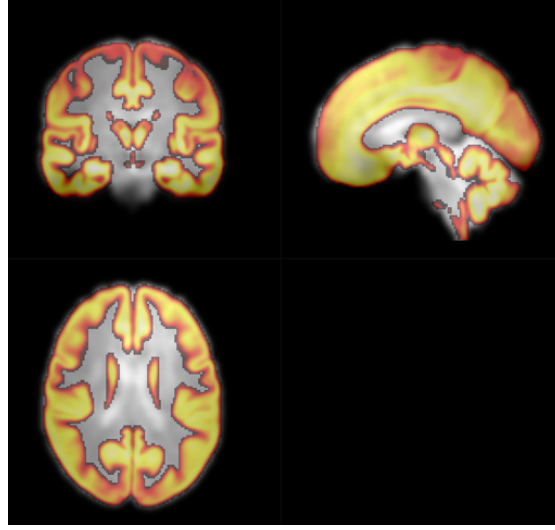
Figure 5.3 – The gray matter (GM) mask used in the present study, resliced and overlaid on the functional volume of a single subject for visualization purposes. Using this mask, the number of GM voxels is $N_{voxels} = 159'459$ per subject and run.

Using these matrices we can define the Accordance and Discordance ($\mathbf{A_{cc}}, \mathbf{D_{isc}}$) matrices as defined in Eq. 5.9 and finally, the normalized Laplacian and modularity matrices (see Eq. 5.10 and Eq. 5.12). However, in reality none of these matrices were built explicitly. On the contrary, using the proposed framework for the non-explicit estimation of the spectra (see Eq. 5.15 and Eq. 5.16 in section 5.2.2.3), we estimated a subset of the laplacian and modularity spectra in two different cases: first, when the adjacency matrix was the Accordance matrix ($\mathbf{A_{cc}}$) and second, when the adjacency matrix was the Discordance matrix ($\mathbf{D_{isc}}$).

The subsets of the spectra were estimated using the ARPACK library (ARPACK Software, 2020) and choosing $M = 1000$. For the normalized Laplacian matrix, we estimated the M smallest and largest eigenvectors for the case of $\mathbf{A_{cc}}$ and $\mathbf{D_{isc}}$, respectively. Discordance captures anti-coupling in brain activity and thus, in that case, we focused on the bipartite structure that can be recovered from the spectrum. For the modularity matrix, we estimated the M leading positive (reflecting community structure) and negative eigenvectors for the case of $\mathbf{A_{cc}}$ and $\mathbf{D_{isc}}$, respectively. We opted for the most negative eigenvectors when Discordance was used as the adjacency to recover anti-modular information that is encoded in the spectrum (Newman, 2006b). We ended up with four matrices $\mathbf{U_{acc}^L}$, $\mathbf{U_{disc}^L}$, $\mathbf{U_{acc}^B}$, $\mathbf{U_{disc}^B}$ with dimension $[N, M]$, where $N = 159'459$ voxels and $M = 1000$, with columns being the laplacian and modularity eigenvectors, respectively.
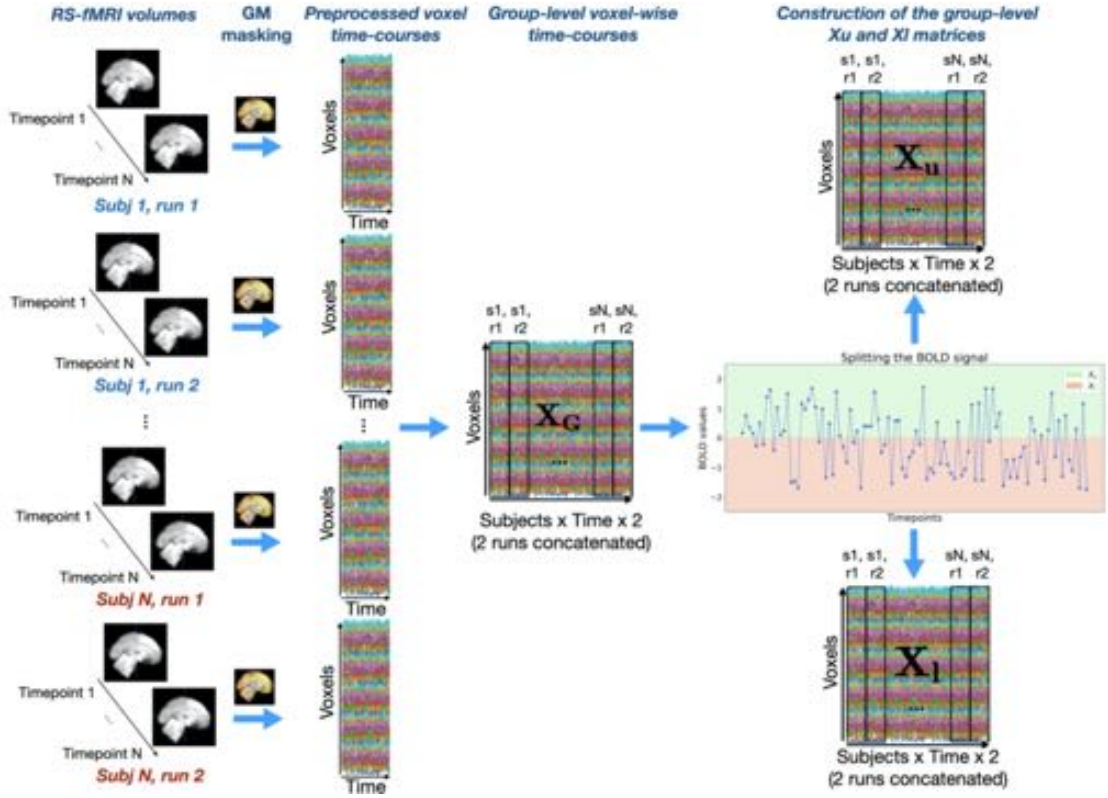
Figure 5.4 – Framework's pipeline. The group-level matrix ($\mathbf{X_G}$) was constructed by concatenating the z-scored voxel-wise time-courses across subjects and time. Next, the BOLD signals were split into their positive and negative parts to build the ($\mathbf{X_u}$) and ($\mathbf{X_l}$) matrices. Finally, these matrices were used for the spectral analysis at the voxel level as described in section Proposed framework & mathematical formulation.

Exploring the spectra

Laplacian and modularity similarities

To explore similarities and differences between the estimated Laplacian ($\mathbf{U^L_{acc}}$, $\mathbf{U^L_{disc}}$) and modularity ($\mathbf{U^B_{acc}}$, $\mathbf{U^B_{disc}}$) spectra at the voxel level, we used the cosine similarity metric. The cosine similarity (CS) of two arbitrary vectors $\mathbf{a}$ and $\mathbf{b}$ is defined as:

$$CS = \cos(\theta) = \frac{\mathbf{ab}}{\|\mathbf{a}\|\|\mathbf{b}\|} = \frac{\sum_{i=1}^{n} a_i b_i}{\sqrt{\sum_{i=1}^{n} a_i^2}\sqrt{\sum_{i=1}^{n} b_i^2}}, \tag{5.19}$$

where a_i and b_i are components of the vectors $\mathbf{a}$ and $\mathbf{b}$, respectively.

The range of the cosine similarity is $[-1, 1]$. For two vectors that are pointing in the same direction CS is 1, while for vectors pointing in opposite directions the CS is -1. Finally, orthogonal vectors have CS equal to 0.

Spatial configuration of large-scale networks

Finally, we investigated whether the estimated leading eigenmodes are associated with the intrinsic spatial configuration of known resting-state networks (RSNs). To this end, we used the seven and seventeen-network Yeo parcellations (Yeo et al., 2011) to examine the network's spatial arrangement with respect to the estimated brain eigenmodes.

5.2.3 Results

5.2.3.1 Group-level spectra at the voxel level

Using the proposed framework (as described in section 5.2.2.4), we estimated a subset ($M =$ 1000) of the Laplacian and modularity spectra at the voxel level in two different cases: first, when the adjacency matrix was the Accordance matrix ($\mathbf{U}_{\mathbf{acc}}^{\mathbf{L}}$ and $\mathbf{U}_{\mathbf{acc}}^{\mathbf{B}}$) and second when the adjacency matrix was the Discordance matrix ($\mathbf{U}_{\mathbf{disc}}^{\mathbf{L}}$ and $\mathbf{U}_{\mathbf{disc}}^{\mathbf{B}}$). The average computation time was $13.8 \pm 0.5h$ on an Ubuntu 18.04.2 LTS system (with 503G MEM and 96 Intel(R) Xeon(R) Platinum 8160 CPU(s) @ 2.10GHz). In the case of the Laplacian spectrum using Accordance as adjacency, the first eigenvector $\mathbf{v_1} = \mathbf{D}^{\frac{1}{2}}\mathbf{1}$ with corresponding eigenvalue $\lambda_1 = 0$ was excluded from further analysis. The scree plots for the aforementioned cases are presented in Fig. 5.5. Moreover, the leading eigenvectors of the Laplacian and modularity matrices are presented in Fig. C.4 and Fig. C.3 in Appendix C.

To investigate similarities and differences between the estimated Laplacian and modularity spectra at the voxel level, we used the cosine similarity metric as described in section 5.2.2.4. The absolute values of the cosine similarity between the eigenvector matrices $\mathbf{U}_{\mathbf{acc}}^{\mathbf{B}}$ and $\mathbf{U}_{\mathbf{acc}}^{\mathbf{L}}$ as well as between $\mathbf{U}_{\mathbf{disc}}^{\mathbf{B}}$ and $\mathbf{U}_{\mathbf{disc}}^{\mathbf{L}}$ are presented in Fig. 5.6 (a) and (b), respectively. Finally, the cosine similarities between $\mathbf{U}_{\mathbf{acc}}^{\mathbf{B}}$ and $\mathbf{U}_{\mathbf{disc}}^{\mathbf{B}}$, and $\mathbf{U}_{\mathbf{acc}}^{\mathbf{L}}$ and $\mathbf{U}_{\mathbf{disc}}^{\mathbf{L}}$ are shown in Fig. C.5 in Appendix C.
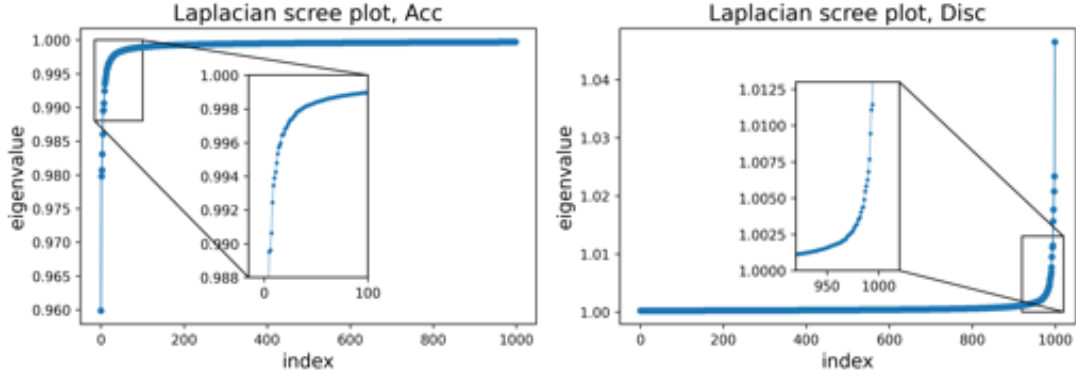
(a) Scree plot of $\mathbf{L}_{sym}$ using A_{cc} and D_{isc}
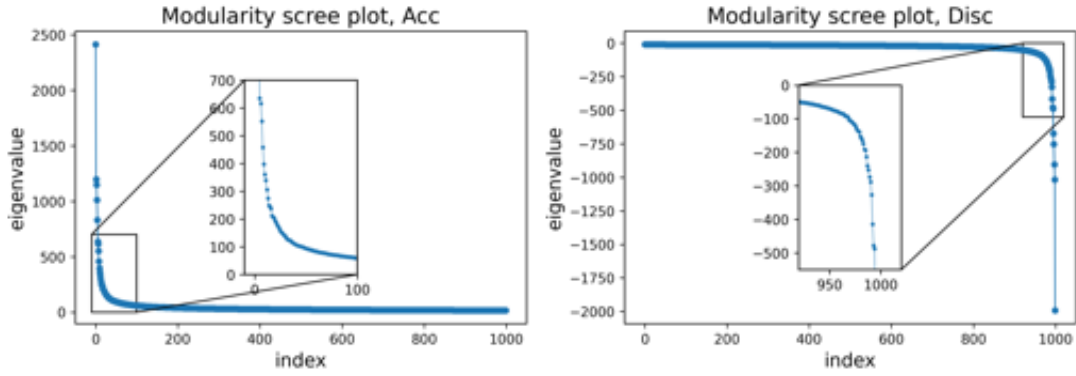
(b) Scree plot of $\mathbf{B}$ using A_{cc} and D_{isc}

Figure 5.5 – The scree plots of the Laplacian (a) and modularity (b) spectra using Accordance (left) and Discordance (right) as adjacency, respectively. In the case of Laplacian with Accordance, the smallest eigenvalue i.e. $\lambda_1 = 0$ is discarded for visualization purposes.

Finally, we examined the relationship between the spatial arrangement of the seven Yeo RSNs and the estimated Laplacian and modularity leading eigenmodes. Fig. 5.7 illustrates that there is indeed a relationship and that the spatial configuration of the seven Yeo RSNs is not random with respect to the estimated Laplacian and modularity leading eigenvectors. Similarly, the results for the seventeen-network Yeo parcellation are presented in Fig. C.6 in Appendix C.
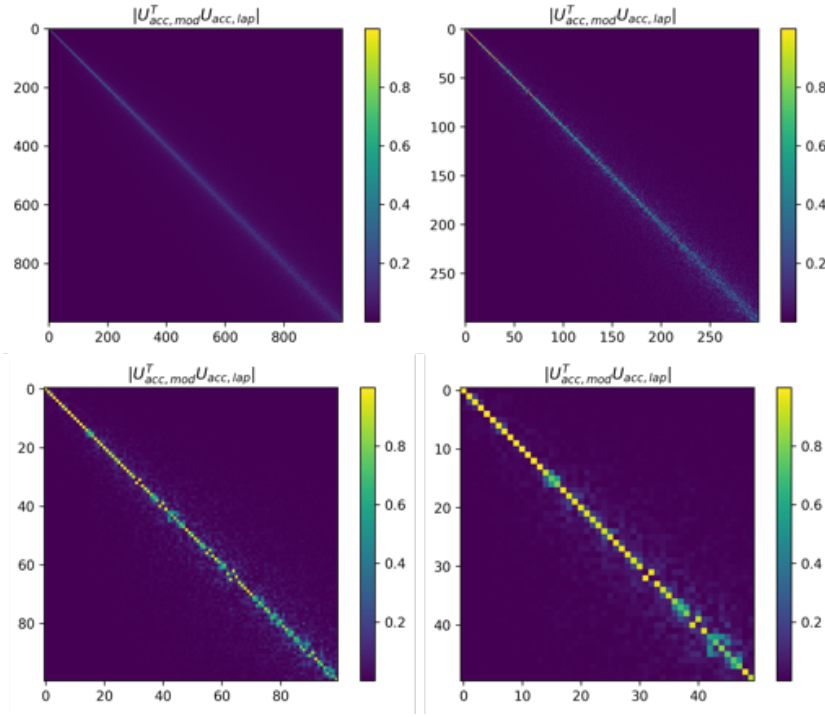
(a) Absolute value of the cosine similarity between U_{acc}^B, U_{acc}^L
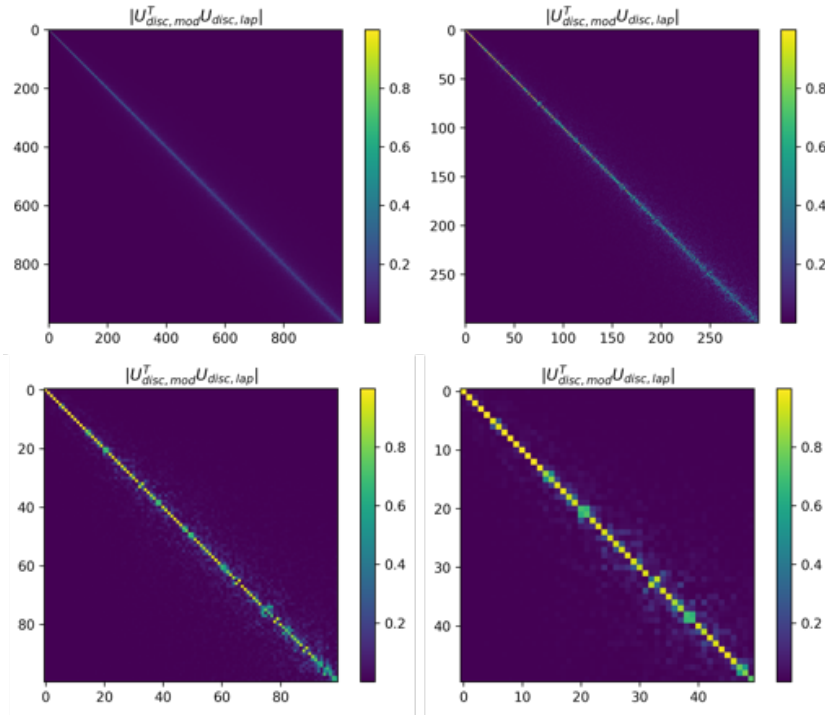
(b) Absolute value of the cosine similarity between U_{disc}^B, U_{disc}^L

Figure 5.6 – Cosine similarity between the spectra: (a) and (b) show the absolute value of the cosine similarity of the eigenvectors when the adjacency was the Accordance or Discordance matrix, for the Laplacian and modularity matrix, respectively.
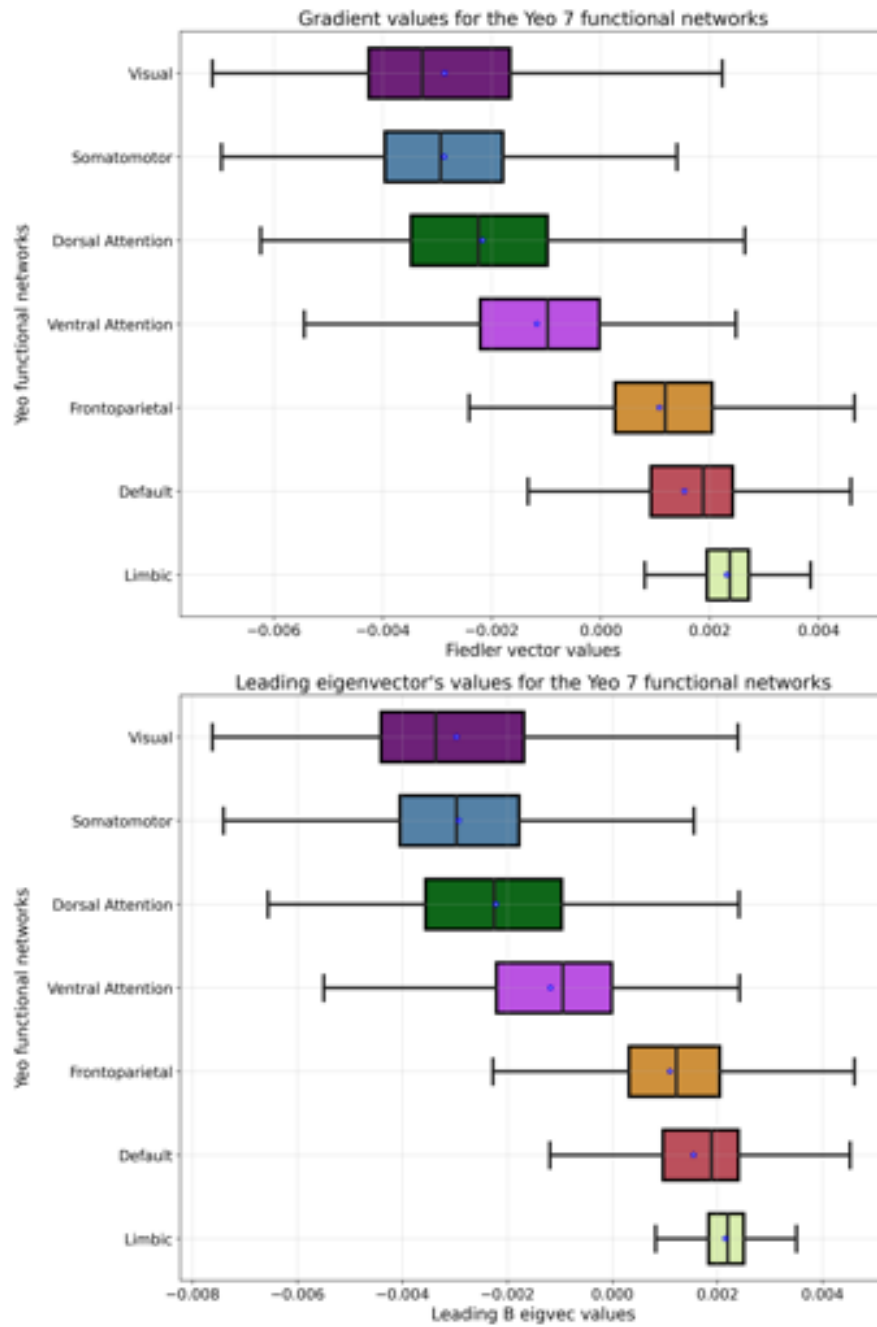
Figure 5.7 – The Laplacian principle gradient's values (top) and the modularity leading eigenvector's values (bottom) for each of the seven Yeo resting-state networks. For the sake of simplicity, here we visualize only the results based on the Accordance as adjacency matrix. The asterisks represent mean values. Colors represent the exact same colors used to describe the networks in Yeo et al. (2011).

5.2.4 Discussion

It is known that the spontaneous fluctuations of brain activity during rest form consistent large-scale functional networks with specific spatial configuration across healthy subjects (Damoiseaux et al., 2006; Yeo et al., 2011). Moreover, each of these resting-state networks (RSNs) has been characterized by a unique functional profile (functional specialization) (Smith et al., 2009). This specialization has been shown to range from basic primary functions (e.g., movement and auditory/visual perception) to higher-order cognitive control (e.g., attention control, working memory demand) (Smith et al., 2009; Petrides, 2005; Rossi et al., 2008; Cole et al., 2012), to finally, even more, abstract demand-free cognitive states such as mind-wandering (Raichle, 2015).

While the spatial configuration (topography) of these RSNs has been previously accurately described (Damoiseaux et al., 2006; Yeo et al., 2011), only recently studies have tried to explore the principles underlying this spatial configuration and its relation to function for each network. Using a diffusion embedding technique that captures the differentiation of functional connectivity patterns, a principal large-scale gradient of organization in the human cortical surface has been recently described (Margulies et al., 2016). This gradient extended between primary unimodal sensorimotor areas and transmodal association regions (i.e., regions of the DMN) and it was related to the intrinsic geometry of the cortex, as well as to the spatial arrangement of the well-known RSNs (Margulies et al., 2016). Thus, this gradient provided a functional organizational principle that expanded between sensorimotor and transmodal regions. However, in that study the compressed group-averaged connectome derived via group-PCA was used and the data were sampled onto a cortical surface with approximately 32'000 nodes after zeroing out negative values explicitly. Moreover, only approximately 300 leading eigenvectors were estimated. In the same context, using seed-based connectivity and a multidimensional scaling technique, it has been shown that the intrinsic functional connectivity of the human brain is organized as three main interdependent gradients (Zhang et al., 2019). The first functional gradient was found to capture a functional contrast between regions that are involved in processing external and internal information. The second gradient captured a contrast between regions implicated in attention modulation and content representation, while the third gradient was characterized by a structural contrast between spatially central and peripheral nodes. Moreover, an interdependence of these connectivity gradients was revealed (Zhang et al., 2019).

While these studies have provided valuable insights into the brain topological organization, the full dimension of the neuroimaging data has not been exploited due to the high spatial resolution of the fMRI data that prohibits connectomic and spectral graph theory analyses at the voxel level. Importantly, studies employing brain parcellation schemes to reduce the dimension of the data assume that the brain can indeed be separated by sharp and strict boundaries. Furthermore, methods that have explored the brain's large-scale cortical organization, such as the diffusion embedding approach, imply smooth underlying structure (Margulies et al., 2016; Huntenburg et al., 2018).

Here, we proposed a novel framework that enables the fast, implicit estimation of the graph Laplacian and modularity spectrum at the voxel level exploiting the full dimension of the resting-state fMRI data. The Laplacian and modularity are the theoretically optimal for the 'gradient-based' and 'specialization' organization principles, respectively, that have been previously described in the literature (Wang et al., 2014; Margulies et al., 2016; Smith et al., 2009; Zeki et al., 1991). In the present study, we explored these two fundamental organizational principles via spectral graph theory at the voxel level.

Even though the eigenvectors of the Laplacian and modularity matrices provide optimal solutions to different optimization problems – namely to the minimization of NCut and maximization of the modularity Q, respectively – our results show that the two spectra at the voxel level are virtually identical (see Fig. 5.6). This similarity is also depicted on the spacial configuration of the leading Laplacian and modularity eigenmodes (see Fig. C.3 and Fig. C.4 in Appendix C). These findings suggest the presence of strong community organization at the voxel level that results in large edge count within communities and small between them, defining in that way, a gradient that is captured by the Laplacian eigenmodes. In other words, these gradients (that gradually reduce as we move away from the center of a community towards the gap between communities) agree with the corresponding modularity splits and capture voxels that agree in terms of the spatial distribution of the connectivity values. Therefore, based on your results, both types of organization are present at the voxel level.

Additionally, the smoothness of the leading eigenvectors of the Laplacian matrix (see Fig. C.3) provides more evidence of the presence of functional gradients at the voxel level. If gradients were not present in the underlying network, the Laplacian eigenmodes would not be expected to be smooth. Similarly, the modularity eigenmodes provide meaningful community-based splits assembling known RSNs, such as the DMN, visual, auditory, and fronto-parietal networks (see Fig. C.7).

Moreover, Fig. 5.7 illustrates that the spatial configuration of known intrinsic functional networks is not random with respect to the estimated Laplacian and modularity leading eigenvectors. Instead, we observe that voxel belonging to the same network are grouped together i.e., they are represented by similar eigenvector values. This grouping places the limbic, DMN, and frontoparietal networks at opposite sides along the gradient (induced by the eigenvector entries) compared to the somatosensory, visual, and dorsal/ventral attention networks. Thus, both the Laplacian and modularity leading eigenvectors provide a natural, intrinsic spatial ordering for these large-scale networks and this ordering distinguishes between primary and multimodal cortical regions. These results are in line with the cortical surface gradients described by Margulies et al. (2016). Finally, the results for the seventeen-network Yeo parcellation case are presented in Fig. C.6 in Appendix C. Taking all these into account, our findings verify the presence of both community structure and functional gradient organization at the voxel level.

Finally, the modularity and Laplacian spectral information based on the Accordance and Discordance seems to agree in terms of the spatial connectivity patterns (see Fig. C.4, Fig. C.3, and Fig. C.5 in Appendix C). This is also evident from the scree plots (Fig. 5.5). A possible explanation could be that accordance and discordance measures reinforce one other. For pairs of voxel time- courses the accordance measure is high, the discordance measure is low and vise versa. Therefore, Discordance captures anti-modular (in the case of modularity) and bipartite (in the case of the Laplacian) information that pushes communities away from each other and eventually converges to the same results as accordance measure.

5.2.4.1 Future extensions of the framework

One extension of the current work can be the integration of the resolution parameter (γ) into the modularity criterion. Modularity works well in most situations however, it is unable to detect community structure in large networks with many small communities. To overcome this, a modified version of the standard modularity has been proposed. In that case, the modularity matrix is defined as $B_{ij} = A_{ij} - (\gamma\, k_i k_j)/M$, where $M = 2m = \sum_{ij} A_{ij}$ and $\gamma \in [0, \infty]$ (Reichardt and Bornholdt, 2006). Smaller and larger values of the γ parameter favor the detection of larger and smaller modules, respectively (Betzel et al., 2017; Newman, 2016). Another interesting extension could be spectral clustering (SC). The eigenvectors of the Laplacian and modularity matrices induce a low-dimensional representation for the data and can serve as inputs for the clustering algorithm. SC does not presume any parametric form for the data and can capture the natural underlying structure of the data (Venkataraman et al., 2009; Craddock et al., 2012; von Luxburg, 2007). To this end, *data-driven* clusters at the voxel level can be obtained. Furthermore, different null models in the modularity criterion can be used. For instance, the Bernoulli random model assumes an equal probability of appearance for all edges, preserving the average degree (Newman, 2006a) while other null models account for the correlation between degrees of nodes (Newman, 2002). Moreover, the configuration model used in this study can be modified to exclude self-loops (Massen and Doye, 2005). Finally, to model *extreme* co-activations/co-deactivations and oppositions of brain activity (i.e., discordant intervals), the threshold for the construction of Acc and Disc can be increased. In that way, Acc and Disc would become 'extreme event detector' as in its initial proposition (Meskaldji et al., 2015c,a) and the mathematical foundation of the proposed framework would be still valid.

5.2.5 Conclusion

We presented a framework that enables the estimation of the Laplacian and modularity spectrum at the voxel level exploiting the full spatial resolution of the fMRI data. Our results suggest the presence of both functional gradients and community structure at the voxel level showing fine-grained, distinct brain connectivity patterns based on the leading Laplacian and modularity eigenvectors. Additionally, a high similarity between the Laplacian and modularity spectra was observed indicating that both functional gradients and community structure are present at the voxel level. Interestingly, we showed that the spatial configuration of known

intrinsic RSNs is not random but instead the Laplacian and modularity leading eigenvectors provide a natural spatial ordering for these networks. Finally, the proposed framework opens a new avenue for spectral graph theory research at the voxel level.

Supportive Information

The Human Connectome Project data release (S900, HCP) is publicly accessible (Human Connectome Project, 2020). All codes used in this study for the implicit estimation of the modularity at the voxel level can be found in the following repository: https://github.com/seralouk/Voxel_wise_Laplace_Modularity. The Yeo brain parcellations (Yeo et al., 2011) are available at the dedicated GitHub repository: https://github.com/ThomasYeoLab/CBIG/tree/master/stable_projects/brain_parcellation/Yeo2011_fcMRI_clustering.

6 | Summary and future perspectives

The present dissertation explored the consequences of preterm birth on brain function and tissue volume as well as investigated the effect of an early music intervention on the functional connectivity in preterm infants. Moreover, the association between brain tissue volumes following preterm birth and adverse neurodevelopmental outcomes was investigated. To this end, both task-based and resting-state fMRI paradigms, as well as brain volumetric analyses were performed. Furthermore, one methodological advancement was developed to enable the spectral graph theory analysis at the voxel-level. Using this framework the characterization of the brain's organizational principles was achieved. In this chapter, a summary of the main findings is presented along with potential avenues for future work that builds upon the analyses and clinical contributions presented in the present thesis.

6.1   Summary of findings

The effects of music intervention on task-based and resting-state brain functional connectivity (FC): To investigate, for the first time, the effects of an early music intervention in preterm infants, we performed both task-based and resting-state fMRI analyses. Brain effective connectivity changes were explored using a Ppsychophysiological interaction (PPI) analysis. We unveiled brain networks involved in familiarity and pleasant music processing in preterm infants and we showed that music exposure during hospitalization promotes brain auditory processing maturation and can have lasting learning effects on music processing. We found increased FC between the auditory cortex and regions involved in familiarity and music processing, such as thalamus, caudate nucleus, putamen, and cingulate cortex, in favor of the preterm group that underwent the early music intervention. Moreover, using a resting-state connectomics-based statistical framework and a multivariate partial least squares (PLS) approach, we demonstrated that preterm infants who were previously repeatedly exposed to music increased their resting-state FC between specific brain regions. These regions included the calcarine, angular gurys, amygdala, superior frontal/superior parietal, and temporal areas that are known to be involved in associative memory and multi-sensory processing. Finally, a multivariate dosage-dependent effect on this modulation was unveiled. Our novel findings

highlighted, for the first time, the beneficial aspects of early musical intervention on *brain function* in preterm infants and brought new insights for supporting early music exposure to preterm infants in the NICU.

Brain tissue volumes at term-equivalent-age (TEA) and long-term outcome: We investigated the longitudinal brain development between birth and TEA in preterm infants and how brain volumes are associated with cognitive and behavioural long-term outcomes. Using multivariate machine learning classifiers (SVM, LDA), we explored the predictive utility of brain volumetric data in terms of cognitive/motor outcomes prediction at 18-24 months and 5 years of age, but also behavioural outcome at 5 years of age. We showed that several perinatal risk factors such as asphyxia, sepsis, and patent ductus arteriosus (PDA) have an impact on brain tissue volumes and their growth between birth and TEA time-points, without however being associated with neurodevelopmental outcome. We also found that children's long-term cognitive outcome was strongly associated with the parental SES variable. The volumetric data at birth and TEA contributed to the prediction of motor outcomes at 18-24 months, while brain volumes at TEA and tissue growth rates contributed to the prediction of cognitive outcome at 5 years of age. Concerning the behavioural long-term outcomes, we found that volumes such as WM, amygdala and CB can predict emotional outcome, while perinatal factors such as sepsis, gender and BPD can predict hyperactivity/inattention problems. Finally, the SES variable was found to add predictive power to the brain volumes in terms of predicting peer, conduct, and hyperactivity/inattention problems. Our results provide more evidence on the prognostic utility of magnetic resonance imaging at TEA, a point that is still controversial. Moreover, our findings suggest that perinatal brain characteristics in preterm infants may influence later functional development and that brain tissues at TEA could serve as moderate biomarkers for the long-term prediction of emotional problems.

Advanced models for neurodevelopment

Prematurity disease progression: Conditions such as preterm birth may change the dynamic process of neurodevelopment and lead to adverse neurodevelopmental outcomes. We unveiled, for the first time, the sequence of biological events along the course of encephalopathy of prematurity by employing an advanced probabilistic model that has been previously used in Alzheimer's disease. It is the first time that such a model is employed in neonatal populations. We provided novel valuable insights into the underlying pathophysiology. Our novel findings suggest that the first biomarkers to become abnormal are the brainstem and white matter whereas the last biomarkers are the cerebellum and the subcortical gray matter. These results might be of clinical use allowing more targeted early interventions aiming to improve long-term outcomes in preterm infants. This study was conducted in the context of the European Progression of Neurological Disease (EuroPOND, http://europond.eu/) consortium. The code used for this analysis has been made available at https://github.com/seralouk/preterm_ebms_open.

Spectral graph theory at the voxel level: Functional connectome-based studies have revealed interesting network-related characteristics such as small-world (Bassett and Bullmore, 2016),

rich-hub (van den Heuvel and Sporns, 2011), and scale-free (power-law degree distribution) organization of the human brain (Eguíluz et al., 2005). Moreover, spectral graph theory analysis of the functional connectomes has revealed the presence of a modular (Kabbara et al., 2019; Betzel et al., 2017; Zhigalov et al., 2017; Sporns and Betzel, 2016), and large-scale cortical gradient-based underlying organization (Margulies et al., 2016; Huntenburg et al., 2018). However, due to the high dimensionality of the fMRI data that prohibits the connectomics and spectral graph theory analysis at the voxel level, the brain is usually parcellated based on a subjective, non-trivial choice of a predefined atlas, at the cost of sacrificing the high resolution of the data. Importantly, different atlases impact the brain network structure and connectome-based statistics, and thus affect the analyses and results (Bellec et al., 2015; Wang et al., 2009; de Reus and van den Heuvel, 2013). In this work, we introduced a framework that enabled the spectral graph theory analysis at the voxel level overcoming the aforementioned limitations. To validate our framework, we estimated the voxel-wise group-level modularity and Laplacian spectrum of 40 subjects from the Human Connectome Project. We identified meaningful, modularity, and Laplacian-driven brain maps of resting-state functional connectivity assembling the Default-Mode-Network (DMN), Visual and Auditory networks. Moreover, our results showed the presence of both functional gradients and community structure at the voxel level revealing fine-grained, dominant, connectivity patterns. We showed that the spatial configuration of known intrinsic RSNs is not random but instead a natural spatial ordering for these networks is provided by the leading eigenvectors of the Laplacian and modularity matrices. Finally, the proposed framework enabled, for the first time, the characterization of the brain's fundamental organizational principles at the voxel level, without the use of a parcellation scheme or dimensionality reduction technique. The code developed to perform the analysis described in this work has been made available at https://github.com/seralouk/Voxel_wise_Laplace_Modularity.

6.2 Perspectives of future work

Dynamic brain functional connectivity

The fMRI studies presented in this thesis characterized features of brain function and explored the effects of an early music intervention on the brain effective and functional connectivity in preterm infants (see chapter 3). Recent research has demonstrated that functional connectivity at rest but also during a task is time-varying and not stationary as initially thought (Preti et al., 2017; Lurie et al., 2020; Fong et al., 2019). Moreover, functional networks can undergo several re-configurations during MRI scan (Chang and Glover, 2010). Both Psychophysiological Interaction (PPI) and static connectomics-based analyses used in this thesis did not explore dynamic features of brain connectivity. Therefore, dynamic methods could provide new insights into the *brain dynamics* during task or rest. To this end, an interesting and promising extension of the PPI analysis presented here would be to investigate the effects of music intervention using dynamic approaches such as the Psychophysiological Interactions of Co-activation Patterns (PPI-CAPs) method. PPI-CAPs is a point process-based approach that

temporally decomposes task-modulated connectivity into dynamic building blocks, which cannot be captured by current methods such as PPI (Freitas et al., 2020). Furthermore, dynamic resting-state functional connectivity traits in preterm infants can be explored by employing a sliding-window and clustering method (Preti et al., 2017). By employing such methods on our data, we will be able to explore dynamic brain connectivity trait changes related to the beneficial effect of the early music intervention. This would thus be a natural and feasible next step for the near future.

Linking brain neural traits and neurodevelopmental outcomes after intervention

This dissertation provided novel findings highlighting the beneficial aspects of early musical intervention on brain function in preterm infants. An interesting future step would be the longitudinal follow-up of the preterm infants that underwent the early intervention and the association of brain functional and structural changes with long-term neurodevelopmental outcomes. Multivariate approaches such as partial least square correlation (PLSC, McIntosh and Lobaugh (2004); Krishnan et al. (2011)) can unveil multivariate brain-outcome associations and shed more light on the neural correlates of adverse or improved long-term outcomes. Recently, Lejeune and colleagues (Lejeune et al., 2019) reported beneficial long-term effects of music listening in the NICU on neurodevelopmental outcomes in preterm children at 12 and 24 months of age, however, the association of long-term outcome and *brain functional and structural changes* related to early musical intervention exposure remains unexplored. This can be another feasible next step for the near future.

Spectral graph theory framework extensions

In Chapter 5, section 5.2 we introduced a novel, data-driven method that enables the fine-grained estimation of the modularity and Laplacian spectra, allowing the spectral graph theory analysis that the voxel level. One interesting way in which this methodology could be extended is the integration of spectral clustering for the construction of a data-driven functional atlas at the voxel level. Spectral clustering (SC) refers to clustering methods that are employed on the eigenvectors of a pairwise affinity matrix constructed from the data points aiming to group the underlying network's nodes. Transitionally, the adjacency (A) and Laplacian (L) matrix have been used as the affinity matrix. The eigenvectors of those matrices induce a low-dimensional representation for the data and serve as inputs for the clustering algorithm. SC does not presume any parametric form for the data and is able to capture the natural underlying structure of the data (Venkataraman et al., 2009; Craddock et al., 2012; von Luxburg, 2007). To this end, SC approaches could be employed on the leading eigenvectors of the modularity matrix (**B**) that correspond to the most positive eigenvalues. By doing so, *data-driven* subdivisions (modules) of the network could be obtained. These modules are, by definition, internally strongly connected and externally weakly connected. In this way, a *data-driven* functional atlas at the *voxel level* can be built, avoiding the sacrifice of the high spatial resolution of the fMRI data (e.g. by parcellating the brain using a predefined coarse

atlas resulting in a network with 100-1000 nodes).

Another interesting extension of the current work is the integration of the resolution parameter (γ) into the proposed modularity framework. Modularity, as defined by Newman (Newman and Girvan, 2004; Newman, 2004, 2006b), works well in most situations however, it suffers from one limitation; it is unable to detect community structure in large networks with many small communities. If the true number of communities is greater than $\sqrt{2m}$, then the maximum modularity will tend to combine communities into larger groups and fail to resolve the smallest divisions in the network (Newman, 2016). To overcome this limitation, a modified version of the standard modularity has been proposed. In this case, the modularity matrix is defined as $B_{ij} = A_{ij} - \gamma \frac{k_i k_j}{M}$, where $M = 2m = \sum_{ij} A_{ij}$ and $\gamma \in [0, \infty]$ (Reichardt and Bornholdt, 2006). Smaller and larger values of the γ parameter favor the detection of larger and smaller modules, respectively (Betzel et al., 2017; Newman, 2016). Thus, this would be a natural and feasible development for the near future, providing more flexibility to the proposed method.

Furthermore, different null models in the modularity criterion could be used. For instance, the Bernoulli random model can be used that assumes equal probability of appearance for all edges, preserving the average degree (Newman, 2006a). Additionally, null models that account for possible correlation between degrees of nodes could be used (Newman, 2002). Also, the configuration model used in the context of this dissertation can be modified to exclude self-loops (Massen and Doye, 2005).

Finally, to model *extreme* co-activations/co-deactivations and oppositions of brain activity (i.e., discordant intervals), the threshold for the construction of Accordance (Acc) and Discordance (Disc) can be increased. In that way, Acc and Disc would become 'extreme event detector' as initially proposed (Meskaldji et al., 2015c,a).

Structure-function relationship

This thesis mainly focused on the relevance of brain function for the study of preterm birth. It is worth mentioning though that the brain's underlying structural architecture can affect brain functional connectivity. It has been shown that the strength and persistence of the resting-state functional connectivity are constrained by the large-scale anatomical structure of the human cerebral cortex (Honey et al., 2009; Das et al., 2014). Therefore, by considering both functional and structural connectivity we could provide novel relevant information that previous studies may have missed.

Graph signal processing (GSP) has recently gained increasing interest in the neuroimaging field as a novel framework for brain data analysis that integrates brain structure and function. GSP tackles the problem of analyzing data defined on irregular domains that can be represented by a graph model (Huang et al., 2018). In this context, the brain structural connectome defines the graph backbone with nodes and edges being the brain regions and the white matter tracts, respectively. Additionally, each frame of BOLD activity is considered a temporal

sample of a signal living on this graph (e.g. at a specific time-point, each node has a value that corresponds to the BOLD signal of that region at the given time-point). Traditionally, most connectomics-based studies in preterm populations have used the functional or structural connectome independently, and therefore, GSP can be characterized as a promising avenue to analyze BOLD signals from a new viewpoint in prematurity, by integrating brain structure with function.

A Supplementary material for Chapter 3

A.1 Supplementary material for Section 3.1

Behavioral response to the music was assessed by a nurse specialized in developmental care using a behavioral assessment tool (Martinet et al., 2013) on 12 preterm newborns between 33 and 37 weeks of gestational age. Also, cardiorespiratory response and oxygen saturation level were taken during 10 minutes before, during and 10 minutes after the music intervention. We observed increased oxygen saturation level during and after music listening and no other modification of the cardiorespiratory system. Furthermore, nurses specialized in developmental care observed the babies listening (or not) to music and did not notice any discomfort behavior. We thus concluded that this music was adapted to preterm newborns (A.2).

Table A.1 – Demographic and perinatal characteristics of the populations. Differences between preterm with and without a musical intervention were calculated using the Mann-Whitney test or the Fisher test. We observed no differences between age at scan between the 3 groups (ANOVA, p 0.11). Socioeconomic status (Largo et al., 1989) was assessed based on maternal education and paternal occupation (range, 2-12, with 2 the highest score).

	Full-term n=9	Preterm music (PM) n=9	Preterm control (PC) n=9	PM versus PC p value
Gestational age at birth, weeks, mean (SD)		28.70 (± 2.5)	28.70 (± 2.0)	0.79
Birth Weight, gram, mean (SD)	3324.4 (± 366.1)	1151.7 (± 329.62)	1051.1 (±265.5)	0.65
Small for gestational age, n(%)	0	1/9 (11%)	2/9 (22%)	1
Birth Height, centimeter, mean (SD)	49.33 (± 1)	37.9 (± 3.4)	35.8 (± 2.7)	0.65
Birth head circumference, (cm) mean (SD)	34.22 (± 1.30)	27 (± 3.1)	25.6 (± 2.4)	0.28
Female, n (%)	4/9 (44.44%)	4/9 (44.44%)	5/9 (55.56%)	1
Neonatal asphyxia, n(%)	0	0	0	N.A
Bronco-pulmonary dysplasia, n(%)	0	3/9 (33%)	4/9 (44%)	1
Intraventricular haemorrhages (grade 1-2), n(%)	0	2/9 (22%)	3/9 (33%)	1
Early and late onset sepsis, n(%)	0	2/9 (22%)	3/9 (33%)	1
Number of music/no-music intervention , mean (SD)	NA	25.2 (± 9.8)	25.9 (± 5.6)	0.75
Gestational age at scan, weeks, mean (SD)	39.63 (± 1.02)	40.25 (± 0.51)	40.40 (± 0.77)	0.53
Socio-economic score (range 2-12), mean (SD)	4.88 (± 2.87)	6.4 (± 3.7)	4.9 (± 2.5)	0.36

Table A.2 – Heart rate, respiratory rate and oxygen saturation level in 12 preterm infants listening to the music created by A. Vollenweider. Each infant listened one time to the music and physiological responses were registered during 10 min before, during music listening and 10 minutes after. We used paired t-test to assess cardio-respiratory and oxygen saturation level responses to music.

	Before Mean	During Mean	After Mean	Paired t-test Before vs During (p-value unco.)	Paired t-test Before vs After (p-value unco.)	Paired t-test During vs After (p-value unco.)
Heart rate (beats/min)	158.74	161.29	161.37	0.453	0.354	0.971
Respiratory rate (breaths/min)	48.94	49.86	48.29	0.723	0.806	0.431
Oxygen saturation level (%)	97.15	97.73	97.83	0.062	0.056	0.651

Table A.3 – Two sample t-test: Significant activations for Preterm-Music >Preterm-Control group comparison (seed: right primary auditory cortex).

Preterm-Music >Preterm-Control, Original-Music >Tempo modification, Seed: Right primary auditory cortex			
Region	Number of voxels	T value	P value (FWE)
R Thalamus	272	6.64	0.009
L Caudate and MCC	257	5.13	0.013

Table A.4 – Two sample t-test: Significant activations for Preterm-Music >Full-Term control group comparison (seed: right primary auditory cortex).

Preterm-Music >Full-Term control, Original Music >Tempo modification, Seed: Right primary auditory cortex			
Region	Number of voxels	T value	P value (FWE)
MCC	474	4.94	0.001

Table A.5 – One sample t-test: Significant activations for Preterm-Music group at group level (seed: Left primary auditory cortex).

Preterm-Music, Original Music >Tempo modification, Seed: Left primary auditory cortex			
Region	Number of voxels	T value	P value (FWE)
MCC	208	8.92	0.007
R Caudate and Putamen	171	7.98	0.01

A.2 Supplementary material for Section 3.2
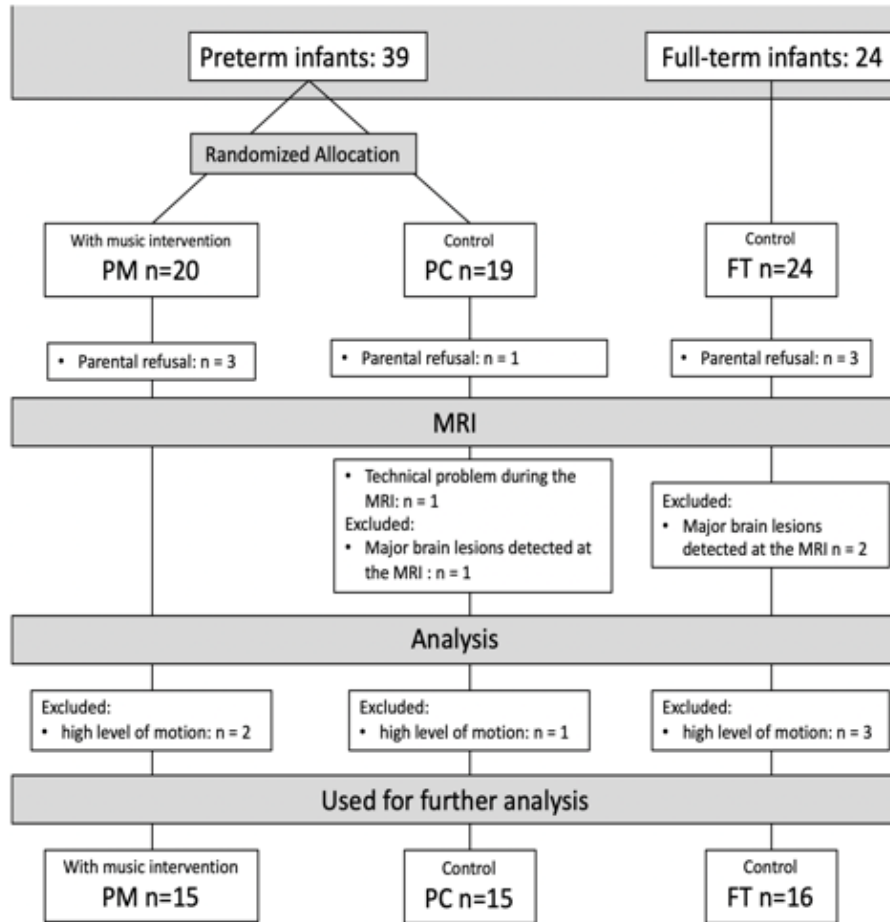
Figure A.1 – The enrollment procedure and further information of the exclusion criteria.

Table A.6 – Population Characteristics.

	PM	PC	FT
N	**15**	**15**	**16**
GA birth (weeks)	29.16 ± 2.14	28.95 ± 1.83	39.50 ± 1.08
GA at scan (weeks)	40.21 ± 0.55	40.50 ± 0.77	39.78 ± 1.05
Socioeconomic status (SES)	6.46 ± 3.54	6.34 ± 3.47	4.53 ± 3.06
Birth weight (g)	1203.67 ± 351	1161 ± 287	3333.43 ± 334
Cranial perimeter at birth (cm)	27.05 ± 2.82	26.17 ± 2.25	34.46 ± 1.14
Height at birth (cm)	37.84 ± 3.20	36.47 ± 4.02	49.68 ± 1.49

Table A.7 – Intervention details for the Preterm-Music group.

PM (n=15) # of music listening during hospitalization	
Subject_001	30
Subject_002	31
Subject_006	7
Subject_007	28
Subject_008	33
Subject_012	25
Subject_016	33
Subject_028	11
Subject_032	30
Subject_044	9
Subject_047	24
Subject_048	24
Subject_051	28
Subject_052	35
Subject_054	27
Mean (std)	**25 (8.92)**

PLSC implementation details

The core of the PLSC method is the singular value decomposition (SVD) of the cross-covariance matrix $\mathbf{R} = \mathbf{USV^T}$ defined as $\mathbf{R} = \mathbf{Y^T X}$, $\mathbf{X} \in \mathbb{R}^{N_{outcomes} \times N_{imaging}}$, where $\mathbf{Y}$ is a matrix storing the outcome variables (one outcome variable in this study) for each subject as rows ($\mathbf{Y} \in \mathbb{R}^{N_{subjects} \times N_{outcomes}}$) and $\mathbf{X}$ is a matrix storing the imaging variables ($\mathbf{X} \in \mathbb{R}^{N_{subjects} \times N_{imaging}}$). In this study, the cross-covariance matrix $\mathbf{R}$ is built using the z-scored (across subjects) matrices $\mathbf{X}$ and $\mathbf{Y}$ ($\mu = 0, \sigma = 1$). Given that we only have one outcome variable in this study, the cross-covariance matrix $\mathbf{R}$ has dimension $[1 \times 90]$.

The SVD of $\mathbf{R}$ results in correlation components each composed of a set of outcomes (columns of $\mathbf{U}$) and brain salience weights (columns of $\mathbf{V}$). In the present study we only have one PLSC component since $\mathbf{R}$ has dimension $[1 \times 90]$ as explained above. Additionally, this component is associated with a corresponding singular value (stored on the diagonal of $\mathbf{S}$) that specifies the explained correlation along this dimension. Outcome ($\mathbf{U}$) and brain imaging ($\mathbf{V}$) salience weights indicate how strongly each input variable contributes to the multivariate outcome behavior-brain correlation in this certain component. In this study the weights range lies between -1 and 1 since we normalized the data (z-scoring of outcome and brain network input features across subjects) before the computation of the cross-covariance matrix $\mathbf{R}$ and thus, these salience weights can be interpreted similarly to correlation values.

To assess the statistical significance of this component, permutation testing was performed. Briefly, the rows of $\mathbf{Y} \in \mathbb{R}^{N_{subjects} \times N_{outcomes}}$ (i.e., the outcome variable's elements) were permuted

Table A.8 – Regions of interest included in AAL-atlas.

Labels	Abbreviation used in figures	Regions full name
1	PreCG	Precental gyrus
2	SFGdor	Superior frontal gyrus, dorsolateral
3	ORBsup	Superior frontal gyrus, orbital part
4	MFG	Middle frontal gyrus
5	ORBmid	Middle frontal gyrus, orbital part
6	IFGoperc	Inferior frontal gyrus, opercular part
7	IFGtriang	Inferior frontal gyrus, triangular part
8	ORBinf	Inferior frontal gyrus, orbital part
9	ROL	Rolandic operculum
10	SMA	Supplementary motor area
11	OLF	Olfactory cortex
12	SFGmed	Superior frontal gyrus, medial
13	ORBsupmed	Superior frontal gyrus, medial orbital
14	REC	Gyrus rectus
15	INS	Insula
16	ACG	Anterior cingulate and paracingulate gyri
17	DCG	Median cingulate and paracingulate gyri
18	PCG	Posterior cingulate gyrus
19	HIP	Hippocampus
20	PHG	Parahippocampal gyrus
21	AMYG	Amygdala
22	CAL	Calcarine fissure and surrounding cortex
23	CUN	Cuneus
24	LING	Lingual gyrus
25	SOG	Superior occipital gyrus
26	MOG	Middle occipital gyrus
27	IOG	Inferior occipital gyrus
28	FFG	Fusiform gyrus
29	PoCG	Postcentral gyrus
30	SPG	Superior parietal gyrus
31	IPL	Inferior parietal, supramarginal and angular gyri
32	SMG	Supramarginal gyrus
33	ANG	Angular gyrus
34	PCUN	Precuneus
35	PCL	Paracentral lobule
36	CAU	Caudate nucleus
37	PUT	Lenticular nucleus, putamen
38	PAL	Lenticular nucleus, pallidum
39	THA	Thalamus
40	HES	Heschl gyrus
41	STG	Superior temporal gyrus
42	TPOsup	Temporal pole: superior temporal gyrus
43	MTG	Middle temporal gyrus
44	TPOmid	Temporal pole: middle temporal gyrus
45	ITG	Inferior temporal gyrus

5000 times and within each iteration, the permuted **Rperm**, **Uperm**, **Sperm**, **Vperm** were estimated. Next, the p-value was estimated from the permutation null distribution by counting the number of permuted singular values (**Sperm**) above the observed singular value (**S**) of the PLSC component.

Finally, to evaluate the stability of brain and outcome salience weights (i.e., the elements of the matrices **U** and **V**) , 200 bootstrap samples of **X** and **Y** with replacement were performed (sampling) and the PLSC analysis was repeated obtaining the bootstrapped outcome and brain salience weights. In this study, we report significant PLSC results (saliences) in terms of bootstrap mean and standard errors for the single PLSC component which was found to be significant based on the permutation testing.

Permutation testing for the PLSC analysis

To assess the statistical significance of the computed PLSC component, 5000 permutation tests were performed. The p-value was estimated from the permutation null distribution by counting the number of times that the permuted singular values (Sp) were above the observed true singular value (S) of the PLSC component. The permutation null distribution is shown in below where in y-axis we have the frequency and in x-axis the singular values obtained by the permutation testing. The red vertical line represents the true observed singular value of the PLSC component which was found to be statistically significant based on the permutation testing (p=0.043).
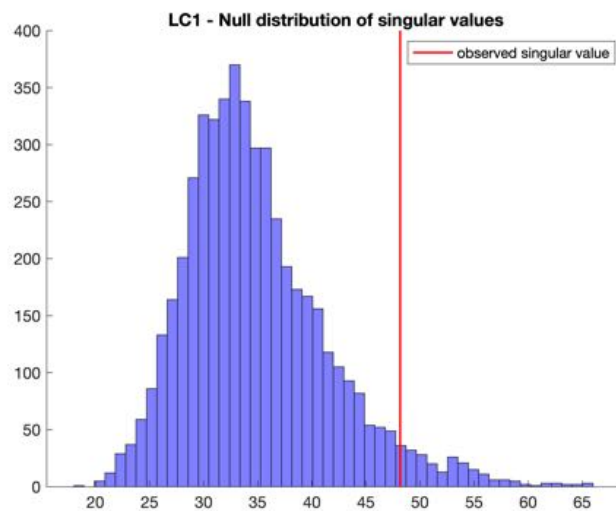
Figure A.2 – The permutation null distribution. The histogram of the null distribution of the singular values is presented among with the observed (red line) singular value of the significant latent component. Y-axis represents frequency and x-axis the singular values obtained by the permutation testing.

Table A.9 – Mean bootstrap weights and 5th to 95th percentiles for the significant component.

Mean bootstrapped brain salience weights	Lower bound of CI	Upper bound of CI
-0.092	-0.167	0.064
-0.101	-0.219	0.03
-0.07	-0.17	0.092
-0.079	-0.172	0.121
0.062	-0.05	0.138
-0.1	-0.2	0.017
-0.048	-0.176	0.157
-0.161	-0.248	-0.073
-0.041	-0.173	0.133
-0.085	-0.175	0.011
-0.034	-0.171	0.097
-0.019	-0.154	0.108
-0.134	-0.233	-0.011
0.034	-0.12	0.127
-0.086	-0.207	0.069
-0.054	-0.169	0.021
0.03	-0.103	0.136
-0.089	-0.218	0.067
-0.015	-0.154	0.133
0.046	-0.127	0.142
0.069	-0.047	0.144
0.028	-0.152	0.137
-0.141	-0.202	0.02
-0.116	-0.2	-0.006
-0.109	-0.177	-0.014
-0.027	-0.134	0.039
0.004	-0.143	0.098
0.034	-0.058	0.102
0.008	-0.171	0.14
-0.048	-0.167	0.108
-0.009	-0.174	0.126
0.033	-0.091	0.138
-0.102	-0.168	0.098
-0.128	-0.204	0.142
-0.09	-0.186	0.073
-0.148	-0.199	-0.077
-0.082	-0.166	0.046
-0.156	-0.229	-0.05
-0.081	-0.183	0.04
-0.116	-0.195	-0.041
0.083	0.005	0.159
-0.054	-0.212	0.08
-0.047	-0.193	0.065

0.009	-0.126	0.116
-0.006	-0.114	0.121
-0.016	-0.135	0.1
-0.083	-0.19	0.041
-0.045	-0.149	0.086
-0.004	-0.127	0.144
0.005	-0.125	0.128
0.041	-0.091	0.127
0.037	-0.078	0.14
-0.153	-0.197	-0.096
-0.002	-0.134	0.122
-0.089	-0.187	0.018
-0.185	-0.236	-0.123
-0.079	-0.169	0.116
-0.056	-0.129	0.044
-0.026	-0.163	0.141
-0.017	-0.144	0.077
-0.134	-0.218	-0.006
-0.135	-0.192	-0.026
-0.148	-0.29	0.01
0.021	-0.103	0.139
-0.098	-0.216	0.057
-0.046	-0.155	0.112
-0.093	-0.184	0.059
-0.081	-0.169	0.11
-0.152	-0.23	-0.065
-0.019	-0.15	0.079
-0.024	-0.139	0.05
-0.014	-0.144	0.139
0.056	-0.038	0.133
0.099	0	0.181
0.041	-0.129	0.126
-0.086	-0.205	0.063
-0.165	-0.22	-0.01
-0.107	-0.185	0.101
-0.124	-0.207	0.03
-0.041	-0.173	0.082
-0.012	-0.134	0.143
-0.067	-0.188	0.083
-0.003	-0.154	0.106
-0.022	-0.129	0.122
-0.099	-0.166	0.003
-0.128	-0.229	-0.003
0.09	0.028	0.17
-0.132	-0.219	0.05
-0.055	-0.195	0.095
-0.002	-0.137	0.066

Table A.10 – Statistical tests for clinical variables.

Clinical Variables	Hypothesis Testing	Conclusion	Critical value & p-value
Gender	FT vs PM vs PC	No significant difference	X2(2) = 0.035, p-value = 0.982
Number of times with headphones	PM versus PC	No significant difference	F(1,29) = 0.147, p-value = 0.703
Number of images (run 1)	FT vs PM vs PC	No significant difference	F(2,43) = 1.806, p-value = 0.176
Number of images (run 2)	FT vs PM vs PC	No significant difference	F(2,43) = 1.259, p-value = 0.294
Coil type	FT vs PM vs PC	No significant difference	F(2,43) = 0.370, p-value = 0.692
GA birth	PM versus PC	No significant difference	F(1,29) = 0.082, p-value = 0.776
GA MRI	FT vs PM vs PC	No significant difference	F(2,43) = 2.687, p-value = 0.079
Socioeconomic Status	PM vs PC	No significant difference	F(1,29) = 0.0108, p-value = 0.917
Birth Weight (g)	PM vs PC	No significant difference	F(1,29) = 0.132, p-value = 0.718
Cranial Perimeter Birth (cm)	PM vs PC	No significant difference	F(1,29) = 0.594, p-value = 0.447
Height birth (cm)	PM vs PC	No significant difference	F(1,29) = 1.05, p-value = 0.312
Intrauterine growth restriction (yes/no)	PM vs PC	No significant difference	X2(1) = 0.0, p-value = 1.0
Microcephaly (yes/no)	PM vs PC	No significant difference	X2(2) = 3.012, p-value = 0.221
Chorioamnionitis (yes/no)	PM vs PC	No significant difference	X2(1) = 0.370, p-value = 0.542
Asphyxia (yes/no)	PM vs PC	No significant difference	X2(1) = 3.334, p-value = 0.067
BPD (yes/no)	PM vs PC	No significant difference	X2(1) = 0.681, p-value = 0.408
IVH (yes/no)	PM vs PC	No significant difference	X2(1) = 0.240, p-value = 0.624
Sepsis (yes/no)	PM vs PC	No significant difference	X2(2) = 1.366, p-value = 0.505
NEC (yes/no)	PM vs PC	No significant difference	X2(1) = 1.034, p-value = 0.309
Patent ductus arteriosus (yes/no)	PM vs PC	No significant difference	X2(1) = 0.370, p-value = 0.542

* ANOVA for numerical variables.

* Chi-squared test for categorical variables.

B Supplementary material for Chapter 4

B.1 Supplementary material for Section 4.1

MRI acquisition parameters

The parameters used for the acquisition of the T2-weighted images in this study are summarized in the following table.

Table B.1 – MRI acquisition parameters for T2-weighted images.

Machine	Field strength (T)	Echo time (ms)	Repetition time (ms)	Echo train length	Voxel size (mm3)	Birth scans	TEA scans
Philips Eclipse	1.5	156	4000	16	0.7 x 0.7 x 1.5	11	8
Philips Achieva	1.5	150	4000	16	0.7 x 0.7 x 1.5	39	41
Siemens Avanto	1.5	150	5700	15	0.8 x 0.8 x 1.2	31	2
Siemens Trio Tim	3	150	4600	15	0.8 x 0.8 x 1.2	3	33

Data dependency on scanner type

Table B.2 – Effect of scanner type on tissue volumes, controlling for GA at birth (analysis of covariance).

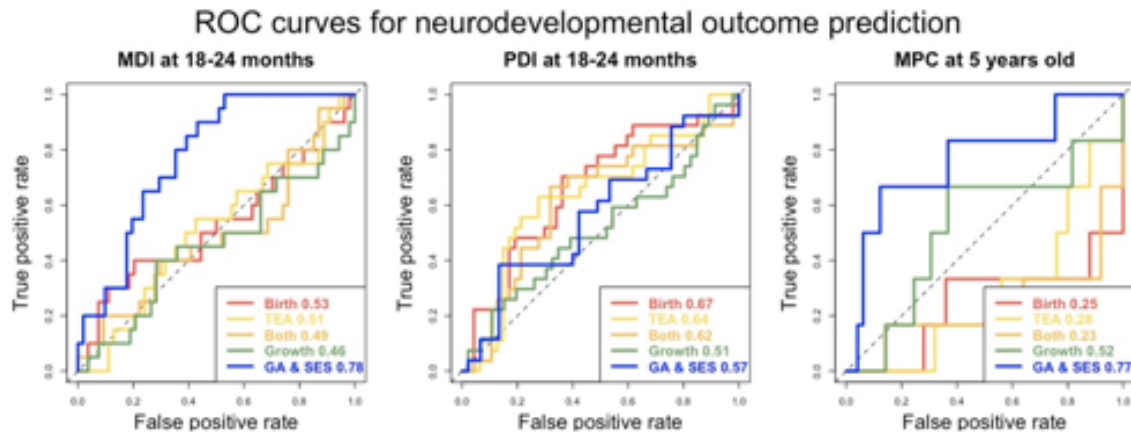| Tissue volume | At birth | | | | At TEA | | | |
| | Scanner type | | GA birth | | Scanner type | | GA birth | |
	F	P-value	F	P-value	F	P-value	F	P-value
GM	.94	.426	202.24	<.001	.71	.552	.10	.758
UWM	1.64	.186	96.54	<.001	.48	.700	.11	.742
SGM	2.31	.083	158.14	<.001	.82	.489	.05	.825
CSF	1.80	.153	28.03	<.001	1.82	.151	.70	.404
CB	.89	.453	173.89	<.001	1.09	.360	.13	.716
IC	1.61	.193	123.74	<.001	.59	.625	.00	.992

Figure B.1 – Classification ROC curves using the following four sets of birth weight normalized features (without GA and SES) (i) only the birth data (red lines), (ii) only the TEA data (yellow lines), (iii) both birth and TEA data (orange lines), (iv) brain volume GR, and, for comparison, (v) only GA and SES.

B.2 Supplementary material for Section 4.2

Cohort characteristics

Table B.3 – The population characteristics

Characteristics	Analysis with volumetric data n = 80	Analysis with clinical data N = 86
Boys, n	36 (45%)	41 (47.7 %)
Mean gestational age (SD), weeks	27.8 (1.64)	27.8 (1.65)
<28 GW, n	46 (57.5%)	49 (57 %)
Extreme, weeks	23.9 - 32	23.9 - 32
Mean birthweight (SD), grams	989 (231)	992 (240.7)
<10th percentile	9 (12%)	10 (11.6%)
Mean birth head circumference, cm	25 (1.9)	25 (1.9)
<10th percentile	9 (11%)	10 (11.6%)
BPD, n	30 (37.5%)	30 (37.5%)
Sepsis infection, n	23 (28.7%)	24 (28%)
Periventricular leukomalcia, n	2 (2.7%)	4 (4.6%)
Low socio-economic status, n	38 (47.5%)	41 (47.7%)
Mean age atbrain MRI, weeks	40.1 (SD 0.8)	40 (SD 0.85)
Median age at assessment (extreme), months	61 (59 – 69)	60 (59 - 69)
Median K-ABC (extreme)	98 (54 – 126)	97 (54 - 126)
K-ABC >85	64 (86.5%)	69 (80%)
K-ABC >70; <85	10 (13.5%)	11 (13%)
K-ABC <70	6 (7.5%)	6 (7%)
K-ABC I	36 (48.5%)	41 (47.7%)

Table B.4 shows the population characteristics of the participants included in this study. The clinical and SES data were available for all n=86 subjects, whereas the volumetric data were available only for n=80 subjects due to amygdala volume missing data. There was no significant difference in gender distribution, GA at birth, birth weight z-score, and birth head circumference between the 86 subjects for whom clinical data were available and the subgroup of 80 (out of the 86) children for whom volumetric data were available. In addition, the rates of BPD, sepsis, and PVL were comparable, as well as the SES.

Table B.4 – The population characteristics of the participants included in this study.

| Population Characteristics	SDQ Total Difficulties score normal N = 75	SDQ Total Difficulties score at risk N = 11	P-value
Perinatal data			
Male gender, n (%)	36 (48%)	5 (45.5 %)	0.567
GA, weeks, mean (SD), range	27.8 (1.68) 24 – 32	27.9 (1.54) 26 - 31	0.887
Birthweight, g, mean (SD)	998 (248)	955 (184)	0.582
Birth head circumference, cm, mean (SD), range	25.1 (1.9) 22 – 30	24.77 (1.7) 23 - 28	0.602
BPD, n (%)	28 (37.3%)	3 (27.3%)	0.387
Sepsis, n (%)	21 (28%)	3 (27.3%)	0.635
PVL, n (%)	4 (5.3%)	0 (0%)	0.572
Parental socio-economic status			
SES score, mean (SD), range	6 (3) 2 - 12	8 (3) 3 – 11	0.080
Cognitive outcome at 5 years			
K-ABC score, mean (SD), range	96 (14.2) 54 - 126	86 (18.7) 54 - 108	0.035
Score <85, n (%)	12 (16%)	3 (27.3%)	0.169
K-ABC I	38 (50.6%)	4 (36.4%)	2.88
K-ABC II	37 (49.4%)	7 (63.6%)	2.88
Brain development at TEA, n=80 **Absolute volumes, ml**	**SDQ normal N = 69**	**SDQ at risk N = 11**	**P-value**
WM , mean (SD)	147.64 (16.15)	148.77 (14.52)	0.830
CGM, mean (SD)	166.02 (24.03)	164.29 (20.53)	0.824
DSGM, mean (SD)	21.14 (2.07)	21.09 (1.09)	0.939
Amygdala , mean (SD)	0.817 (0.14)	0.87 (0.19)	0.212
CB, mean (SD)	22.96 (3.71)	21.14 (2.32)	0.123
CSF, mean (SD)	101.77 (25.19)	95.31 (26.71)	0.441
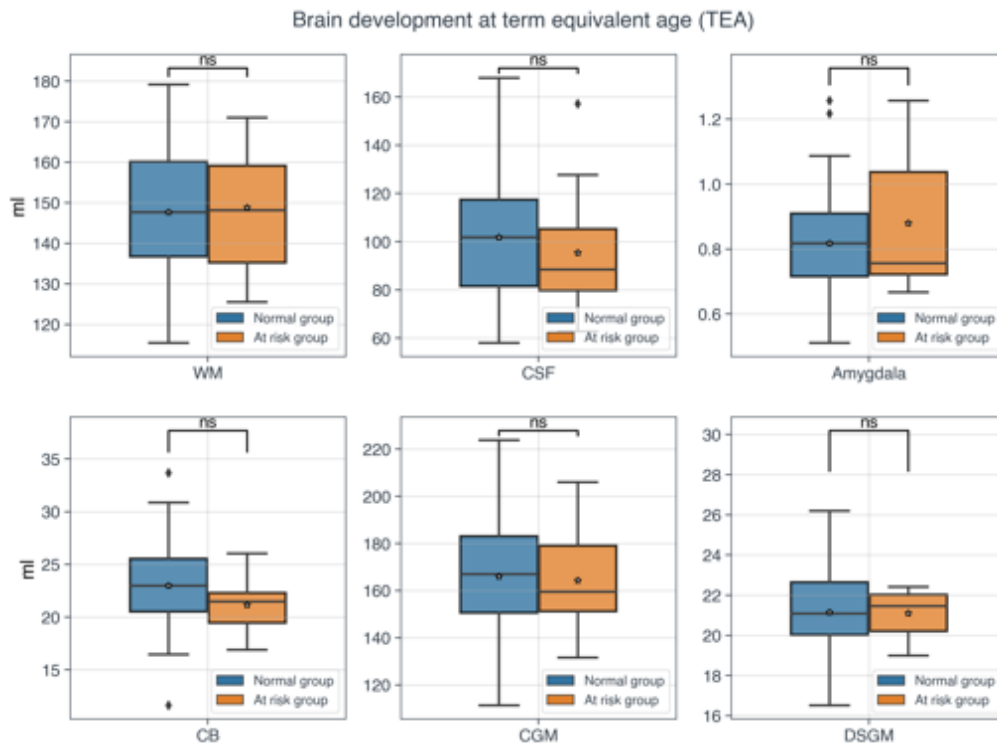
Figure B.2 – Averages of brain absolute volumes at TEA. Boxplots showing the brain absolute volumes for white matter (WM), cerebrospinal fluid (CSF), amygdala, cerebellum (CB), cortical gray matter (CGM) and deep subcortical gray matter (DSGM) of the two groups of participants based on the SDQ total difficulties score variable. Blue and orange color represents the normal and at risk group, respectively. No statistically significant differences between the volumetric data of the two groups were observed. The asterisk represents the mean value whereas the black line inside the bodies of the boxplots depicts the median values.
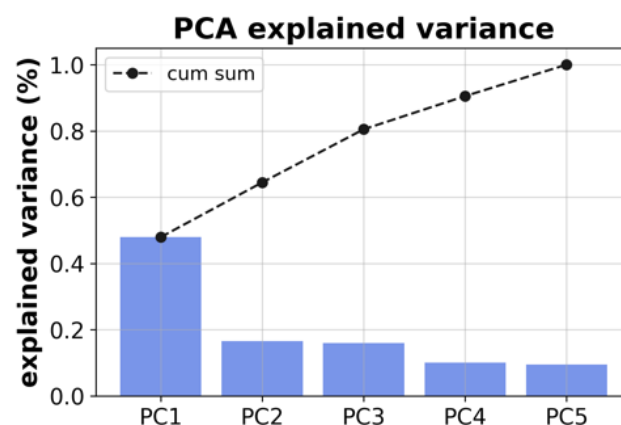

Figure B.3 – The PCA explained variance. The first component (PC1) captures 50% of the variance whereas the second (PC2) captures 20% of the variance. The contribution of the remaining components is negligible for this analysis (each explains less than 15%).
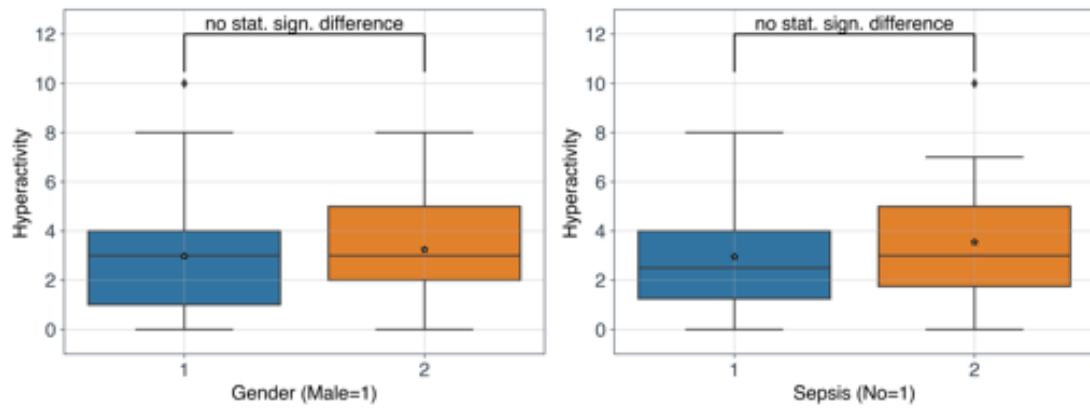
Figure B.4 – Post hoc analysis: Boxplots (star marker: mean value) of the behavioral variable of interest i.e., Hyperactivity/inattention subscale, grouped by the most important features (i.e., Gender, Sepsis) based on the Mean Decrease Accuracy (MDA) method. The asterisk represents the mean value, whereas the black horizontal line in the boxes depicts the median value.

C Supplementary material for Chapter 5

C.1 Supplementary material for Section 5.1

Table C.1 shows the ANCOVA results for the effect of scanner on the brain volumes. No significant effects of the scanner type on the brain volumes after controlling for the GA at birth were observed.

Tissue volume	Scanner type		GA at birth	
	F	P-value	F	P-value
CGM	1.55	.193	12.44	<.001
WM	.825	.512	.863	.355
SGM	1.58	.198	6.24	.014
CSF	.388	.816	.729	.395
Cerebellum	1.41	.236	5.31	.023
Brainstem	.967	.429	12.56	<.001

Table C.1 – Analysis of Covariance for the effect of scanner type on tissue brain volumes, controlling for the GA at birth.

To test for statistically significant differences in the brain tissue volumes at TEA between the two groups, student t-tests are used. The exact p-values of the statistical tests are reported in Table C.2. The white matter, CSF and brainstem tissue volumes were found to be statistically different.

Table C.2 – Absolute cerebral tissue volumes measured at TEA. Student t-tests were performed to test for statistical significant differences between the PM and FT groups.

Tissue volume mean (SD)	PM	FT	P-value
CGM	.354 (.022)	.359 (.027)	.165
WM	.327 (.022)	.354 (.019)	<.001
SGM	.047 (.003)	.048 (.004)	.213
CSF	.209 (.037)	.174 (.033)	<.001
Cerebellum	.05 (.006)	.052 (.006)	.052
Brainstem	.012 (.001)	.014 (.001)	<.001

Figure C.1 shows the boxplots of the volumetric data for the cortical gray matter (CGM), white matter (WM), subcortical gray matter (SGM), cerebrospinal fluid (CSF), cerebellum (CB) and brainstem of the two groups of participants. Student t-tests were performed to test for statistical significant differences between the PM and FT groups.

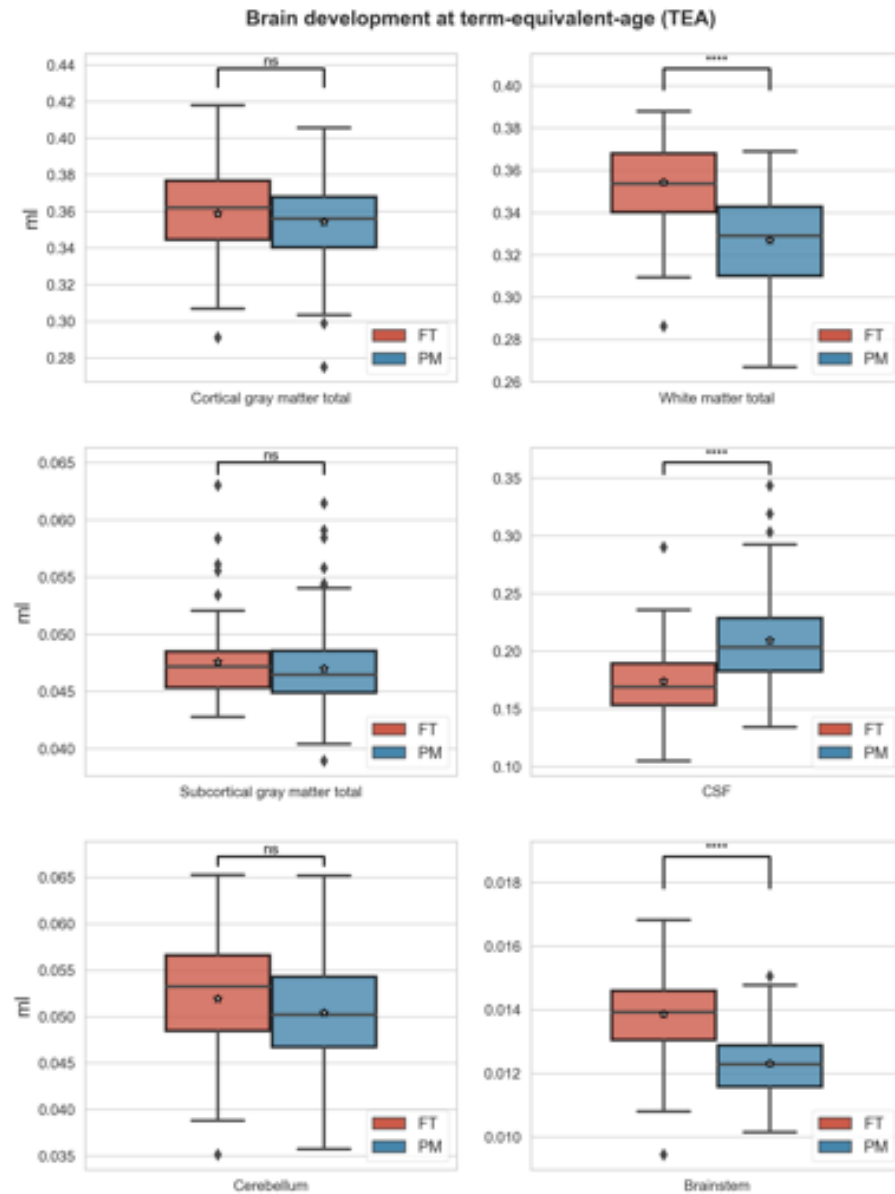Figure C.1 – Boxplots of the absolute cerebral tissue volumes (in ml) at TEA (expressed as medians and means with 25/75 percentile box, 10th/90th percentile error bars, and outliers). Student t-tests were performed to test for statistical significant differences between the PM and FT groups. ns refers to "no significant" outcome with a P-value > 0.05 whereas, four asterisks (****) indicate statistical significance at P ≤ 0.0001.

Figure C.2 shows the event probabilities of the input biomarkers. We observe an overlap in the distributions of the biomarkers across groups and a tendency of decreased volumes for the preterm infants compared to control full-terms (except for CSF volume, see also Figure C.1).
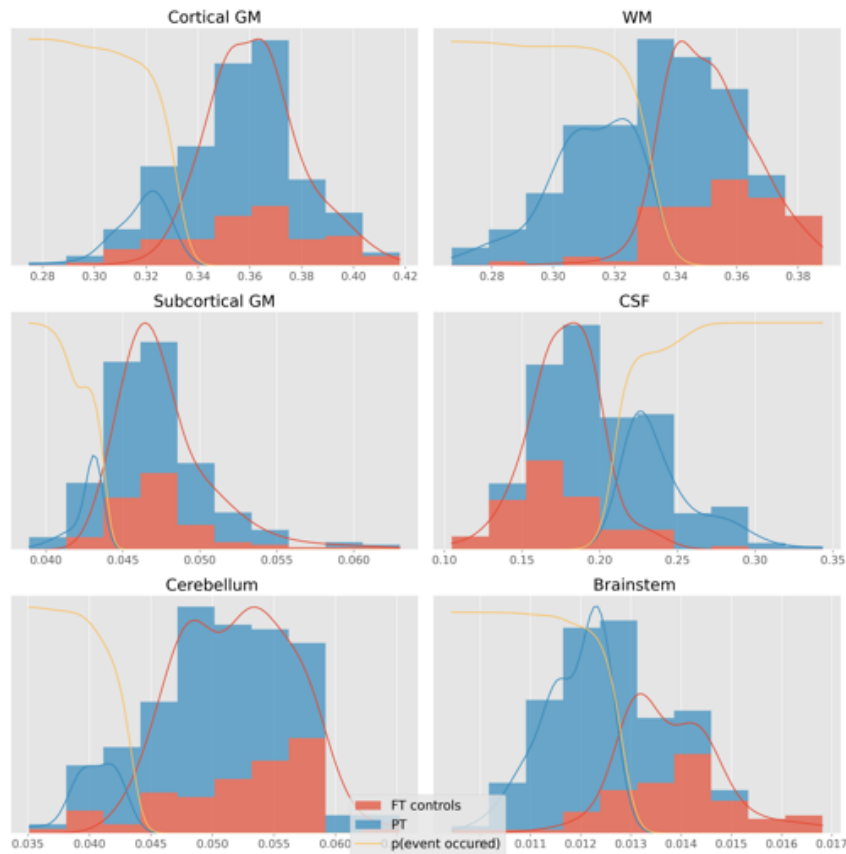
Figure C.2 – The individual event probabilities of the input biomarkers as estimated by the KDE-EBM model for the two groups: PT (blue) and FT (red) among with the probability of event transition (yellow line).

C.2 Supplementary material for Section 5.2

Fig. C.3 (a) & (b) show the eigenvectors of the normalized graph Laplacian matrix corresponding to the first smallest (omitting the first i.e, $\lambda_1 = 0, \mathbf{v_1} = \mathbf{D}^{\frac{1}{2}}\mathbf{1}$) and largest eigenvalues using $\mathbf{A_{cc}}$ and $\mathbf{D_{isc}}$, respectively.
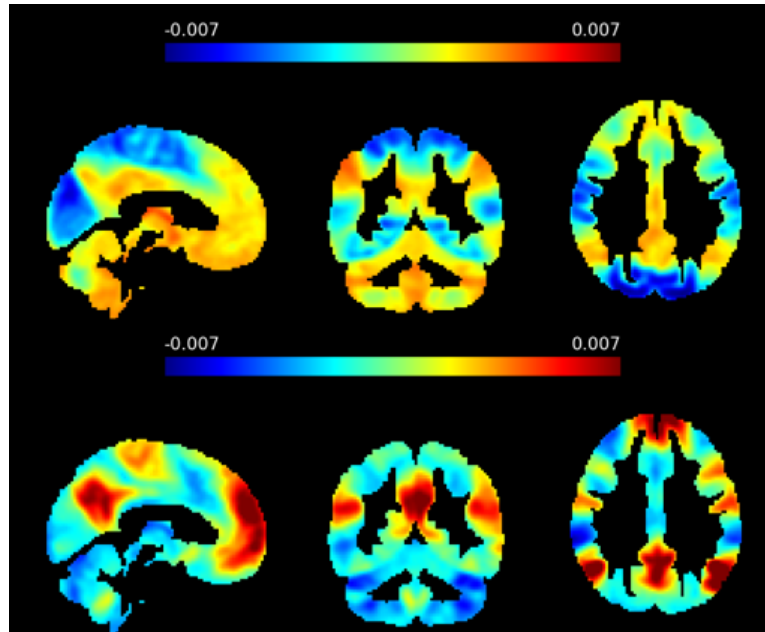
(a) Leading smallest eigenvectors of L using A_{cc}
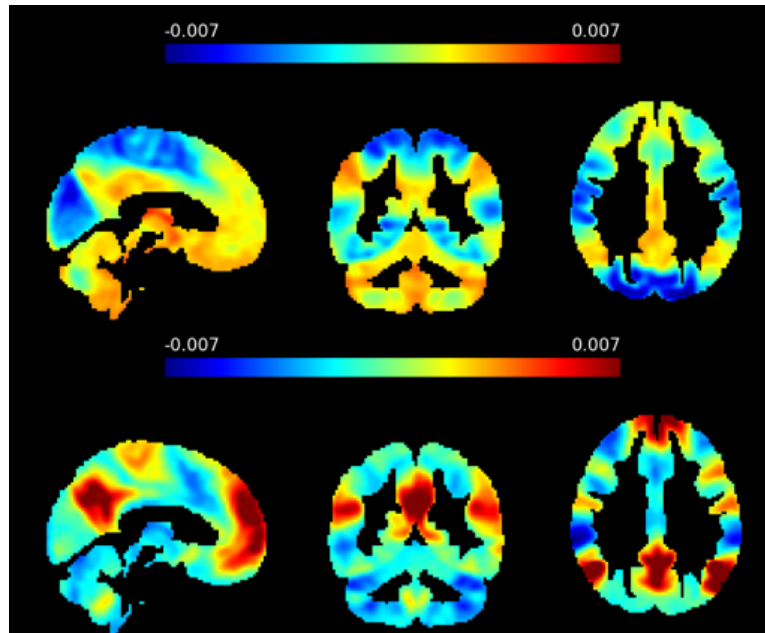
(b) Leading largest eigenvectors of L using D_{isc}

Figure C.3 – Laplacian leading eigenvectors: (a) and (b) show the first two leading modularity eigenvectors in the case where the adjacency was the Accordance matrix or the Discordance matrix, respectively. Positive and negative eigenvector entries are represented by red and blue colors, respectively. MNI coordinates: x=4, y=-50, z=29.

Fig. C.4 (a) & (b) show the modularity eigenvectors corresponding to the first most positive and most negative eigenvalues using $\mathbf{A_{cc}}$ and $\mathbf{D_{isc}}$, respectively.
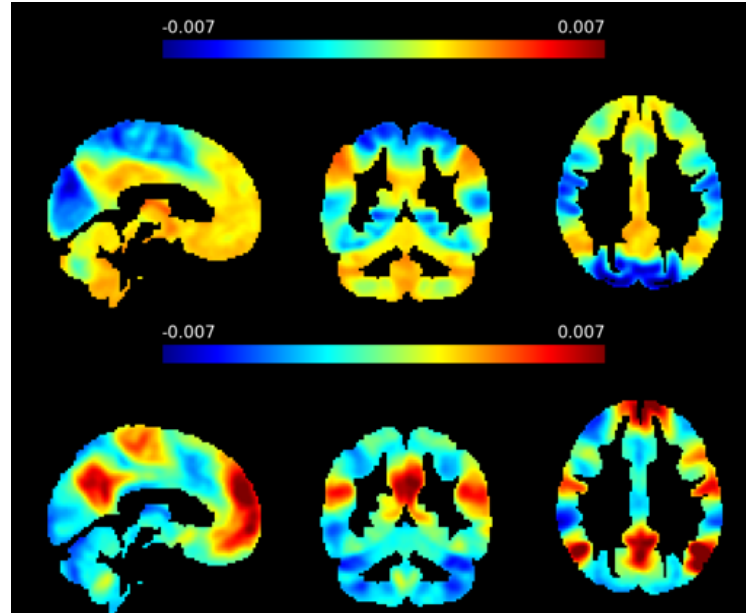
(a) First two leading positive eigenvectors of B using A_{cc}
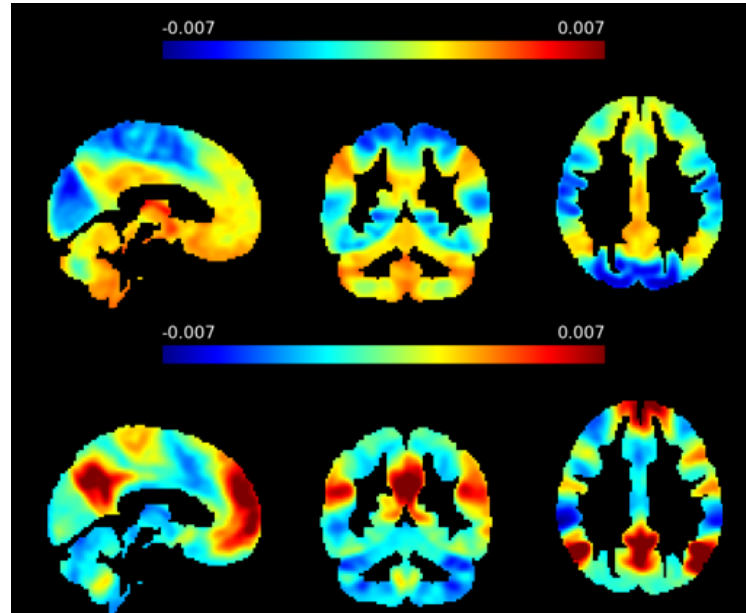
(b) First two leading negative eigenvectors of B using D_{isc}

Figure C.4 – Modularity leading eigenvectors: (a) and (b) show the first two leading modularity eigenvectors in the case where the adjacency was the Accordance matrix or the Discordance matrix, respectively. Positive and negative eigenvector entries are represented by red and blue colors, respectively. MNI coordinates: x=4, y=-50, z=29.

Fig. C.5 (a) shows the absolute value of the cosine similarity between the eigenvectors of the normalized graph Laplacian when constructed using $\mathbf{A_{cc}}$ and $\mathbf{D_{isc}}$ as adjacency, respectively. Fig. C.5 (b) shows the same information for the modularity matrix.
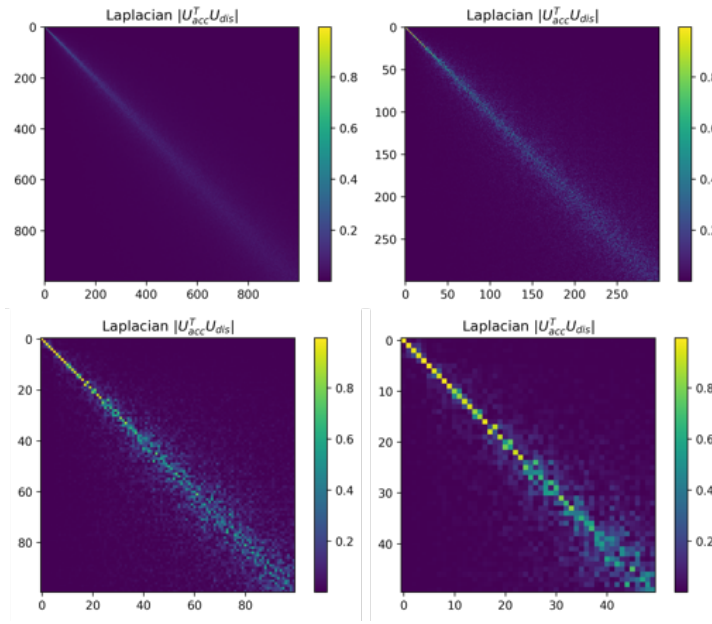
(a) Cosine similarity between U^L_{acc}, U^L_{disc}
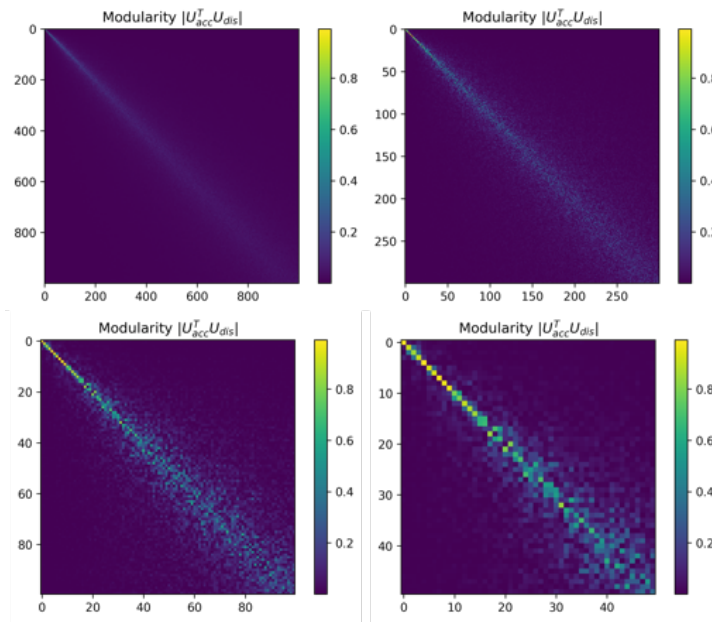
(b) Cosine similarity between U^B_{acc}, U^B_{disc}

Figure C.5 – Cosine similarity between the spectra: (a) and (b) show the absolute value of the cosine similarity of the eigenvectors when the adjacency was the Accordance or Discordance matrix, for the Laplacian and modularity matrix, respectively.

Fig. C.6 shows that the spatial configuration of the seventeen Yeo RSNs is not random with respect to the estimated Laplacian and modularity leading eigenvectors.
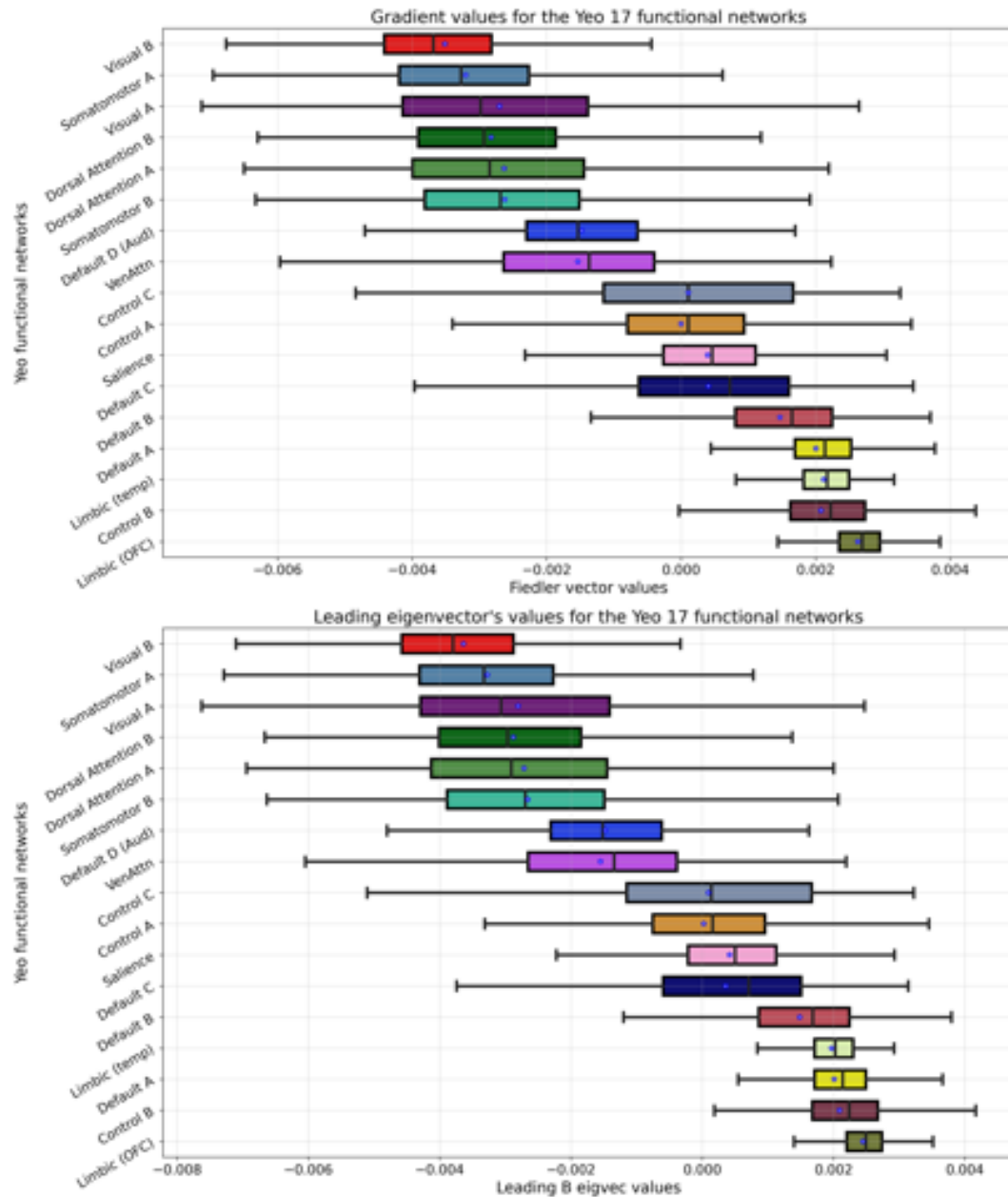
Figure C.6 – The Laplacian principle gradient's values (top) and the modularity leading eigen-vector's values (bottom) for each of the seventeen Yeo resting-state networks. For the sake of simplicity, here we visualize only the results based on the Accordance as adjacency matrix. The asterisks represent mean values. Colors represent the exact same colors used to describe the networks in Yeo et al. (2011).

Fig. C.7 illustrates an example of four resting-state networks (RSN) encoded in the leading modularity eigenvectors.
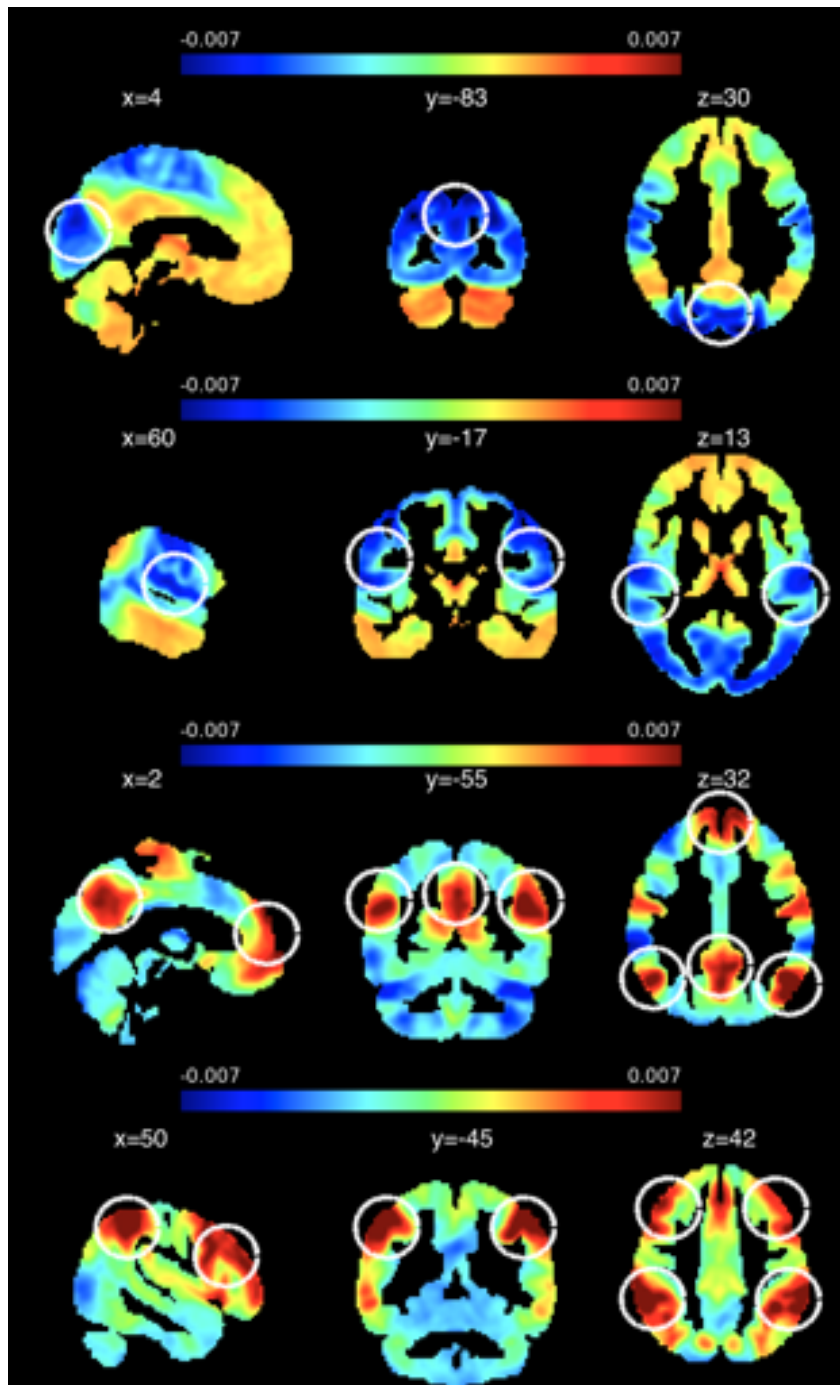
Figure C.7 – Example of four resting-state networks (RSN) recovered based on the leading modularity eigenvectors. Numbers indicate slice coordinates in MNI space. Positive and negative eigenvector entries are represented by red and blue colors, respectively. First row: visual, second row: auditory, third row: DMN and fourth row: fronto-parietal.

Bibliography

Aarnoudse-Moens, C. S. H., Weisglas-Kuperus, N., van Goudoever, J. B., and Oosterlaan, J. (2009). Meta-analysis of neurobehavioral outcomes in very preterm and/or very low birth weight children. *PEDIATRICS*, 124(2):717–728.

Adam-Darque, A., Pittet, M. P., Grouiller, F., Rihs, T. A., Leuchter, R. H.-V., Lazeyras, F., Michel, C. M., and Hüppi, P. S. (2020). Neural correlates of voice perception in newborns and the influence of preterm birth. *Cerebral Cortex*, 30(11):5717–5730.

Akiki, T. J. and Abdallah, C. G. (2019). Determining the hierarchical architecture of the human brain using subject-level clustering of functional networks. *Scientific Reports*, 9(1).

Alexander, B., Kelly, C. E., Adamson, C., Beare, R., Zannino, D., Chen, J., Murray, A. L., Loh, W. Y., Matthews, L. G., Warfield, S. K., Anderson, P. J., Doyle, L. W., Seal, M. L., Spittle, A. J., Cheong, J. L., and Thompson, D. K. (2019). Changes in neonatal regional brain volume associated with preterm birth and perinatal factors. *NeuroImage*, 185:654–663.

Ali, S. O. and Peynircioğğlu, Z. F. (2010). Intensity of emotions conveyed and elicited by familiar and unfamiliar music. *Music Perception*, 27(3):177–182.

Aljobouri, H. K., Jaber, H. A., Koçak, O. M., Algin, O., and Çankaya, I. (2018). Clustering fMRI data with a robust unsupervised learning algorithm for neuroscience data mining. *Journal of Neuroscience Methods*, 299:45–54.

Allen, K. (2014). Music therapy in the NICU: Is there evidence to support integration for procedural support ? *Adv Neonatal Care.*, 13(5).

Alluri, V., Toiviainen, P., Jääskeläinen, I. P., Glerean, E., Sams, M., and Brattico, E. (2012). Large-scale brain networks emerge from dynamic processing of musical timbre, key and rhythm. *NeuroImage*, 59(4):3677–3689.

Aly, H. A. and Ahmed, A. M. (2016). Effect of noise on neonatal vital data and behavior in nicu. *Clinical Medicine and Diagnostics*, 6:1–6.

Anderson, D. and Patel, A. (2018). Infants born preterm, stress, and neurodevelopment in the neonatal intensive care unit: might music have an impact? *Dev Med Child Neurol.*, 60(3).

Bibliography

Anderson, P. J., Cheong, J. L., and Thompson, D. K. (2015). The predictive validity of neonatal MRI for neurodevelopmental outcome in very preterm children. *Seminars in Perinatology*, 39(2):147–158.

Anderson, P. J. and Doyle, L. W. (2006). Neurodevelopmental outcome of bronchopulmonary dysplasia. *Seminars in Perinatology*, 30(4):227–232.

Andescavage, N. N., du Plessis, A., McCarter, R., Serag, A., Evangelou, I., Vezina, G., Robertson, R., and Limperopoulos, C. (2016). Complex trajectories of brain development in the healthy human fetus. *Cerebral Cortex*.

Ansermet, F. and Magistretti, P. (2019). *Biology of Freedom*. Routledge.

Arichi, T., Fagiolo, G., Varela, M., Melendez-Calderon, A., Allievi, A., Merchant, N., Tusor, N., Counsell, S. J., Burdet, E., Beckmann, C. F., and Edwards, A. D. (2012). Development of BOLD signal hemodynamic responses in the human brain. *NeuroImage*, 63(2):663–673.

ARPACK Software (2020). https://www.caam.rice.edu/software/ARPACK/. Accessed: 2020-03-17.

Arpino, C., Compagnone, E., Montanaro, M., Cacciatore, D., De Luca, A., Cerulli, A., Di Girolamo, S., and Curatolo, P. (2010). Preterm birth and neurodevelopmental outcome: a review. *Childs. Nerv. Syst.*, 26(9).

Atasoy, S., Donnelly, I., and Pearson, J. (2016). Human brain networks function in connectome-specific harmonic waves. *Nature Communications*, 7(1).

Atay, F. M., Bıyıkoğlu, T., and Jost, J. (2006). Network synchronization: Spectral versus statistical properties. *Physica D: Nonlinear Phenomena*, 224(1-2):35–41.

Avants, B. B., Tustison, N. J., Song, G., Cook, P. A., Klein, A., and Gee, J. C. (2011). A reproducible evaluation of ANTs similarity metric performance in brain image registration. *NeuroImage*, 54(3):2033–2044.

Baird, A. E. and Warach, S. (1998). Magnetic resonance imaging of acute stroke. *Journal of Cerebral Blood Flow & Metabolism*, 18(6):583–609.

Ball, G., Aljabar, P., Arichi, T., Tusor, N., Cox, D., Merchant, N., Nongena, P., Hajnal, J., Edwards, A., and Counsell, S. (2016). Machine-learning to characterise neonatal functional connectivity in the preterm brain. *NeuroImage*, 124.

Barnes, E. R. (1982). An algorithm for partitioning the nodes of a graph. *SIAM Journal on Algebraic Discrete Methods*, 3(4):541–550.

Barnes-Davis, M. E., Williamson, B. J., Merhar, S. L., Holland, S. K., and Kadis, D. S. (2020). Rewiring the extremely preterm brain: Altered structural connectivity relates to language function. *NeuroImage: Clinical*, 25:102194.

Baroncelli, L., Braschi, C., Spolidoro, M., Begenisic, T., Sale, A., and Maffei, L. (2010). Nurturing brain plasticity: impact of environmental enrichment. *Cell Death & Differentiation*, 17(7):1092–1103.

Bartal, T., Adams, M., Natalucci, G., Borradori-Tolsa, C., and Latal, B. (2020). Behavioral problems in very preterm children at five years of age using the strengths and difficulties questionnaire: A multicenter cohort study. *Early Human Development*, 151:105200.

Baruch, C. and Drake, C. (1997). Tempo discrimination in infants. *Infant Behavior and Development*, 20(4):573–577.

Basser, P., Mattiello, J., and LeBihan, D. (1994). MR diffusion tensor spectroscopy and imaging. *Biophysical Journal*, 66(1):259–267.

Basser, P. J. and Jones, D. K. (2002). Diffusion-tensor MRI: theory, experimental design and data analysis - a technical review. *NMR in Biomedicine*, 15(7-8):456–467.

Bassett, D. S. and Bullmore, E. T. (2016). Small-world brain networks revisited. *The Neuroscientist*, 23(5):499–516.

Baumgartner, T., Lutz, K., Schmidt, C. F., and Jäncke, L. (2006). The emotional power of music: How music enhances the feeling of affective pictures. *Brain Research*, 1075(1):151–164.

Bayer, S. (2003). *Atlas of human central nervous system development.* CRC Press, Boca Raton.

Bayley (1993). Bayley scales of infant development-second edition (BSID-II), mental scale and mental development index.

Beam, A. L., Fried, I., Palmer, N., Agniel, D., Brat, G., Fox, K., Kohane, I., Sinaiko, A., Zupancic, J. A. F., and Armstrong, J. (2020). Estimates of healthcare spending for preterm and low-birthweight infants in a commercially insured population: 2008–2016. *Journal of Perinatology*, 40(7):1091–1099.

Beauchamp, M. H., Thompson, D. K., Howard, K., Doyle, L. W., Egan, G. F., Inder, T. E., and Anderson, P. J. (2008). Preterm infant hippocampal volumes correlate with later working memory deficits. *Brain*, 131(11):2986–2994.

Behrens, T., Berg, H. J., Jbabdi, S., Rushworth, M., and Woolrich, M. (2007). Probabilistic diffusion tractography with multiple fibre orientations: What can we gain? *NeuroImage*, 34(1):144–155.

Bellec, P., Benhajali, Y., Carbonell, F., Dansereau, C., Albouy, G., Pelland, M., Craddock, C., Collignon, O., Doyon, J., Stip, E., and Orban, P. (2015). Impact of the resolution of brain parcels on connectome-wide association studies in fMRI. *NeuroImage*, 123:212–228.

Benarroch, E. E. (2018). Brainstem integration of arousal, sleep, cardiovascular, and respiratory control. *Neurology*, 91(21):958–966.

Bibliography

Benders, M. J., Palmu, K., Menache, C., Borradori-Tolsa, C., Lazeyras, F., Sizonenko, S., Dubois, J., Vanhatalo, S., and Hüppi, P. S. (2015). Early brain activity relates to subsequent brain growth in premature infants. *Cerebral Cortex*, 25(9):3014–3024.

Bengtsson, S. L. and Ullén, F. (2006). Dissociation between melodic and rhythmic processing during piano performance from musical scores. *NeuroImage*, 30(1):272–284.

Bernat, J. and Stępień, S. (2010). Induction motor analysis employing optimal torque predictor and massive conductor approach. *Archives of Electrical Engineering*, 59(1-2):99–107.

Betzel, R. F., Medaglia, J. D., Papadopoulos, L., Baum, G. L., Gur, R., Gur, R., Roalf, D., Satterthwaite, T. D., and Bassett, D. S. (2017). The modular organization of human anatomical brain networks: Accounting for the cost of wiring. *Network Neuroscience*, 1(1):42–68.

Bhutta, A. T., Cleves, M. A., Casey, P. H., Cradock, M. M., and Anand, K. J. S. (2002). Cognitive and behavioral outcomes of school-aged children who were born preterm. *JAMA*, 288(6):728.

Bihan, D. L. (2014). Diffusion MRI: what water tells us about the brain. *EMBO Molecular Medicine*, 6(5):569–573.

Biswal, B., Yetkin, F. Z., Haughton, V. M., and Hyde, J. S. (1995). Functional connectivity in the motor cortex of resting human brain using echo-planar mri. *Magnetic Resonance in Medicine*, 34(4):537–541.

Blackford, J. U., Buckholtz, J. W., Avery, S. N., and Zald, D. H. (2010). A unique role for the human amygdala in novelty detection. *NeuroImage*, 50(3):1188–1193.

Blencowe, H., Cousens, S., Chou, D., Oestergaard, M., Say, L., Moller, A.-B., Kinney, M., and and, J. L. (2013). Born too soon: The global epidemiology of 15 million preterm births. *Reproductive Health*, 10(Suppl 1):S2.

Blood, A. J. and Zatorre, R. J. (2001). Intensely pleasurable responses to music correlate with activity in brain regions implicated in reward and emotion. *Proceedings of the National Academy of Sciences*, 98(20):11818–11823.

Boardman, J. P., Counsell, S. J., Rueckert, D., Hajnal, J. V., Bhatia, K. K., Srinivasan, L., Kapellou, O., Aljabar, P., Dyet, L. E., Rutherford, M. A., Allsop, J. M., and Edwards, A. D. (2007). Early growth in brain volume is preserved in the majority of preterm infants. *Annals of Neurology*, 62(2):185–192.

Bobin-Bègue, A., Provasi, J., Marks, A., and Pouthas, V. (2006). Influence of auditory tempo on the endogenous rhythm of non-nutritive sucking. *European Review of Applied Psychology*, 56(4):239–245.

Bocchio, M., Nabavi, S., and Capogna, M. (2017). Synaptic plasticity, engrams, and network oscillations in amygdala circuits for storage and retrieval of emotional memories. *Neuron*, 94(4):731–743.

Bodini, B. and Ciccarelli, O. (2014). Diffusion MRI in neurological disorders. In *Diffusion MRI*, pages 241–255. Elsevier.

Bøe, T., Øverland, S., Lundervold, A. J., and Hysing, M. (2011). Socioeconomic status and children's mental health: results from the bergen child study. *Social Psychiatry and Psychiatric Epidemiology*, 47(10):1557–1566.

Bogert, B., Numminen-Kontti, T., Gold, B., Sams, M., Numminen, J., Burunat, I., Lampinen, J., and Brattico, E. (2016). Hidden sources of joy, fear, and sadness: Explicit versus implicit neural processing of musical emotions. *Neuropsychologia*, 89:393–402.

Bolas, N. (2016). Basic MRI principles. In *Equine MRI*, pages 1–37. John Wiley & Sons, Ltd.

Bonnici, H. M., Richter, F. R., Yazar, Y., and Simons, J. S. (2016). Multimodal feature integration in the angular gyrus during episodic and semantic retrieval. *Journal of Neuroscience*, 36(20):5462–5471.

Bora, S., Pritchard, V. E., Moor, S., Austin, N. C., and Woodward, L. J. (2011). Emotional and behavioural adjustment of children born very preterm at early school age. *Journal of Paediatrics and Child Health*, 47(12):863–869.

Bourgoin, L., Cipierre, C., Hauet, Q., Basset, H., Gournay, V., Rozé, J.-C., Flamant, C., and Gascoin, G. (2016). Neurodevelopmental outcome at 2 years of age according to patent ductus arteriosus management in very preterm infants. *Neonatology*, 109(2):139–146.

Bouyssi-Kobar, M., du Plessis, A. J., McCarter, R., Brossard-Racine, M., Murnick, J., Tinkleman, L., Robertson, R. L., and Limperopoulos, C. (2016). Third trimester brain growth in preterm infants compared with in utero healthy fetuses. *Pediatrics*, 138(5):e20161640.

Bowman, F. D. (2005). Spatio-temporal modeling of localized brain activity. *Biostatistics*, 6(4):558–575.

Bradley, R. H. and Corwyn, R. F. (2002a). Socioeconomic status and child development. *Annual Review of Psychology*, 53(1):371–399.

Bradley, R. H. and Corwyn, R. F. (2002b). Socioeconomic status and child development. *Annual Review of Psychology*, 53(1):371–399.

Bravo, F., Cross, I., Hopkins, C., Gonzalez, N., Docampo, J., Bruno, C., and Stamatakis, E. A. (2019). Anterior cingulate and medial prefrontal cortex response to systematically controlled tonal dissonance during passive music listening. *Human Brain Mapping*, 41(1):46–66.

Breiman, L. (2001). Random forests. *Machine Learning*, 45(1):5–32.

Brindle, K. (2008). New approaches for imaging tumour responses to treatment. *Nature Reviews Cancer*, 8(2):94–107.

Bibliography

Brodmann, K. (1994). Localization in the cerebral cortex.(lj garey, trans.). *London: Smith-Gordon.(Original work published 1909).*

Brown, G. D., Yamada, S., and Sejnowski, T. J. (2001). Independent component analysis at the neural cocktail party. *Trends in Neurosciences*, 24(1):54–63.

Brown, M. A. and Semelka, R. C. (2011). *MRI: basic principles and applications.* John Wiley & Sons.

Brown, S., Martinez, M. J., and Parsons, L. M. (2004). Passive music listening spontaneously engages limbic and paralimbic systems. *NeuroReport*, 15(13):2033–2037.

Buckner, R. L., Sepulcre, J., Talukdar, T., Krienen, F. M., Liu, H., Hedden, T., Andrews-Hanna, J. R., Sperling, R. A., and Johnson, K. A. (2009). Cortical hubs revealed by intrinsic functional connectivity: Mapping, assessment of stability, and relation to alzheimers disease. *Journal of Neuroscience*, 29(6):1860–1873.

Bullmore, E. and Sporns, O. (2009). Complex brain networks: graph theoretical analysis of structural and functional systems. *Nature Reviews Neuroscience*, 10(3):186–198.

Burnett, A. C., Youssef, G., Anderson, P. J., Duff, J., Doyle, L. W., and and, J. L. C. (2019). Exploring the "preterm behavioral phenotype" in children born extremely preterm. *Journal of Developmental & Behavioral Pediatrics*, 40(3):200–207.

Bäuml, J. G., Daamen, M., Meng, C., Neitzel, J., Scheef, L., Jaekel, J., Busch, B., Baumann, N., Bartmann, P., Wolke, D., Boecker, H., Wohlschläger, A. M., and Sorg, C. (2015). Correspondence between aberrant intrinsic network connectivity and gray-matter volume in the ventral brain of preterm born adults. *Cerebral Cortex*, 25(11):4135–4145.

Canals, S., Beyerlein, M., Merkle, H., and Logothetis, N. K. (2009). Functional MRI evidence for LTP-induced neural network reorganization. *Current Biology*, 19(5):398–403.

Cancedda, L. (2004). Acceleration of visual system development by environmental enrichment. *Journal of Neuroscience*, 24(20):4840–4848.

Cantou, P., Platel, H., Desgranges, B., and Groussard, M. (2018). How motor, cognitive and musical expertise shapes the brain: Focus on fMRI and EEG resting-state functional connectivity. *Journal of Chemical Neuroanatomy*, 89:60–68.

Capaldi, D. M. (1992). Co-occurrence of conduct problems and depressive symptoms in early adolescent boys: II. a 2-year follow-up at grade 8. *Development and Psychopathology*, 4(1):125–144.

Chang, C. and Glover, G. H. (2010). Time–frequency dynamics of resting-state brain connectivity measured with fMRI. *NeuroImage*, 50(1):81–98.

Chen, G., Adleman, N. E., Saad, Z. S., Leibenluft, E., and Cox, R. W. (2014). Applications of multivariate modeling to neuroimaging group analysis: A comprehensive alternative to univariate general linear model. *NeuroImage*, 99:571–588.

Chenevert, T. L., Brunberg, J. A., and Pipe, J. G. (1990). Anisotropic diffusion in human white matter: demonstration with MR techniques in vivo. *Radiology*, 177(2):401–405.

Cheong, J. L. and Doyle, L. W. (2018). An update on pulmonary and neurodevelopmental outcomes of bronchopulmonary dysplasia. *Seminars in Perinatology*, 42(7):478–484.

Cheong, J. L., Thompson, D. K., Spittle, A. J., Potter, C. R., Walsh, J. M., Burnett, A. C., Lee, K. J., Chen, J., Beare, R., Matthews, L. G., Hunt, R. W., Anderson, P. J., and Doyle, L. W. (2016). Brain volumes at term-equivalent age are associated with 2-year neurodevelopment in moderate and late preterm children. *The Journal of Pediatrics*, 174:91–97.e1.

Chou, E. T. and Carrino, J. A. (2007). Magnetic resonance imaging. In *Pain Management*, pages 106–117. Elsevier.

Christensen, D., Schieve, L., Devine, O., and Drews-Botschc, C. (2014). Socioeconomic status, child enrichment factors, and cognitive performance among preschool-age children: Results from the follow-up of growth and development experiences study. *Res Dev Disabil.*, 35(7).

Chung, E. H., Chou, J., and Brown, K. A. (2020). Neurodevelopmental outcomes of preterm infants: a recent literature review. *Translational Pediatrics*, 9(S1):S3–S8.

Chung, F. (1996). *Spectral Graph Theory*. American Mathematical Society.

Cismaru, A. L., Gui, L., Vasung, L., Lejeune, F., Barisnikov, K., Truttmann, A., Tolsa, C. B., and Hüppi, P. S. (2016). Altered amygdala development and fear processing in prematurely born infants. *Frontiers in Neuroanatomy*, 10.

Cole, M. W., Yarkoni, T., Repovs, G., Anticevic, A., and Braver, T. S. (2012). Global connectivity of prefrontal cortex predicts cognitive control and intelligence. *Journal of Neuroscience*, 32(26):8988–8999.

Conrad, A. L., Richman, L., Lindgren, S., and Nopoulos, P. (2010). Biological and environmental predictors of behavioral sequelae in children born preterm. *PEDIATRICS*, 125(1):e83–e89.

Conturo, T. E., Lori, N. F., Cull, T. S., Akbudak, E., Snyder, A. Z., Shimony, J. S., McKinstry, R. C., Burton, H., and Raichle, M. E. (1999). Tracking neuronal fiber pathways in the living human brain. *Proceedings of the National Academy of Sciences*, 96(18):10422–10427.

Counsell, S. and Boardman, J. (2005). Differential brain growth in the infant born preterm: Current knowledge and future developments from brain imaging. *Seminars in Fetal & Neonatal Medicine*, 10(5).

Bibliography

Craddock, R. C., James, G. A., Holtzheimer, P. E., Hu, X. P., and Mayberg, H. S. (2012). A whole brain fMRI atlas generated via spatially constrained spectral clustering. *Human Brain Mapping*, 33(8):1914–1928.

Crooks, L. E. and Hylton, N. M. (1994). *MR Principles and Technology*, pages 353–373. Springer Berlin Heidelberg, Berlin, Heidelberg.

Curran, K. M., Emsell, L., and Leemans, A. (2016). Quantitative DTI measures. In *Diffusion Tensor Imaging*, pages 65–87. Springer New York.

Cusack, R., McCuaig, O., and Linke, A. C. (2018). Methodological challenges in the comparison of infant fMRI across age groups. *Developmental Cognitive Neuroscience*, 33:194–205.

Damadian, R., Goldsmith, M., and Minkoff, L. (1977). NMR in cancer: XVI. FONAR image of the live human body. *Physiol Chem Phys*, 9(1):97–100.

Damoiseaux, J. S., Rombouts, S. A. R. B., Barkhof, F., Scheltens, P., Stam, C. J., Smith, S. M., and Beckmann, C. F. (2006). Consistent resting-state networks across healthy subjects. *Proceedings of the National Academy of Sciences*, 103(37):13848–13853.

Das, T. K., Abeyasinghe, P. M., Crone, J. S., Sosnowski, A., Laureys, S., Owen, A. M., and Soddu, A. (2014). Highlighting the structure-function relationship of the brain with the ising model and graph theory. *BioMed Research International*, 2014:1–14.

de Almeida, J. S., Meskaldji, D.-E., Loukas, S., Lordier, L., Gui, L., Lazeyras, F., and Hüppi, P. S. (2021). Preterm birth leads to impaired rich-club organization and fronto-paralimbic/limbic structural connectivity in newborns. *NeuroImage*, 225:117440.

de Groot, J. C., de Leeuw, F.-E., Oudkerk, M., Hofman, A., Jolles, J., and Breteler, M. M. B. (2000). Cerebral white matter lesions and depressive symptoms in elderly adults. *Archives of General Psychiatry*, 57(11):1071.

de KIEVIET, J. F., ZOETEBIER, L., van ELBURG, R. M., VERMEULEN, R. J., and OOSTERLAAN, J. (2012). Brain development of very preterm and very low-birthweight children in childhood and adolescence: a meta-analysis. *Developmental Medicine & Child Neurology*, 54(4):313–323.

de Laat, S. A. A., Essink-Bot, M.-L., van Wassenaer-Leemhuis, A. G., and Vrijkotte, T. G. (2016). Effect of socioeconomic status on psychosocial problems in 5- to 6-year-old preterm- and term-born children: the ABCD study. *European Child & Adolescent Psychiatry*, 25(7):757–767.

de Reus, M. A. and van den Heuvel, M. P. (2013). The parcellation-based connectome: Limitations and extensions. *NeuroImage*, 80:397–404.

de Silva, A., Neel, M. L., Maitre, N., Busch, T., and Taylor, H. G. (2020). Resilience and vulnerability in very preterm 4-year-olds. *The Clinical Neuropsychologist*, pages 1–21.

Dehaene-Lambertz, G., Montavont, A., Jobert, A., Allirol, L., Dubois, J., Hertz-Pannier, L., and Dehaene, S. (2010). Language or music, mother or mozart? structural and environmental influences on infants' language networks. *Brain and Language*, 114(2):53–65.

Delobel-Ayoub, M. (2006). Behavioral outcome at 3 years of age in very preterm infants: The EPIPAGE study. *PEDIATRICS*, 117(6):1996–2005.

Delobel-Ayoub, M., Arnaud, C., White-Koning, M., Casper, C., Pierrat, V., Garel, M., Burguet, A., Roze, J., Matis, J., Picaud, J., Kaminski, M., and Larroque, B. (2009). Behavioral problems and cognitive performance at 5 years of age after very preterm birth: The EPIPAGE study. *Pediatrics*, 123(6).

Demertzi, A., Soddu, A., Faymonville, M.-E., Bahri, M., Gosseries, O., Vanhaudenhuyse, A., Phillips, C., Maquet, P., Noirhomme, Q., Luxen, A., and Laureys, S. (2011). Hypnotic modulation of resting state fMRI default mode and extrinsic network connectivity. In *Slow Brain Oscillations of Sleep, Resting State and Vigilance*, pages 309–322. Elsevier.

Dewey, D., Thompson, D. K., Kelly, C. E., Spittle, A. J., Cheong, J. L. Y., Doyle, L. W., and Anderson, P. J. (2019). Very preterm children at risk for developmental coordination disorder have brain alterations in motor areas. *Acta Paediatrica*, 108(9):1649–1660.

Dhond, R. P., Yeh, C., Park, K., Kettner, N., and Napadow, V. (2008). Acupuncture modulates resting state connectivity in default and sensorimotor brain networks. *Pain*, 136(3):407–418.

Diez, I., Bonifazi, P., Escudero, I., Mateos, B., Muñoz, M. A., Stramaglia, S., and Cortes, J. M. (2015). A novel brain partition highlights the modular skeleton shared by structure and function. *Scientific Reports*, 5(1).

Dijk, K. R. A. V., Hedden, T., Venkataraman, A., Evans, K. C., Lazar, S. W., and Buckner, R. L. (2010). Intrinsic functional connectivity as a tool for human connectomics: Theory, properties, and optimization. *Journal of Neurophysiology*, 103(1):297–321.

Doran, M., Hajnal, J. V., Bruggen, N. V., King, M. D., Young, I. R., and Bydder, G. M. (1990). Normal and abnormal white matter tracts shown by MR imaging using directional diffusion weighted sequences. *Journal of Computer Assisted Tomography*, 14(6):865–873.

Doria, V., Beckmann, C. F., Arichi, T., Merchant, N., Groppo, M., Turkheimer, F. E., Counsell, S. J., Murgasova, M., Aljabar, P., Nunes, R. G., Larkman, D. J., Rees, G., and Edwards, A. D. (2010). Emergence of resting state networks in the preterm human brain. *Proceedings of the National Academy of Sciences*, 107(46):20015–20020.

Dosenbach, N. U. F., Nardos, B., Cohen, A. L., Fair, D. A., Power, J. D., Church, J. A., Nelson, S. M., Wig, G. S., Vogel, A. C., Lessov-Schlaggar, C. N., Barnes, K. A., Dubis, J. W., Feczko, E., Coalson, R. S., Pruett, J. R., Barch, D. M., Petersen, S. E., and Schlaggar, B. L. (2010). Prediction of individual brain maturity using fMRI. *Science*, 329(5997):1358–1361.

Bibliography

Doucet, G., Naveau, M., Petit, L., Delcroix, N., Zago, L., Crivello, F., Jobard, G., Tzourio-Mazoyer, N., Mazoyer, B., Mellet, E., and Joliot, M. (2011). Brain activity at rest: a multiscale hierarchical functional organization. *Journal of Neurophysiology*, 105(6):2753–2763.

Doyle, L. and Anderson, P. (2010). Adult outcome of extremely preterm infants. *Pediatrics*, 126(2).

Doyle, L. W. and Anderson, P. J. (2009). Long-term outcomes of bronchopulmonary dysplasia. *Seminars in Fetal and Neonatal Medicine*, 14(6):391–395.

Dubois, J., Alison, M., Counsell, S. J., Hertz-Pannier, L., Hüppi, P. S., and Benders, M. J. (2020). MRI of the neonatal brain: A review of methodological challenges and neuroscientific advances. *Journal of Magnetic Resonance Imaging*.

Dubois, J., Benders, M., Borradori-Tolsa, C., Cachia, A., Lazeyras, F., Leuchter, R. H.-V., Sizonenko, S. V., Warfield, S. K., Mangin, J. F., and Hüppi, P. S. (2008). Primary cortical folding in the human newborn: an early marker of later functional development. *Brain*, 131(8):2028–2041.

Eguíluz, V. M., Chialvo, D. R., Cecchi, G. A., Baliki, M., and Apkarian, A. V. (2005). Scale-free brain functional networks. *Phys. Rev. Lett.*, 94:018102.

Eickhoff, S. B., Constable, R. T., and Yeo, B. T. (2018). Topographic organization of the cerebral cortex and brain cartography. *NeuroImage*, 170:332–347.

Elgen, I. (2002). Population based, controlled study of behavioural problems and psychiatric disorders in low birthweight children at 11 years of age. *Archives of Disease in Childhood - Fetal and Neonatal Edition*, 87(2):128F–132.

ElHassan, N. O., Bai, S., Gibson, N., Holland, G., Robbins, J. M., and Kaiser, J. R. (2018). The impact of prematurity and maternal socioeconomic status and education level on achievement-test scores up to 8th grade. *PLOS ONE*, 13(5):e0198083.

Elton, A. and Gao, W. (2015). Task-related modulation of functional connectivity variability and its behavioral correlations. *Human Brain Mapping*, 36(8):3260–3272.

Eryilmaz, H., Ville, D. V. D., Schwartz, S., and Vuilleumier, P. (2011). Impact of transient emotions on functional connectivity during subsequent resting state: A wavelet correlation approach. *NeuroImage*, 54(3):2481–2491.

Escobar, C., Ansermet, F., and Magistretti, P. J. (2017). A historical review of diachrony and semantic dimensions of trace in neurosciences and lacanian psychoanalysis. *Frontiers in Psychology*, 8.

Essen, D. C. V., Smith, S. M., Barch, D. M., Behrens, T. E., Yacoub, E., and Ugurbil, K. (2013). The WU-minn human connectome project: An overview. *NeuroImage*, 80:62–79.

Farah, M. J., Shera, D. M., Savage, J. H., Betancourt, L., Giannetta, J. M., Brodsky, N. L., Malmud, E. K., and Hurt, H. (2006). Childhood poverty: Specific associations with neurocognitive development. *Brain Research*, 1110(1):166–174.

Favrais, G. and Saliba, E. (2019). Neurodevelopmental outcome of late-preterm infants: Literature review. *Archives de Pédiatrie*, 26(8):492–496.

Feinberg, D. A., Moeller, S., Smith, S. M., Auerbach, E., Ramanna, S., Glasser, M. F., Miller, K. L., Ugurbil, K., and Yacoub, E. (2010). Multiplexed echo planar imaging for sub-second whole brain FMRI and fast diffusion imaging. *PLoS ONE*, 5(12):e15710.

Fernández-Gil, M. Á., Palacios-Bote, R., Leo-Barahona, M., and Mora-Encinas, J. (2010). Anatomy of the brainstem: A gaze into the stem of life. *Seminars in Ultrasound, CT and MRI*, 31(3):196–219.

Fevang, S. K. E., Hysing, M., Sommerfelt, K., and Elgen, I. (2017). Mental health assessed by the strengths and difficulties questionnaire for children born extremely preterm without severe disabilities at 11 years of age: a norwegian, national population-based study. *European Child & Adolescent Psychiatry*, 26(12):1523–1531.

Fiedler, M. (1973). Czechoslovak Mathematical Journal Miroslav Fiedler Algebraic connectivity of graphs ALGEBRAIC CONNECTIVITY OF GRAPHS*). *Czechoslovak Mathematical Journal*, 23(2398):298–305.

Filippa, M., Frassoldati, R., Talucci, G., and Ferrari, F. (2015). Mothers singing and speaking to preterm infants in nicu. *J Pediatr Neonat Individual Med.*, 4(2).

Filippa, M., Panza, C., Ferrari, F., Frassoldati, R., Kuhn, P., Balduzzi, S., and D'Amico, R. (2017). Systematic review of maternal voice interventions demonstrates increased stability in preterm infants. *Acta Paediatr.*, 106(8).

Fink, G. R. (2007). Functional magnetic resonance imaging. In *Neurobiology of Disease*, pages 839–848. Elsevier.

Fink, K. R. T. and Fink, J. R. (2018). Principles of modern neuroimaging. In *Principles of Neurological Surgery*, pages 62–86.e2. Elsevier.

Finn, E. S., Shen, X., Scheinost, D., Rosenberg, M. D., Huang, J., Chun, M. M., Papademetris, X., and Constable, R. T. (2015). Functional connectome fingerprinting: identifying individuals using patterns of brain connectivity. *Nature Neuroscience*, 18(11):1664–1671.

Firth, N. C., Primativo, S., Brotherhood, E., Young, A. L., Yong, K. X., Crutch, S. J., Alexander, D. C., and Oxtoby, N. P. (2020). Sequences of cognitive decline in typical alzheimer's disease and posterior cortical atrophy estimated using a novel event-based model of disease progression. *Alzheimer's & Dementia*, 16(7):965–973.

Bibliography

Fischi-Gómez, E., Vasung, L., Meskaldji, D., Lazeyras, F., Borradori-Tolsa, C., Hagmann, P., Barisnikov, K., Thiran, J., and Huppi, P. (2015). Structural brain connectivity in school-age preterm infants provides evidence for impaired networks relevant for higher order cognitive skills and social cognition. *Cereb Cortex.*, 25(9).

Fluss, J., Ziegler, J. C., Warszawski, J., Ducot, B., Richard, G., and Billard, C. (2009). Poor reading in french elementary school: The interplay of cognitive, behavioral, and socioeconomic factors. *Journal of Developmental & Behavioral Pediatrics*, 30(3):206–216.

Fong, A. H. C., Yoo, K., Rosenberg, M. D., Zhang, S., Li, C.-S. R., Scheinost, D., Constable, R. T., and Chun, M. M. (2019). Dynamic functional connectivity during task performance and rest predicts individual differences in attention across studies. *NeuroImage*, 188:14–25.

Fonteijn, H. M., Modat, M., Clarkson, M. J., Barnes, J., Lehmann, M., Hobbs, N. Z., Scahill, R. I., Tabrizi, S. J., Ourselin, S., Fox, N. C., and Alexander, D. C. (2012). An event-based model for disease progression and its application in familial alzheimer's disease and huntington's disease. *NeuroImage*, 60(3):1880–1889.

Formisano, E., Martino, F. D., and Valente, G. (2008). Multivariate analysis of fMRI time series: classification and regression of brain responses using machine learning. *Magnetic Resonance Imaging*, 26(7):921–934.

Fornito, A., Zalesky, A., and Breakspear, M. (2015). The connectomics of brain disorders. *Nature Reviews Neuroscience*, 16(3):159–172.

Fortunato, S. (2010). Community detection in graphs. *Physics Reports*, 486(3-5):75–174.

Fox, M. D. (2010). Clinical applications of resting state functional connectivity. *Frontiers in Systems Neuroscience*.

Frankland, P. W., Josselyn, S. A., and Köhler, S. (2019). The neurobiological foundation of memory retrieval. *Nature Neuroscience*, 22(10):1576–1585.

Freitas, C., Manzato, E., Burini, A., Taylor, M. J., Lerch, J. P., and Anagnostou, E. (2018). Neural correlates of familiarity in music listening: A systematic review and a neuroimaging meta-analysis. *Frontiers in Neuroscience*, 12.

Freitas, L. G., Bolton, T. A., Krikler, B. E., Jochaut, D., Giraud, A.-L., Hüppi, P. S., and Ville, D. V. D. (2020). Time-resolved effective connectivity in task fMRI: Psychophysiological interactions of co-activation patterns. *NeuroImage*, 212:116635.

Friston, K., Buechel, C., Fink, G., Morris, J., Rolls, E., and Dolan, R. (1997). Psychophysiological and modulatory interactions in neuroimaging. *NeuroImage*, 6(3):218–229.

Friston, K., Frith, C., Frackowiak, R., and Turner, R. (1995a). Characterizing dynamic brain responses with fMRI: A multivariate approach. *NeuroImage*, 2(2):166–172.

Friston, K., Harrison, L., and Penny, W. (2003). Dynamic causal modelling. *NeuroImage*, 19(4):1273–1302.

Friston, K., Holmes, A., Poline, J.-B., Grasby, P., Williams, S., Frackowiak, R., and Turner, R. (1995b). Analysis of fMRI time-series revisited. *NeuroImage*, 2(1):45–53.

Friston, K. J. (2005). Models of brain function in neuroimaging. *Annual Review of Psychology*, 56(1):57–87.

Friston, K. J., Josephs, O., Rees, G., and Turner, R. (1998). Nonlinear event-related responses in fMRI. *Magnetic Resonance in Medicine*, 39(1):41–52.

Friston, K. J., Williams, S., Howard, R., Frackowiak, R. S. J., and Turner, R. (1996). Movement-related effects in fMRI time-series. *Magnetic Resonance in Medicine*, 35(3):346–355.

Gano, D. and Ferriero, D. M. (2017). Altered cerebellar development in preterm newborns: Chicken or egg? *The Journal of Pediatrics*, 182:11–13.

Gardner, F. (2004). Behavioral and emotional adjustment of teenagers in mainstream school who were born before 29 weeks' gestation. *PEDIATRICS*, 114(3):676–682.

Garza-Villarreal, E. A., Jiang, Z., Vuust, P., Alcauter, S., Vase, L., Pasaye, E. H., Cavazos-Rodriguez, R., Brattico, E., Jensen, T. S., and Barrios, F. A. (2015). Music reduces pain and increases resting state fMRI BOLD signal amplitude in the left angular gyrus in fibromyalgia patients. *Frontiers in Psychology*, 6.

Gilmore, J. H., Lin, W., Prastawa, M. W., Looney, C. B., Vetsa, Y. S. K., Knickmeyer, R. C., Evans, D. D., Smith, J. K., Hamer, R. M., Lieberman, J. A., and Gerig, G. (2007). Regional gray matter growth, sexual dimorphism, and cerebral asymmetry in the neonatal brain. *Journal of Neuroscience*, 27(6):1255–1260.

Gimenez, M., Junque, C., Vendrell, P., Narberhaus, A., Bargallo, N., Botet, F., and Mercader, J. (2006). Abnormal orbitofrontal development due to prematurity. *Neurology*, 67(10).

Girouard, P. C., BAILLARGEON, R. H., TREMBLAY, R. E., GLORIEUX, J., LEFEBVRE, F., and ROBAEY, P. (1998). Developmental pathways leading to externalizing behaviors in 5 year olds born before 29 weeks of gestation. *Journal of Developmental & Behavioral Pediatrics*, 19(4):244–253.

Glasser, M. F., Coalson, T. S., Robinson, E. C., Hacker, C. D., Harwell, J., Yacoub, E., Ugurbil, K., Andersson, J., Beckmann, C. F., Jenkinson, M., Smith, S. M., and Essen, D. C. V. (2016). A multi-modal parcellation of human cerebral cortex. *Nature*, 536(7615):171–178.

Glasser, M. F., Sotiropoulos, S. N., Wilson, J. A., Coalson, T. S., Fischl, B., Andersson, J. L., Xu, J., Jbabdi, S., Webster, M., Polimeni, J. R., Essen, D. C. V., and Jenkinson, M. (2013). The minimal preprocessing pipelines for the human connectome project. *NeuroImage*, 80:105–124.

Bibliography

Goodman, R. (1997). The strengths and difficulties questionnaire: A research note. *Journal of Child Psychology and Psychiatry*, 38(5):581–586.

Goodman, R., Ford, T., Simmons, H., Gatward, R., and Meltzer, H. (2003). Using the strengths and difficulties questionnaire (SDQ) to screen for child psychiatric disorders in a community sample. *International Review of Psychiatry*, 15(1-2):166–172.

Goodman, R., Renfrew, D., and Mullick, M. (2000a). Predicting type of psychiatric disorder from strengths and difficulties questionnaire (SDQ) scores in child mental health clinics in london and dhaka. *European Child & Adolescent Psychiatry*, 9(2):129–134.

Goodman, R., Renfrew, D., and Mullick, M. (2000b). Predicting type of psychiatric disorder from strengths and difficulties questionnaire (SDQ) scores in child mental health clinics in london and dhaka. *European Child & Adolescent Psychiatry*, 9(2):129–134.

Gordon, C. L., Cobb, P. R., and Balasubramaniam, R. (2018). Recruitment of the motor system during music listening: An ALE meta-analysis of fMRI data. *PLOS ONE*, 13(11):e0207213.

Gore, J. C. (2003). Principles and practice of functional MRI of the human brain. *Journal of Clinical Investigation*, 112(1):4–9.

Grahn, J. A. and Rowe, J. B. (2009). Feeling the beat: Premotor and striatal interactions in musicians and nonmusicians during beat perception. *Journal of Neuroscience*, 29(23):7540–7548.

Grahn, J. A. and Rowe, J. B. (2013). Finding and feeling the musical beat: Striatal dissociations between detection and prediction of regularity. *Cerebral Cortex*, 23(4):913–921.

Granier-Deferre, C., Bassereau, S., Ribeiro, A., Jacquet, A.-Y., and DeCasper, A. J. (2011). A melodic contour repeatedly experienced by human near-term fetuses elicits a profound cardiac reaction one month after birth. *PLoS ONE*, 6(2):e17304.

Gray, R. F. (2004a). Prevalence, stability, and predictors of clinically significant behavior problems in low birth weight children at 3, 5, and 8 years of age. *PEDIATRICS*, 114(3):736–743.

Gray, R. F. (2004b). Prevalence, stability, and predictors of clinically significant behavior problems in low birth weight children at 3, 5, and 8 years of age. *PEDIATRICS*, 114(3):736–743.

Graybiel, A. M. (2008). Habits, rituals, and the evaluative brain. *Annual Review of Neuroscience*, 31(1):359–387.

Graz, M. B., Tolsa, J.-F., and Fumeaux, C. J. F. (2015). Being small for gestational age: Does it matter for the neurodevelopment of premature infants? a cohort study. *PLOS ONE*, 10(5):e0125769.

194

Gregory, M. D., Agam, Y., Selvadurai, C., Nagy, A., Vangel, M., Tucker, M., Robertson, E. M., Stickgold, R., and Manoach, D. S. (2014). Resting state connectivity immediately following learning correlates with subsequent sleep-dependent enhancement of motor task performance. *NeuroImage*, 102:666–673.

Greicius, M. D., Krasnow, B., Reiss, A. L., and Menon, V. (2002). Functional connectivity in the resting brain: A network analysis of the default mode hypothesis. *Proceedings of the National Academy of Sciences*, 100(1):253–258.

Groussard, M., Joie, R. L., Rauchs, G., Landeau, B., Chételat, G., Viader, F., Desgranges, B., Eustache, F., and Platel, H. (2010a). When music and long-term memory interact: Effects of musical expertise on functional and structural plasticity in the hippocampus. *PLoS ONE*, 5(10):e13225.

Groussard, M., Rauchs, G., Landeau, B., Viader, F., Desgranges, B., Eustache, F., and Platel, H. (2010b). The neural substrates of musical memory revealed by fMRI and two semantic tasks. *NeuroImage*, 53(4):1301–1309.

Grover, V. P., Tognarelli, J. M., Crossey, M. M., Cox, I. J., Taylor-Robinson, S. D., and McPhail, M. J. (2015). Magnetic resonance imaging: Principles and techniques: Lessons for clinicians. *Journal of Clinical and Experimental Hepatology*, 5(3):246–255.

Gui, L., Lisowski, R., Faundez, T., Hüppi, P. S., Lazeyras, F., and Kocher, M. (2012). Morphology-driven automatic segmentation of MR images of the neonatal brain. *Medical Image Analysis*, 16(8):1565–1579.

Gui, L., Loukas, S., Lazeyras, F., Hüppi, P., Meskaldji, D., and Tolsa, C. B. (2019). Longitudinal study of neonatal brain tissue volumes in preterm infants and their ability to predict neurodevelopmental outcome. *NeuroImage*, 185:728–741.

Guzzetta, A., Baldini, S., Bancale, A., Baroncelli, L., Ciucci, F., Ghirri, P., Putignano, E., Sale, A., Viegi, A., Berardi, N., Boldrini, A., Cioni, G., and Maffei, L. (2009). Massage accelerates brain development and the maturation of visual function. *Journal of Neuroscience*, 29(18):6042–6051.

Háden, G. P., Honing, H., Török, M., and Winkler, I. (2015). Detecting the temporal structure of sound sequences in newborn infants. *International Journal of Psychophysiology*, 96(1):23–28.

Háden, G. P., Stefanics, G., Vestergaard, M. D., Denham, S. L., Sziller, I., and Winkler, I. (2009). Timbre-independent extraction of pitch in newborn infants. *Psychophysiology*, 46(1):69–74.

Hamano, Y. H., Sugawara, S. K., Yoshimoto, T., and Sadato, N. (2020). The motor engram as a dynamic change of the cortical network during early sequence learning: An fMRI study. *Neuroscience Research*, 153:27–39.

Bibliography

Hampson, M., Olson, I. R., Leung, H.-C., Skudlarski, P., and Gore, J. C. (2004). Changes in functional connectivity of human MT/v5 with visual motion input. *NeuroReport*, 15(8):1315–1319.

Harrison, B. J., Pujol, J., Ortiz, H., Fornito, A., Pantelis, C., and Yücel, M. (2008). Modulation of brain resting-state networks by sad mood induction. *PLoS ONE*, 3(3):e1794.

Haslbeck, F. (2012). Music therapy for premature infants and their parents: an integrative review. *Nordic Journal of Music Therapy*, 21(3).

Healy, E., Reichenberg, A., Nam, K. W., Allin, M. P., Walshe, M., Rifkin, L., Murray, S. R. M., and Nosarti, C. (2013). Preterm birth and adolescent social functioning–alterations in emotion-processing brain areas. *The Journal of Pediatrics*, 163(6):1596–1604.

Hearst, M., Dumais, S., Osuna, E., Platt, J., and Scholkopf, B. (1998). Support vector machines. *IEEE Intelligent Systems and their Applications*, 13(4):18–28.

Heckemann, R. A., Hajnal, J. V., Aljabar, P., Rueckert, D., and Hammers, A. (2006). Automatic anatomical brain MRI segmentation combining label propagation and decision fusion. *NeuroImage*, 33(1):115–126.

Honey, C. J., Sporns, O., Cammoun, L., Gigandet, X., Thiran, J. P., Meuli, R., and Hagmann, P. (2009). Predicting human resting-state functional connectivity from structural connectivity. *Proceedings of the National Academy of Sciences*, 106(6):2035–2040.

Hoogman, M., Bralten, J., Hibar, D. P., Mennes, M., Zwiers, M. P., Schweren, L. S. J., Kimm J E van Hulzen, ..., and Franke, B. (2017). Subcortical brain volume differences in participants with attention deficit hyperactivity disorder in children and adults: a cross-sectional mega-analysis. *The Lancet Psychiatry*, 4(4):310–319.

Hosokawa, R. and Katsura, T. (2018). Effect of socioeconomic status on behavioral problems from preschool to early elementary school – a japanese longitudinal study. *PLOS ONE*, 13(5):e0197961.

Hou, J., Chen, C., and Dong, Q. (2015). Resting-state functional connectivity and pitch identification ability in non-musicians. *Frontiers in Neuroscience*, 9.

Hu, R.-F., Jiang, X.-Y., Hegadoren, K. M., and Zhang, Y.-H. (2015). Effects of earplugs and eye masks combined with relaxing music on sleep, melatonin and cortisol levels in ICU patients: a randomized controlled trial. *Critical Care*, 19(1).

Huang, W., Bolton, T. A. W., Medaglia, J. D., Bassett, D. S., Ribeiro, A., and Ville, D. V. D. (2018). A graph signal processing perspective on functional brain imaging. *Proceedings of the IEEE*, 106(5):868–885.

Huettel, S. A. (2010). Functional MRI (fMRI). In *Encyclopedia of Spectroscopy and Spectrometry*, pages 741–748. Elsevier.

Human Connectome Project (2020). 900 subjects data release. https://www.humanconnectome.org/study/hcp-young-adult/document/900-subjects-data-release. Accessed: 2021-03-14.

Hung, Y., Uchida, M., Gaillard, S. L., Woodworth, H., Kelberman, C., Capella, J., Kadlec, K., Goncalves, M., Ghosh, S., Yendiki, A., Chai, X. J., Hirshfeld-Becker, D. R., Whitfield-Gabrieli, S., Gabrieli, J. D., and Biederman, J. (2020). Cingulum-callosal white-matter microstructure associated with emotional dysregulation in children: A diffusion tensor imaging study. *NeuroImage: Clinical*, 27:102266.

Huntenburg, J. M., Bazin, P.-L., and Margulies, D. S. (2018). Large-scale gradients in human cortical organization. *Trends in Cognitive Sciences*, 22(1):21–31.

Hüppi, P. S., Warfield, S., Kikinis, R., Barnes, P. D., Zientara, G. P., Jolesz, F. A., Tsuji, M. K., and Volpe, J. J. (1998). Quantitative magnetic resonance imaging of brain development in premature and mature newborns. *Annals of Neurology*, 43(2):224–235.

Ikeda, K., Kawakami, K., Onimaru, H., Okada, Y., Yokota, S., Koshiya, N., Oku, Y., Iizuka, M., and Koizumi, H. (2016). The respiratory control mechanisms in the brainstem and spinal cord: integrative views of the neuroanatomy and neurophysiology. *The Journal of Physiological Sciences*, 67(1):45–62.

Inder, T. E. (2005). Abnormal cerebral structure is present at term in premature infants. *PEDIATRICS*, 115(2):286–294.

Indredavik, M. S. (2004). Psychiatric symptoms and disorders in adolescents with low birth weight. *Archives of Disease in Childhood - Fetal and Neonatal Edition*, 89(5):F445–F450.

Indredavik, M. S., Vik, T., Heyerdahl, S., Kulseng, S., and Brubakk, A.-M. (2005). Psychiatric symptoms in low birth weight adolescents, assessed by screening questionnaires. *European Child & Adolescent Psychiatry*, 14(4):226–236.

Ingoldsby, E. M., Kohl, G. O., McMahon, R. J., and and, L. L. (2006). Conduct problems, depressive symptomatology and their co-occurring presentation in childhood as predictors of adjustment in early adolescence. *Journal of Abnormal Child Psychology*, 34(5):602–620.

Ion-Margineanu, A. (2018). *Machine learning for classifying abnormal brain tissue progression based on multi-parametric Magnetic Resonance data*. PhD thesis, Arenberg Doctoral School.

Isaacs, E. B., Lucas, A., Chong, W. K., Wood, S. J., Johnson, C. L., Marshall, C., Vargha-Khadem, F., and Gadian, D. G. (2000). Hippocampal volume and everyday memory in children of very low birth weight. *Pediatric Research*, 47(6):713–720.

Jaekel, J., Baumann, N., and Wolke, D. (2013). Effects of gestational age at birth on cognitive performance: A function of cognitive workload demands. *PLoS ONE*, 8(5):e65219.

Bibliography

Jednoróg, K., Altarelli, I., Monzalvo, K., Fluss, J., Dubois, J., Billard, C., Dehaene-Lambertz, G., and Ramus, F. (2012). The influence of socioeconomic status on children's brain structure. *PLoS ONE*, 7(8):e42486.

Jobe, A. and Bancalari, E. (2001). Bronchopulmonary dysplasia. *American Journal of Respiratory and Critical Care Medicine*, 163(7):1723–1729.

Johansson, B. B. (2011). Current trends in stroke rehabilitation. a review with focus on brain plasticity. *Acta Neurologica Scandinavica*, 123(3):147–159.

Johns, C. B., Lacadie, C., Vohr, B., Ment, L. R., and Scheinost, D. (2019). Amygdala functional connectivity is associated with social impairments in preterm born young adults. *NeuroImage: Clinical*, 21:101626.

Johnson, S., Hollis, C., Kochhar, P., Hennessy, E., Wolke, D., and Marlow, N. (2010). Autism spectrum disorders in extremely preterm children. *The Journal of Pediatrics*, 156(4):525–531.e2.

Johnson, S., Hollis, C., Marlow, N., Simms, V., and Wolke, D. (2014). Screening for childhood mental health disorders using the strengths and difficulties questionnaire: the validity of multi-informant reports. *Developmental Medicine & Child Neurology*, 56(5):453–459.

Johnson, S. and Marlow, N. (2011). Preterm birth and childhood psychiatric disorders. *Pediatric Research*, 69(5 Part 2):11R–18R.

Johnson, S. and Marlow, N. (2014). Growing up after extremely preterm birth: Lifespan mental health outcomes. *Seminars in Fetal and Neonatal Medicine*, 19(2):97–104.

Jolliffe, I. T. (1986). *Principal Component Analysis.* Springer New York.

Jones, D. K. and Leemans, A. (2010). Diffusion tensor imaging. In *Methods in Molecular Biology*, pages 127–144. Humana Press.

Joshi, G. and Tada, N. (2017). Effect of noise intensity on vital parameters of newborns in a tertiary care hospital. *Sri Lanka Journal of Child Health*, 46(1):66.

Josselyn, S. A., Köhler, S., and Frankland, P. W. (2015). Finding the engram. *Nature Reviews Neuroscience*, 16(9):521–534.

Josselyn, S. A. and Tonegawa, S. (2020). Memory engrams: Recalling the past and imagining the future. *Science*, 367(6473):eaaw4325.

Joyce, K. E., Laurienti, P. J., Burdette, J. H., and Hayasaka, S. (2010). A new measure of centrality for brain networks. *PLoS ONE*, 5(8):e12200.

Kabbara, A., Khalil, M., O'Neill, G., Dujardin, K., Traboulsi, Y. E., Wendling, F., and Hassan, M. (2019). Detecting modular brain states in rest and task. *Network Neuroscience*, 3(3):878–901.

Kapellou, O., Counsell, S. J., Kennea, N., Dyet, L., Saeed, N., Stark, J., Maalouf, E., Duggan, P., Ajayi-Obe, M., Hajnal, J., Allsop, J. M., Boardman, J., Rutherford, M. A., Cowan, F., and Edwards, A. D. (2006). Abnormal cortical development after premature birth shown by altered allometric scaling of brain growth. *PLoS Medicine*, 3(8):e265.

Karmonik, C., Brandt, A., Anderson, J. R., Brooks, F., Lytle, J., Silverman, E., and Frazier, J. T. (2016). Music listening modulates functional connectivity and information flow in the human brain. *Brain Connectivity*, 6(8):632–641.

Karolis, V. R., Froudist-Walsh, S., Kroll, J., Brittain, P. J., Tseng, C.-E. J., Nam, K.-W., Reinders, A. A., Murray, R. M., Williams, S. C., Thompson, P. M., and Nosarti, C. (2017). Volumetric grey matter alterations in adolescents and adults born very preterm suggest accelerated brain maturation. *NeuroImage*, 163:379–389.

Kaufman, A. S. and Kaufman, N. L. (1983). Kaufman assessment battery for children.

Kavas, N., Arısoy, A. E., Bayhan, A., Kara, B., Günlemez, A., Türker, G., Oruç, M., and Gökalp, A. S. (2017). Neonatal sepsis and simple minor neurological dysfunction. *Pediatrics International*, 59(5):564–569.

Kay, B. P., Meng, X., DiFrancesco, M. W., Holland, S. K., and Szaflarski, J. P. (2012). Moderating effects of music on resting state networks. *Brain Research*, 1447:53–64.

Kelly, C. E., Thompson, D. K., Cheong, J. L., Chen, J., Olsen, J. E., Eeles, A. L., Walsh, J. M., Seal, M. L., Anderson, P. J., Doyle, L. W., and Spittle, A. J. (2018). Brain structure and neurological and behavioural functioning in infants born preterm. *Developmental Medicine & Child Neurology*, 61(7):820–831.

Kelly, C. E., Thompson, D. K., Spittle, A. J., Chen, J., Seal, M. L., Anderson, P. J., Doyle, L. W., and Cheong, J. L. (2020). Regional brain volumes, microstructure and neurodevelopment in moderate–late preterm children. *Archives of Disease in Childhood - Fetal and Neonatal Edition*, 105(6):593–599.

Kersbergen, K. J., Leroy, F., Išgum, I., Groenendaal, F., de Vries, L. S., Claessens, N. H., van Haastert, I. C., Moeskops, P., Fischer, C., Mangin, J.-F., Viergever, M. A., Dubois, J., and Benders, M. J. (2016a). Relation between clinical risk factors, early cortical changes, and neurodevelopmental outcome in preterm infants. *NeuroImage*, 142:301–310.

Kersbergen, K. J., Makropoulos, A., Aljabar, P., Groenendaal, F., de Vries, L. S., Counsell, S. J., and Benders, M. J. (2016b). Longitudinal regional brain development and clinical risk factors in extremely preterm infants. *The Journal of Pediatrics*, 178:93–100.e6.

Keunen, K., Išgum, I., van Kooij, B. J., Anbeek, P., van Haastert, I. C., Koopman-Esseboom, C., van Stam, P. C. F., Nievelstein, R. A., Viergever, M. A., de Vries, L. S., Groenendaal, F., and Benders, M. J. (2016). Brain volumes at term-equivalent age in preterm infants: Imaging biomarkers for neurodevelopmental outcome through early school age. *The Journal of Pediatrics*, 172:88–95.

Bibliography

Keunen, K., Kersbergen, K. J., Groenendaal, F., Isgum, I., de Vries, L. S., and Benders, M. J. N. L. (2012). Brain tissue volumes in preterm infants: prematurity, perinatal risk factors and neurodevelopmental outcome: A systematic review. *The Journal of Maternal-Fetal & Neonatal Medicine*, 25(sup1):89–100.

Koelsch, S. (2014). Brain correlates of music-evoked emotions. *Nature Reviews Neuroscience*, 15(3):170–180.

Koelsch, S. and Skouras, S. (2014). Functional centrality of amygdala, striatum and hypothalamus in a "small-world" network underlying joy: An fMRI study with music. *Human Brain Mapping*, 35(7):3485–3498.

Kono, K., Inoue, Y., Nakayama, K., Shakudo, M., Morino, M., Ohata, K., Wakasa, K., and Yamada, R. (2001). The role of diffusion-weighted imaging in patients with brain tumors. *American Journal of Neuroradiology*, 22(6):1081–1088.

Koshino, H., Minamoto, T., Yaoi, K., Osaka, M., and Osaka, N. (2014). Coactivation of the default mode network regions and working memory network regions during task preparation. *Scientific Reports*, 4(1).

Kotilahti, K., Nissilä, I., Näsi, T., Lipiäinen, L., Noponen, T., Meriläinen, P., Huotilainen, M., and Fellman, V. (2010). Hemodynamic responses to speech and music in newborn infants. *Human Brain Mapping*, pages NA–NA.

Krishnan, A., Williams, L. J., McIntosh, A. R., and Abdi, H. (2011). Partial least squares (PLS) methods for neuroimaging: A tutorial and review. *NeuroImage*, 56(2):455–475.

Lahav, A. (2015). Questionable sound exposure outside of the womb: frequency analysis of environmental noise in the neonatal intensive care unit. *Acta Paediatrica*, 104(1):e14–e19.

Lahav, A. and Skoe, E. (2014). An acoustic gap between the NICU and womb: a potential risk for compromised neuroplasticity of the auditory system in preterm infants. *Frontiers in Neuroscience*, 8.

Landi, S., Sale, A., Berardi, N., Viegi, A., Maffei, L., and Cenni, M. C. (2007). Retinal functional development is sensitive to environmental enrichment: a role for BDNF. *The FASEB Journal*, 21(1):130–139.

Largo, R. H., Pfister, D., Molinari, L., Kundu, S., Lipp, A., and Due, G. (1989). SIGNIFICANCE OF PRENATAL, PERINATAL AND POSTNATAL FACTORS IN THE DEVELOPMENT OF AGA PRETERM INFANTS AT FIVE TO SEVEN YEARS. *Developmental Medicine & Child Neurology*, 31(4):440–456.

Larmor, J. (1897). LXIII. on the theory of the magnetic influence on spectra and on the radiation from moving ions. *The London, Edinburgh, and Dublin Philosophical Magazine and Journal of Science*, 44(271):503–512.

Larroque, B. (2004). Survival of very preterm infants: Epipage, a population based cohort study. *Archives of Disease in Childhood - Fetal and Neonatal Edition*, 89(2):139F–144.

Larroque, B., Ancel, P., Marret, S., Marchand, L., Andre, M., Arnaud, C., Pierrat, V., Roze, J., Messer, J., Thiriez, G., Burguet, A., Picaud, J., Breart, G., and Kaminski, M. (2008). Neurodevelopmental disabilities and special care of 5-year-old children born before 33 weeks of gestation (the EPIPAGE study): a longitudinal cohort study. *Lancet.*, 371(9615).

Larsson, H., Thomsen, C., Frederiksen, J., Stubgaard, M., and Henriksen, O. (1992). In vivo magnetic resonance diffusion measurement in the brain of patients with multiple sclerosis. *Magnetic Resonance Imaging*, 10(1):7–12.

Lauterbur, P. C. (1973). Image formation by induced local interactions: Examples employing nuclear magnetic resonance. *Nature*, 242(5394):190–191.

Lee, C.-H., Lee, C.-Y., Hsu, M.-Y., Lai, C.-L., Sung, Y.-H., Lin, C.-Y., and Lin, L.-Y. (2017). Effects of music intervention on state anxiety and physiological indices in patients undergoing mechanical ventilation in the intensive care unit. *Biological Research For Nursing*, 19(2):137–144.

Lee, I., Neil, J. J., Huettner, P. C., Smyser, C. D., Rogers, C. E., Shimony, J. S., Kidokoro, H., Mysorekar, I. U., and Inder, T. E. (2014). The impact of prenatal and neonatal infection on neurodevelopmental outcomes in very preterm infants. *Journal of Perinatology*, 34(10):741–747.

Lee, M., Smyser, C., and Shimony, J. (2012). Resting-state fMRI: A review of methods and clinical applications. *American Journal of Neuroradiology*, 34(10):1866–1872.

Lee, W., Al-Dossary, H., Raybaud, C., Young, J. M., Morgan, B. R., Whyte, H. E., Sled, J. G., Taylor, M. J., and Shroff, M. M. (2016). Longitudinal cerebellar growth following very preterm birth. *Journal of Magnetic Resonance Imaging*, 43(6):1462–1473.

Leech, R., Kamourieh, S., Beckmann, C. F., and Sharp, D. J. (2011). Fractionating the default mode network: Distinct contributions of the ventral and dorsal posterior cingulate cortex to cognitive control. *Journal of Neuroscience*, 31(9):3217–3224.

Lejeune, F., Lordier, L., Pittet, M. P., Schoenhals, L., Grandjean, D., Hüppi, P. S., Filippa, M., and Tolsa, C. B. (2019). Effects of an early postnatal music intervention on cognitive and emotional development in preterm children at 12 and 24 months: Preliminary findings. *Frontiers in Psychology*, 10.

Lejeune, F., Tolsa, C. B., Graz, M. B., Hüppi, P. S., and Barisnikov, K. (2015). Emotion, attention, and effortful control in 24-month-old very preterm and full-term children. *L'Année psychologique*, 115(02):241–264.

Lemmers, P. M. A., Benders, M. J. N. L., DAscenzo, R., Zethof, J., Alderliesten, T., Kersbergen, K. J., Isgum, I., de Vries, L. S., Groenendaal, F., and van Bel, F. (2016). Patent ductus arteriosus and brain volume. *PEDIATRICS*, 137(4):e20153090–e20153090.

Bibliography

Leonardi, N., Richiardi, J., Gschwind, M., Simioni, S., Annoni, J.-M., Schluep, M., Vuilleumier, P., and Ville, D. V. D. (2013). Principal components of functional connectivity: A new approach to study dynamic brain connectivity during rest. *NeuroImage*, 83:937–950.

Limperopoulos, C. (2005). Late gestation cerebellar growth is rapid and impeded by premature birth. *PEDIATRICS*, 115(3):688–695.

Limperopoulos, C., Bassan, H., Gauvreau, K., Robertson, R. L., Sullivan, N. R., Benson, C. B., Avery, L., Stewart, J., MD, J. S. S., Ringer, S. A., Volpe, J. J., and duPlessis, A. J. (2007). Does cerebellar injury in premature infants contribute to the high prevalence of long-term cognitive, learning, and behavioral disability in survivors? *PEDIATRICS*, 120(3):584–593.

Limperopoulos, C., Bassan, H., Sullivan, N. R., Soul, J. S., Robertson, R. L., Moore, M., Ringer, S. A., Volpe, J. J., and du Plessis, A. J. (2008). Positive screening for autism in ex-preterm infants: Prevalence and risk factors. *PEDIATRICS*, 121(4):758–765.

Limperopoulos, C., Chilingaryan, G., Sullivan, N., Guizard, N., Robertson, R. L., and du Plessis, A. J. (2014). Injury to the premature cerebellum: Outcome is related to remote cortical development. *Cerebral Cortex*, 24(3):728–736.

Lind, A., , Haataja, L., Rautava, L., Väliaho, A., Lehtonen, L., Lapinleimu, H., Parkkola, R., and Korkman, M. (2010). Relations between brain volumes, neuropsychological assessment and parental questionnaire in prematurely born children. *European Child & Adolescent Psychiatry*, 19(5):407–417.

Lind, A., , Parkkola, R., Lehtonen, L., Munck, P., Maunu, J., Lapinleimu, H., and Haataja, L. (2011). Associations between regional brain volumes at term-equivalent age and development at 2 years of age in preterm children. *Pediatric Radiology*, 41(8):953–961.

Lindquist, M. A. (2008). The statistical analysis of fMRI data. *Statistical Science*, 23(4):439–464.

Lindstrom, K., Lindblad, F., and Hjern, A. (2011). Preterm birth and attention-deficit/hyperactivity disorder in schoolchildren. *PEDIATRICS*, 127(5):858–865.

Linsell, L., Malouf, R., Morris, J., Kurinczuk, J. J., and Marlow, N. (2015). Prognostic factors for poor cognitive development in children born very preterm or with very low birth weight. *JAMA Pediatrics*, 169(12):1162.

Liu, L., Oza, S., Hogan, D., Chu, Y., Perin, J., Zhu, J., Lawn, J. E., Cousens, S., Mathers, C., and Black, R. E. (2016). Global, regional, and national causes of under-5 mortality in 2000–15: an updated systematic analysis with implications for the sustainable development goals. *The Lancet*, 388(10063):3027–3035.

Lodygensky, G. A., Seghier, M. L., Warfield, S. K., Tolsa, C. B., Sizonenko, S., Lazeyras, F., and Hüppi, P. S. (2008). Intrauterine growth restriction affects the preterm infant's hippocampus. *Pediatric Research*, 63(4):438–443.

Logothetis, N. K., Pauls, J., Augath, M., Trinath, T., and Oeltermann, A. (2001). Neurophysiological investigation of the basis of the fMRI signal. *Nature*, 412(6843):150–157.

Lohmann, G., Margulies, D. S., Horstmann, A., Pleger, B., Lepsien, J., Goldhahn, D., Schloegl, H., Stumvoll, M., Villringer, A., and Turner, R. (2010). Eigenvector centrality mapping for analyzing connectivity patterns in fMRI data of the human brain. *PLoS ONE*, 5(4):e10232.

Lordier*, L., Loukas*, S., Grouiller, F., Vollenweider, A., Vasung, L., Meskaldji, D.-E., Lejeune, F., Pittet, M. P., Borradori-Tolsa, C., Lazeyras, F., Grandjean, D., Ville, D. V. D., and Hüppi, P. S. (2018). Music processing in preterm and full-term newborns: A psychophysiological interaction (PPI) approach in neonatal fMRI. *NeuroImage*, 185:857–864.

Lordier, L., Meskaldji, D.-E., Grouiller, F., Pittet, M. P., Vollenweider, A., Vasung, L., Borradori-Tolsa, C., Lazeyras, F., Grandjean, D., Ville, D. V. D., and Hüppi, P. S. (2019). Music in premature infants enhances high-level cognitive brain networks. *Proceedings of the National Academy of Sciences*, page 201817536.

Lowe, M. J. (2010). A historical perspective on the evolution of resting-state functional connectivity with MRI. *Magnetic Resonance Materials in Physics, Biology and Medicine*, 23(5-6):279–288.

Lurie, D. J., Kessler, D., Bassett, D. S., Betzel, R. F., Breakspear, M., Kheilholz, S., Kucyi, A., Liégeois, R., Lindquist, M. A., McIntosh, A. R., Poldrack, R. A., Shine, J. M., Thompson, W. H., Bielczyk, N. Z., Douw, L., Kraft, D., Miller, R. L., Muthuraman, M., Pasquini, L., Razi, A., Vidaurre, D., Xie, H., and Calhoun, V. D. (2020). Questions and controversies in the study of time-varying functional connectivity in resting fMRI. *Network Neuroscience*, 4(1):30–69.

Machado, B. H. and Brody, M. J. (1988). Role of the nucleus ambiguus in the regulation of heart rate and arterial pressure. *Hypertension*, 11(6_pt_2):602–607.

Maclaren, J., Han, Z., Vos, S. B., Fischbein, N., and Bammer, R. (2014). Reliability of brain volume measurements: A test-retest dataset. *Scientific Data*, 1(1).

Mahmoudzadeh, M., Dehaene-Lambertz, G., Fournier, M., Kongolo, G., Goudjil, S., Dubois, J., Grebe, R., and Wallois, F. (2013). Syllabic discrimination in premature human infants prior to complete formation of cortical layers. *Proceedings of the National Academy of Sciences*, 110(12):4846–4851.

Mahon, B. Z. and Cantlon, J. F. (2011). The specialization of function: Cognitive and neural perspectives. *Cognitive Neuropsychology*, 28(3-4):147–155.

Mai, J. and Paxinos, G. (2012). *The human nervous system*. Elsevier Academic Press, Amsterdam Boston.

Makropoulos, A., Aljabar, P., Wright, R., Hüning, B., Merchant, N., Arichi, T., Tusor, N., Hajnal, J. V., Edwards, A. D., Counsell, S. J., and Rueckert, D. (2016). Regional growth and atlasing of the developing human brain. *NeuroImage*, 125:456–478.

Bibliography

Mangin, K. S., Horwood, L. J., and Woodward, L. J. (2016). Cognitive development trajectories of very preterm and typically developing children. *Child Development*, 88(1):282–298.

Mangin, K. S., Horwood, L. J., and Woodward, L. J. (2017). Cognitive development trajectories of very preterm and typically developing children. *Child Development*, 88(1):282–298.

Mansfield, P. (1984). Real-time echo-planar imaging by NMR. *British Medical Bulletin*, 40(2):187–190.

Manto, M., Bower, J. M., Conforto, A. B., Delgado-García, J. M., da Guarda, S. N. F., Gerwig, M., Habas, C., Hagura, N., Ivry, R. B., Mariën, P., Molinari, M., Naito, E., Nowak, D. A., Taib, N. O. B., Pelisson, D., Tesche, C. D., Tilikete, C., and Timmann, D. (2011). Consensus paper: Roles of the cerebellum in motor control—the diversity of ideas on cerebellar involvement in movement. *The Cerebellum*, 11(2):457–487.

Margulies, D. S., Ghosh, S. S., Goulas, A., Falkiewicz, M., Huntenburg, J. M., Langs, G., Bezgin, G., Eickhoff, S. B., Castellanos, F. X., Petrides, M., Jefferies, E., and Smallwood, J. (2016). Situating the default-mode network along a principal gradient of macroscale cortical organization. *Proceedings of the National Academy of Sciences*, 113(44):12574–12579.

Markett, S., Montag, C., Heeren, B., Saryiska, R., Lachmann, B., Weber, B., and Reuter, M. (2015). Voxelwise eigenvector centrality mapping of the human functional connectome reveals an influence of the catechol-o-methyltransferase val158met polymorphism on the default mode and somatomotor network. *Brain Structure and Function*, 221(5):2755–2765.

Marlow, N., Wolke, D., Bracewell, M., and Samara, M. (2005). Neurologic and developmental disability at six years of age after extremely preterm birth. *N. Engl. J. Med*, 352(1).

Martinet, M., Tolsa, C. B., Jelidi, M. R., Bullinger, A., Perneger, T., and Pfister, R. (2013). Élaboration et validation de contenu d'une grille d'observation du comportement sensorimoteur du nouveau-né à l'usage du personnel soignant. *Archives de Pédiatrie*, 20(2):137–145.

Mason, M. F., Norton, M. I., Horn, J. D. V., Wegner, D. M., Grafton, S. T., and Macrae, C. N. (2007). Wandering minds: The default network and stimulus-independent thought. *Science*, 315(5810):393–395.

Massen, C. P. and Doye, J. P. K. (2005). Identifying communities within energy landscapes. *Physical Review E*, 71(4).

McCarthy, P., Benuskova, L., and Franz, E. A. (2014). The age-related posterior-anterior shift as revealed by voxelwise analysis of functional brain networks. *Frontiers in Aging Neuroscience*, 6.

McCormick, M. C., Workman-Daniels, K., and Brooks-Gunn, J. (1996). The behavioral and emotional well-being of school-age children with different birth weights. *Pediatrics*, 97(1):18–25.

McIntosh, A. R. and Lobaugh, N. J. (2004). Partial least squares analysis of neuroimaging data: applications and advances. *NeuroImage*, 23:S250–S263.

McKeown, M. (2003). Independent component analysis of functional MRI: what is signal and what is noise? *Current Opinion in Neurobiology*, 13(5):620–629.

McLaren, D. G., Ries, M. L., Xu, G., and Johnson, S. C. (2012). A generalized form of context-dependent psychophysiological interactions (gPPI): A comparison to standard approaches. *NeuroImage*, 61(4):1277–1286.

Ment, L. R., Hirtz, D., and Hüppi, P. S. (2009). Imaging biomarkers of outcome in the developing preterm brain. *The Lancet Neurology*, 8(11):1042–1055.

Meskaldji, D.-E., Morgenthaler, S., and Van De Ville, D. (2015a). Functional brain connectivity evaluated by an effective and more sufficient estimator based on extreme events. *Traitement du Signal , GRETSI*.

Meskaldji, D.-E., Morgenthaler, S., and Van De Ville, D. (2015b). New measures of brain functional connectivity by temporal analysis of extreme events. In *2015 IEEE 12th International Symposium on Biomedical Imaging (ISBI)*, pages 26–29. IEEE.

Meskaldji, D.-E., Morgenthaler, S., and Ville, D. V. D. (2015c). New measures of brain functional connectivity by temporal analysis of extreme events. In *2015 IEEE 12th International Symposium on Biomedical Imaging (ISBI)*. IEEE.

Mewes, A. U., Huppi, P. S., Als, H., Rybicki, F. J., Inder, T. E., McAnulty, G. B., Mulkern, R. V., Robertson, R. L., Rivkin, M. J., and Warfield, S. K. (2006). Regional brain development in serial magnetic resonance imaging of low-risk preterm infants. *PEDIATRICS*, 118(1):23–33.

Miller, S. P., Ferriero, D. M., Leonard, C., Piecuch, R., Glidden, D. V., Partridge, J. C., Perez, M., Mukherjee, P., Vigneron, D. B., and Barkovich, A. J. (2005a). Early brain injury in premature newborns detected with magnetic resonance imaging is associated with adverse early neurodevelopmental outcome. *The Journal of Pediatrics*, 147(5):609–616.

Miller, S. P., Ferriero, D. M., Leonard, C., Piecuch, R., Glidden, D. V., Partridge, J. C., Perez, M., Mukherjee, P., Vigneron, D. B., and Barkovich, A. J. (2005b). Early brain injury in premature newborns detected with magnetic resonance imaging is associated with adverse early neurodevelopmental outcome. *The Journal of Pediatrics*, 147(5):609–616.

Mitterschiffthaler, M. T., Fu, C. H., Dalton, J. A., Andrew, C. M., and Williams, S. C. (2007). A functional MRI study of happy and sad affective states induced by classical music. *Human Brain Mapping*, 28(11):1150–1162.

Moeller, S., Yacoub, E., Olman, C. A., Auerbach, E., Strupp, J., Harel, N., and Uğurbil, K. (2010). Multiband multislice GE-EPI at 7 tesla, with 16-fold acceleration using partial parallel imaging with application to high spatial and temporal whole-brain fMRI. *Magnetic Resonance in Medicine*, 63(5):1144–1153.

Moeskops, P., Išgum, I., Keunen, K., Claessens, N. H. P., van Haastert, I. C., Groenendaal, F., de Vries, L. S., Viergever, M. A., and Benders, M. J. N. L. (2017). Prediction of cognitive

and motor outcome of preterm infants based on automatic quantitative descriptors from neonatal MR brain images. *Scientific Reports*, 7(1).

Mohanty, R., Sethares, W. A., Nair, V. A., and Prabhakaran, V. (2020). Rethinking measures of functional connectivity via feature extraction. *Scientific Reports*, 10(1).

Monson, B. B., Anderson, P. J., Matthews, L. G., Neil, J. J., Kapur, K., Cheong, J. L. Y., Doyle, L. W., Thompson, D. K., and Inder, T. E. (2016). Examination of the pattern of growth of cerebral tissue volumes from hospital discharge to early childhood in very preterm infants. *JAMA Pediatrics*, 170(8):772.

Montagna, A., Karolis, V., Batalle, D., Counsell, S., Rutherford, M., Arulkumaran, S., Happe, F., Edwards, D., and Nosarti, C. (2020). ADHD symptoms and their neurodevelopmental correlates in children born very preterm. *PLOS ONE*, 15(3):e0224343.

Monti, M. (2011). Statistical analysis of fMRI time-series: A critical review of the GLM approach. *Frontiers in Human Neuroscience*, 5.

Moore, T., Hennessy, E. M., Myles, J., Johnson, S. J., Draper, E. S., Costeloe, K. L., and Marlow, N. (2012). Neurological and developmental outcome in extremely preterm children born in england in 1995 and 2006: the EPICure studies. *BMJ*, 345(dec04 3):e7961–e7961.

Mori, S. and van Zijl, P. (2005). Mr tractography using diffusion tensor mr imaging. *Clinical MR neuroimaging: diffusion, perfusion and spectroscopy*, pages 86–99.

Morishita, H., Miwa, J. M., Heintz, N., and Hensch, T. K. (2010). Lynx1, a cholinergic brake, limits plasticity in adult visual cortex. *Science*, 330(6008):1238–1240.

Morsing, E., Malova, M., Kahn, A., Lätt, J., Björkman-Burtscher, I. M., Maršál, K., and Ley, D. (2018). Brain volumes and developmental outcome in childhood following fetal growth restriction leading to very preterm birth. *Frontiers in Physiology*, 9.

Mourão-Miranda, J., Bokde, A. L., Born, C., Hampel, H., and Stetter, M. (2005). Classifying brain states and determining the discriminating activation patterns: Support vector machine on functional MRI data. *NeuroImage*, 28(4):980–995.

Mueller, S., Wang, D., Fox, M. D., Yeo, B. T., Sepulcre, J., Sabuncu, M. R., Shafee, R., Lu, J., and Liu, H. (2013). Individual variability in functional connectivity architecture of the human brain. *Neuron*, 77(3):586–595.

Mulder, H., Pitchford, N. J., Hagger, M. S., and Marlow, N. (2009). Development of executive function and attention in preterm children: A systematic review. *Developmental Neuropsychology*, 34(4):393–421.

Murphy, K., Bodurka, J., and Bandettini, P. A. (2007). How long to scan? the relationship between fMRI temporal signal to noise ratio and necessary scan duration. *NeuroImage*, 34(2):565–574.

Naze, S., Proix, T., Atasoy, S., and Kozloski, J. R. (2021). Robustness of connectome harmonics to local gray matter and long-range white matter connectivity changes. *NeuroImage*, 224:117364.

Newman, M. E. J. (2002). Assortative mixing in networks. *Physical Review Letters*, 89(20).

Newman, M. E. J. (2004). Detecting community structure in networks. *The European Physical Journal B - Condensed Matter*, 38(2):321–330.

Newman, M. E. J. (2006a). Finding community structure in networks using the eigenvectors of matrices. *Phys. Rev. E*, 74:036104.

Newman, M. E. J. (2006b). Modularity and community structure in networks. *Proceedings of the National Academy of Sciences*, 103(23):8577–8582.

Newman, M. E. J. (2016). Equivalence between modularity optimization and maximum likelihood methods for community detection. *Physical Review E*, 94(5).

Newman, M. E. J. and Girvan, M. (2004). Finding and evaluating community structure in networks. *Phys. Rev. E*, 69:026113.

Nicholson, J. M., Lucas, N., Berthelsen, D., and Wake, M. (2010). Socioeconomic inequality profiles in physical and developmental health from 0–7 years: Australian national study. *Journal of Epidemiology and Community Health*, 66(1):81–87.

Noble, K. G., Engelhardt, L. E., Brito, N. H., Mack, L. J., Nail, E. J., Angal, J., Barr, R., Fifer, W. P., and and, A. J. E. (2015). Socioeconomic disparities in neurocognitive development in the first two years of life. *Developmental Psychobiology*, 57(5):535–551.

Nosarti, C., Nam, K. W., Walshe, M., Murray, R. M., Cuddy, M., Rifkin, L., and Allin, M. P. (2014). Preterm birth and structural brain alterations in early adulthood. *NeuroImage: Clinical*, 6:180–191.

O'Connor, E. E. and Zeffiro, T. A. (2019). Why is clinical fMRI in a resting state? *Frontiers in Neurology*, 10.

Olsson, M. (2009). DSM diagnosis of conduct disorder (CD)—a review. *Nordic Journal of Psychiatry*, 63(2):102–112.

O'Reilly, J. X., Woolrich, M. W., Behrens, T. E., Smith, S. M., and Johansen-Berg, H. (2012). Tools of the trade: psychophysiological interactions and functional connectivity. *Social Cognitive and Affective Neuroscience*, 7(5):604–609.

Otte, R., Winkler, I., Braeken, M., Stekelenburg, J., van der Stelt, O., and den Bergh, B. V. (2013). Detecting violations of temporal regularities in waking and sleeping two-month-old infants. *Biological Psychology*, 92(2):315–322.

Bibliography

Oxtoby, N. P., Young, A. L., Cash, D. M., Benzinger, T. L. S., Fagan, A. M., Morris, J. C., Bateman, R. J., Fox, N. C., Schott, J. M., and Alexander, D. C. (2018). Data-driven models of dominantly-inherited alzheimer's disease progression. *Brain*, 141(5):1529–1544.

Padilla, N., Alexandrou, G., Blennow, M., Lagercrantz, H., and Ådén, U. (2014). Brain growth gains and losses in extremely preterm infants at term. *Cerebral Cortex*, 25(7):1897–1905.

Padilla, N., Alexandrou, G., Blennow, M., Lagercrantz, H., and Ådén, U. (2015). Brain growth gains and losses in extremely preterm infants at term. *Cerebral Cortex*, 25(7):1897–1905.

Palomar-García, M.-Á., Zatorre, R. J., Ventura-Campos, N., Bueichekú, E., and Ávila, C. (2017). Modulation of functional connectivity in auditory–motor networks in musicians compared with nonmusicians. *Cerebral Cortex*, page bhw120.

Pandit, A. S., Ball, G., Edwards, A. D., and Counsell, S. J. (2013). Diffusion magnetic resonance imaging in preterm brain injury. *Neuroradiology*, 55(S2):65–95.

Panteleeva, Y., Ceschi, G., Glowinski, D., Courvoisier, D. S., and Grandjean, D. (2017). Music for anxiety? meta-analysis of anxiety reduction in non-clinical samples. *Psychology of Music*, 46(4):473–487.

Papile, L.-A., Munsick-Bruno, G., and Schaefer, A. (1983). Relationship of cerebral intraventricular hemorrhage and early childhood neurologic handicaps. *The Journal of Pediatrics*, 103(2):273–277.

Papini, C., White, T. P., Montagna, A., Brittain, P. J., Froudist-Walsh, S., Kroll, J., Karolis, V., Simonelli, A., Williams, S. C., Murray, R. M., and Nosarti, C. (2016). Altered resting-state functional connectivity in emotion-processing brain regions in adults who were born very preterm. *Psychological Medicine*, 46(14):3025–3039.

Parbery-Clark, A., Skoe, E., Lam, C., and Kraus, N. (2009). Musician enhancement for speech-in-noise. *Ear & Hearing*, 30(6):653–661.

Partanen, E., Kujala, T., Naatanen, R., Liitola, A., Sambeth, A., and Huotilainen, M. (2013a). Learning-induced neural plasticity of speech processing before birth. *Proceedings of the National Academy of Sciences*, 110(37):15145–15150.

Partanen, E., Kujala, T., Tervaniemi, M., and Huotilainen, M. (2013b). Prenatal music exposure induces long-term neural effects. *PLoS ONE*, 8(10):e78946.

Paschal, C. B. and Morris, H. D. (2004). K-space in the clinic. *Journal of Magnetic Resonance Imaging*, 19(2):145–159.

Pehrs, C., Deserno, L., Bakels, J.-H., Schlochtermeier, L. H., Kappelhoff, H., Jacobs, A. M., Fritz, T. H., Koelsch, S., and Kuchinke, L. (2014). How music alters a kiss: superior temporal gyrus controls fusiform–amygdalar effective connectivity. *Social Cognitive and Affective Neuroscience*, 9(11):1770–1778.

Peralta-Carcelen, M., Carlo, W. A., Pappas, A., Vaucher, Y. E., Yeates, K. O., Phillips, V. A., Gustafson, K. E., Payne, A. H., Duncan, A. F., Newman, J. E., and and, C. M. B. (2017). Behavioral problems and socioemotional competence at 18 to 22 months of extremely premature children. *Pediatrics*, 139(6):e20161043.

Perani, D., Saccuman, M. C., Scifo, P., Spada, D., Andreolli, G., Rovelli, R., Baldoli, C., and Koelsch, S. (2010). Functional specializations for music processing in the human newborn brain. *Proceedings of the National Academy of Sciences*, 107(10):4758–4763.

Pereira, C. S., Teixeira, J., Figueiredo, P., Xavier, J., Castro, S. L., and Brattico, E. (2011). Music and emotions in the brain: Familiarity matters. *PLoS ONE*, 6(11):e27241.

Peretz, I., Gaudreau, D., and Bonnel, A.-M. (1998). Exposure effects on music preference and recognition. *Memory & Cognition*, 26(5):884–902.

Peretz, I. and Zatorre, R. J. (2005). Brain organization for music processing. *Annual Review of Psychology*, 56(1):89–114.

Pernet, C. R. (2014). Misconceptions in the use of the general linear model applied to functional MRI: a tutorial for junior neuro-imagers. *Frontiers in Neuroscience*, 8.

Péron, J., Frühholz, S., Vérin, M., and Grandjean, D. (2013). Subthalamic nucleus: A key structure for emotional component synchronization in humans. *Neuroscience & Biobehavioral Reviews*, 37(3):358–373.

Peterson, B., Anderson, A., Ehrenkranz, R., Staib, L., Tageldin, M., Colson, E., Gore, J., Duncan, C., Makuch, R., and Ment, L. (2003). Regional brain volumes and their later neurodevelopmental correlates in term and preterm infants. *Pediatrics*, 111(5).

Peterson, B. S. (2000). Regional brain volume abnormalities and long-term cognitive outcome in preterm infants. *JAMA*, 284(15):1939.

Petrides, M. (2005). Lateral prefrontal cortex: architectonic and functional organization. *Philosophical Transactions of the Royal Society B: Biological Sciences*, 360(1456):781–795.

Piccolo, L. R., Merz, E. C., He, X., Sowell, E. R., and and, K. G. N. (2016). Age-related differences in cortical thickness vary by socioeconomic status. *PLOS ONE*, 11(9):e0162511.

Pineda, R., Guth, R., Herring, A., Reynolds, L., Oberle, S., and Smith, J. (2016). Enhancing sensory experiences for very preterm infants in the NICU: an integrative review. *Journal of Perinatology*, 37(4):323–332.

Pineda, R., Guth, R., Herring, A., Reynolds, L., Oberle, S., and Smith, J. (2017). Enhancing sensory experiences for very preterm infants in the NICU: an integrative review. *J Perinatol.*, 37(4).

Bibliography

Pineda, R. G., Neil, J., Dierker, D., Smyser, C. D., Wallendorf, M., Kidokoro, H., Reynolds, L. C., Walker, S., Rogers, C., Mathur, A. M., Essen, D. C. V., and Inder, T. (2014). Alterations in brain structure and neurodevelopmental outcome in preterm infants hospitalized in different neonatal intensive care unit environments. *The Journal of Pediatrics*, 164(1):52–60.e2.

Plantinga, J. and Trainor, L. J. (2005). Memory for melody: infants use a relative pitch code. *Cognition*, 98(1):1–11.

Platel, H., Baron, J.-C., Desgranges, B., Bernard, F., and Eustache, F. (2003). Semantic and episodic memory of music are subserved by distinct neural networks. *NeuroImage*, 20(1):244–256.

Plewes, D. B. and Kucharczyk, W. (2012). Physics of MRI: A primer. *Journal of Magnetic Resonance Imaging*, 35(5):1038–1054.

Poldrack, R. A., Huckins, G., and Varoquaux, G. (2020). Establishment of best practices for evidence for prediction. *JAMA Psychiatry*, 77(5):534.

Pothen, A., Simon, H. D., and Liou, K.-P. (1990). Partitioning sparse matrices with eigenvectors of graphs. *SIAM journal on matrix analysis and applications*, 11(3):430–452.

Power, J. D., Mitra, A., Laumann, T. O., Snyder, A. Z., Schlaggar, B. L., and Petersen, S. E. (2014). Methods to detect, characterize, and remove motion artifact in resting state fMRI. *NeuroImage*, 84:320–341.

Power, J. D., Plitt, M., Gotts, S. J., Kundu, P., Voon, V., Bandettini, P. A., and Martin, A. (2018). Ridding fMRI data of motion-related influences: Removal of signals with distinct spatial and physical bases in multiecho data. *Proceedings of the National Academy of Sciences*, 115(9):E2105–E2114.

Preti, M. G., Bolton, T. A., and Ville, D. V. D. (2017). The dynamic functional connectome: State-of-the-art and perspectives. *NeuroImage*, 160:41–54.

Preti, M. G. and Van De Ville, D. (2017). Dynamics of functional connectivity at high spatial resolution reveal long-range interactions and fine-scale organization. *Scientific Reports*, 7(1).

Pruett, J. R., Kandala, S., Hoertel, S., Snyder, A. Z., Elison, J. T., Nishino, T., Feczko, E., Dosenbach, N. U., Nardos, B., Power, J. D., Adeyemo, B., Botteron, K. N., McKinstry, R. C., Evans, A. C., Hazlett, H. C., Dager, S. R., Paterson, S., Schultz, R. T., Collins, D. L., Fonov, V. S., Styner, M., Gerig, G., Das, S., Kostopoulos, P., Constantino, J. N., Estes, A. M., Petersen, S. E., Schlaggar, B. L., and Piven, J. (2015). Accurate age classification of 6 and 12 month-old infants based on resting-state functional connectivity magnetic resonance imaging data. *Developmental Cognitive Neuroscience*, 12:123–133.

Puonti, O., Iglesias, J. E., and Leemput, K. V. (2016). Fast and sequence-adaptive whole-brain segmentation using parametric bayesian modeling. *NeuroImage*, 143:235–249.

Puthussery, S., Chutiyami, M., Tseng, P.-C., Kilby, L., and Kapadia, J. (2018). Effectiveness of early intervention programs for parents of preterm infants: a meta-review of systematic reviews. *BMC Pediatrics*, 18(1).

Raichle, M. E. (2015). The brain's default mode network. *Annual Review of Neuroscience*, 38(1):433–447.

Raichle, M. E., MacLeod, A. M., Snyder, A. Z., Powers, W. J., Gusnard, D. A., and Shulman, G. L. (2001). A default mode of brain function. *Proceedings of the National Academy of Sciences*, 98(2):676–682.

Rangaprakash, D., Wu, G.-R., Marinazzo, D., Hu, X., and Deshpande, G. (2018). Hemodynamic response function (HRF) variability confounds resting-state fMRI functional connectivity. *Magnetic Resonance in Medicine*, 80(4):1697–1713.

Rathbone, R., Counsell, S. J., Kapellou, O., Dyet, L., Kennea, N., Hajnal, J., Allsop, J. M., Cowan, F., and Edwards, A. D. (2011). Perinatal cortical growth and childhood neurocognitive abilities. *Neurology*, 77(16):1510–1517.

Reichardt, J. and Bornholdt, S. (2006). Statistical mechanics of community detection. *Physical Review E*, 74(1).

Reineberg, A. E., Andrews-Hanna, J. R., Depue, B. E., Friedman, N. P., and Banich, M. T. (2015). Resting-state networks predict individual differences in common and specific aspects of executive function. *NeuroImage*, 104:69–78.

Richiardi, J., Altmann, A., Milazzo, A.-C., Chang, C., Chakravarty, M. M., Banaschewski, T., et al. (2015). Correlated gene expression supports synchronous activity in brain networks. *Science*, 348(6240):1241–1244.

Risius, O. J., Onur, O. A., Dronse, J., von Reutern, B., Richter, N., Fink, G. R., and Kukolja, J. (2019). Neural network connectivity during post-encoding rest: Linking episodic memory encoding and retrieval. *Frontiers in Human Neuroscience*, 12.

Rogers, C. E., Anderson, P. J., Thompson, D. K., Kidokoro, H., Wallendorf, M., Treyvaud, K., Roberts, G., Doyle, L. W., Neil, J. J., and Inder, T. E. (2012). Regional cerebral development at term relates to school-age social–emotional development in very preterm children. *Journal of the American Academy of Child & Adolescent Psychiatry*, 51(2):181–191.

Rogers, C. E., Sylvester, C. M., Mintz, C., Kenley, J. K., Shimony, J. S., Barch, D. M., and Smyser, C. D. (2017). Neonatal amygdala functional connectivity at rest in healthy and preterm infants and early internalizing symptoms. *Journal of the American Academy of Child & Adolescent Psychiatry*, 56(2):157–166.

Rommel, A.-S., James, S.-N., McLoughlin, G., Brandeis, D., Banaschewski, T., Asherson, P., and Kuntsi, J. (2017). Association of preterm birth with attention-deficit/hyperactivity disorder–like and wider-ranging neurophysiological impairments of attention and inhibition. *Journal of the American Academy of Child & Adolescent Psychiatry*, 56(1):40–50.

Bibliography

Rossi, A. F., Pessoa, L., Desimone, R., and Ungerleider, L. G. (2008). The prefrontal cortex and the executive control of attention. *Experimental Brain Research*, 192(3):489–497.

Rubinov, M. and Sporns, O. (2010). Complex network measures of brain connectivity: Uses and interpretations. *NeuroImage*, 52(3):1059–1069.

Rutherford, M. (2002). Magnetic resonance imaging of the brain in preterm infants 24 weeks' gestation to term. *MRI of the Neonatal Brain*.

Samara, M., Marlow, N., and and, D. W. (2008). Pervasive behavior problems at 6 years of age in a total-population sample of children born at <=25 weeks of gestation. *PEDIATRICS*, 122(3):562–573.

Särkämö, T. (2017). Cognitive, emotional, and neural benefits of musical leisure activities in aging and neurological rehabilitation: A critical review. *Annals of Physical and Rehabilitation Medicine*, 61(6):414–418.

Särkämö, T., Ripollés, P., Vepsäläinen, H., Autti, T., Silvennoinen, H. M., Salli, E., Laitinen, S., Forsblom, A., Soinila, S., and Rodríguez-Fornells, A. (2014). Structural changes induced by daily music listening in the recovering brain after middle cerebral artery stroke: A voxel-based morphometry study. *Frontiers in Human Neuroscience*, 8:245.

Schellenberg, E. G., Peretz, I., and Vieillard, S. (2008). Liking for happy- and sad-sounding music: Effects of exposure. *Cognition & Emotion*, 22(2):218–237.

Schirmer, A., Fox, P. M., and Grandjean, D. (2012). On the spatial organization of sound processing in the human temporal lobe: A meta-analysis. *NeuroImage*, 63(1):137–147.

Schwartze, M., Keller, P. E., Patel, A. D., and Kotz, S. A. (2011). The impact of basal ganglia lesions on sensorimotor synchronization, spontaneous motor tempo, and the detection of tempo changes. *Behavioural Brain Research*, 216(2):685–691.

Seghier, M. L. (2013). The angular gyrus. *The Neuroscientist*, 19(1):43–61.

Setsompop, K., Gagoski, B. A., Polimeni, J. R., Witzel, T., Wedeen, V. J., and Wald, L. L. (2011). Blipped-controlled aliasing in parallel imaging for simultaneous multislice echo planar imaging with reduced g-factor penalty. *Magnetic Resonance in Medicine*, 67(5):1210–1224.

Shah, D. K., Anderson, P. J., Carlin, J. B., Pavlovic, M., Howard, K., Thompson, D. K., Warfield, S. K., and Inder, T. E. (2006). Reduction in cerebellar volumes in preterm infants: Relationship to white matter injury and neurodevelopment at two years of age. *Pediatric Research*, 60(1):97–102.

Shi, F., Yap, P.-T., Wu, G., Jia, H., Gilmore, J. H., Lin, W., and Shen, D. (2011). Infant brain atlases from neonates to 1- and 2-year-olds. *PLoS ONE*, 6(4):e18746.

Short, E. J., Klein, N. K., Lewis, B. A., Fulton, S., Eisengart, S., Kercsmar, C., Baley, J., and Singer, L. T. (2003). Cognitive and academic consequences of bronchopulmonary dysplasia and very low birth weight: 8-year-old outcomes. *PEDIATRICS*, 112(5):e359–e359.

Sikka, R., Cuddy, L. L., Johnsrude, I. S., and Vanstone, A. D. (2015). An fMRI comparison of neural activity associated with recognition of familiar melodies in younger and older adults. *Frontiers in Neuroscience*, 9.

Silveira, R. C., Mendes, E. W., Fuentefria, R. N., Valentini, N. C., and Procianoy, R. S. (2018). Early intervention program for very low birth weight preterm infants and their parents: a study protocol. *BMC Pediatrics*, 18(1).

Simpson, J. R., Drevets, W. C., Snyder, A. Z., Gusnard, D. A., and Raichle, M. E. (2001). Emotion-induced changes in human medial prefrontal cortex: II. during anticipatory anxiety. *Proceedings of the National Academy of Sciences*, 98(2):688–693.

Sinclair, L. (2012). Premature birth linked to mental illness in adults. *Psychiatric News*, 47(15):24a–24a.

Skellern, C., Rogers, Y., and O'Callaghan, M. (2001). A parent-completed developmental questionnaire: Follow up of ex-premature infants. *Journal of Paediatrics and Child Health*, 37(2):125–129.

Skiöld, B., Alexandrou, G., Padilla, N., Blennow, M., Vollmer, B., and Ådén, U. (2014). Sex differences in outcome and associations with neonatal brain morphology in extremely preterm children. *The Journal of Pediatrics*, 164(5):1012–1018.

Smith, S. M., Fox, P. T., Miller, K. L., Glahn, D. C., Fox, P. M., Mackay, C. E., Filippini, N., Watkins, K. E., Toro, R., Laird, A. R., and Beckmann, C. F. (2009). Correspondence of the brain's functional architecture during activation and rest. *Proceedings of the National Academy of Sciences*, 106(31):13040–13045.

Soher, B. J., Dale, B. M., and Merkle, E. M. (2007). A review of MR physics: 3t versus 1.5t. *Magnetic Resonance Imaging Clinics of North America*, 15(3):277–290.

Soleimani, F., Zaheri, F., and Abdi, F. (2014). Long-term neurodevelopmental outcomes after preterm birth. *Iran. Red Crescent Med. J.*, 16(6).

Soria-Pastor, S., Padilla, N., Zubiaurre-Elorza, L., Ibarretxe-Bilbao, N., Botet, F., Costas-Moragas, C., Falcon, C., Bargallo, N., Mercader, J. M., and Junque, C. (2009). Decreased regional brain volume and cognitive impairment in preterm children at low risk. *PEDIATRICS*, 124(6):e1161–e1170.

Spittle, A., Orton, J., Anderson, P., Boyd, R., and Doyle, L. (2015). Early developmental intervention programmes provided posthospital discharge to prevent motor and cognitive impairmentin preterm infants (review). *The Cochrane Database of Systematic Reviews*, 59(11).

Spittle, A. and Treyvaud, K. (2016). The role of early developmental intervention to influence neurobehavioral outcomes of children born preterm. *Seminars in Perinatology*, 40(8):542–548.

Spittle, A. J. and Orton, J. (2014). Cerebral palsy and developmental coordination disorder in children born preterm. *Seminars in Fetal and Neonatal Medicine*, 19(2):84–89.

Spittle, A. J., Treyvaud, K., Doyle, L. W., Roberts, G., Lee, K. J., Inder, T. E., Cheong, J. L., Hunt, R. W., Newnham, C. A., and Anderson, P. J. (2009). Early emergence of behavior and social-emotional problems in very preterm infants. *Journal of the American Academy of Child & Adolescent Psychiatry*, 48(9):909–918.

Sporns, O. (2011). The human connectome: a complex network. *Annals of the New York Academy of Sciences*, 1224(1):109–125.

Sporns, O. and Betzel, R. F. (2016). Modular brain networks. *Annual Review of Psychology*, 67(1):613–640.

Sporns, O., Tononi, G., and Kötter, R. (2005). The human connectome: A structural description of the human brain. *PLoS Computational Biology*, 1(4):e42.

Statistical Parametric Mapping (2020). https://www.fil.ion.ucl.ac.uk/spm/software/spm12/. Accessed: 2020-03-17.

Stephens, K., Silk, T. J., Anderson, V., Hazell, P., Enticott, P. G., and Sciberras, E. (2020). Associations between limbic system white matter structure and socio-emotional functioning in children with adhd + asd. *Journal of Autism and Developmental Disorders*.

Stevens, C., Lauinger, B., and Neville, H. (2009). Differences in the neural mechanisms of selective attention in children from different socioeconomic backgrounds: an event-related brain potential study. *Developmental Science*, 12(4):634–646.

Sutton, P. and Darmstadt, G. (2013). Preterm birth and neurodevelopment: A review of outcomes and recommendations for early identification and cost-effective interventions. *Journal Of Tropical Pediatrics*, 59(4).

Symington, A. J. and Pinelli, J. (2006). Developmental care for promoting development and preventing morbidity in preterm infants. *Cochrane Database of Systematic Reviews*.

Tambini, A., Ketz, N., and Davachi, L. (2010). Enhanced brain correlations during rest are related to memory for recent experiences. *Neuron*, 65(2):280–290.

Tavano, A., Grasso, R., Gagliardi, C., Triulzi, F., Bresolin, N., Fabbro, F., and Borgatti, R. (2007). Disorders of cognitive and affective development in cerebellar malformations. *Brain*, 130(10):2646–2660.

Taylor, H. G., Minich, N., Schluchter, M., Espy, K. A., and Klein, N. (2019). Resilience in extremely preterm/extremely low birth weight kindergarten children. *Journal of the International Neuropsychological Society*, 25(04):362–374.

Teie, D. (2016). A comparative analysis of the universal elements of music and the fetal environment. *Frontiers in Psychology*, 07.

Tharwat, A., Gaber, T., Ibrahim, A., and Hassanien, A. E. (2017). Linear discriminant analysis: A detailed tutorial. *AI Communications*, 30(2):169–190.

Thompson, D. K., Chen, J., Beare, R., Adamson, C. L., Ellis, R., Ahmadzai, Z. M., Kelly, C. E., Lee, K. J., Zalesky, A., Yang, J. Y., Hunt, R. W., Cheong, J. L., Inder, T. E., Doyle, L. W., Seal, M. L., and Anderson, P. J. (2016). Structural connectivity relates to perinatal factors and functional impairment at 7 years in children born very preterm. *NeuroImage*, 134:328–337.

Thompson, D. K., Warfield, S. K., Carlin, J. B., Pavlovic, M., Wang, H. X., Bear, M., Kean, M. J., Doyle, L. W., Egan, G. F., and Inder, T. E. (2007). Perinatal risk factors altering regional brain structure in the preterm infant. *Brain*, 130(3):667–677.

Thompson, D. K., Wood, S. J., Doyle, L. W., Warfield, S. K., Lodygensky, G. A., Anderson, P. J., Egan, G. F., and Inder, T. E. (2008). Neonate hippocampal volumes: Prematurity, perinatal predictors, and 2-year outcome. *Annals of Neurology*, 63(5):642–651.

Thornburgh, C. L., Narayana, S., Rezaie, R., Bydlinski, B. N., Tylavsky, F. A., Papanicolaou, A. C., Choudhri, A. F., and Völgyi, E. (2017). Concordance of the resting state networks in typically developing, 6-to 7-year-old children and healthy adults. *Frontiers in Human Neuroscience*, 11.

Tolsa, C. B., Zimine, S., Warfield, S. K., Freschi, M., Rossignol, A. S., Lazeyras, F., Hanquinet, S., Pfizenmaier, M., and Hüppi, P. S. (2004). Early alteration of structural and functional brain development in premature infants born with intrauterine growth restriction. *Pediatric Research*, 56(1):132–138.

Tommiska, V., Tuominen, R., and Fellman, V. (2003). Economic costs of care in extremely low birthweight infants during the first 2 years of life. *Pediatric Critical Care Medicine*, 4(2):157–163.

Trainor, L. J., Wu, L., and Tsang, C. D. (2004). Long-term memory for music: infants remember tempo and timbre. *Developmental Science*, 7(3):289–296.

Trehub, S. E. and Hannon, E. E. (2009). Conventional rhythms enhance infants' and adults' perception of musical patterns. *Cortex*, 45(1):110–118.

Treyvaud, K., Ure, A., Doyle, L. W., Lee, K. J., Rogers, C. E., Kidokoro, H., Inder, T. E., and Anderson, P. J. (2013). Psychiatric outcomes at age seven for very preterm children: rates and predictors. *Journal of Child Psychology and Psychiatry*, 54(7):772–779.

Bibliography

Trost, W., Ethofer, T., Marcel, and Vuilleumier, P. (2011). Mapping aesthetic musical emotions in the brain. *Cerebral Cortex*, 22(12):2769–2783.

Trost, W., Frühholz, S., Schön, D., Labbé, C., Pichon, S., Grandjean, D., and Vuilleumier, P. (2014). Getting the beat: Entrainment of brain activity by musical rhythm and pleasantness. *NeuroImage*, 103:55–64.

Twilhaar, E. S., Wade, R. M., de Kieviet, J. F., van Goudoever, J. B., van Elburg, R. M., and Oosterlaan, J. (2018). Cognitive outcomes of children born extremely or very preterm since the 1990s and associated risk factors. *JAMA Pediatrics*, 172(4):361.

van den Bosch, I., Salimpoor, V. N., and Zatorre, R. J. (2013). Familiarity mediates the relationship between emotional arousal and pleasure during music listening. *Frontiers in Human Neuroscience*, 7.

van den Heuvel, M. P. and Pol, H. E. H. (2010). Exploring the brain network: A review on resting-state fMRI functional connectivity. *European Neuropsychopharmacology*, 20(8):519–534.

van den Heuvel, M. P. and Sporns, O. (2011). Rich-club organization of the human connectome. *Journal of Neuroscience*, 31(44):15775–15786.

van der Heijden, M., Oliai, A., Jeekel, J., Reiss, I., Hunink, M., and van Dijk, M. (2016). Do hospitalized premature infants benefit from music interventions? a systematic review of randomized controlled trials. *PLOS ONE*, 11(9).

van Houdt, C. A., Oosterlaan, J., Aarnoudse-Moens, C. S., van Kaam, A. H., and van Wassenaer-Leemhuis, A. G. (2020). Subtypes of behavioral functioning in 8–12 year old very preterm children. *Early Human Development*, 142:104968.

Van Kooij, B. J., Benders, M. J., Anbeek, P., Van Haastert, I. C., De Vries, L. S., and Groenendaal, F. (2012). Cerebellar volume and proton magnetic resonance spectroscopy at term, and neurodevelopment at 2 years of age in preterm infants. *Developmental Medicine & Child Neurology*, 54(3):260–266.

van Marle, H. J., Hermans, E. J., Qin, S., and Fernández, G. (2010). Enhanced resting-state connectivity of amygdala in the immediate aftermath of acute psychological stress. *NeuroImage*, 53(1):348–354.

Varoquaux, G., Buitinck, L., Louppe, G., Grisel, O., Pedregosa, F., and Mueller, A. (2015). Scikit-learn. *GetMobile: Mobile Computing and Communications*, 19(1):29–33.

Veijola, J., Guo, J. Y., Moilanen, J. S., Jääskeläinen, E., Miettunen, J., Kyllönen, M., et al. (2014). Longitudinal changes in total brain volume in schizophrenia: Relation to symptom severity, cognition and antipsychotic medication. *PLoS ONE*, 9(7):e101689.

Venkataraman, A., Van Dijk, K. R., Buckner, R. L., and Golland, P. (2009). Exploring functional connectivity in fMRI via clustering. *ICASSP, IEEE International Conference on Acoustics, Speech and Signal Processing - Proceedings*, pages 441–444.

Versace, A., Acuff, H., Bertocci, M. A., Bebko, G., Almeida, J. R. C., Perlman, S. B., Leemans, A., Schirda, C., Aslam, H., Dwojak, A., Bonar, L., Travis, M., Gill, M. K., Demeter, C., Diwadkar, V. A., Sunshine, J. L., Holland, S. K., Kowatch, R. A., Birmaher, B., Axelson, D., Horwitz, S. M., Frazier, T. W., Arnold, L. E., Fristad, M. A., Youngstrom, E. A., Findling, R. L., and Phillips, M. L. (2015). White matter structure in youth with behavioral and emotional dysregulation disorders. *JAMA Psychiatry*, 72(4):367.

Voigt, M., Fusch, C., Olbertz, D., Hartmann, K., Rochow, N., Renken, C., and Schneider, K. (2006). Analyse des neugeborenenkollektivs der bundesrepublik deutschland. *Geburtshilfe und Frauenheilkunde*, 66(10):956–970.

Volkova, A., Trehub, S. E., and Schellenberg, E. G. (2006). Infants' memory for musical performances. *Developmental Science*, 9(6):583–589.

Volpe, J. J. (2008). *Neurology of the newborn E-book*. Elsevier Health Sciences.

Volpe, J. J. (2009). Brain injury in premature infants: a complex amalgam of destructive and developmental disturbances. *The Lancet Neurology*, 8(1):110–124.

von Luxburg, U. (2007). A tutorial on spectral clustering. *Statistics and Computing*, 17(4):395–416.

Wang, D., Buckner, R. L., and Liu, H. (2014). Functional specialization in the human brain estimated by intrinsic hemispheric interaction. *Journal of Neuroscience*, 34(37):12341–12352.

Wang, J., Wang, L., Zang, Y., Yang, H., Tang, H., Gong, Q., Chen, Z., Zhu, C., and He, Y. (2009). Parcellation-dependent small-world brain functional networks: A resting-state fMRI study. *Human Brain Mapping*, 30(5):1511–1523.

Watts, D. J. and Strogatz, S. H. (1998). Collective dynamics of 'small-world' networks. *Nature*, 393(6684):440–442.

Wehrle, F. M., Michels, L., Guggenberger, R., Huber, R., Latal, B., O'Gorman, R. L., and Hagmann, C. F. (2018). Altered resting-state functional connectivity in children and adolescents born very preterm short title. *NeuroImage: Clinical*, 20:1148–1156.

Wheelock, M., Austin, N., Bora, S., Eggebrecht, A., Melzer, T., Woodward, L., and Smyser, C. (2018). Altered functional network connectivity relates to motor development in children born very preterm. *NeuroImage*, 183:574–583.

White, R. D., , Smith, J. A., and Shepley, M. M. (2013). Recommended standards for newborn ICU design, eighth edition. *Journal of Perinatology*, 33(S1):S2–S16.

Wilson-Ching, M., Molloy, C. S., Anderson, V. A., Burnett, A., Roberts, G., Cheong, J. L., Doyle, L. W., and Anderson, P. J. (2013). Attention difficulties in a contemporary geographic cohort of adolescents born extremely preterm/extremely low birth weight. *Journal of the International Neuropsychological Society*, 19(10):1097–1108.

Bibliography

Wink, A. M., de Munck, J. C., van der Werf, Y. D., van den Heuvel, O. A., and Barkhof, F. (2012). Fast eigenvector centrality mapping of voxel-wise connectivity in functional magnetic resonance imaging: Implementation, validation, and interpretation. *Brain Connectivity*, 2(5):265–274. PMID: 23016836.

Winkler, I., Haden, G. P., Ladinig, O., Sziller, I., and Honing, H. (2009). Newborn infants detect the beat in music. *Proceedings of the National Academy of Sciences*, 106(7):2468–2471.

Witt, A., Theurel, A., Tolsa, C. B., Lejeune, F., Fernandes, L., van Hanswijck de Jonge, L., Monnier, M., Graz, M. B., Barisnikov, K., Gentaz, E., and Hüppi, P. S. (2014). Emotional and effortful control abilities in 42-month-old very preterm and full-term children. *Early Human Development*, 90(10):565–569.

Wong, H. S. and Edwards, P. (2013). Nature or nurture: A systematic review of the effect of socio-economic status on the developmental and cognitive outcomes of children born preterm. *Maternal and Child Health Journal*, 17(9):1689–1700.

Wood, N. S. (2005). The EPICure study: associations and antecedents of neurological and developmental disability at 30 months of age following extremely preterm birth. *Archives of Disease in Childhood - Fetal and Neonatal Edition*, 90(2):F134–F140.

Woodward, L. J., Anderson, P. J., Austin, N. C., Howard, K., and Inder, T. E. (2006). Neonatal MRI to predict neurodevelopmental outcomes in preterm infants. *New England Journal of Medicine*, 355(7):685–694.

Woodward, L. J., Edgin, J. O., Thompson, D., and Inder, T. E. (2005). Object working memory deficits predicted by early brain injury and development in the preterm infant. *Brain*, 128(11):2578–2587.

Woodward, L. J., Lu, Z., Morris, A. R., and Healey, D. M. (2017). Preschool self regulation predicts later mental health and educational achievement in very preterm and typically developing children. *The Clinical Neuropsychologist*, 31(2):404–422.

Woodward, L. J., Moor, S., Hood, K. M., Champion, P. R., Foster-Cohen, S., Inder, T. E., and Austin, N. C. (2009). Very preterm children show impairments across multiple neurodevelopmental domains by age 4 years. *Archives of Disease in Childhood - Fetal and Neonatal Edition*, 94(5):339–344.

Wright, C. I., Martis, B., Schwartz, C. E., Shin, L. M., Fischer, H., McMullin, K., and Rauch, S. L. (2003). Novelty responses and differential effects of order in the amygdala, substantia innominata, and inferior temporal cortex. *NeuroImage*, 18(3):660–669.

Wu, Y., Stoodley, C., Brossard-Racine, M., Kapse, K., Vezina, G., Murnick, J., du Plessis, A. J., and Limperopoulos, C. (2020). Altered local cerebellar and brainstem development in preterm infants. *NeuroImage*, 213:116702.

Xiong, T., Gonzalez, F., and Mu, D.-Z. (2012). An overview of risk factors for poor neurodevelopmental outcome associated with prematurity. *World Journal of Pediatrics*, 8(4):293–300.

Yan (2010). DPARSF: a MATLAB toolbox for "pipeline" data analysis of resting-state fMRI. *Frontiers in System Neuroscience*.

Yang, S., Fombonne, E., and Kramer, M. S. (2011). Duration of gestation, size at birth and later childhood behaviour. *Paediatric and Perinatal Epidemiology*, 25(4):377–387.

Yeo, B. T. T., Krienen, F. M., Eickhoff, S. B., Yaakub, S. N., Fox, P. T., Buckner, R. L., Asplund, C. L., and Chee, M. W. (2014). Functional specialization and flexibility in human association cortex. *Cerebral Cortex*, 25(10):3654–3672.

Yeo, B. T. T., Krienen, F. M., Sepulcre, J., Sabuncu, M. R., Lashkari, D., Hollinshead, M., Roffman, J. L., Smoller, J. W., Zöllei, L., Polimeni, J. R., Fischl, B., Liu, H., and Buckner, R. L. (2011). The organization of the human cerebral cortex estimated by intrinsic functional connectivity. *Journal of Neurophysiology*, 106(3):1125–1165.

Yoshikawa, A., Masaoka, Y., Yoshida, M., Koiwa, N., Honma, M., Watanabe, K., Kubota, S., Natsuko, I., Ida, M., and Izumizaki, M. (2020). Heart rate and respiration affect the functional connectivity of default mode network in resting-state functional magnetic resonance imaging. *Frontiers in Neuroscience*, 14.

Young, A. L., Oxtoby, N. P., Daga, P., Cash, D. M., Fox, N. C., Ourselin, S., Schott, J. M., and Alexander, D. C. (2014). A data-driven model of biomarker changes in sporadic alzheimer's disease. *Brain*, 137(9):2564–2577.

Young, J. M., Morgan, B. R., Powell, T. L., Moore, A. M., Whyte, H. E., Smith, M. L., and Taylor, M. J. (2016). Associations of perinatal clinical and magnetic resonance imaging measures with developmental outcomes in children born very preterm. *The Journal of Pediatrics*, 170:90–96.

Young, J. M., Vandewouw, M. M., Whyte, H. E. A., Leijser, L. M., and Taylor, M. J. (2020). Resilience and vulnerability: Neurodevelopment of very preterm children at four years of age. *Frontiers in Human Neuroscience*, 14.

Yushkevich, P. A., Piven, J., Hazlett, H. C., Smith, R. G., Ho, S., Gee, J. C., and Gerig, G. (2006). User-guided 3d active contour segmentation of anatomical structures: Significantly improved efficiency and reliability. *NeuroImage*, 31(3):1116–1128.

Zamorano, A. M., Cifre, I., Montoya, P., Riquelme, I., and Kleber, B. (2017). Insula-based networks in professional musicians: Evidence for increased functional connectivity during resting state fMRI. *Human Brain Mapping*, 38(10):4834–4849.

Zeki, S., Watson, J., Lueck, C., Friston, K., Kennard, C., and Frackowiak, R. (1991). A direct demonstration of functional specialization in human visual cortex. *The Journal of Neuroscience*, 11(3):641–649.

Bibliography

Zentner, M. and Eerola, T. (2010). Rhythmic engagement with music in infancy. *Proceedings of the National Academy of Sciences*, 107(13):5768–5773.

Zhang, J., Abiose, O., Katsumi, Y., Touroutoglou, A., Dickerson, B. C., and Barrett, L. F. (2019). Intrinsic functional connectivity is organized as three interdependent gradients. *Scientific Reports*, 9(1).

Zhang, W., Wang, J., Fan, L., Zhang, Y., Fox, P. T., Eickhoff, S. B., Yu, C., and Jiang, T. (2016). Functional organization of the fusiform gyrus revealed with connectivity profiles. *Human Brain Mapping*, 37(8):3003–3016.

Zhao, T. C. and Kuhl, P. K. (2016). Musical intervention enhances infants' neural processing of temporal structure in music and speech. *Proceedings of the National Academy of Sciences*, 113(19):5212–5217.

Zhigalov, A., Arnulfo, G., Nobili, L., Palva, S., and Palva, J. M. (2017). Modular co-organization of functional connectivity and scale-free dynamics in the human brain. *Network Neuroscience*, 1(2):143–165.

Zhong, Y., Wang, H., Lu, G., Zhang, Z., Jiao, Q., and Liu, Y. (2009). Detecting functional connectivity in fMRI using PCA and regression analysis. *Brain Topography*, 22(2):134–144.

Zhu, C. Z., Zang, Y. F., Liang, M., Tian, L. X., He, Y., Li, X. B., Sui, M. Q., Wang, Y. F., and Jiang, T. Z. (2005). Discriminative analysis of brain function at resting-state for attention-deficit/hyperactivity disorder. In *Lecture Notes in Computer Science*, pages 468–475. Springer Berlin Heidelberg.

Zöller, D., Sandini, C., Karahanoğlu, F. I., Padula, M. C., Schaer, M., Eliez, S., and Ville, D. V. D. (2019). Large-scale brain network dynamics provide a measure of psychosis and anxiety in 22q11.2 deletion syndrome. *Biological Psychiatry: Cognitive Neuroscience and Neuroimaging*, 4(10):881–892.

Serafeim Loukas

Nationality: *Greek*

G seralouk@gmail.com

in www.linkedin.com/in/serafeim-loukas
☉ https://github.com/seralouk
🎓 https://bit.ly/3vPS3l8

Education

2017– Present	**PhD student in Electrical Engineering school** Swiss Federal Institute of Technology Lausanne, Lausanne, Switzerland.
2015–2017	**Master in Neuroscience (M.Sc.)** University of Geneva, Geneva, Switzerland *-Thesis title: "Effective connectivity analysis of brain networks in preterm infants". Supervision*: Prof. Dimitri Van De Ville, Prof. Petra Huppi
2010–2015	**Diploma in Electrical and Computer Engineering** Five years program at National Technical University of Athens, Athens, Greece *-Thesis title: "Analysis of biochemical phenotypes of the carotid atherosclerosis: Correlations with image-based and clinical indicators using clustering methods". Supervision*: Prof. Konstantina Nikita
2007–2010	**General Lyceum Certificate** Aristotelian General Lyceum, Corinth, Greece *-Participation to the Pan-Hellenic Exams 2009-2010, (19.242/20.000 points)*

Awards and distinctions

- **Summa Cum Laude Merit Award** at the International Society for Magnetic Resonance in Medicine Annual Meeting (ISMRM) 2020.

- **Best poster presentation award**, Neuroscience Day (2016) at Campus Biotech, Geneva
  Best poster award among 30 neuroscience posters

Research Experience

2017 - 2021	**Doctoral Candidate** - Swiss Federal Institute of Technology Lausanne & University of Geneva Lausanne & Geneva, Switzerland *-Responsibilities: Research, scientific writing, project management, supervision of students, teaching activities.* *-Dissertation Title: "Brain connectomics: multivariate and predictive models for neurodevelopment".*
2015–2017	**Master Thesis** - University of Geneva, Geneva, Switzerland *-Thesis title: "Effective connectivity analysis of brain networks in preterm infants".*
2010–2015	**Bachelor Thesis** - National Technical University of Athens, Athens, Greece *-Thesis title: "Analysis of biochemical phenotypes of the carotid atherosclerosis: Correlations with image-based and clinical indicators using clustering methods".*

Teaching activities

2017 - 2021

- Image Processing I (MICRO-511)* & Image Processing II (MICRO-512)*

- Signal processing for functional brain imaging (MICRO-513)*

   * Master courses at the Swiss Federal Institute of Technology Lausanne (EPFL)

Professional experience

2020 - Present	**Official author at Medium** *Objective*: Publishing high-quality scientific articles for Towards Data Science & AI In Plain English publications
2017 - Present	**Ambassador of the E3 – EPFL Excellence in Engineering Summer internship program** EPFL, Geneva, Switzerland *Responsibilities: Contact and motivate students to apply for the E3 program. Promotion of the engineering school and research activities*

Foreign Languages

Greek	**Native**
English	**Proficient User: C2**
French	**Intermediate User: B1**

List of Publications & Presentations

Journal Papers

- **Loukas, S.***, Lordier, L.*, Grouiller, F., Vollenweider, A., Vasung, L., Meskaldji, D.-E., Lejeune, F., Pittet, M.P., Borradori-Tolsa, C., Lazeyras, F., Grandjean, D., Van De Ville, D., Hüppi, P.S., 2019. Music processing in preterm and full-term newborns: A psychophysiological interaction (PPI) approach in neonatal fMRI. NeuroImage 185, 857–864.
  DOI: https://doi.org/10.1016/j.neuroimage.2018.03.078

- **Loukas, S.***, Lordier, L.*, Meskaldji, D.-E., Filippa, M., Sa de Almeida, J., Van De Ville, D., Hüppi, P.S., 2020. Musical memories in newborns: A resting-state functional connectivity study (Submitted to Human Brain Mapping Journal, 2021)

- Gui, L., **Loukas, S***., Lazeyras, F., Hüppi, P.S., Meskaldji, D.-E., Borradori Tolsa, C., 2019. Longitudinal study of neonatal brain tissue volumes in preterm infants and their ability to predict neurodevelopmental outcome. NeuroImage 185, 728–741.
  DOI: https://doi.org/10.1016/j.neuroimage.2018.06.034

Oral Presentations

- **Loukas, S.,** (2017). *"Music training enhances functional connectivity in preterm newborns"*, CIBM/BBL day 2017, Geneva, Switzerland

- **Loukas, S.,** (2019). *"Investigating the effects of an early intervention in preterm newborns: A resting-state functional connectivity study"*, ISMRM Annual Meeting 2019, Montreal, Canada

Conference Abstracts Presentations

- **Loukas, S.**, et al., (2020). "*Resting State Functional Connectivity and Angiogenesis-related Gene Co-Expression Networks in early brain development*", Proc. Intl. Soc. Mag. Reson. Med. 28, ISMRM, Virtual conference.
  (Link: https://index.mirasmart.com/ISMRM2020/PDFfiles/4588.html)

- **Loukas, S.**, et al., (2019). "*Investigating the effects of an early intervention in preterm newborns: A resting-state functional connectivity study*", Proc. Intl. Soc. Mag. Reson. Med. 27, ISMRM, Montreal, Canada.
  (Link: https://index.mirasmart.com/ISMRM2019/PDFfiles/0045.html)

- **Loukas, S.**, et al., (2018). "*Adaptive linear discriminant analysis for complex networks to study extreme prematurity and intrauterine growth restriction effects at school age*", Proc. Intl. Soc. Mag. Reson. Med. 26, ISMRM, Paris, France.
  (Link: https://index.mirasmart.com/ISMRM2018/PDFfiles/5214.html)

- **Loukas, S.**, et al., (2017). "*Music training enhances functional connectivity in preterm newborns*", Proc. Intl. Soc. Mag. Reson. Med. 25 (2017), ISMRM, Hawaii, USA.
  (Link: http://indexsmart.mirasmart.com/ISMRM2017/PDFfiles/4103.html)